

Alessandro de Iaco Veris

Fundamental Concepts of Liquid-Propellant Rocket Engines

Springer Aerospace Technology

Series Editors

Sergio De Rosa, DII, University of Naples Federico II, NAPOLI, Italy

Yao Zheng, School of Aeronautics and Astronautics, Zhejiang University,
Hangzhou, Zhejiang, China

The series explores the technology and the science related to the aircraft and spacecraft including concept, design, assembly, control and maintenance. The topics cover aircraft, missiles, space vehicles, aircraft engines and propulsion units. The volumes of the series present the fundamentals, the applications and the advances in all the fields related to aerospace engineering, including:

- structural analysis,
- aerodynamics,
- aeroelasticity,
- aeroacoustics,
- flight mechanics and dynamics
- orbital maneuvers,
- avionics,
- systems design,
- materials technology,
- launch technology,
- payload and satellite technology,
- space industry, medicine and biology.

The series' scope includes monographs, professional books, advanced textbooks, as well as selected contributions from specialized conferences and workshops.

The volumes of the series are single-blind peer-reviewed.

To submit a proposal or request further information, please contact:

Mr. Pierpaolo Riva at pierpaolo.riva@springer.com (Europe and Americas)
Mr. Mengchu Huang at mengchu.huang@springer.com (China)

More information about this series at <http://www.springer.com/series/8613>

Alessandro de Iaco Veris

Fundamental Concepts of Liquid-Propellant Rocket Engines



Springer

Alessandro de Iaco Veris
Rome, Italy

ISSN 1869-1730
Springer Aerospace Technology
ISBN 978-3-030-54703-5
<https://doi.org/10.1007/978-3-030-54704-2>

ISSN 1869-1749 (electronic)
ISBN 978-3-030-54704-2 (eBook)

© The Editor(s) (if applicable) and The Author(s), under exclusive license to Springer Nature Switzerland AG 2021

This work is subject to copyright. All rights are solely and exclusively licensed by the Publisher, whether the whole or part of the material is concerned, specifically the rights of translation, reprinting, reuse of illustrations, recitation, broadcasting, reproduction on microfilms or in any other physical way, and transmission or information storage and retrieval, electronic adaptation, computer software, or by similar or dissimilar methodology now known or hereafter developed.

The use of general descriptive names, registered names, trademarks, service marks, etc. in this publication does not imply, even in the absence of a specific statement, that such names are exempt from the relevant protective laws and regulations and therefore free for general use.

The publisher, the authors and the editors are safe to assume that the advice and information in this book are believed to be true and accurate at the date of publication. Neither the publisher nor the authors or the editors give a warranty, expressed or implied, with respect to the material contained herein or for any errors or omissions that may have been made. The publisher remains neutral with regard to jurisdictional claims in published maps and institutional affiliations.

Cover illustration: This cover image is taken from NASA website (https://www.nasa.gov/audience/foreducators/rocketry/imagegallery/rpd_spaceX.jpg.html).

This Springer imprint is published by the registered company Springer Nature Switzerland AG
The registered company address is: Gewerbestrasse 11, 6330 Cham, Switzerland

Preface

The present book is conceived for undergraduate or graduate aerospace engineers and in particular for those who design liquid-propellant engines for rocket propulsion.

This book gives several data on existing engines, typical values of design parameters, and worked examples of application of the concepts discussed with their numerical results. This enables the reader to apply the concepts introduced to cases of practical interest.

This book uses only the metric system (SI).

Rome, Italy
October 2019

Alessandro de Iaco Veris

Contents

1 Fundamental Concepts on Liquid-Propellant Rocket Engines	1
1.1 The Generation of Thrust	1
1.2 The Gas Flow Through the Combustion Chamber and the Nozzle	7
1.3 Performance Indicators	27
1.4 Liquid Propellants for High-Thrust Rocket Engines	39
1.5 Combustion of Propellants in Steady State	49
1.6 Combustion of Propellants in Unsteady State	53
1.7 Principal Components of a Liquid-Propellant Rocket Engine	57
References	59
2 The Thrust Chamber Assembly	63
2.1 The Principal Components of a Thrust Chamber	63
2.2 The Design of a Thrust Chamber for Thrust Vector Control	67
2.3 Performance of a Thrust Chamber	79
2.4 Configuration and Design of a Thrust Chamber	83
2.5 Cooling of a Thrust Chamber	110
2.6 Injectors	152
2.7 Gas-generator and Other Engine Cycles	166
2.8 Igniters	175
2.9 Combustion Instability	185
References	197
3 Feed Systems Using Gases Under Pressure	203
3.1 Fundamental Concepts	203
3.2 Requirements for Gases Stored Under Pressure	204
3.3 Feed Systems Using Gases Stored for Bi-Propellants	210
3.4 Feed Systems Using Evaporation of Two Propellants	230
3.5 Feed Systems Using Gases Stored for Mono-Propellants	235
3.6 Feed Systems Using Combustion Products	239

3.7	Control Systems for Liquid-Propellant Gas Generators	244
3.8	Feed Systems Using Direct Injection into the Main Propellant Tanks	247
3.9	Choice of a Feed System Using Gases Under Pressure	248
	References	249
4	Feed Systems Using Turbo-Pumps	251
4.1	Fundamental Concepts	251
4.2	Pumps for Propellants	252
4.3	Turbines Driving the Pumps	259
4.4	Sources of Energy for Turbines	269
4.5	Description of a Typical Turbo-Pump	271
4.6	Turbo-Pump Performance	276
4.7	Turbo-Pump Design Parameters	278
4.8	Heads and Mass Flow Rates of Pumps	284
4.9	Design of Centrifugal-Flow Pumps	302
4.10	Design of Axial-Flow Pumps	348
4.11	Design of Turbines	379
4.12	Bearings for Turbo-Pumps	430
4.13	Seals for Turbo-Pumps	436
4.14	Gears for Turbo-Pumps	440
	References	444
5	Control Systems and Valves	447
5.1	Fundamental Concepts on Control Systems	447
5.2	Control Systems for Rocket Engines	452
5.3	Control of Thrust Magnitude	456
5.4	Control of Propellant Mixture Ratio	458
5.5	Control of Propellant Consumption	459
5.6	Control of Thrust Direction	465
5.7	Principal Components of Flow Control Systems	469
5.8	Static and Dynamic Seals for Leakage Control in Valves	478
5.9	Design of Propellant Valves	491
5.10	Design of Pilot Valves	505
5.11	Design of Flow Regulating Devices of the Fixed-Area Type	515
5.12	Design of Servo-Valves	520
5.13	Design of Pressure-Reducing Regulators	532
5.14	Design of Differential Pressure Regulators	538
5.15	Design of Relief Valves	540
5.16	Design of Check Valves	548
5.17	Design of Burst Discs	553
5.18	Design of Explosive Valves	556
	References	560

6 Tanks for Propellants	563
6.1 Fundamental Concepts	563
6.2 Tanks Subject Only to Membrane Stresses	564
6.3 Tanks Subject to Membrane and Bending Stresses	571
6.4 Multi-element Tanks	584
6.5 Tanks Subject to Loads Due to Propellant Sloshing	593
6.6 Slosh-Suppression Devices for Tanks	606
6.7 Materials, Processes, and Environmental Conditions of Tanks	614
6.8 Fracture Control of Metals Used for Tanks	628
6.9 Structural Elements of Tanks	637
References	654
7 Interconnecting Components and Structures	657
7.1 Fundamental Concepts	657
7.2 Interconnecting Ducts and Structures in a Rocket Engine	659
7.3 Materials Used for Tubing in Rocket Engines	671
7.4 Coupling Components for Tubing	673
7.5 Control of Pressure Loss in Tubing	680
7.6 Control of Vibrations at the Inlet of Pumps	683
7.7 Bellows Joints	687
7.8 Flexible Hoses	701
7.9 Filters	710
7.10 Design of a Flange Joint	720
7.11 Gaskets and Other Seals for Flange Joints	729
7.12 Design of a Bellows Joint for a Flexible Duct	735
References	746

Chapter 1

Fundamental Concepts

on Liquid-Propellant Rocket Engines

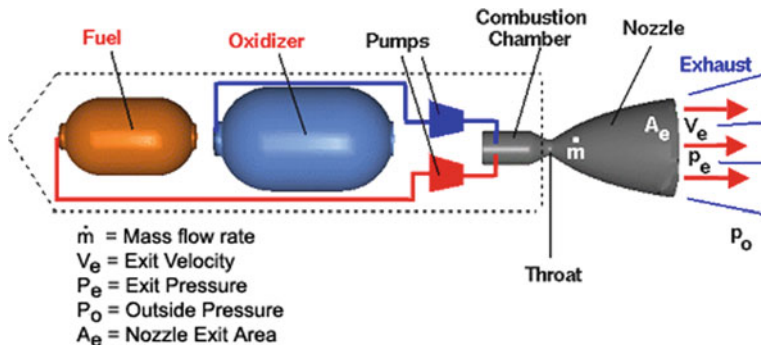


1.1 The Generation of Thrust

A rocket is a vehicle which moves through space by ejecting a propellant gas at high velocity oppositely to the direction in which the vehicle is desired to move. High-thrust propulsion systems for rocket engines use chemical propellants, which are burned in the combustion chamber of a rocket to generate thrust. According to Newton's third law of motion (to every action there is always opposed an equal reaction), the continuous ejection of a stream of hot gases in one direction causes a steady motion of the rocket in the opposite direction.

A couple of propellants comprises a fuel and an oxidiser. A fuel is a substance, such as liquid hydrogen (H_2) or a mixture of hydrocarbons, which burns in the presence of oxygen to form the hot gases which are accelerated and then ejected at high speed through a nozzle. An oxidiser is either liquid oxygen (O_2) or a substance releasing oxygen, such as hydrogen peroxide (H_2O_2), nitrous oxide (N_2O), nitronium perchlorate (NO_2ClO_4), or another substance, such as fluorine (F_2), having a strong tendency to accept electrons. The oxidiser combines with the fuel in a proper mixture ratio, as will be shown in Sect. 1.2.

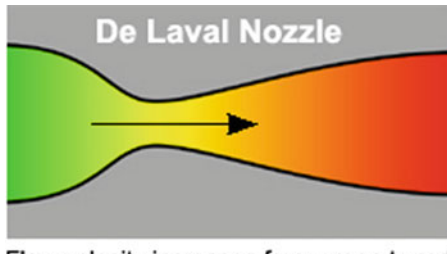
Four categories of high-thrust rocket motors may be identified, according to the physical state of the propellants carried within such rockets. These categories are solid-propellant motors, liquid-propellant engines, gaseous-propellant engines and hybrid-propellant engines, the last of them being those which use propellants stored in at least two of the three (solid, liquid, and gaseous) physical states of matter. The following figure, due to the courtesy of NASA-JPL [1], shows a scheme of a pump-fed liquid bi-propellant rocket engine.



$$\text{Thrust} = \mathbf{F} = \dot{m} V_e + (P_e - P_o) A_e$$

A rocket carries a combination of propellants (a fuel and an oxidiser) within itself in order to be capable of operating inside or outside the atmosphere of the Earth. In the rocket engine illustrated above, the magnitude F of the thrust vector \mathbf{F} depends on the propellant mass flow rate $\dot{m} \equiv dm/dt$ through the engine, on the magnitude v_e of the exit velocity vector \mathbf{v}_e of the exhaust gas, and on the pressure p_e of the gas at the exit plane of the nozzle.

The principle of functioning of a converging-diverging nozzle (also known as a de Laval nozzle, after the name of its inventor, Gustaf de Laval) is illustrated in the following figure, due to the courtesy of NASA-JPL [1].



Flow velocity increases from green to red.

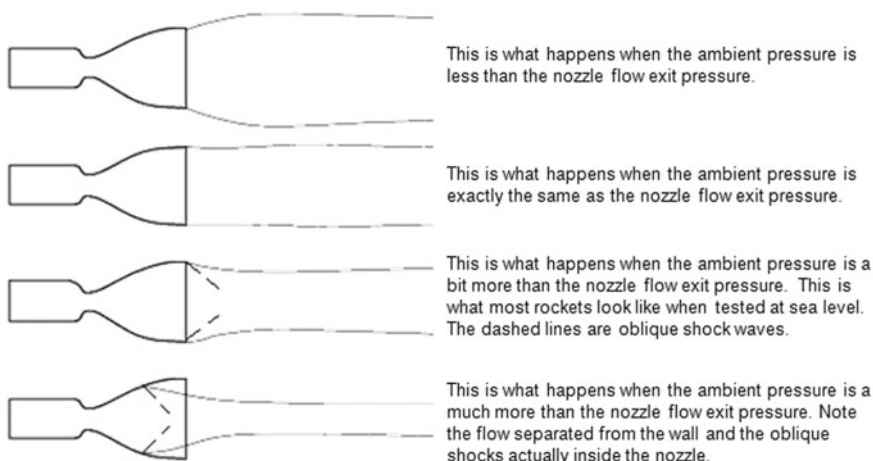
As has been shown by Crown [2], a compressible fluid at virtually zero velocity in the combustion chamber is accelerated through the converging portion of the nozzle to sonic speed ($M = 1$) in the throat where, if the converging portion is properly designed, the flow is uniform and parallel. The fluid is then expanded in the diverging portion of the nozzle until the desired Mach number $M > 1$ is reached in the test section, where the flow is again uniform and parallel.

In other words, the cross-section (perpendicular to the gas flow) of the nozzle immediately downstream of the combustion chamber decreases, in order for the subsonic flow ($M < 1$) to increase its speed up to the speed of sound ($M = 1$).

The sonic flow condition is reached in the throat, where the cross-sectional area A of the nozzle reaches its minimum value A_t . In order for the flow to increase further its

speed in supersonic conditions ($M > 1$), the exhaust gases must expand downstream of the throat, and therefore the cross-sectional area A of the nozzle must increase ($A > A_t$). This is because, in the converging portion of the nozzle, the maximum uniform velocity which can be reached by the flow in any section is the velocity corresponding to the local velocity of sound. Further increases in velocity can only be obtained by expanding the gas in the subsequent diverging portion of the nozzle.

For optimum performance in terms of thrust, the gas pressure, p_e , at the exit plane of the nozzle should be exactly equal to the pressure, p_0 , due to the environment around it. In the vacuum of space ($p_0 = 0$), this is impossible. The bigger the exit area, A_e , of the nozzle, the closer the rocket gets to the optimum thrust. However, at some point, the additional thrust gained is not worth the added mass which is necessary to make the exit area bigger. In conditions of optimum expansion ratio, the rocket motor produces the maximum thrust. A nozzle, which ends before the exhaust gas reaches the pressure of the outside environment, is called an under-expanded nozzle. In these conditions, the rocket does not get all the thrust available from its engine, because the expansion ratio is too low, and therefore the exhaust gas pressure is greater than the environmental pressure. By contrast, a nozzle, whose cross-sectional area at the exit plane is too large, is called an over-expanded nozzle. This occurs when the expansion ratio A_e/A_t is too high, and the pressure of the exhaust gas is less than the environmental pressure. Since the cross-sectional area at the exit plane A_e is too large, then the exhaust gas completely expands before reaching the exit plane of the nozzle. The gas flow downstream of the exit plane, as a function of the ambient pressure, is shown in the following figure, due to the courtesy of NASA [3].



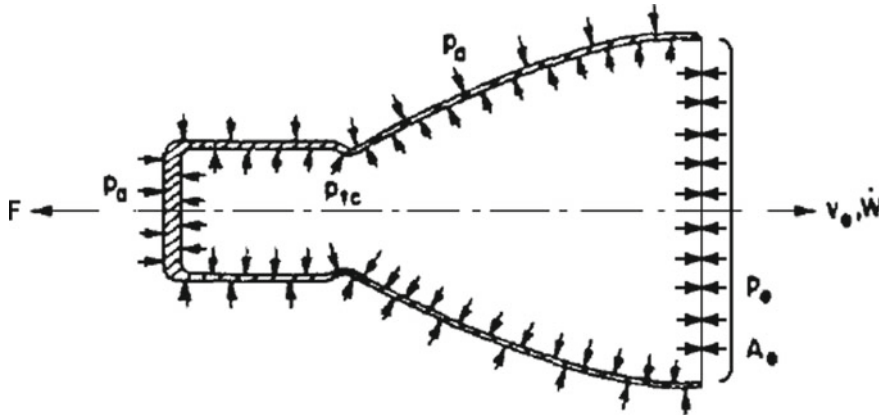
In the atmosphere, it is difficult to get the optimum expansion ratio, because the air pressure changes with temperature and altitude. Since a given expansion ratio results in the optimum expansion only at a specific altitude, then the design expansion ratio

of the nozzle must be selected in such a way as to give the best average performance during powered flight.

With reference to the following figure, due to the courtesy of NASA [4], the thrust imparted to the spacecraft by the gas flow can be expressed as follows

$$F = \dot{m} v_e$$

where \dot{m} is the mass flow rate of the exhaust gas, and v_e is its velocity at the exit plane of the nozzle. Therefore, for a constant mass flow rate \dot{m} or weight flow rate $\dot{W} = g_0 \dot{m}$ of exhaust gas, the thrust F is proportional to the velocity v_e of the gas at the exit plane.



A spacecraft is subject not only to the thrust due to its engine, but also to the pressure, p_0 , due to the environment around it. At high altitudes, p_0 can be assumed to be equal to zero. In these conditions, the net force acting on the gas contained in the thrust chamber (comprising the combustion chamber and the nozzle) is the sum of the reactions coming from the walls and of the reaction of the absolute pressure of gas at the exit plane. These two reaction forces are opposed, as shown in the preceding figure.

Therefore, according to the second principle of dynamics, the net force acting on the gas must be equal to the momentum flux out of the thrust chamber, which is

$$\int_{A_{tc}}^0 p_{tc} dA - A_e p_e = \dot{m} v_e$$

where A_{tc} and p_{tc} are respectively the area and the pressure of the thrust chamber, A_e , v_e , and p_e are respectively the area, the gas velocity, and the static absolute pressure of the gas at the exit plane of the nozzle, and \dot{m} is the steady mass flow rate of the gas. The integral, that is, the first term on the left-hand side of the preceding equation,

represent the integral of the pressure forces (resultant) acting on the thrust chamber (combustion chamber and nozzle) and projected onto a plane normal to the axis of symmetry of the thrust chamber, as shown in the preceding figure. This integral is just the force, F , which acts on the thrust chamber (and, therefore, on the spacecraft). Consequently, the preceding equation may also be written as follows

$$F = \dot{m}v_e + A_e p_e$$

This equality holds under the following hypotheses:

- the injection flow velocity of the propellants is negligible;
- the flow is constant and does not change with time during the burn;
- the products of combustion are in chemical equilibrium after the burn;
- the flow of gas through the exit plane of the nozzle is one-dimensional, that is, all the molecules of the ejected gas move on straight lines which are parallel to the axis of symmetry of the nozzle;
- the flow is compressible, that is, the gas density is subject to significant changes;
- the flow is isentropic, that is, frictionless and adiabatic (without heat loss), and therefore depends only on the cross-sectional areas of the nozzle; and
- the gas flowing in the nozzle is a perfect gas, so that the well-known equation of state $p = \rho RT$ involving pressure p , density ρ , and temperature T can be used, where R is the constant of the specific gas (the universal gas constant $R^* = 8314.460 \text{ N m kmol}^{-1} \text{ K}^{-1}$ divided by the average molar mass \mathcal{M} (kg/kmol) of the exhaust gas; for example, if the exhaust gas were water, H_2O , then $R = 8314.460/18 = 461.9 \text{ N m kg}^{-1} \text{ K}^{-1}$).

In the thrust equation written above, the quantity \dot{m} is called the momentum thrust, and the quantity $A_e p_e$ is called the pressure thrust. The latter term indicates that some (but not all) of the total forces due to the pressure p_{tc} in the thrust chamber contribute to the kinetic energy possessed by the exhaust gases flowing in the nozzle. In other words, a part of the gas pressure generated by the release of chemical energy is used to increase the gas momentum, whereas another part is not. The greater the part of gas pressure used for this purpose, the greater the efficiency of the nozzle.

Let us assume now that the rocket is fired at an ambient pressure p_0 greater than zero, that is, at low-altitudes. In these conditions, the pressure forces due to the environment and acting on the outside of the thrust chamber walls have no effect on the gas inside. However, such pressure forces subtract a part ($A_e p_0$) from the total pressure thrust ($A_e p_e$). Since the exhaust gas flows at supersonic velocity through the exit plane of area A_e , then the ambient pressure p_0 cannot gain access to it. Therefore, the ambient pressure generates a net unbalanced force onto the projected thrust chamber area, in the direction opposed to the thrust, of magnitude $A_e p_0$. This fact is taken into account by re-writing the equation of thrust as follows

$$F = \dot{m}v_e + A_e(p_e - p_0)$$

which is just the equation given in [1]. The same equation may also be written as follows

$$F = \dot{m}v_e + A_e(p_e - p_0) = \dot{m}c$$

where

$$c = v_e + \frac{A_e(p_e - p_0)}{\dot{m}}$$

is called the effective exhaust velocity, whose value is the same as that of the exhaust gas velocity v_e at the exit plane of the nozzle only when the gas pressure p_e at the same plane is equal to the ambient pressure p_0 . As has been shown above, the presence of the second addend on the right-hand side of the preceding equation indicates that the optimum value of v_e has not been reached.

As an application of these concepts to a practical case, taken from [4], it is required to compute the exhaust gas velocity v_e at the exit plane of the nozzle, the thrust in space, and the effective exhaust velocities at sea level (c) and in space (c_s), for a rocket engine having a thrust $F = 4.448 \times 10^5$ N at sea level, a mass flow rate $\dot{m} = 167.5$ kg/s due to propellant consumption, an area $A_e = 0.4905$ m² at the exit plane of the nozzle, and an absolute pressure $p_e = 7.377 \times 10^4$ N/m² at the same plane. The atmospheric pressure p_0 at sea level has the standard value $101325 \approx 1.013 \times 10^5$ N/m².

In order to compute the value of v_e , we use the equation of thrust written above solved for v_e , as follows

$$\begin{aligned} v_e &= \frac{F - A_e(p_e - p_0)}{\dot{m}} = \frac{4.448 \times 10^5 - 0.4905 \times (0.7377 - 1.013) \times 10^5}{167.5} \\ &= 2736 \text{ m/s} \end{aligned}$$

Since the pressure p_e of the exhaust gas at the exit plane of the nozzle is smaller than the atmospheric pressure p_0 at sea level, then the nozzle of the rocket engine considered in the present example is too long for sea level conditions.

During the ascent of the rocket, the value of the atmospheric pressure decreases continuously. When the rocket reaches a certain altitude h^* above the sea level, the atmospheric pressure at that altitude and the exhaust gas pressure p_e at the exit plane of the nozzle have the same value (in the present case, this value is 7.377×10^4 N/m²), and therefore the value of the component $A_e(p_e - p_0)$ of the thrust becomes equal to zero. This event represents an ideal expansion of the gas flow. At an altitude h greater than h^* , the value of the atmospheric pressure p_0 becomes less than 7.377×10^4 N/m², and is equal to zero in space. When this happens, the value of the term $A_e p_0$, which appears on the right-hand side of the equation of thrust, is also equal to zero. The two equations which express the thrust F at sea level and the thrust F_s in space are respectively

$$F = \dot{m}v_e + A_e(p_e - p_0)$$

$$F_s = \dot{m}v_e + A_e p_e$$

By subtracting F from F_s and solving for F_s , there results

$$F_s = F + A_e p_0 = 4.448 \times 10^5 + 0.4905 \times 1.013 \times 10^5 = 4.945 \times 10^5 \text{ N}$$

The effective exhaust velocity at sea level results from the preceding equation

$$c = v_e + \frac{A_e(p_e - p_0)}{\dot{m}} = 2736 + \frac{0.4905 \times (0.7377 - 1.013) \times 10^5}{167.5} = 2655 \text{ m/s}$$

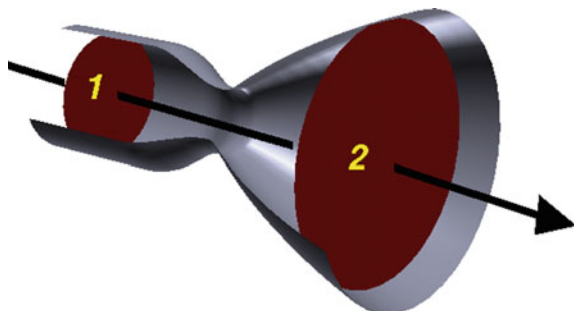
The effective exhaust velocity in space (where $p_0 = 0$) is

$$c_s = v_e + \frac{A_e p_e}{\dot{m}} = 2736 + \frac{0.4905 \times 0.7377 \times 10^5}{167.5} = 2952 \text{ m/s}$$

1.2 The Gas Flow Through the Combustion Chamber and the Nozzle

Under the seven hypotheses indicated in Sect. 1.1, it is possible to compute the exhaust gas velocity, v_e , at the exit plane of the nozzle as a function of the physical properties of the gas. Three of the four fundamental equations used for this purpose express the conservation of energy, mass, and momentum, and the fourth is the equation of state of perfect gases. They are shown below.

The energy equation (also known as the Bernoulli equation) states the principle of conservation of energy. In the hypotheses of Sect. 1.1, let us consider an adiabatic flow between two cross-sections (1 and 2) of a nozzle perpendicular to its axis of symmetry, as shown in the following figure, due to the courtesy of NASA [5].



The energy equation for an adiabatic flow between the two cross-sections shown above can be written as follows [6]

$$h_1 - h_2 = c_p(T_1 - T_2) = \frac{1}{2} \frac{v_2^2 - v_1^2}{J}$$

where J is the mechanical equivalent of heat ($J = 1$ because the SI is used in this book, that is, because heat is measured in joules), $h = u + p/\rho$ is the enthalpy per unit mass of the fluid, u is the internal energy per unit mass of the fluid, c_p is the specific heat of the fluid at constant pressure, and T is the temperature of the fluid. The enthalpy measures the total energy of a thermodynamic system, and includes the internal energy of the gas and the amount of energy required to make room for it by displacing its environment and establishing its density and its pressure.

The energy equation states that the energy per unit mass available for heat transfer, $h_1 - h_2$, is converted into kinetic energy per unit mass, $\frac{1}{2}(v_2^2 - v_1^2)$, of the flow. In other words, an amount of energy in form of heat possessed by the gas is used to increase the velocity of the flow. The term $c_p(T_1 - T_2)$ indicates the decrease in temperature resulting from the energy conversion. The specific heat at constant pressure, c_p , has been assumed constant, and depends on the composition of the gas resulting from the combustion. In particular, when the cross-section 1 is located at the exit of the combustion chamber (subscript c), as shown in the preceding figure, then there results $v_1 \approx 0$, $T_1 = (T_c)_{ns}$, $v_2 \equiv v$, and $T_2 \equiv T_i$. Therefore, for an isentropic flow ($p/\rho^\gamma = \text{constant}$), the energy equation can be written as follows

$$\begin{aligned} (T_c)_{ns} &= T_i \left(1 + \frac{\gamma - 1}{2} M_i^2 \right) \\ (p_c)_{ns} &= p_i \left(1 + \frac{\gamma - 1}{2} M_i^2 \right)^{\frac{1}{\gamma-1}} \\ (\rho_c)_{ns} &= \rho_i \left(1 + \frac{\gamma - 1}{2} M_i^2 \right)^{\frac{1}{\gamma-1}} \end{aligned}$$

where $M_i = v_i/a_i$ is the Mach number at the nozzle inlet, $\gamma \equiv c_p/c_v$ is the specific heat ratio of the gas, R is the specific constant of the gas, and $a_i = (\gamma RT_i)^{1/2}$ is the sonic velocity of the flow at the nozzle inlet.

The second of the four fundamental equations mentioned above states the principle of mass conservation. Since the flow is constant, then the rate \dot{m} at which a quantity of mass m passes through a cross-section A of the nozzle must be independent of the position of this cross-section along the axis of symmetry of the nozzle, that is,

$$\dot{m} = \rho A v = \text{constant}$$

where ρ , A , and v are respectively the local density of the gas, the local cross-sectional area of the nozzle, and the local velocity of the flow.

Since the mass flow rate through the nozzle must be constant in all sections of the nozzle, the continuity equation may also be written as follows

$$\rho A v = \rho_t A_t v_t$$

where the subscript t indicates the throat of the nozzle, where the Mach number is equal to unity. By using the equations written above, it is possible to express the area ratio between any cross-sectional area A_x (where $M = M_x$) and the throat cross-sectional area A_t (where $M_t = 1$) of the nozzle as follows [2]:

$$\left(\frac{A_x}{A_t}\right)^2 = \frac{1}{M_x^2} \left[\left(\frac{2}{\gamma + 1} \right) \left(1 + \frac{\gamma - 1}{2} M_x^2 \right) \right]^{\frac{\gamma+1}{\gamma-1}}$$

Let 1 and 2 be two cross-sections of the nozzle at two arbitrary points along its axis of symmetry. With reference to these sections, the equation of energy can be written as follows

$$h_1 - h_2 = \frac{1}{2} (v_2^2 - v_1^2)$$

The preceding equation, solved for v_2 , yields

$$v_2 = [2(h_1 - h_2) + v_1^2]^{\frac{1}{2}}$$

which can also be written as follows [6]:

$$v_2 = \left\{ \frac{2\gamma}{\gamma - 1} R T_1 \left[1 - \left(\frac{p_2}{p_1} \right)^{\frac{\gamma-1}{\gamma}} \right] + v_1^2 \right\}^{\frac{1}{2}}$$

By choosing the cross-section 2 as the exit plane of the nozzle (subscript e) and the cross-section 1 as the exit plane of the combustion chamber (subscript c), the second addend ($v_1^2 \equiv v_c^2$) within curly brackets becomes negligible in comparison with the first. Therefore, the velocity of the exhaust gas at the exit plane of the nozzle is expressible as follows

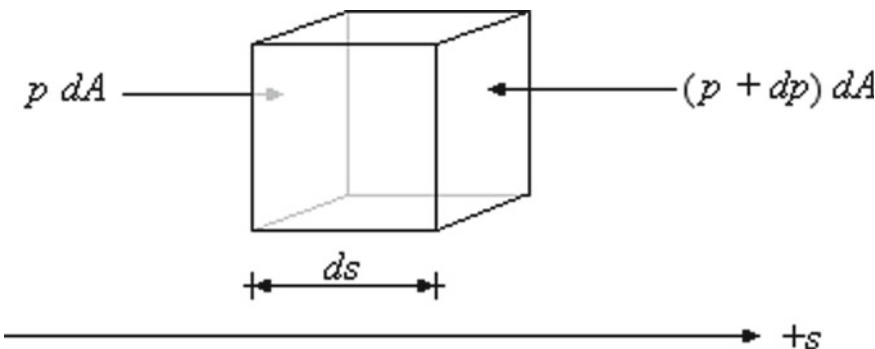
$$v_e = \left\{ \frac{2\gamma}{\gamma - 1} R T_c \left[1 - \left(\frac{p_e}{p_c} \right)^{\frac{\gamma-1}{\gamma}} \right] \right\}^{\frac{1}{2}}$$

This is because the cross-section of the combustion chamber is larger than that of the throat. Therefore, the flow velocity, v_c , at the exit plane of the combustion chamber can be neglected in the expression given above. In addition, the temperature, T_c , of the combustion chamber and of the nozzle inlet differs very little, in isentropic conditions, from the stagnation temperature.

The maximum theoretical value of the exhaust gas velocity, v_e , at the exit plane of the nozzle is reached when the pressure value, p_e , at the same plane is zero (infinite expansion). Setting $p_e = 0$ in the preceding equation yields

$$(v_e)_{MAX} = \left(\frac{2\gamma}{\gamma - 1} RT_c \right)^{\frac{1}{2}}$$

The third of the fundamental equations mentioned above expresses the principle of conservation of momentum in a steady one-dimensional flow. With reference to the following figure, let us consider an infinitesimal particle of gas moving along a streamline, s , in a steady, one-dimensional flow, that is, in a flow whose velocity, v , is independent of time ($dv/dt = 0$).



We consider here, of all forces which may act on the gaseous particle, only those due to pressure imbalances. Therefore, gravitational, magnetic, and viscous forces are neglected. By applying the second law of dynamics to the motion of the infinitesimal particle of gas along the streamline, the sum of the forces, $\sum F$, in the stream direction, s , is equal to the mass, m , of the particle multiplied by the rate of change, dv/dt , of its velocity, that is,

$$\sum F = m \frac{dv}{dt} = pdA - (p + dp)dA$$

Since the mass, m , of the infinitesimal particle is equal to its density, ρ , times the infinitesimal distance, ds , times the infinitesimal area, dA , then there results

$$m = \rho ds dA$$

In addition, since the velocity vector of the particle is always tangent to the streamline, then the rate of change of velocity with time is expressible as follows

$$\frac{dv}{dt} = \left(\frac{dv}{ds} \right) \left(\frac{ds}{dt} \right) = v \frac{dv}{ds}$$

By substituting the expressions of mass and acceleration in the equation written above, there results

$$pdA - (p + dp)dA = (\rho ds dA) \left(v \frac{dv}{ds} \right)$$

that is,

$$-dp = \rho v dv$$

which is the momentum equation. The minus sign in front of dp is due to the fact that the gas particle moves along the streamline, s , from a region of high pressure to a region of low pressure; therefore, when the velocity of the particle increases with s , then its pressure decreases. In other words, to each increase in the flow velocity of a particle there corresponds a decrease in its pressure. The preceding equation, also known as the Euler equation, is a particular case of the general Navier-Stokes equations [7]. Since the flow is not only steady but also isentropic ($p/\rho^\gamma = \text{constant}$), then the following equality holds

$$\frac{dp}{p} = \gamma \frac{d\rho}{\rho}$$

The two equations written above, combined together, yield

$$v dv = -\frac{dp}{\rho} = -\left(\frac{dp}{d\rho}\right)\left(\frac{d\rho}{\rho}\right) = -a^2 \frac{d\rho}{\rho}$$

where

$$a = \left(\frac{dp}{d\rho}\right)^{\frac{1}{2}}$$

is the velocity of sound in the flowing gas.

Since $M = v/a$ is the Mach number, then by multiplying and dividing the quantity on the left-hand side of the preceding equation by v there results

$$v^2 \frac{dv}{v} = -a^2 \frac{d\rho}{\rho}$$

that is,

$$M^2 \frac{dv}{v} = -\frac{d\rho}{\rho}$$

By combining the preceding equation with the equation ($\rho Av = \text{constant}$) which expresses the principle of mass conservation, there results

$$(1 - M^2) \frac{dv}{v} = \frac{dA}{A}$$

For subsonic flow ($M < 1$), a decrease in the cross-sectional area ($dA < 0$) of the nozzle causes the flow velocity to increase ($dv > 0$). This is what happens in the convergent portion of the nozzle, downstream of the combustion chamber, until the sonic condition ($M = 1$) is reached in the throat. By contrast, for supersonic flow, an increase in the cross-sectional area ($dA > 0$) of the nozzle causes the flow velocity to increase ($dv > 0$). This is what happens in the divergent portion of the nozzle, downstream of the throat. The equations written above (energy, continuity, momentum, and state) make it possible to express the propellant mass flow rate and the thrust in terms of the pressure of the fluid in the combustion chamber (subscript c) and the area of the nozzle throat (subscript t), as will be shown below. The energy equation for the combustion chamber (where $v_c \approx 0$) is

$$\frac{\rho_c}{\rho} = \left(1 + \frac{\gamma - 1}{2} M^2 \right)^{\frac{1}{\gamma-1}}$$

When M^2 is much smaller than unity, then the preceding equation yields $\rho \approx \rho_c$, and consequently

$$\frac{p_c}{p} = 1 + \frac{1}{2} M^2 = 1 + \frac{v^2}{2RT} = 1 + \frac{\rho v^2}{2p}$$

Hence

$$p_c = p + \frac{1}{2} \rho v^2$$

The mass flow rate per unit area is

$$\frac{\dot{m}}{A} = \rho v$$

Since $M = v/a$, $a = (\gamma RT)^{\frac{1}{2}}$, and $T_c/T = 1 + \frac{1}{2}(\gamma - 1)M^2$, then

$$v = M \left[\frac{\gamma RT_c}{1 + \frac{\gamma-1}{2} M^2} \right]^{\frac{1}{2}}$$

and therefore

$$\frac{\dot{m}}{A} = \rho v = \frac{p_c \gamma^{\frac{1}{2}} M}{(RT_c)^{\frac{1}{2}}} \left[\frac{1}{1 + \frac{\gamma-1}{2} M^2} \right]^{\frac{\gamma+1}{2(\gamma-1)}}$$

The preceding equation, written for the throat (where $A = A_t$ and $M = 1$), yields

$$\frac{\dot{m}}{A_t} = \frac{p_c \gamma^{\frac{1}{2}}}{(RT_c)^{\frac{1}{2}}} \left[\frac{2}{\gamma + 1} \right]^{\frac{\gamma+1}{2(\gamma-1)}}$$

that is,

$$\dot{m} = \Gamma(\gamma) \frac{A_t p_c}{(RT_c)^{\frac{1}{2}}}$$

where

$$\Gamma(\gamma) = \gamma^{\frac{1}{2}} \left(\frac{2}{\gamma + 1} \right)^{\frac{\gamma+1}{2(\gamma-1)}}$$

is the Vandenkerkhove function. By introducing the expressions of \dot{m}_n and v_e derived above in the equation of thrust

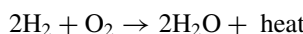
$$F = \dot{m} v_e + A_e (p_e - p_0)$$

it is possible to re-write this equation as follows [8]:

$$F = A_t p_c \left\{ \frac{2\gamma^2}{\gamma - 1} \left(\frac{2}{\gamma + 1} \right)^{\frac{\gamma+1}{\gamma-1}} \left[1 - \left(\frac{p_e}{p_c} \right)^{\frac{\gamma-1}{\gamma}} \right] \right\}^{\frac{1}{2}} + A_e (p_e - p_0)$$

which expresses the thrust in terms of the pressure of the fluid in the combustion chamber and of the area of the nozzle throat. In other words, when the pressure thrust is zero, which occurs when $p_e = p_0$, then the thrust is directly proportional to the throat area, A_t , and nearly directly proportional to the pressure, p_c , of the fluid within the combustion chamber.

The chemical reaction, which takes place in the combustion chamber when the fuel combines with the oxidiser, is an oxidation. When the fuel is hydrogen (H_2) and the oxidiser is oxygen (O_2), the product of the combustion is water (H_2O) in its gaseous state, due to of the high temperature generated when hydrogen burns in the presence of oxygen, according to the well-known reaction



This means that, in each second, two kilomoles of hydrogen (that is, $2 \times 2 \times 1 = 4$ kg of hydrogen) react with one kilomole of oxygen (that is, $2 \times 16 = 32$ kg of

oxygen) to form two kilomoles of water (that is, $2 \times (2 + 16) = 36$ kg of water). The corresponding stoichiometric mixture ratio (*o/f*) of the oxidiser (*o*) to the fuel (*f*) is

$$\frac{o}{f} \equiv \frac{\dot{m}_o}{\dot{m}_f} = \frac{32}{4} = 8$$

In other words, 8 kg of oxygen are necessary to burn 1 kg of hydrogen in 1 s. When used for rockets, hydrogen and oxygen are most often stored in their liquid state of aggregation, at very low temperatures (cryogenic propellants). This is because they take less space in the liquid state than in the gaseous state at normal temperature and pressure conditions. Hydrogen remains liquid without evaporating at atmospheric pressure (101325 N/m^2) at a temperature not higher than 20 K, and oxygen does the same at a temperature not higher than 90 K [9].

Another cryogenic fuel used for space propulsion is liquid methane (CH_4), which requires a storage at a temperature not higher than 111 K [10]. The related chemical reaction with liquid oxygen is [10]:



In each second, one kilomole of methane (that is, $12 + 4 \times 1 = 16$ kg of methane) reacts with two kilomoles of oxygen (that is, $2 \times 2 \times 16 = 64$ kg of oxygen) to form one kilomole of carbon dioxide (that is, $12 + 2 \times 16 = 44$ kg of carbon dioxide) and two kilomoles of water (that is, $2 \times (2 + 16) = 36$ kg of water). The corresponding stoichiometric mixture ratio (*o/f*) between the oxidiser (*o*) and the fuel (*f*) is

$$\frac{o}{f} \equiv \frac{\dot{m}_o}{\dot{m}_f} = \frac{64}{16} = 4$$

A cryogenic oxidiser which can be used either alone or in combination with liquid oxygen is liquid fluorine (F_2), which requires a storage at a temperature not higher than 85 K. Fluorine is extremely toxic and reacts violently with most substances [10]. Cryogenic propellants are difficult to store over long periods of time, due to the low temperatures required by them. Therefore, they are not used in military rockets, which must be taken in a state of readiness for launch over times of several months. In addition, liquid hydrogen requires a storage volume many times greater than that required by other fuels, because of its very low density (70.85 kg/m^3). On the other hand, the higher performance made available by cryogenic propellants makes them particularly attractive when constraints of storage and reaction time are not critical. For example, according to Aerojet Rocketdyne [11], the RS-25 engines aboard the Space Shuttle orbiter use liquid hydrogen and liquid oxygen and have a specific impulse in space (see Sect. 1.3) of 451 s. The RL10 engines on the Centaur, the US first liquid-hydrogen/liquid-oxygen rocket stage, have a specific impulse in space of 433 s [12]. The J-2 engines used on the Saturn V second and third stages and on the second stage of the Saturn 1B also burn the liquid-hydrogen/liquid-oxygen combination. They have a specific impulse in space of 424 s [13]. By comparison,

the liquid-oxygen/kerosene combination used in the cluster of five F-1 engines in the Saturn V first stage has a specific impulse in space of 304 s [14]. In a few words, liquid hydrogen, in comparison with other fuels (such as kerosene), yields more power per unit volume of storage.

When the fuel is a hydrocarbon (for example, kerosene), the oxidation reaction may be represented [10] as follows



In each second, two kilomoles of dodecane (that is, $2 \times 12 \times 12 + 2 \times 26 = 340$ kg of dodecane) react with twenty-five kilomoles of oxygen (that is, $25 \times 2 \times 16 = 800$ kg of oxygen) to form twenty-four kilomoles of carbon monoxide (that is, $24 \times (12 + 16) = 672$ kg of carbon monoxide) and twenty-six kilomoles of water (that is, $26 \times (2 + 16) = 468$ kg of water). The corresponding stoichiometric mixture ratio (*of*/*f*) between the oxidiser (*o*) and the fuel (*f*) is

$$\frac{o}{f} \equiv \frac{\dot{m}_o}{\dot{m}_f} = \frac{800}{340} \approx 2.35$$

It is to be noted that kerosene is a mixture of hydrocarbons. The chemical composition of kerosene depends on its source. It usually consists of about ten different hydrocarbons, each of them containing from 10 to 16 carbon atoms per molecule; the constituents include n-dodecane, alkyl benzenes, and naphthalene and its derivatives. Kerosene is usually represented by the single compound n-dodecane. In particular, RP-1 is a special type of highly-refined kerosene which conforms to Military Specification MIL-R-25576 and is used as a fuel for rocket engines [10]. For example, RP-1 is used in the first-stage boosters of the Delta and Atlas-Centaur rockets. It also powered the first stages of the Saturn 1B and Saturn V [10]. Hydrocarbon-based fuels do not pose the severe constraints of storage which are peculiar to cryogenic fuels. On the other hand, as has been shown above, the specific impulse yielded by them is considerably less than that made available by cryogenic fuels.

Another class of substances used for space propulsion includes the hypergolic propellants, that is, specific couples of fuels and oxidisers which ignite spontaneously and violently when one gets in touch with the other, without the need for any ignition source. Such propellants remain liquid at normal temperatures. These properties make them particularly suitable for propulsion and hydraulic power systems carried aboard spacecraft, and in particular for those which are meant to be used for orbital manoeuvring. On the other hand, hypergolic propellants are extremely toxic and/or corrosive and must be handled with the highest care. The most common fuels used in hypergolic propellants are hydrazine (N_2H_4), monomethyl hydrazine ($\text{CH}_3(\text{NH})\text{NH}_2$), unsymmetrical dimethyl hydrazine ($\text{H}_2\text{NN}(\text{CH}_3)_2$), and Aerozine 50, the last being an equal mixture of hydrazine and unsymmetrical dimethyl hydrazine.

According to Nufer [15], the oxidisers used in combination with the fuels named above are usually nitrogen tetroxide (N_2O_4) and various blends of nitrogen tetroxide

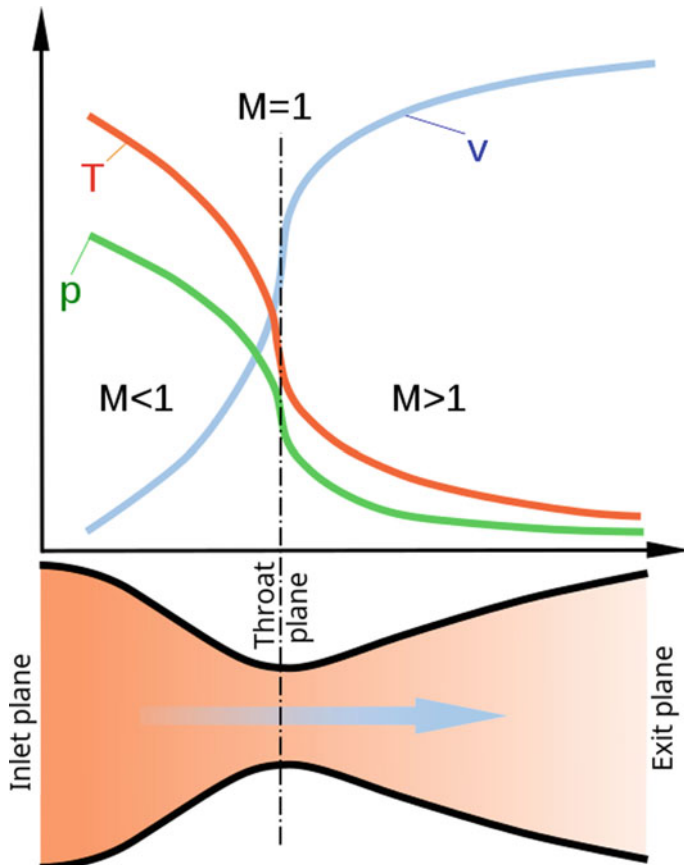
with nitric oxide (NO). Hybergolic propellants are used in the core liquid-propellant stages of the Titan family of launch vehicles, and on the Delta launcher. The Space Shuttle orbiter uses hybergolic propellants in its orbital manoeuvring subsystem for orbital insertion, main orbital manoeuvres, and de-orbit. It also uses hybergols in its reaction control system for attitude control [10]. The efficiency (in terms of specific impulse) reached in the Space Shuttle by combining monomethyl hydrazine with nitrogen tetroxide ranges from 260 to 280 s in the reaction control system, and to 313 s in the orbital manoeuvring subsystem, the higher efficiency of the latter being attributed by NASA [10] to higher expansion ratios in the nozzles and higher pressures in the combustion chambers.

In a liquid-propellant rocket, the fuel and the oxidiser are stored in two separate containers, and are sent to the combustion chamber by means of two separate systems of pipes, valves, and pumps. As the sequel will show, a liquid-propellant engine is more complex than a solid-propellant motor, but has several advantages over the latter. This is because the former offers the possibility of controlling the flow of propellant towards the combustion chamber, thereby permitting of throttling, stopping, or re-starting the engine.

The liquid propellants are introduced into the combustion chamber at the injecting plane with a small axial velocity, v_{inj} , which is assumed to be equal to zero in the present calculation. The combustion proceeds throughout the length of the combustion chamber, and is presumed to be complete at the inlet plane of the nozzle. The density of the gas decreases from one section of the combustion chamber to the other, due to the heat of combustion released between these sections. Since the mass flow rate remains constant, the gas accelerates toward the inlet section of the nozzle, and its pressure decreases.

In practice, the gas flow within the combustion chamber is not entirely isentropic, that is, the expansion process within the combustion chamber is neither fully irreversible nor fully adiabatic. The stagnation temperature, T_s , remains nearly constant, but the stagnation pressure, p_s , decreases. This causes an energy loss, which depends on the specific heat ratio, γ , of the gas, and also on the nozzle contraction area ratio, A_c/A_t , where A_c is the area of the cross-section of the combustion chamber, and A_t is the area of the cross-section of the throat. The energy loss occurs where the acceleration of gases is affected by expansion due to heat release, as is the case in the combustion chamber, rather than by a change of area, as is the case in the nozzle. The greater the acceleration of the gas flow given by the nozzle, the more efficient the process is.

The following figure, adapted from [16], shows the static pressure p , the temperature T , and the velocity v of a gas flowing from the inlet plane to the exit plane of a converging-diverging nozzle.



Neglecting the velocity of the gas flow at the injecting plane ($v_{inj} = 0$) and assuming the total pressure of the combustion chamber at the injecting plane $(p_c)_{inj}$ to be equal to the pressure of the injector p_{inj} (that is, assuming $(p_c)_{inj} = p_{inj}$), the total pressure ratio $(p_c)_{inj}/(p_c)_{ns}$ can be expressed as follows [4]:

$$\frac{(p_c)_{inj}}{(p_c)_{ns}} = \frac{1 + \gamma M_i^2}{\left(1 + \frac{\gamma-1}{2} M_i^2\right)^{\frac{\gamma}{\gamma-1}}}$$

where $(p_c)_{ns}$ is the total pressure in the combustion chamber at the nozzle inlet, M_i is the Mach number at the nozzle inlet plane, and $\gamma \equiv c_p/c_v$ is the specific heat ratio of the gas. The preceding equation results from the equation of energy written for the converging portion of nozzle, which goes from the inlet plane (where the Mach number of the gas flow is M_i) to the throat plane (where the Mach number of the gas flow is $M_t = 1$). In case of the static pressure ratio p_{inj}/p_i , the preceding equation can be simplified as follows

$$\frac{p_{inj}}{p_i} = 1 + \gamma M_i^2$$

In order to reduce the energy loss mentioned above, a small value (that is, considerably smaller than unity) is desirable for M_i . A typical value of 0.31 is indicated by Huzel and Huang [4] for a thrust chamber having a contraction area ratio, A_c/A_t , equal to 2 and a gas having a specific heat ratio, γ , equal to 1.2.

In this manner, a combustion chamber performs efficiently its function of converting a propellant into a gas of high temperature and pressure through combustion. This gas is then accelerated within the nozzle, as will be shown below. The nozzles used in rocket engines are of the converging-diverging (de Laval) type, as has been shown in Sect. 1.1. In a nozzle of this type, the area of the cross-section decreases and reaches its minimum value at the throat. Downstream of the throat, this area increases to the exit plane of the nozzle. The velocity of the gas flow increases, reaches the sonic value at the throat, and then increases further to supersonic values in the diverging portion of the nozzle.

As has been shown in Sect. 1.1, the gas flow through the nozzle is assumed to be an isentropic expansion. The total temperature and the total pressure of the gas are also assumed to remain constant throughout the nozzle. In these conditions, the pressure ratio, $p_t/(p_c)_{ns}$, between the static pressure at the throat and the total pressure in the combustion chamber at the nozzle inlet is the critical pressure ratio, which depends only on the specific heat ratio, γ , as follows

$$\frac{p_t}{(p_c)_{ns}} = \left(\frac{2}{\gamma + 1} \right)^{\frac{\gamma}{\gamma - 1}}$$

which results from the energy equation. The sonic velocity ($M_t = 1$) of the gas flow is reached in the throat independently of whether the value of the ambient pressure (p_0) at the exit plane of the nozzle be, or be not, less than the value of the gas pressure at the throat.

In case of an ideal expansion ($p_0 = p_e$), the pressure of the gas flowing in the diverging portion of the nozzle continues to decrease, as shown in the preceding figure. Otherwise, an increase in pressure occurs in the diverging portion of the nozzle. This increase in pressure may take place either by isentropic subsonic deceleration of the gas flow, or by non-isentropic discontinuities (called shock waves), or by a combination of both of these manners.

An example of shock waves in a gas flow is shown in the following figure, which is due to the courtesy of NASA [17].



The blue cones of light, which appear below the three main engines of the Space Shuttle, are known as shock (or Mach) diamonds. They are due to the formation of shock waves in the exhaust plume of the three main engines. The exhaust gas (H_2O) flowing from the engines reaches the speed of Mach 10, and the increase in pressure results in the shock diamonds.

Lower values of pressure than that of the ambient pressure (p_0) can be reached in the diverging portion of a nozzle, where the exhaust gas flows at supersonic speed. The higher ambient pressure cannot advance upstream of the nozzle, because the gas flows at supersonic speed. However, along the nozzle walls, due to the friction, there may be a boundary layer of gas moving at low speeds. Within this boundary layer, the gas moves at subsonic speeds, and therefore the ambient pressure can advance upstream for a distance. Therefore, the low-pressure central flow is forced away from the nozzle walls.

The following example shows a calculation relating to an ideal liquid-propellant rocket engine. The following data are known (from [4]): propellant mass flow rate in the combustion chamber $\dot{m}_{tc} = 163.6 \text{ kg/s}$, total pressure in the combustion chamber at the nozzle inlet $(p_c)_{ns} = p_i[1 + \frac{1}{2}(\gamma - 1)M_i^2]^{\gamma/\gamma-1} = 6.895 \times 10^6 \text{ N/m}^2$, total temperature of the combustion chamber $(T_c)_{ns} = T_i[1 + \frac{1}{2}(\gamma - 1)M_i^2] = 3633 \text{ K}$ (T_i and M_i being respectively the flow temperature and the Mach number at the nozzle inlet), molar mass of the combustion products $\mathcal{M} = 22.67 \text{ kg/kmol}$, specific heat ratio of the combusted gas $\gamma = 1.20$, and expansion area ratio of the nozzle $A_e/A_t = 12$. The Mach number M_{inj} at the injection plane is assumed to be equal to zero, and the Mach number M_i at the inlet plane of the nozzle is assumed to be equal to 0.4. In practice, the design values used for M_i range from 0.15 to 0.45. We want to compute the static pressures p_{inj} , p_t , p_x (at a cross-section x of area $A_x = 4A_t$), and p_e of the gas. As has been shown above, the total pressure ratio $(p_c)_{inj}/(p_c)_{ns}$ can be expressed by means of the following equation

$$\frac{(p_c)_{inj}}{(p_c)_{ns}} = \frac{1 + \gamma M_i^2}{\left(1 + \frac{\gamma-1}{2} M_i^2\right)^{\frac{\gamma}{\gamma-1}}}$$

In the present case, there results

$$\frac{(p_c)_{inj}}{(p_c)_{ns}} = \frac{1 + 1.20 \times 0.4^2}{\left(1 + \frac{1.20-1}{2} \times 0.4^2\right)^{\frac{1.20}{1.20-1}}} = 1.084$$

Since $(p_c)_{ns} = 6.895 \times 10^6 \text{ N/m}^2$, then the total pressure at the injection plane is

$$(p_c)_{inj} = 6.895 \times 10^6 \times 1.084 = 7.474 \times 10^6 \text{ N/m}^2$$

Since M_{inj} has been assumed to be equal to zero, then the static pressure at the injecting plane is

$$p_{inj} = (p_c)_{inj} = 7.474 \times 10^6 \text{ N/m}^2$$

At the inlet plane of the nozzle, the Mach number is assumed to be $M_i = 0.4$. Since the static pressure ratio p_{inj}/p_i is expressed by the preceding equation

$$\frac{p_{inj}}{p_i} = 1 + \gamma M_i^2$$

then the static pressure at the inlet plane of the nozzle is

$$p_i = \frac{p_{inj}}{1 + \gamma M_i^2} = \frac{7.474 \times 10^6}{1 + 1.20 \times 0.4^2} = 6.270 \times 10^6 \text{ N/m}^2$$

The static pressure of the gas at the throat results from the preceding equation

$$\frac{p_t}{(p_c)_{ns}} = \left(\frac{2}{\gamma + 1}\right)^{\frac{\gamma}{\gamma-1}}$$

In the present case, since $(p_c)_{ns} = 6.895 \times 10^6 \text{ N/m}^2$ and $\gamma = 1.20$, then

$$p_t = 6.895 \times 10^6 \times \left(\frac{2}{1.2 + 1}\right)^{\frac{1.2}{1.2-1}} = 3.892 \times 10^6 \text{ N/m}^2$$

The static pressure p_x at the cross-section x of area $A_x = 4A_t$ results from the following equation given in [4]:

$$\frac{A_x}{A_t} = \frac{\left(\frac{2}{\gamma+1}\right)^{\frac{1}{\gamma-1}} \left(\frac{(p_c)_{ns}}{p_x}\right)^{\frac{1}{\gamma}}}{\left\{ \frac{\gamma+1}{\gamma-1} \left[1 - \left(\frac{p_x}{(p_c)_{ns}} \right)^{\frac{\gamma-1}{\gamma}} \right] \right\}^{\frac{1}{2}}}$$

The unknown value of p_x can be computed numerically, as will be shown below. For convenience, we set $z = p_x/(p_c)_{ns}$, where z is an auxiliary variable.

Müller's method of root finding uses a quadratic interpolation and consequently requires the knowledge of three points in the vicinity of the unknown value of the root z to be found. This method is briefly described below.

Let z_2 and z_1 be the endpoints of an interval $z_2 \leq z \leq z_1$ containing the unknown value, z , of the root of a given equation. Let $f(z)$ be the function which is required to be equal to zero in the point z . The existence of at least one real root of $f(z) = 0$ lying between z_2 and z_1 is assured if $f_2 \equiv f(z_2)$ and $f_1 \equiv f(z_1)$ have opposite signs. Following Gerald and Wheatley [18], the computation is performed as follows:

- take a third point z_0 placed between z_2 and z_1 and compute $f_0 \equiv f(z_0)$;
- set $h_1 = z_1 - z_0$, $h_2 = z_0 - z_2$, and $k = h_2/h_1$;
- compute the following three coefficients

$$A = \frac{kf_1 - f_0(1+k) + f_2}{kh_1^2(1+k)}$$

$$B = \frac{f_1 - f_0 - Ah_1^2}{h_1}$$

$$C = f_0$$

of the interpolating parabola $f(z) = A(z - z_0)^2 + B(z - z_0) + C$;

- compute the estimated root of $f(z) = 0$ as follows

$$z = z_0 - \frac{2C}{B \pm (B^2 - 4AC)^{\frac{1}{2}}}$$

where the sign plus or the sign minus is chosen so that the denominator should have the maximum absolute value (that is, if $B > 0$, choose plus; if $B < 0$, choose minus; if $B = 0$, choose either) and compute $f \equiv f(z)$;

- check the computed value of z to determine which set of three points should be used in the next iteration (if z is greater than z_0 , take z_0, z_1 , and the root z for the next iteration; if z is less than z_0 , take z_0, z_2 , and the root z for the next iteration); and

- reset the subscripts 0, 1, and 2 so that z_0 should be placed between z_2 and z_1 , and repeat the cycle while the computed value of z does not satisfy the condition $f(z) = 0$ to some acceptable degree of tolerance.

In the present case ($A_x/A_t = 4$ and $\gamma = 1.2$), we define a function $f(z)$ such that

$$f(z) \equiv 4^2 - \frac{\left(\frac{2}{1.2+1}\right)^{\frac{2}{1.2-1}} \left(\frac{1}{z}\right)^{\frac{2}{1.2}}}{\left(\frac{1.2+1}{1.2-1}\right) \left(1 - z^{\frac{1.2-1}{1.2}}\right)}$$

Since $p_t = 3.892 \times 10^6 \text{ N/m}^2$ and $(p_c)_{ns} = 6.895 \times 10^6 \text{ N/m}^2$, then the unknown value of the pressure ratio $z \equiv p_x/(p_c)_{ns}$ is less than $p_t/(p_c)_{ns} = 0.5645$. Therefore, we search the unknown value of z by trying values which are progressively smaller than 0.5645. By so doing, we find the following interval

$$0.04 \leq z \leq 0.05$$

in which the function $f(z)$ changes sign, as will be shown below. At the upper end ($z_1 = 0.05$) of the interval indicated above, there results

$$f_1 \equiv f(0.05) = 2.859$$

At the lower end ($z_2 = 0.04$) of the same interval, there results

$$f_2 \equiv f(0.04) = -2.044$$

Since the product $f_1 f_2$ is less than zero, then the function $f(z)$ defined above has at least one zero in the interval $0.04 \leq z \leq 0.05$. We choose arbitrarily another point $z_0 = 0.045$ between 0.04 and 0.05, and compute

$$f_0 \equiv f(0.045) = 0.7464$$

Starting from the values f_2, f_0 , and f_1 obtained above, we compute

$$\begin{aligned} h_1 &= z_1 - z_0 = 0.050 - 0.045 = 0.005 \\ h_2 &= z_0 - z_2 = 0.045 - 0.040 = 0.005 \\ k &= h_2/h_1 = 0.005/0.005 = 1 \end{aligned}$$

and then the three coefficients (A , B , and C) of the quadratic polynomial which interpolates the three points (z_2, f_2) , (z_0, f_0) , and (z_1, f_1) , as follows

$$\begin{aligned} A &= \frac{kf_1 - f_0(1+k) + f_2}{kh_1^2(1+k)} = \frac{1 \times 2.859 - 0.7464 \times (1+1) - 2.044}{1 \times 0.005^2 \times (1+1)} \\ &= -1.355 \times 10^4 \end{aligned}$$

$$B = \frac{f_1 - f_0 - Ah_1^2}{h_1} = \frac{2.859 - 0.7464 + 1.355 \times 10^4 \times 0.005^2}{0.005} = 490.3$$

$$C = f_0 = 0.7464$$

The estimated root z of $f(z) = 0$ is computed as follows

$$\begin{aligned} z &= z_0 - \frac{2C}{B + (B^2 - 4AC)^{\frac{1}{2}}} \\ &= 0.045 - \frac{2 \times 0.7404}{490.3 + (490.3^2 - 4 \times 1.355 \times 10^4 \times 0.7464)^{\frac{1}{2}}} = 0.04354 \end{aligned}$$

By applying repeatedly Müller's method, we find, with four significant figures, $z = 0.04351$. Therefore, remembering the definition of the auxiliary variable z , we have

$$p_x = z(p_c)_{ns} = 0.04351 \times 6.895 \times 10^6 = 3.0 \times 10^5 \text{ N/m}^2$$

The static pressure p_e at the exit plane of the nozzle such that $A_e = 12A_t$, results from the same equation given above

$$\frac{A_x}{A_t} = \frac{\left(\frac{2}{\gamma+1}\right)^{\frac{1}{\gamma-1}} \left(\frac{(p_c)_{ns}}{p_x}\right)^{\frac{1}{\gamma}}}{\left\{\frac{\gamma+1}{\gamma-1} \left[1 - \left(\frac{p_x}{(p_c)_{ns}}\right)^{\frac{\gamma-1}{\gamma}}\right]\right\}^{\frac{1}{2}}}$$

In order to compute p_e , the preceding equation is re-written by replacing p_x with p_e , and A_x with A_e , as follows

$$\frac{A_e}{A_t} = \frac{\left(\frac{2}{\gamma+1}\right)^{\frac{1}{\gamma-1}} \left(\frac{(p_c)_{ns}}{p_e}\right)^{\frac{1}{\gamma}}}{\left\{\frac{\gamma+1}{\gamma-1} \left[1 - \left(\frac{p_e}{(p_c)_{ns}}\right)^{\frac{\gamma-1}{\gamma}}\right]\right\}^{\frac{1}{2}}}$$

In the present case ($A_e/A_t = 12$ and $\gamma = 1.2$), we define a function $f(z)$ such that

$$f(z) \equiv 12^2 - \frac{\left(\frac{2}{1.2+1}\right)^{\frac{2}{1.2-1}} \left(\frac{1}{z}\right)^{\frac{2}{1.2}}}{\left(\frac{1.2+1}{1.2-1}\right) \left(1 - z^{\frac{1.2-1}{1.2}}\right)}$$

where the auxiliary variable z is defined as follows $z \equiv p_e/(p_c)_{ns}$.

By applying repeatedly Müller's method, we find, with four significant figures, $z = 0.009859$. Therefore, according to the definition of z , we have

$$p_e = z(p_c)_{ns} = 0.009859 \times 6.895 \times 10^6 = 6.798 \times 10^4 \text{ N/m}^2$$

Now, we want to compute the flow temperatures at the injection plane (T_{inj}), at the nozzle inlet (T_i), at the throat (T_t), at the cross-section x defined above (T_x), and at the exit plane of the nozzle (T_e).

Since the Mach number at the injection plane, M_{inj} , has been assumed to be equal to zero, then the flow temperature at the injection plane of the nozzle, T_{inj} , is equal to the total temperature of the combustion chamber ($T_c)_{ns} = 3633 \text{ K}$.

By definition, the following equation holds between total temperature of the combustion chamber ($T_c)_{ns}$ and the temperature at the nozzle inlet T_i :

$$T_i = \frac{(T_c)_{ns}}{1 + \frac{1}{2}(\gamma - 1)M_i^2}$$

Since the Mach number of the flow at the inlet plane of the nozzle, M_i , has been assumed equal to 0.4, then there results

$$T_i = \frac{3633}{1 + 0.5 \times (1.2 - 1) \times 0.4^2} = 3576 \text{ K}$$

In case of an isentropic flow ($p/\rho^\gamma = \text{constant}$), the energy equation, written for any two points 1 and 2 placed along the axis of symmetry of the nozzle, yields

$$\frac{T_1}{T_2} = \left(\frac{p_1}{p_2} \right)^{\frac{\gamma-1}{\gamma}}$$

Since $(T_c)_{ns} = 3633 \text{ K}$ and $(p_c)_{ns} = 6.895 \times 10^6 \text{ N/m}^2$ are respectively the total temperature and the total pressure of the combustion chamber at the inlet plane of the nozzle, then the preceding equation, written for respectively the throat, the section x , and the exit plane of the nozzle, yields

$$T_t = (T_c)_{ns} \left[\frac{p_t}{(p_c)_{ns}} \right]^{\frac{\gamma-1}{\gamma}} = 3633 \times \left(\frac{3.892 \times 10^6}{6.895 \times 10^6} \right)^{\frac{1.2-1}{1.2}} = 3303 \text{ K}$$

$$T_x = (T_c)_{ns} \left[\frac{p_x}{(p_c)_{ns}} \right]^{\frac{\gamma-1}{\gamma}} = 3633 \times \left(\frac{3.0 \times 10^5}{6.895 \times 10^6} \right)^{\frac{1.2-1}{1.2}} = 2155 \text{ K}$$

$$T_e = (T_c)_{ns} \left[\frac{p_e}{(p_c)_{ns}} \right]^{\frac{\gamma-1}{\gamma}} = 3633 \times \left(\frac{6.798 \times 10^4}{6.895 \times 10^6} \right)^{\frac{1.2-1}{1.2}} = 1682 \text{ K}$$

Now, we want to compute the densities of gas at the injection plane (ρ_{inj}), at the nozzle inlet (ρ_i), at the throat (ρ_t), at the cross-section x defined above (ρ_x), and at the exit plane of the nozzle (ρ_e). The law of perfect gases states that

$$p = \rho RT$$

Since the molar mass of the combustion products is $\mathcal{M} = 22.67 \text{ kg/kmol}$, and the universal gas constant is $R^* = 8314.460 \text{ N m kmol}^{-1} \text{ K}^{-1}$, then the densities of gas at the sections of interest are

$$\rho_{inj} = \frac{\mathcal{M} p_{inj}}{R^* T_{inj}} = \frac{22.67 \times 7.474 \times 10^6}{8314.46 \times 3633} = 5.609 \text{ kg/m}^3$$

$$\rho_i = \frac{\mathcal{M} p_i}{R^* T_i} = \frac{22.67 \times 6.270 \times 10^6}{8314.46 \times 3576} = 4.781 \text{ kg/m}^3$$

$$\rho_t = \frac{\mathcal{M} p_t}{R^* T_t} = \frac{22.67 \times 3.892 \times 10^6}{8314.46 \times 3303} = 3.213 \text{ kg/m}^3$$

$$\rho_x = \frac{\mathcal{M} p_x}{R^* T_x} = \frac{22.67 \times 3.0 \times 10^5}{8314.46 \times 2155} = 0.3796 \text{ kg/m}^3$$

$$\rho_e = \frac{\mathcal{M} p_e}{R^* T_e} = \frac{22.67 \times 6.798 \times 10^4}{8314.46 \times 1682} = 0.1102 \text{ kg/m}^3$$

We also want to compute the flow velocities at the nozzle inlet (v_i), at the throat (v_t), at the cross-section x defined above (v_x), and at the exit plane of the nozzle (v_e). The sonic velocity at the nozzle inlet is expressed by the following equation

$$a_i = (\gamma R T_i)^{\frac{1}{2}}$$

The flow velocity at the nozzle inlet, where $M_i = 0.4$ and $T_i = 3576 \text{ K}$, is

$$v_i = M_i a_i = 0.4 \times (1.2 \times 366.8 \times 3576)^{\frac{1}{2}} = 501.8 \text{ m/s}$$

The flow velocity at the throat, where $M_t = 1$ and $T_t = 3303 \text{ K}$, is

$$v_t = M_t a_t = 1 \times (1.2 \times 366.8 \times 3303)^{\frac{1}{2}} = 1206 \text{ m/s}$$

The flow velocity at the cross-section x , where $A_x/A_t = 4$ and $p_x = 3.0 \times 10^5 \text{ N/m}^2$, is expressed by the following equation of [4]:

$$v_x = \left\{ \frac{2\gamma}{\gamma - 1} R(T_c)_{ns} \left[1 - \left(\frac{p_x}{(p_c)_{ns}} \right)^{\frac{\gamma-1}{\gamma}} \right] \right\}^{\frac{1}{2}}$$

where $(T_c)_{ns} = 3633 \text{ K}$ and $(p_c)_{ns} = 6.895 \times 10^6 \text{ N/m}^2$ are respectively the total temperature and the total pressure of the combustion chamber at the nozzle inlet.

After substituting these values into the preceding equation, there results

$$v_x = \left\{ \frac{2 \times 1.2}{1.2 - 1} \times 366.8 \times 3633 \times \left[1 - \left(\frac{3.0 \times 10^5}{6.895 \times 10^6} \right)^{\frac{1.2-1}{1.2}} \right] \right\}^{\frac{1}{2}} = 2551 \text{ m/s}$$

Likewise, the flow velocity at the exit plane of the nozzle, where the static pressure $p_e = 6.798 \times 10^4 \text{ N/m}^2$, is expressed by the following equation

$$v_e = \left\{ \frac{2\gamma}{\gamma-1} R(T_c)_{ns} \left[1 - \left(\frac{p_e}{(p_c)_{ns}} \right)^{\frac{\gamma-1}{\gamma}} \right] \right\}^{\frac{1}{2}}$$

After substituting this value into the preceding equation, there results

$$v_e = \left\{ \frac{2 \times 1.2}{1.2 - 1} \times 366.8 \times 3633 \times \left[1 - \left(\frac{6.798 \times 10^4}{6.895 \times 10^6} \right)^{\frac{1.2-1}{1.2}} \right] \right\}^{\frac{1}{2}} = 2930 \text{ m/s}$$

Now, we want to compute the Mach numbers of the gas flow at the cross-section x (M_x) and at the exit plane of the nozzle (M_e).

The sonic velocity of the gas flow at the cross-section x of the nozzle is

$$a_x = (\gamma R T_x)^{\frac{1}{2}} = (1.2 \times 366.8 \times 2155)^{\frac{1}{2}} = 973.8 \text{ m/s}$$

Therefore, the Mach number of the gas flow at the cross-section x of the nozzle is

$$M_x = \frac{v_x}{a_x} = \frac{2551}{973.8} = 2.619$$

Likewise, the sonic velocity of the gas flow at the exit plane of the nozzle is

$$a_e = (\gamma R T_e)^{\frac{1}{2}} = (1.2 \times 366.8 \times 1682)^{\frac{1}{2}} = 860.5 \text{ m/s}$$

Therefore, the Mach number of the gas flow at the exit plane of the nozzle is

$$M_e = \frac{v_e}{a_e} = \frac{2930}{860.5} = 3.405$$

Finally, we want to compute the areas of the cross-sections of the gas flow at the inlet plane of the nozzle (A_i), at the combustion chamber (A_c), at the throat (A_t), at the section x of the nozzle (A_x), and at the exit plane of the nozzle (A_e).

As has been shown in Sect. 1.2, owing to the principle of mass conservation, the rate at which a quantity of mass passes through a cross-section of the nozzle is independent of the position of this cross-section along the axis of symmetry of the nozzle, that is,

$$\dot{m} = \rho A v = \text{constant}$$

In the present case, we know the mass flow rate of the propellant in the combustion chamber to be $\dot{m}_{tc} = 163.6 \text{ kg/s}$, which value is also constant at any cross-section of the nozzle. Therefore, the areas of the cross-sections of the gas flow at the inlet plane of the nozzle (A_i), at the combustion chamber (A_c), and at the throat (A_t) are

$$A_i = \frac{\dot{m}_{tc}}{v_i \rho_i} = \frac{163.6}{501.8 \times 4.781} = 0.06819 \text{ m}^2$$

$$A_c = A_i = 0.06819 \text{ m}^2$$

$$A_t = \frac{\dot{m}_{tc}}{v_t \rho_t} = \frac{163.6}{1206 \times 3.213} = 0.04222 \text{ m}^2$$

By definition, the areas of the cross-sections of the gas flow at the section x of the nozzle (A_x) and at the exit plane of the nozzle (A_e) are

$$A_x = 4A_t = 4 \times 0.04222 = 0.1689 \text{ m}^2$$

$$A_e = 12A_t = 12 \times 0.04222 = 0.5066 \text{ m}^2$$

1.3 Performance Indicators

The performance of a rocket engine, independently of whether its propellant may be liquid or solid, is measured by a quantity, which is called specific impulse (I_s). This quantity is defined as the ratio of the thrust F (N) imparted to the rocket to the weight flow rate \dot{W} (N/s) of the propellant on the surface of the Earth and at the sea level, as follows

$$I_s = \frac{F}{\dot{W}} = \frac{F}{\dot{m} g_0}$$

This quantity is measured in seconds. The following table, due to the courtesy of the Government of the United States ([19], page 44), gives the specific impulse of some typical chemical propellants for rockets.

In case of liquid-propellant engines, it is important to specify whether a given specific impulse takes account of the thrust chamber only, in which case it is denoted here by $(I_s)_{tc}$, or of the overall engine, in which case it is denoted here by $(I_s)_{oa}$. This distinction is necessary, because, when a rocket engine is fed by turbo-pumps, then its specific impulse relating to the overall engine may include the power required by

its turbines, by its Vernier rockets (by the way, a Vernier rocket is a small additional engine, which is placed at the bottom of the main rocket for the purpose of generating a control torque), and by its devices used for attitude control. The propellant necessary to feed the devices indicated above may come from one or more tanks carried on board a rocket. The amount by which $(I_s)_{tc}$ is greater than $(I_s)_{oa}$ is usually 1 or 2%.

TABLE 1.—*Specific impulse of some typical chemical propellants*¹

Propellant combinations:	Isp range (sec)
Monopropellants (liquid):	
Low-energy monopropellants.....	160 to 190.
Hydrazine	
Ethylene oxide	
Hydrogen peroxide	
High-energy monopropellants.....	
Nitromethane.....	190 to 230.
Bipropellants (liquid):	
Low-energy bipropellants.....	200 to 230.
Perchloryl fluoride—Available fuel	
Analine—Acid	
JP-4—Acid	
Hydrogen peroxide—JP-4	
Medium-energy bipropellants.....	230 to 260.
Hydrazine—Acid	
Ammonia—Nitrogen tetroxide	
High-energy bipropellants.....	250 to 270.
Liquid oxygen—JP-4	
Liquid oxygen—Alcohol	
Hydrazine—Chlorine trifluoride	
Very high-energy bipropellants.....	270 to 330.
Liquid oxygen and fluorine—JP-4	
Liquid oxygen and ozone—JP-4	
Liquid oxygen—Hydrazine	
Super high-energy bipropellants.....	300 to 385.
Fluorine—Hydrogen	
Fluorine—Ammonia	
Ozone—Hydrogen	
Fluorine—Diborane	
Oxidizer-binder combinations (solid):	
Potassium perchlorate:	
Thiokol or asphalt.....	170 to 210.
Ammonium perchlorate:	
Thiokol.....	170 to 210.
Rubber.....	170 to 210.
Polyurethane.....	210 to 250.
Nitropolymer.....	210 to 250.
Ammonium nitrate:	
Polyester.....	170 to 210.
Rubber.....	170 to 210.
Nitropolymer.....	210 to 250.
Double base.....	170 to 250.
Boron metal components and oxidant.....	200 to 250.
Lithium metal components and oxidant.....	200 to 250.
Aluminum metal components and oxidant.....	200 to 250.
Magnesium metal components and oxidant.....	200 to 250.
Perfluoro-type propellants.....	250 and above.

¹ Some Considerations Pertaining to Space Navigation, Aerojet-General Corp., Special Rept. No. 1450, May 1958.

Another performance indicator is the propellant mass fraction, R_p , of the whole vehicle which is propelled by a rocket engine. The propellant mass fraction is defined as the ratio of the mass of the usable propellant (m_p) to the initial mass of the rocket (m_0), as follows

$$R_p = \frac{m_p}{m_0}$$

where the initial mass of the rocket (m_0) includes the masses due to the engine at burnout, the structure, the guidance system, the propellant, and the payload.

Let $\dot{m}_e > 0$ be the rate at which the exhaust gas flows through the exit plane of the nozzle. Due to this flow, the mass m of the rocket decreases in time at the rate dm/dt . According to the principle of mass conservation, this decrease in mass must be equal to the exhaust gas flowing through the nozzle, as follows

$$\frac{dm}{dt} = -\dot{m}_e$$

Assuming $\dot{m}_e = \text{constant}$, the mass m of the rocket decreases in time as follows

$$m = m_0 - \dot{m}_e t$$

Let m and v be respectively the total mass and the velocity of the rocket with respect to the Earth at a given time t . At the same time t , the linear momentum of the rocket is mv . After an infinitesimal interval of time dt , due to the flow of propellant, the mass m of the rocket decreases by dm , and the velocity v of the rocket increases by dv . This is because a positive mass $-dm$ has been expelled from the rocket at a velocity $-v_e$ (with respect to the rocket) and $v - v_e$ (with respect to the Earth). Therefore, at the time $t + dt$, the mass of the rocket becomes $m + dm$ (with $dm < 0$), and its velocity becomes $v + dv$ (with $dv > 0$).

The total linear momentum of the system (comprising the rocket and the exhaust gas) at the time $t + dt$ results from the linear momentum due to the rocket plus the linear momentum due to the exhaust gas, as follows

$$(m + dm)(v + dv) + (-dm)(v - v_e)$$

The principle of conservation of linear momentum states that the linear momentum of the system (gas and rocket) at the time t is equal to the linear momentum of the system at the time $t + dt$, as follows

$$mv = (m + dm)(v + dv) + (-dm)(v - v_e)$$

This is because the acceleration of the ejected mass of gas and the corresponding reaction (thrust) acting on the rocket (which are two forces equal in magnitude

and oppositely directed) are the sole forces considered as acting on the system. Aerodynamic forces (lift and drag) and gravitational attraction are neglected.

After executing the operations on the right-hand side of the preceding equation, neglecting the second-order differential $dm \, dv$, and cancelling the two terms mv , there results

$$0 = mdv + v_e dm$$

which, solved for dv , yields

$$dv = -v_e \frac{dm}{m}$$

The preceding differential equation, integrated over the time interval going from $t = 0$ to the time of burnout t_{bo} , yields

$$\Delta v = -v_e \ln\left(\frac{m_{bo}}{m_0}\right) = v_e \ln\left(\frac{m_0}{m_{bo}}\right)$$

where $m_{bo} = m_0 - m_p$ is the mass of the rocket at burnout, m_0 is the initial mass of the rocket, and m_p is the mass of propellant. The preceding equation was derived in 1903 by the Russian scientist Konstantin Eduardovich Tsiolkovsky, and is known as the rocket equation.

In the ideal case, in which the ambient pressure p_0 is equal to the pressure p_e of the exhaust gas at the exit plane of the nozzle, the equation of thrust

$$F = \dot{m}v_e + A_e(p_e - p_0)$$

reduces to

$$F = \dot{m}v_e$$

Remembering the definition of specific impulse

$$I_s = \frac{F}{\dot{W}} = \frac{F}{\dot{m}g_0}$$

and substituting $F = \dot{m}v_e$ into the preceding equation, the equation of rocket may also be written as follows

$$\Delta v = -I_s g_0 \ln\left(\frac{m_{bo}}{m_0}\right) = I_s g_0 \ln\left(\frac{m_0}{m_{bo}}\right)$$

In addition, since $m_{bo} = m_0 - m_p$, and $R_p = m_p/m_0$, then the rocket equation may also be written as follows

$$\Delta v = I_s g_0 \ln\left(\frac{m_0}{m_0 - m_p}\right) = I_s g_0 \ln\left(\frac{1}{1 - R_p}\right)$$

As has been shown above, the preceding equation holds in the ideal case, in which gravitational and aerodynamic forces are neglected. When these forces and the losses due to power requirements are taken into account, the preceding equation may be written as follows

$$\Delta v = C_{vc}(I_s)_{oa} g_0 \ln\left(\frac{1}{1 - R_p}\right)$$

where C_{vc} is a coefficient which takes account of the gravitational and aerodynamic forces, and $(I_s)_{oa}$ is the specific impulse of the overall engine.

In particular, when the initial velocity v_0 is equal to zero and the final velocity is the velocity of the rocket at burnout v_{bo} , then the preceding equation may be written as follows

$$v_{bo} = C_{vc}(I_s)_{oa} g_0 \ln\left(\frac{1}{1 - R_p}\right)$$

The performance of a thrust chamber only is measured by the corresponding specific impulse $(I_s)_{tc}$. This performance depends on the propellant (fuel and oxidiser) combination, the combustion efficiency in the combustion chamber, and the expansion of the exhaust gas in the nozzle. When the thrust and the weight flow rate of the thrust chamber are known for a given rocket engine, then the specific impulse relating to the thrust chamber can be determined as follows

$$(I_s)_{tc} = \frac{F}{\dot{W}_{tc}}$$

As an option, when we know the effective exhaust velocity (c), defined in Sect. 1.1, then the specific impulse relating to the thrust chamber can be determined as follows

$$(I_s)_{tc} = \frac{c}{g_0}$$

The effective exhaust velocity (c) may also be defined as the product of two quantities, namely c^* and C_F , as follows

$$c = c^* C_F$$

where c^* is the characteristic velocity, which depends on the combustion performance of the propellant, and C_F is a dimensionless quantity, called the thrust coefficient, which measures the performance of the gas expansion through the nozzle. By using this definition of c , the specific impulse relating to the thrust chamber can be determined as follows

$$(I_s)_{tc} = \frac{c^* C_F}{g_0}$$

Of the performance indicators defined above, the specific impulse (I_s) and the propellant mass fraction (R_p) are of great importance to the designer of a rocket vehicle as a whole. On the other hand, the characteristic velocity (c^*) and the thrust coefficient (C_F) are of great importance to the designer of a rocket engine, as will be shown below.

The characteristic velocity (c^*) of a rocket engine, in which the sonic velocity of the gas flow is reached at the throat, measures the energy possessed by the propellant and the quality level characterising the injector and the combustion chamber. It may be expressed by the following equation [4]:

$$c^* = \frac{(p_c)_{ns} A_t}{\dot{m}_{tc}} = \frac{(p_c)_{ns} A_t g_0}{\dot{W}_{tc}}$$

where $(p_c)_{ns} = p_i [1 + \frac{1}{2}(\gamma - 1)M_i^2]^{\gamma/(\gamma-1)}$ is the total pressure at the nozzle inlet, p_i is the static pressure at the nozzle inlet, $\gamma \equiv c_p/c_v$ is the specific heat ratio of the combusted gas, M_i is the Mach number at the nozzle inlet, A_t is the area of the cross-section at the throat, \dot{m}_{tc} and \dot{W}_{tc} are respectively the mass flow rate and the weight flow rate of the propellant at the thrust chamber, and $g_0 = 9.80665 \text{ m/s}^2$ is the acceleration of gravity at sea level. This equation indicates the mass or the weight flow rate of propellant which must be burned to maintain the required total pressure ($p_c)_{ns}$ at the nozzle inlet. A smaller value of propellant consumption \dot{m}_{tc} or \dot{W}_{tc} corresponds to a higher value of c^* .

Another expression of the characteristic velocity c^* is given in [4] as follows

$$c^* = \frac{[\gamma R(T_c)_{ns}]^{\frac{1}{2}}}{\gamma \left[\left(\frac{2}{\gamma+1} \right)^{\frac{\gamma+1}{\gamma-1}} \right]^{\frac{1}{2}}}$$

where $(T_c)_{ns} = T_i [1 + \frac{1}{2}(\gamma - 1)M_i^2]$ is the total temperature of the combustion chamber at the nozzle inlet, M_i is the Mach number at the nozzle inlet, $\gamma \equiv c_p/c_v$ is the specific heat ratio of the combusted gas, and R is the constant of the specific gas (that is, the universal gas constant $R^* = 8314.460 \text{ N m kmol}^{-1} \text{ K}^{-1}$ divided by the average molar mass \mathcal{M} of the combusted gas). The preceding equation shows that the characteristic velocity c^* depends on the properties of the combusted gas at the nozzle inlet, such properties being the specific heat ratio γ , the constant R of the specific gas, and the total temperature of the combustion chamber at the nozzle inlet $(T_c)_{ns}$.

The thrust coefficient C_F depends on the expansion of the exhaust gas and also on the design of the nozzle. By combining the three following equations derived above

$$(I_s)_{tc} = \frac{F}{\dot{W}_{tc}}$$

$$(I_s)_{tc} = \frac{c^* C_F}{g_0}$$

$$c^* = \frac{(p_c)_{ns} A_t g_0}{\dot{W}_{tc}}$$

the thrust coefficient can be expressed as follows

$$C_F = \frac{F}{A_t (p_c)_{ns}}$$

The thrust coefficient, put in this form, is the ratio of the actual thrust F acting on the rocket to the force $A_t (p_c)_{ns}$ which would act on the rocket if there were no expansion of the exhaust gas downstream of the throat, that is, if the total pressure on the combustion chamber acted only on the area of the throat.

The following equation, given in [4], expresses the theoretical value of the thrust coefficient at any altitude:

$$C_F = \left\{ \frac{2\gamma^2}{\gamma - 1} \left(\frac{2}{\gamma + 1} \right)^{\frac{\gamma+1}{\gamma-1}} \left[1 - \left(\frac{p_e}{(p_c)_{ns}} \right)^{\frac{\gamma-1}{\gamma}} \right] \right\}^{\frac{1}{2}} + \frac{A_e}{A_t} \left[\frac{p_e - p_0}{(p_c)_{ns}} \right]$$

where $\gamma \equiv c_p/c_v$ is the specific heat ratio of the combusted gas, p_e is the pressure of the exhaust gas at the exit plane of the nozzle, $(p_c)_{ns}$ is the total pressure in the combustion chamber at the nozzle inlet, p_0 is the ambient pressure, and A_e/A_t is the ratio of the area of the cross-section at the exit plane of the nozzle to the area of the cross-section at the throat. As has been shown in Sect. 1.1, when the ambient pressure increases from zero (in space) to $p_0 > 0$, then the thrust generated by a rocket engine decreases from F_s (in space) to F by an amount $A_e p_0$. Such is also the case with the thrust coefficient of a rocket engine, which decreases from $(C_F)_s$ (in space) to C_F by an amount $(A_e/A_t) p_0 / (p_c)_{ns}$, as shown by the preceding equation. The same equation may also be rewritten as follows

$$C_F = (C_F)_s - \frac{A_e}{A_t} \left[\frac{p_0}{(p_c)_{ns}} \right]$$

In other words, higher values of thrust F and thrust coefficient C_F correspond to lower values of ambient pressure p_0 .

For a given value p_0 of ambient pressure, the optimum value of thrust is reached when the expansion area ratio A_e/A_t of the nozzle is such that $p_e = p_0$. Let us consider a region in the divergent portion of a nozzle where $p_e > p_0$. In this region, the thrust of a rocket engine increases, and reaches its maximum value at the plane where $p_e = p_0$. When the divergent portion of a nozzle extends downstream of this plane, then

the pressure p_e of the exhaust gas at the exit plane becomes less than the ambient pressure p_0 , causing a decrease in the value of thrust. The value of the expansion area ratio A_e/A_t of the nozzle corresponding to the condition $p_e = p_0$ is called the optimum expansion area ratio.

Since the value of the ambient pressure decreases with altitude, no value of A_e/A_t is optimum at all altitudes, and therefore the design value of A_e/A_t is to be found on the basis of a compromise. This compromise is not necessary in case of upper stages of rockets, which operate at ambient pressures of zero or near zero. In case of rockets operating in space ($p_0 = 0$), a value of expansion area ratio greater than 25 has been found to be scarcely useful [4]. Therefore, in order to reduce weight, this value is not exceeded.

The specific heat ratio $\gamma \equiv c_p/c_v$ is an indicator of the quantity of energy stored in the molecules of exhaust gas. In particular, a small value of γ indicates a high capacity of storing energy, which results in a high performance of a rocket engine. The equations given above, which express c^* and C_F as functions of γ , indicate high values of c^* and C_F for low values of γ . These equations are re-written below for convenience of the reader.

$$c^* = \frac{[\gamma R(T_c)_{ns}]^{\frac{1}{2}}}{\gamma \left[\left(\frac{2}{\gamma+1} \right)^{\frac{\gamma+1}{\gamma-1}} \right]^{\frac{1}{2}}}$$

$$C_F = \left\{ \frac{2\gamma^2}{\gamma-1} \left(\frac{2}{\gamma+1} \right)^{\frac{\gamma+1}{\gamma-1}} \left[1 - \left(\frac{p_e}{(p_c)_{ns}} \right)^{\frac{\gamma-1}{\gamma}} \right] \right\}^{\frac{1}{2}} + \frac{A_e}{A_t} \left[\frac{p_e - p_0}{(p_c)_{ns}} \right]$$

In order for the specific heat ratio γ of the exhaust gas to have a small value, it is necessary to choose accurately the propellant to be used.

The effect of the constant $R = R^*/M$ of the specific exhaust gas on the performance of a rocket engine is shown by the first of the two preceding equations, which expresses the characteristic velocity c^* as a function of R . Since c^* is proportional to the square root of R , then the value of c^* increases for increasing values of R .

The effect of the total pressure in the combustion chamber at the nozzle inlet, $(p_c)_{ns}$, is shown by the second of two equations written above, which expresses the thrust coefficient C_F as a function of $(p_c)_{ns}$. It is to be noted that the total pressure $(p_c)_{ns}$ appears above in the two pressure ratios $p_e/(p_c)_{ns}$ and $p_0/(p_c)_{ns}$.

The following equation of Sect. 1.2

$$\frac{A_e}{A_t} = \frac{\left(\frac{2}{\gamma+1} \right)^{\frac{1}{\gamma-1}} \left(\frac{(p_c)_{ns}}{p_e} \right)^{\frac{1}{\gamma}}}{\left\{ \frac{\gamma+1}{\gamma-1} \left[1 - \left(\frac{p_e}{(p_c)_{ns}} \right)^{\frac{\gamma-1}{\gamma}} \right] \right\}^{\frac{1}{2}}}$$

shows that, for given values of A_e/A_t and γ , the ratio $p_e/(p_c)_{ns}$ has a singular value, corresponding to the condition $1 - (p_e/(p_c)_{ns})^{(\gamma-1)/\gamma} = 0$. The preceding equation

$$C_F = \left\{ \frac{2\gamma^2}{\gamma-1} \left(\frac{2}{\gamma+1} \right)^{\frac{\gamma+1}{\gamma-1}} \left[1 - \left(\frac{p_e}{(p_c)_{ns}} \right)^{\frac{\gamma-1}{\gamma}} \right] \right\}^{\frac{1}{2}} + \frac{A_e}{A_t} \left[\frac{p_e - p_0}{(p_c)_{ns}} \right]$$

shows that the ratio $p_e/(p_c)_{ns}$ affects the thrust coefficient C_F only through of the term $-p_0/(p_c)_{ns}$. When $(p_c)_{ns}$ increases, then $-p_0/(p_c)_{ns}$ decreases, and therefore C_F increases. This effect is particularly important for high values of the ambient pressure p_0 . The preceding equation

$$C_F = \frac{F}{A_t(p_c)_{ns}}$$

shows that, for a given area of the cross-section of the nozzle at the throat A_t , the thrust F is proportional to both the total pressure in the combustion chamber at the nozzle inlet $(p_c)_{ns}$ and the thrust coefficient C_F . Therefore, when the total pressure $(p_c)_{ns}$ increases in a given combustion chamber, then the thrust F also increases. Increasing values of $(p_c)_{ns}$ also cause the values of the total temperature in the combustion chamber $(T_c)_{ns}$ to increase, and the values of γ and R to decrease. According to Huzel and Huang [4], these effects are slight, especially when the value of the total pressure $(p_c)_{ns}$ is greater than $2.068 \times 10^6 \text{ N/m}^2$.

The performance indicators considered so far refer to an ideal rocket engine, which differs from a real rocket engine for the following reasons. A real engine is subject to friction, heat transfer, effects due to non-perfect gases, misalignment of the gas flow with respect to the axis of symmetry of the nozzle, non-uniform reacting substances and flow distribution, and changes in the composition of the exhaust gas. A change in gas composition, in turn, is due to non-uniform values of the quantities γ , M , and R along the axis of symmetry of the nozzle.

The actual quantities result from multiplying the corresponding theoretical quantities by correction factors.

In particular, the correction factor η_F , whose values range from 0.92 to 1.00 [4], makes it possible to compute the actual values of thrust (\bar{F}) and thrust coefficient (\bar{C}_F) from the corresponding theoretical values (F and C_F), as follows

$$\begin{aligned}\bar{F} &= \eta_F F \\ \bar{C}_F &= \eta_F C_F\end{aligned}$$

The correction factor η_v , whose values range from 0.85 to 0.98 [4], makes it possible to compute the actual values of exhaust velocity (\bar{v}) and specific impulse (\bar{I}_s) from the corresponding theoretical values (v and I_s), as follows

$$\begin{aligned}\bar{v} &= \eta_v v \\ \bar{I}_s &= \eta_v I_s\end{aligned}$$

The correction factor η_{c^*} , whose values range from 0.87 to 1.03 [4], makes it possible to compute the actual values of characteristic velocity (c^*) from the corresponding theoretical values (c^*), as follows

$$\bar{c}^* = \eta_{c^*} c^*$$

The correction factor η_W , whose values range from 0.98 to 1.15 [4], makes it possible to compute the actual values of weight flow rate ($\dot{\bar{W}}$) from the corresponding theoretical values (\dot{W}), as follows

$$\dot{\bar{W}} = \eta_W \dot{W}$$

According to Huzel and Huang [4], the following relations exist for the correction factors defined above

$$\eta_v = \eta_{c^*} \eta_F$$

$$\eta_v = \frac{1}{\eta_W}$$

Ranges of the actual values of the quantities relating to liquid-propellant rocket engines are given in the following table (from [4]).

Gas temperature, T (K)	2220–3890
Nozzle stagnation pressure, $(p_c)_{ns}$ (N/m ²)	68950–1.723 × 10 ⁷
Molar mass, \mathcal{M} (kg/kmol)	2–30
Specific gas constant, R (N m kg ⁻¹ K ⁻¹)	143.815–2157.23
Mach number of gas flow, M	0–4.5
Specific heat ratio, γ	1.13–1.66
Nozzle expansion area ratio, A_e/A_t	3.5–100
Nozzle contraction area ratio, A_c/A_t	1.3–6.0
Thrust coefficient, C_F	1.3–2.0
Characteristic velocity, c^* (m/s)	914–2440
Effective exhaust velocity, c (m/s)	1220–3660
Specific impulse in vacuo, I_s (s)	150–480

An example of application is given below. The rocket motor of Sect. 1.2 has the following data: propellant weight flow rate in the combustion chamber $\dot{W}_{tc} = 9.807 \times 163.6 = 1604$ N/s, total pressure in the combustion chamber at the nozzle inlet $(p_c)_{ns} = p_i [1 + \frac{1}{2}(\gamma - 1)M_i^2]^{\gamma/(\gamma-1)} = 6.895 \times 10^6$ N/m², total temperature of the combustion chamber $(T_c)_{ns} = T_i [1 + \frac{1}{2}(\gamma - 1)M_i^2] = 3633$ K (T_i and M_i being

respectively the flow temperature and the Mach number at the nozzle inlet), molar mass of the combustion products $\mathcal{M} = 22.67 \text{ kg/kmol}$, specific ratio of the gas $\gamma = 1.20$, and expansion area ratio of the nozzle $A_e/A_t = 12$. The Mach number at the injection plane, M_{inj} , is assumed to be equal to zero, and the Mach number at the inlet plane of the nozzle, M_i , is assumed to be equal to 0.4. The correction factors for respectively the characteristic velocity and the coefficient of thrust are $\eta_{c^*} = 0.97$ and $\eta_F = 0.983$.

It is required to compute the theoretical value of the characteristic velocity, the theoretical values of the thrust coefficient at sea level and in space, the theoretical values of the specific impulse (due to the thrust chamber only) at sea level and in space, the actual value of the characteristic velocity assuming a correction factor $\eta_{c^*} = 0.97$, the actual values of the thrust coefficient at sea level and in space assuming a correction factor $\eta_F = 0.983$, the actual values of the specific impulse (due to the thrust chamber only) at sea level and in space, the correction factor for the specific impulse (due to the thrust chamber only), the actual values of the thrust at sea level and in space, and the actual values of the areas of the cross-sections at the throat and at the exit section of the nozzle.

The theoretical value of the characteristic velocity, c^* , results from

$$c^* = \frac{\left[\gamma R(T_c)_{ns} \right]^{\frac{1}{2}}}{\gamma \left[\left(\frac{2}{\gamma+1} \right)^{\frac{\gamma+1}{\gamma-1}} \right]^{\frac{1}{2}}} = \frac{(1.2 \times 366.8 \times 3633)^{\frac{1}{2}}}{1.2 \times \left[\left(\frac{2}{1.2+1} \right)^{\frac{1.2+1}{1.2-1}} \right]^{\frac{1}{2}}} = 1780 \text{ m/s}$$

where the value of R has been determined in Sect. 1.2 as follows

$$R = \frac{R^*}{\mathcal{M}} = \frac{8314.460}{22.67} = 366.8 \text{ N m kg}^{-1}\text{K}^{-1}$$

The theoretical value of the thrust coefficient at sea level, C_F , results from

$$C_F = \left\{ \frac{2\gamma^2}{\gamma-1} \left(\frac{2}{\gamma+1} \right)^{\frac{\gamma+1}{\gamma-1}} \left[1 - \left(\frac{p_e}{(p_c)_{ns}} \right)^{\frac{\gamma-1}{\gamma}} \right] \right\}^{\frac{1}{2}} + \frac{A_e}{A_t} \left[\frac{p_e - p_0}{(p_c)_{ns}} \right]$$

Remembering that p_e has been determined in Sect. 1.2 as follows

$$p_e = z(p_c)_{ns} = 0.009859 \times 6.895 \times 10^6 = 6.798 \times 10^4 \text{ N/m}^2$$

and substituting $\gamma = 1.2$, $(p_c)_{ns} = 6.895 \times 10^6 \text{ N/m}^2$, $A_e/A_t = 12$, and $p_0 = 1.013 \times 10^5 \text{ N/m}^2$ into the expression of C_F , we find

$$C_F = 1.588$$

The theoretical value of the thrust coefficient in space, $(C_F)_s$, results from

$$(C_F)_s = C_F + \frac{A_e}{A_t} \left[\frac{p_0}{(p_c)_{ns}} \right] = 1.588 + 12 \times \frac{1.013 \times 10^5}{6.895 \times 10^6} = 1.764$$

Since the theoretical values of the characteristic velocity and the thrust coefficient (c^* and C_F) have been computed above, the theoretical value of the specific impulse at sea level relating to the thrust chamber only, $(I_s)_{tc}$, results from

$$(I_s)_{tc} = \frac{c^* C_F}{g_0} = \frac{1780 \times 1.588}{9.807} = 288.2 \text{ s}$$

Likewise, the theoretical value of the specific impulse in space relating to the thrust chamber only, $(I_s)_{tcs}$, results from

$$(I_s)_{tcs} = \frac{c^*(C_F)_s}{g_0} = \frac{1780 \times 1.764}{9.807} = 320.2 \text{ s}$$

Since the correction factor for the characteristic velocity is $\eta_{c^*} = 0.97$, then the actual value of the characteristic velocity results from

$$\bar{c}^* = \eta_{c^*} c^* = 0.97 \times 1780 = 1727 \text{ m/s}$$

Since the correction factor for the coefficient of thrust is $\eta_F = 0.983$, then the actual value of the coefficient of thrust at sea level results from

$$\bar{C}_F = \eta_E C_F = 0.983 \times 1.588 = 1.561$$

Likewise, the actual value of the coefficient of thrust in space results from

$$(\bar{C}_F)_s = \eta_E (C_F)_s = 0.983 \times 1.764 = 1.734$$

The actual value of the specific impulse at sea level relating to the thrust chamber only results from

$$(\bar{I}_s)_{tc} = \frac{\bar{c}^* \bar{C}_F}{g_0} = \frac{1727 \times 1.561}{9.807} = 274.9 \text{ s}$$

Likewise, the actual value of the specific impulse in space relating to the thrust chamber only results from

$$(\bar{I}_s)_{tcs} = \frac{\bar{c}^* (\bar{C}_F)_s}{g_0} = \frac{1727 \times 1.734}{9.807} = 310.6 \text{ s}$$

The correction factor η_v for the actual values of exhaust velocity and specific impulse results from

$$\eta_v = \frac{(\bar{I}_s)_{tc}}{(I_s)_{tc}} = \frac{274.9}{288.2} = 0.9539$$

The actual value of the thrust at sea level results from

$$\bar{F} = (\bar{I}_s)_{tc} \dot{W}_{tc} = 274.9 \times 1604 = 4.409 \times 10^5 \text{ N}$$

Likewise, the actual value of the thrust in space results from

$$(\bar{F})_s = (\bar{I}_s)_{tcs} \dot{W}_{tc} = 310.6 \times 1604 = 4.982 \times 10^5 \text{ N}$$

The actual values of the areas of the cross-sections of respectively the throat (\bar{A}_t) and the exit plane of the nozzle (\bar{A}_e) result from

$$\bar{A}_t = \frac{\bar{F}}{\bar{C}_F(p_c)_{ns}} = \frac{4.409 \times 10^5}{1.561 \times 6.895 \times 10^6} = 0.04096 \text{ m}^2$$

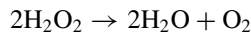
$$\bar{A}_e = 12\bar{A}_t = 12 \times 0.04096 = 0.4916 \text{ m}^2$$

1.4 Liquid Propellants for High-Thrust Rocket Engines

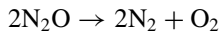
Some fundamental concepts on solid, liquid, and gaseous propellants for high-thrust rockets have been given in Sects. 1.1 and 1.2. The present paragraph deals specifically with liquid propellants. They may be classified into the following categories:

- mono-propellants;
- bi-propellants;
- cryogenic propellants; and
- storable propellants.

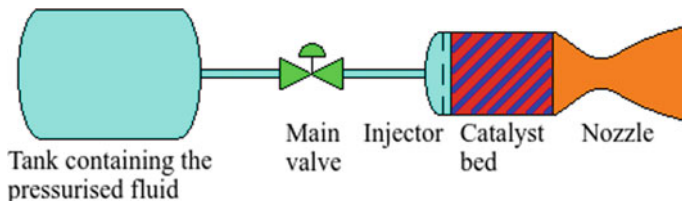
A mono-propellant is either a mixture of a fuel with an oxidiser, or a single substance which decomposes into a hot gas in a thrust chamber, in the presence of an appropriate catalyst. This chemical decomposition releases thermal energy, which is contained within the chemical bonds of the molecules involved in the reaction. For example, hydrogen peroxide (H_2O_2) decomposes into hot water vapour (H_2O) and gaseous oxygen (O_2) when made to pass through a platinum catalyst mesh, according to the following reaction:



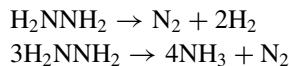
The gases resulting from this reaction are ejected through a nozzle to generate thrust. A gaseous mono-propellant, which can be used instead of hydrogen peroxide, is nitrous oxide (N_2O). This substance, when heated or passed over a catalyst bed, decomposes exothermically into gaseous nitrogen (N_2) and gaseous oxygen (O_2), according to the following reaction:



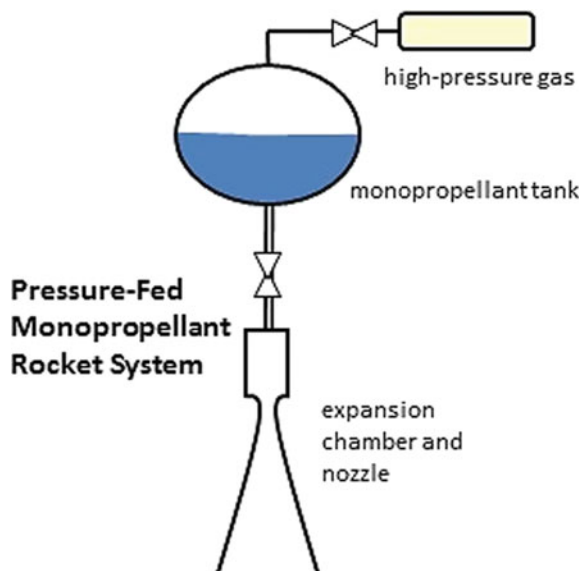
A scheme, which illustrates a rocket engine fed by nitrous oxide, is shown in the following figure, (re-drawn from [20]). Further information on this type of mono-propellant can be found, for example, in [20].



The most widely used mono-propellant is hydrazine (anhydrous N_2H_4 , also written H_2NNH_2), which is a strong reducer, that is, a substance which donates electrons to another substance in a redox chemical reaction. In a mono-propellant engine, hydrazine decomposes (in the presence of a catalyst such as iridium metal supported by high-surface-area alumina, or carbon nanofibres, or molybdenum nitride on alumina) into gaseous nitrogen (N_2) and gaseous hydrogen (H_2), or into ammonia (NH_3) and gaseous nitrogen (N_2), according to the following exothermic reactions [21]:



A scheme illustrating a mono-propellant rocket engine fed by hydrazine is shown in the following figure, which is due to the courtesy of NASA [22].



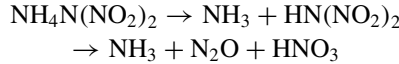
With reference to the preceding figure, the working principle of a hydrazine monopropellant engine can be described as follows. An electric solenoid valve, placed between the hydrazine tank and the thrust chamber, opens in order to allow liquid hydrazine, in a pulsed or continuous flow, to reach the injector. This hydrazine enters the thrust chamber as a spray and gets in touch with the catalyst bed. This bed consists of alumina (Al_2O_3) pellets impregnated with iridium. The catalyst bed and the hot gases leaving the catalyst particles cause the liquid hydrazine to vaporise, and its temperature to rise to a point where the chemical reaction of dissociation is self-sustaining. Then, the gases resulting from hydrazine decomposition leave the catalyst bed and exit from the chamber through a nozzle of high expansion ratio to produce thrust.

Mono-propellant hydrazine engines produce a specific impulse of about 230–240 s. Mono-propellant engines using hydrogen peroxide and nitrous oxide have a lower performance than that obtained with hydrazine, since their specific impulses are respectively about 150 and 170 s [10].

Since hydrazine is corrosive, highly toxic and carcinogenic, and is also dangerous to handle and store, then new substances, called green propellants, are being studied and tested for its replacement. A green propellant is an aqueous solution of a high-energy oxidiser (such as hydroxyl ammonium nitrate, ammonium dinitramide, and others) and a fuel (such as methanol, ethanol, glycerol, and others). Hydroxyl ammonium nitrate, also known as HAN, whose chemical formula is NH_3OHNO_3 , is a salt derived from hydroxyl amine (NH_2OH) and nitric acid (HNO_3), which can be used as a solution in mono-propellants, or also as a solid oxidiser in bi-propellants. The Air Force Research Laboratory at Edwards Air Force Base in California, USA, has developed a hydroxyl ammonium nitrate-based propellant known as AF-M315E. This propellant is less toxic and easier to handle than hydrazine, and has a specific

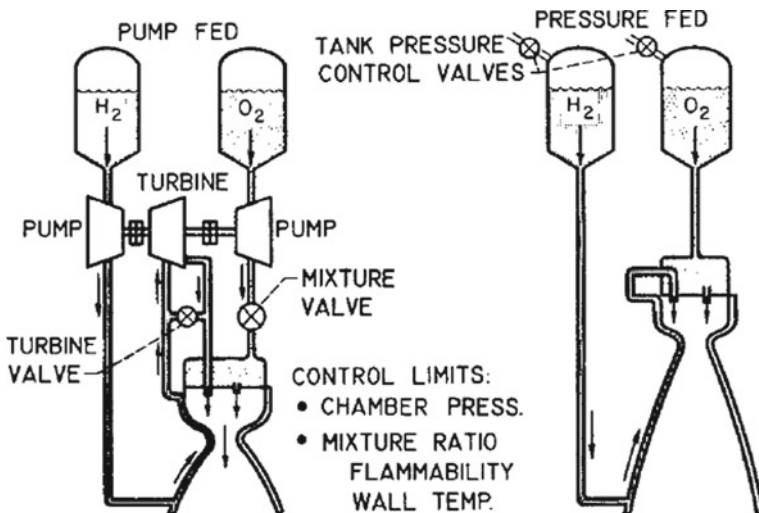
impulse $I_s = 257$ s, which is about 12% greater than the specific impulse of hydrazine, the latter being $I_s = 230$ s. It requires a catalyst bed preheating at a temperature exceeding 558 K to be ready for general operation [23].

Ammonium dinitramide, also known as ADN, whose chemical formula is $\text{NH}_4\text{N}(\text{NO}_2)_2$, is the ammonium (NH_4^+) salt of the dinitraminic acid ($\text{HN}(\text{NO}_2)_2$), and was invented in the 1970s in the former Soviet Union and independently invented again in 1989 in the United States by SRI International. Gaseous ammonium dinitramide decomposes under heat into ammonia (NH_3), nitrous oxide (N_2O), and nitric acid (HNO_3), according to the following two-branch reaction [24]:



The Swedish company EURENCO Bofors produces a liquid mono-propellant, called LMP-103S, as a substitute for hydrazine by dissolving 65% ammonium dinitramide in 35% water solution of methanol (CH_3OH) and ammonia (NH_3). LMP-103S has 6% higher specific impulse and 30% higher impulse density (see below) than hydrazine mono-propellant [25]. LMP-103S has been tested on the PRISMA (Prototype Research Instruments and Space Mission technology Advance-ment, COSPAR designation 2010-028B and 2010-028F) mission in 2010. Rocket engines using mono-propellants are simple, require only one tank for the propellant, and can be readily turned on and off. They are mainly used to perform such functions as orbit maintenance and attitude control of satellites.

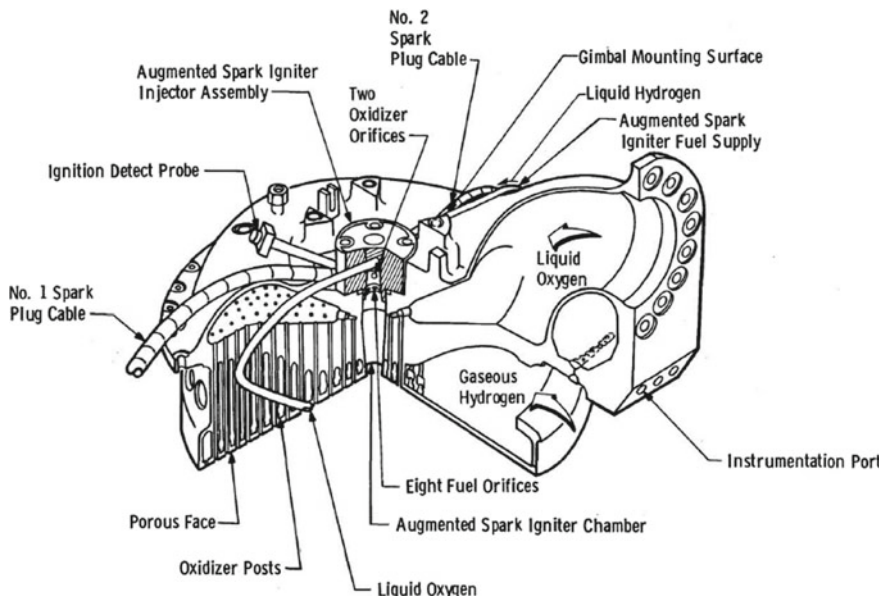
A liquid bi-propellant comprises two substances, namely a fuel and an oxidiser, which are held in separate tanks. They are not mixed before being injected into the combustion chamber of a rocket engine. They may be fed to the combustion chamber either by pumps or by pressure in the tanks, as shown in the following figure, due to the courtesy of NASA [26]. In a pump-fed engine (left), the liquid fuel (H_2) picks up heat, as it circulates through the coolant jacket of the thrust chamber, becomes gaseous, and drives a turbine. The gas exhausted by the turbine is then injected into the combustion chamber. This arrangement is called the expander cycle. Control in this cycle is achieved by using: (a) the turbine valve to regulate the thrust, and (b) the mixture valve to maintain the desired mixture ratio. In a pressure-fed engine (right), the pressure in the propellant tanks is sufficient to force the two propellants (H_2 and O_2) through the injector into the combustion chamber. The fuel (H_2) first circulates through the coolant jacket, and is then delivered to the combustion chamber. In a pressure-fed engine, the pressures in the supply tanks can be regulated to yield the desired pressure and mixture ratio in the combustion chamber [26].



Liquid-propellant rocket engines using bi-propellants have higher performance than those using mono-propellants, as shown in the general table of Sect. 1.3. In addition, the former are often easier to operate than the latter, particularly in consideration of the risks connected with the use of hydrazine.

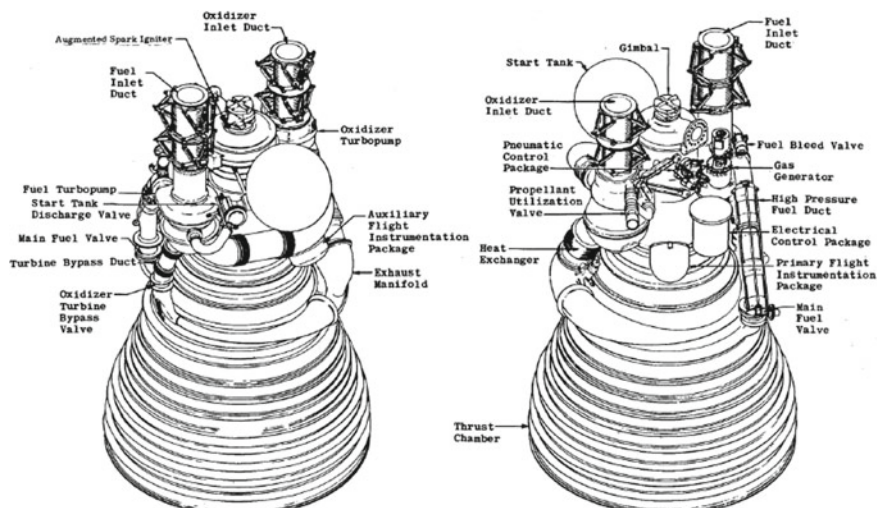
When the fuel and the oxidiser react spontaneously, as is the case with the hypergolic substances described in Sect. 1.2, then no ignition device is needed in a liquid-propellant engine. Otherwise, an ignition device is necessary in the combustion chamber of a bi-propellant rocket engine. Some of these devices are briefly described below. One of them is a spark plug igniter. A spark plug igniter is a small combustion chamber having two spark plugs. It provides the flame to ignite the propellant (fuel and oxidiser) in the main thrust chamber. When the engine is started, the spark excitors energise the spark plugs as the oxidiser and the fuel flow to the spark igniter. As the gaseous oxidiser and fuel enter this small combustion chamber, they mix and are touched off by an electrical spark. The pilot flame provided by the spark igniter lights off the main combustion chamber. A spark plug igniter is capable of multiple re-ignitions.

The Rocketdyne J-2 rocket engine had a particular spark plug igniter unit, called augmented spark igniter or spark torch igniter, which formed an integral part of the thrust chamber injector, as shown in the following figure, which is due to the courtesy of the United States Air Force [27].

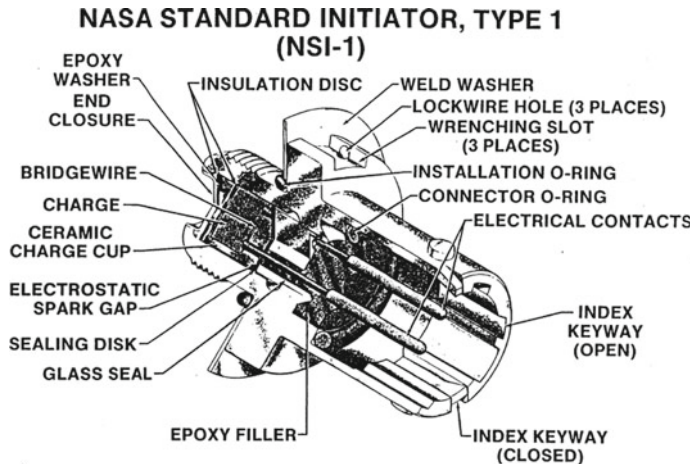


The J-2 rocket engine was used for the Saturn IB and Saturn V launch vehicles for the NASA Apollo programme. The main engines of the Space Shuttle also had an augmented spark igniter, whose chamber was located in the centre of the injector. The dual-redundant igniter was used during the engine start sequence to initiate combustion. The igniters were turned off after approximately three seconds because the combustion process is self-sustaining [28].

The following figure, due to the courtesy of the United States Air Force [27], shows the position of the augmented spark igniter in the J-2 rocket engine.

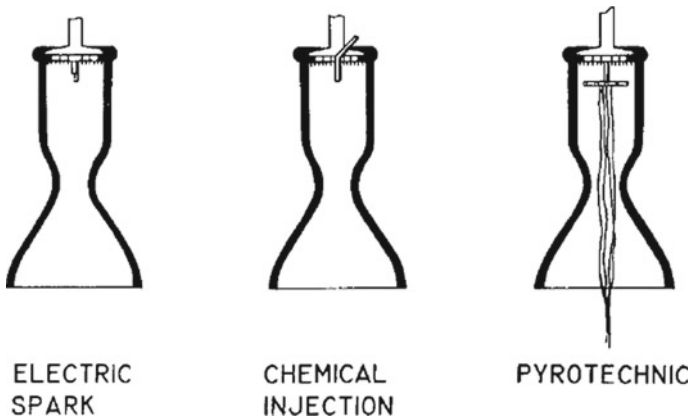


Another ignition device is a pyrotechnic igniter, which is shown in the following figure, due to the courtesy of NASA [29].



A pyrotechnic igniter is set off by an electric current, which heats a bridge wire enclosed in a clump of easily ignited materials. Each of these materials, in turn, comprises an oxidiser (usually potassium perchlorate or potassium nitrate) and a fuel (usually titanium, or titanium hydride, or zirconium, or zirconium hydride, or boron). Such materials, when ignited by the hot wire, generate sparks and hot gases due to the chemical reaction between the oxidiser and the fuel. These, in turn, ignite the mixture of gaseous propellant in the combustion chamber. Pyrotechnic igniters are safe and reliable. They are one-shot devices, and therefore cannot be used to re-start a rocket engine [30].

Still another ignition method used for liquid propellants consists in injecting some spontaneously ignitable fluid, called a pyrophoric fluid, ahead of the propellant. Pyrophoric substances (for example, ferrous sulphide and many reactive metals) have the property of igniting spontaneously, that is, without an external source of heat, upon exposure to air, moisture in the air, oxygen, or water. Such substances may be solid, liquid, or gaseous. Most of them are metals and react spontaneously with oxygen only when they are in a very finely divided state. Pyrophoric substances are a special class of hypergolic substances (described in Sect. 1.2), because the oxidising agent for the former class is restricted to atmospheric oxygen [31]. They can be handled safely in atmospheres of argon or, with a few exceptions, nitrogen. A list of pyrophoric materials can be found in [32]. These three methods of ignition (electric spark, chemical injection, and pyrotechnic) are shown together in the following figure, due to the courtesy of NASA [33].



Finally, liquid propellants can also be ignited by using a small combustor, wherein pyrotechnic devices or electric spark plugs ignite the propellant. The hot gas produced, in turn, ignites the propellant in the main combustion chamber.

Fundamental concepts on cryogenic propellants have been given in Sect. 1.2. The scope of cryogenics has been defined by NASA ([34], page 1) as follows: “Cryogenics is the discipline that involves the properties and use of materials at extremely low temperatures; it includes the production, storage, and use of cryogenic fluids. A gas is considered to be cryogenic if it can be changed to a liquid by the removal of heat and by subsequent temperature reduction to a very low value. The temperature range that is of interest in cryogenics is not defined precisely; however, most researchers consider a gas to be cryogenic if it can be liquefied at or below -240°F . The most common cryogenic fluids are air, argon, helium, hydrogen, methane, neon, nitrogen, and oxygen. Other gases that are being used in space probes and high-energy liquid-propellant rockets include fluorine and nitrogen trifluoride.”. In accordance with the preceding definition, by cryogenic propellants we mean gases which can be liquefied at or below 122 K. The most common cryogenic propellants for rocket applications are liquid oxygen (O_2), liquid hydrogen (H_2), liquid fluorine (F_2), and oxygen difluoride (OF_2), or mixtures of some of these substances.

These propellants should be stored and handled in such a way as to reduce the increase in their temperature of storage to a minimum. This temperature depends on the particular propellant and also on the time of storage. The thermal insulation techniques used for reservoirs should reduce the increase in temperature. The gases developed from the evaporating liquids should have a venting system, in order to allow them to escape. Accurate control should be exerted on the environmental humidity. In addition, the design adopted and the materials selected for rocket engines using cryogenic propellants should take account of the properties of such propellants. These disadvantages are offset by high values of specific impulse, as has been shown in Sect. 1.2.

In contrast with cryogenic liquid propellants, storable liquid propellants are stable over a wide range of temperature and pressure, and are also scarcely reactive with the materials used for their reservoirs. Therefore, they can be stored for periods of

a year or more. These properties make them readily available and reliable. They are used in military vehicles and in upper stages of space vehicles.

For example, a liquid storable fuel is Aerozine 50 (see Sect. 1.2), which is a 50/50 mixture by weight of hydrazine (H_2NNH_2) and unsymmetrical dimethyl hydrazine ($\text{H}_2\text{NN}(\text{CH}_3)_2$). Aerozine 50 is used with nitrogen tetroxide (N_2O_4) as the oxidiser, with which it is hypergolic. This combination of fuel and oxidiser is storable at room temperature, and therefore a loaded missile can be stored for several years without the maintenance requirements associated with cryogenic propellants. This fuel was developed in 1950s by Aerojet General Corporation for the Titan II ICBM rocket engines, and has been used in Aerojet's Titan liquid rocket engine [35] and Delta II stage 2 engine [36]. Aerozine 50 is mainly used for interplanetary probes and spacecraft propulsion, and is also used for intercontinental ballistic missiles, which require long-term storage and launch on short notice. Another liquid storable fuel, also used with nitrogen tetroxide (N_2O_4) as the oxidiser, is UH 24, which is a mixture of 75% unsymmetrical dimethyl hydrazine ($\text{H}_2\text{NN}(\text{CH}_3)_2$) and 25% hydrazine hydrate ($\text{H}_2\text{NNH}_2 \cdot \text{H}_2\text{O}$). This combination is also hypergolic, and has been used in the Ariane rocket versions 2 through 4 [37], and also in the Indian Geosynchronous Satellite Launch Vehicle Mark III [38].

The liquid propellants indicated above are sometimes mixed with additive substances, which are meant to either facilitate ignition, or stabilise combustion, or reduce corrosive effects, or lower freezing point, or improve cooling properties of propellants. Some attempts have been made to promote hypergolicity in propellants by adding substances in the cryogenic oxidiser or in the fuel. An account on these attempts has been given by Clark [39].

In particular, it has been proposed to add aluminium tri-ethyl ($\text{Al}_2(\text{C}_2\text{H}_5)_6$) to the fuel, or ozone fluoride (O_3F_2) to the oxidiser. According to Dickinson [40], using hypergolic additives to fuels is not a good practice, because it increases the danger of inadvertent ignition on exposure of the fuel to air. The additive might be injected as a secondary stream in the fuel ahead of the combustion chamber, but this would imply an added complication in the design of a rocket engine. It seems better to mix additives to the oxidiser, because the danger is confined to direct mixing of fluid with oxidiser, or to direct spilling of the oxidiser on combustible materials.

As has been shown in Sect. 1.2, there is a mixture ratio (o/f), called the stoichiometric mixture ratio, between the oxidiser (o) and the fuel (f). The stoichiometric mixture ratio for a rocket engine is the ideal ratio of oxidiser to fuel that burns all fuel with no excess oxidiser. In practice, there is another mixture ratio, called the optimum mixture ratio, between the oxidiser and the fuel which leads to the maximum value of performance. The optimum mixture ratio is less than the stoichiometric mixture ratio, because the temperature of the flame reaches its maximum value when the quantity of fuel exceeds the value defined by the stoichiometric mixture ratio. This happens because a combustion richer in fuel generates an exhaust gas having a lower molar mass. The optimum mixture ratio varies slightly with the pressure in the combustion chamber. In practice, the actual value chosen for the mixture ratio may differ from the optimum value, because the temperature of the combustion chamber must be

kept within the limits imposed by the materials, or because of the coolant flow, or because the combustion must be made stable.

The performance of a liquid propellant depends not only on its specific impulse, I_s , but also on its density, because a low-density propellant implies large storage tanks, which in turn imply a high mass of a rocket engine. By contrast, a high-density propellant can be stored in small tanks and requires small pumps to be fed to the combustion chamber. This indicator of performance of a propellant combination is taken into account by means of the so-called impulse density, I_d , which is defined as follows [6]:

$$I_d = I_s \delta_{av}$$

where δ_{av} is a dimensionless quantity, called average specific gravity of a propellant combination (oxidiser and fuel), defined as follows

$$\delta_{av} = \frac{\delta_o \delta_f (1 + r)}{r \delta_f + \delta_o}$$

$r \equiv o/f$ is the oxidiser-to-fuel weight mixture ratio, δ_o is the specific gravity (ratio of the density of a given substance to the density of water at 277 K and atmospheric pressure) of the oxidiser, and δ_f is the specific gravity of the fuel. Since δ_{av} is a dimensionless quantity, then the impulse density, I_d , of a propellant combination is measured in seconds, as is the case with the specific impulse, I_s . Specific gravities of various propellants as a function of temperature are given in [6], page 243. Values of I_s and I_d for various propellants are given in [4], pages 25, 26, and 27. Further performance data, in terms of I_s and I_d , concerning liquid hydrocarbons and aluminium-hydrocarbon fuels, are given in [41], pages 5, 6, and 8.

A propellant combination for a specific application is chosen taking into account the advantages and the disadvantages of each combination. It is often necessary to adopt a compromise. Some criteria to be considered in a choice have been identified by Huzel and Huang [4]. They are:

- high release of energy per unit mass of propellant, combined with low molar mass of the gases resulting from combustion or decomposition, in order to have high values of specific impulse;
- easiness of igniting the propellant;
- stability of combustion;
- high density of the propellant or high impulse density, in order to reduce the volume and the weight of the tanks and the pumps;
- capability possessed by the propellant of cooling effectively the thrust chamber;
- low vapour pressure of the propellant at a temperature of about 344 K, for low weight of tanks and pumps;
- low freezing point of the propellant, possibly less than 219 K, for easy engine operation at low temperatures;

- absence of corrosiveness and compatibility of the propellant with the materials used for the engine;
- high boiling point, possibly above 344 K, for storable propellants;
- low viscosity, possibly less than 0.01 Ns/m², to reduce pressure drops through the feed system and the injector;
- high thermal and shock stability, to reduce risks of explosion and fire;
- low toxicity of the propellant itself and its reaction products;
- low cost; and
- ready availability.

1.5 Combustion of Propellants in Steady State

The combustion process which occurs in steady-state conditions in a liquid-propellant rocket engine can be described by the following sequence of events.

The propellants are injected from a distributing manifold into the combustion chamber of the engine through orifices. The propellants are in the form of liquid jets. These jets are made to break up into small droplets, which then vaporise at high temperature in the combustion chamber. The breakup of the jets is often achieved by causing two or three of like (or sometimes unlike) substances to impinge. The impinging jets produce thin liquid sheets or fans which disintegrate rapidly. In bipropellant engines, the reactive vapours containing fuel and oxidiser get mixed one with the other. The mixed vapours interact, and the hot gases resulting from the combustion process flow out of the combustion chamber toward the throat of the nozzle. Due to various reasons, the actual combustion process in steady state may be more complex than the ideal process described above, as shown in the following figure, due to the courtesy of NASA [42].

A reason is the internal shape of some injectors, which are designed so that the liquid propellants flowing through them are partially or totally mixed, or broken up into droplets, or vaporised before entering the combustion chamber. This effect can also be obtained by injecting controlled streams of gases into the injector passages, or by using other means.

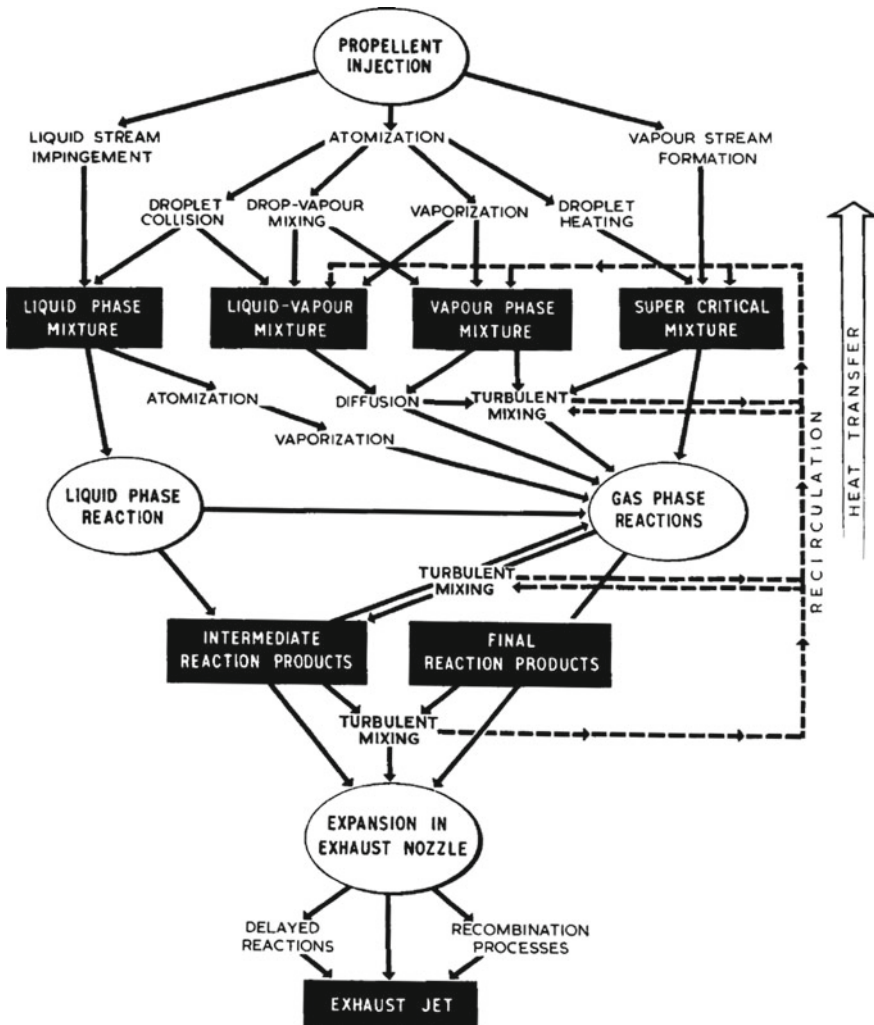
Another reason is the occurrence of combustion reactions in condensed phase with certain propellants, before their mixture or vaporisation.

Still another reason is the occurrence of heterogeneous reactions in the absence of mixing in liquid phase, as is the case with some combinations of hypergolic propellants.

Still another reason is an incomplete mixture of fuel with oxidiser in gaseous phase. This happens near the walls of the combustion chamber, where fuel-rich streams are intentionally sprayed for purposes of cooling. This also happens because of condensed phases which may be present in the mixture of the combustion products, when the propellants used contain either metals or carbon. This also happens because part of combustion products may recirculate back to the vicinity of the injector plate

between spray fans, instead of going directly toward the nozzle, thereby causing a fraction of gas to remain in the combustion chamber for a long time.

Still another reason is the pressure level in the combustion chamber, which may increase above the critical point of one or both of the propellants, thereby causing the sharp distinction between liquid and gas to disappear.



Due to one or more of these reasons, the actual combustion process may differ from the simple process indicated above. Analytical models of the combustion phenomena are described at length in [42, 43].

The phenomena which occur in a combustion chamber of cylindrical shape can be described by dividing the combustion chamber into a series of adjacent cylindrical

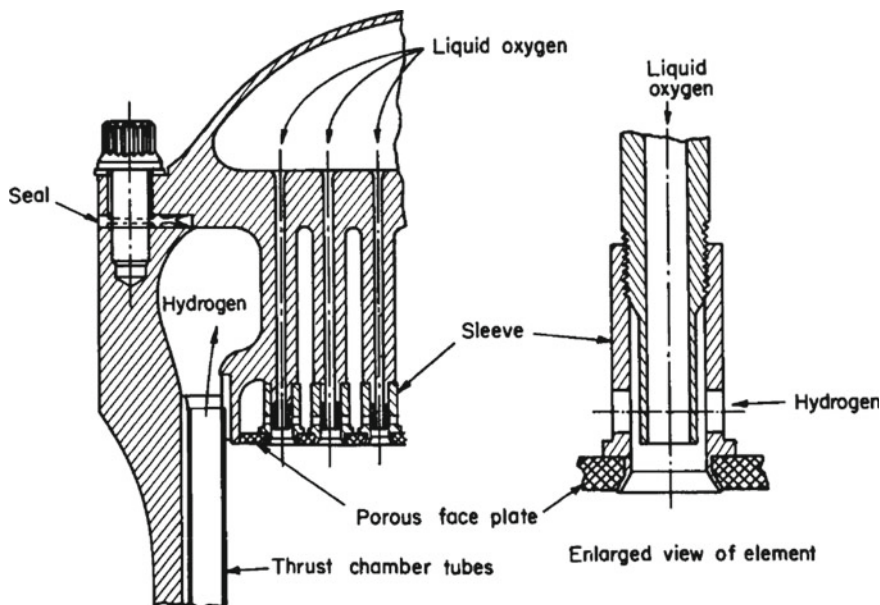
segments, stacked onto one another in the axial direction from the injection plane to the inlet plane of the nozzle. The thickness of each segment, the phenomena which actually occur into it, and the shape of its surfaces of separation from the adjacent segments depend on factors such as the specific combination of propellants used, the operating conditions (pressure, temperature, mixture ratio, et c.), and the type of injectors. The surfaces which separate two adjacent cylindrical segments are not planar, but have undulations which vary with time.

The combustion phenomena in a rocket engine depend on the combination of propellants used. For example, when the fuel is liquid hydrogen which has been used, before injection, to cool the walls of the combustion chamber, then this fuel is in the gaseous state at a temperature varying from 60 to 500 K [6]. In such conditions, there are neither droplets of liquid hydrogen nor evaporation.

When the liquid propellants used are hypergolic, then an initial chemical reaction occurs in liquid phase at the moment in which a droplet of fuel impinges on a droplet of oxidiser. Therefore, care must be taken by the designer to avoid local explosions and excessive releases of energy which could generate shock waves.

The cylindrical segment immediately adjacent to the injector plate is known as the injection-and-breakup zone, where two different liquid propellants enter through the orifices of the injector. This happens with either storable propellants or combinations of liquid oxygen with hydrocarbons. The injection velocities range from about 7 to 60 m/s [6]. The type of injector used (including the pattern, the size, the number, and the distribution of the orifices) has a strong influence on the behaviour and in particular on the stability of the combustion in this zone. The same influence have the pressure drop, the configuration of the manifold, or the roughness of the walls of the injection ducts. In this zone, the individual jets or streams of propellants break up into droplets by impingement of one jet with another or with a surface, or by inherent instability of liquid sprays, or by interactions of liquids with gases having different velocities and temperatures. These droplets are heated by radiation coming from the next zone (called rapid combustion zone) and also by convection of gas in the injection-and-breakup zone. This heat causes the droplets to evaporate and create regions rich in either fuel vapour or oxidiser vapour. The injection-and-breakup zone is heterogeneous, because it contains liquid propellants, vaporised propellants, and hot gases resulting from combustion products. Since the propellants in liquid phase are located at discrete places, then large variations are present in mass flow rates, mixture ratios, sizes and distributions of droplets, and properties of resulting gases. The chemical reactions occurring in the injection-and-breakup zone generate heat at low rates, and hot gases may recirculate back to the injector plate. Such gases create vortices and turbulent motions which contribute to the initial evaporation of the liquids injected. The processes described above occur in a different manner when one of the propellants is in the gaseous state. Such is the case with gaseous hydrogen coming in contact with liquid oxygen. Gaseous hydrogen has no droplets and does not evaporate. Since the injection velocity of gaseous hydrogen is much higher (above 120 m/s, according to [6]) than that of liquid oxygen, then shear forces act on the liquid jets, and such forces foster the formation and the evaporation of droplets. This case requires the use of an injector of a particular type, which differs

from the injectors used for two propellants entering the combustion chamber in the liquid state. To this regard, the following figure, due to the courtesy of NASA [42], shows an injector assembly of coaxial-tube injection elements like that used in the J-2 rocket engine. In this assembly, which is typical of an O₂/H₂ concentric orifice injector, the oxygen tubes are recessed and hydrogen enters the injection elements through inlet holes or slots in their sleeves.



The cylindrical sector contiguous to the injection-and-breakup zone in the direction of the nozzle is called rapid combustion zone. In this zone, rapid and intense chemical reactions occur at increasing high temperatures. Droplets of propellants which may be left are vaporised by convective heat. Consequently, fuel-rich and fuel-lean gases are mixed. The oxidation of the fuel occurs rapidly in this zone, and generates heat at higher rates than those of the preceding zone, with consequent decrease in density and increase in velocity of the burning gas. The chemical composition and the mixture ratio become more uniform as the burning gas moves through this zone. The axial component of the velocity vector of a molecule of combusted gas moving along a stream line becomes gradually greater than its transverse component.

The cylindrical sector contiguous to the rapid combustion zone in the axial direction is called stream tube combustion zone. In this zone, oxidation reactions continue to occur, but at a lower rate than that of the previous zone. The gas mixture approaches an equilibrium composition. The axial component of the velocity vector (ranging from 200 to 600 m/s, according to [6]) of a gas molecule is much higher than its transverse component, and therefore there is little turbulent mixing between gaseous layers. The residence time of a gaseous molecule in the stream tube combustion zone is little in comparison with its residence time in the previous zones. The shape of the

stream lines, the inviscid flow, and the tendency of the combustion products toward chemical equilibrium persist in the stream tube combustion zone.

The burning process which actually takes place in a combustion chamber is to be considered as a series of events which occur rather simultaneously than sequentially. Due to turbulence phenomena occurring in various degrees in all of the three zones indicated above, the flame front in a combustion chamber is not a planar surface.

The time spent by single molecules of reactants or combustion products in the combustion chamber of a liquid-propellant rocket engine is of the order of magnitude of 10 ms. The heat release per unit volume is about $3.7 \times 10^5 \text{ J/m}^3$, which value is much higher than in a turbojet. In addition, the higher temperatures reached in the combustion chamber of a rocket engine cause chemical reactions to occur at much higher rates than in a turbojet [6].

1.6 Combustion of Propellants in Unsteady State

Transients can be induced in the process of combustion either intentionally, as is the case with engine start-up or shut-down, or because of the insurgence of undesired phenomena of instability.

As will be shown at length in Chap. 2, the combustion chamber of a liquid-propellant rocket engine is normally designed to operate in steady state or in conditions which vary slowly with time. However, an unstable behaviour may occur there as a result of small perturbations, which cause self-sustaining oscillations of pressure in the burning gas. The frequencies of these oscillations vary in a wide range. Specifically, frequencies going from less than 100 Hz to over 15,000 Hz have been measured in the combustion chamber at amplitudes going from 10 to 1000% of the pressure in steady state [42].

According to Culick and Kuentzmann [43], the energy taken by these oscillations is only a small part of the chemical energy made available by the propellants. Therefore, except in very severe instances, the mean thrust or the steady power of the engine is not affected by the oscillations. However, serious problems may arise because of structural vibrations excited by the oscillating pressure in the combustion chamber, and also because of oscillations of the thrust generated by the engine. In addition, the heat transfer rates between the hot gas and the internal surface of the combustion chamber can be highly increased, with consequent erosion of the chamber wall.

The unstable motion of the hot gas is self-excited as a result of an interaction of the combustion process with the structural modes of the rocket vehicle. This instability arises because a very small part of the chemical energy contained in the propellants is sufficient to produce large unsteady motions, and also because the processes tending to attenuate such motions are weak, unless appropriate steps are taken.

An example of these self-sustained oscillations is provided by the so-called pogo instability (see Chap. 2, Sect. 2.9, and Chap. 7, Sect. 7.6), which occurs in the feed lines of large liquid-propellant rocket vehicles, such as space launch vehicles or ballistic missiles. This particular instability is due to a feedback interaction between

the propulsion system and the structure of a rocket stage, and occurs principally in the first longitudinal mode of the structure of the vehicle during operation of its first stage.

The most destructive type of combustion instability is characterised by oscillations of high frequency, and is also known as acoustic instability. The frequencies of these oscillations are equal to or greater than 1000 Hz [4].

The term acoustic instability is due to an observed correspondence, in both frequency and phase, between the pressure oscillations observed experimentally in a combustion chamber and the oscillations calculated for the acoustic resonance of the chamber. High-frequency instability includes both longitudinal and transverse modes, and the latter include, in turn, radial and tangential modes.

In general terms, a source of oscillating energy is necessary to sustain instability. In the particular case of high-frequency instability, the source of oscillating energy is the combustion of the propellants used in a rocket engine, and depends weakly on the feed system of the engine. The oscillating energy must, to sustain instability, be properly phased in time with the oscillating pressure, as will be shown at length in Chap. 2, Sect. 2.9.

Sustaining mechanisms which have been proposed for high-frequency instability include loss of ignition, sensitive chemical preparation time, physical time delays, detonation processes, pressure or temperature sensitive chemical kinetics, the burst of droplets heated beyond their critical temperature and pressure, and the shattering and mixing of the streams, fans, or drops by the motion of gas particles [42].

Instability in a combustion chamber may start either spontaneously or as a result of some artificial perturbation. Acoustic instability may have a threshold amplitude, above which a perturbation is sustained and below which the same perturbation is damped. A rocket engine is said to be inherently stable, when it can absorb large perturbations and yet return to its operation in steady state. The degree of inherent stability of a rocket engine can be measured by rating devices which provide artificial perturbations to its combustion chamber. Such perturbations involve operating conditions, such as mixture ratio of the propellants, pressure in the combustion chamber, temperature of the fuel, and so on.

An instability of the spontaneous type requires no initial perturbation to start, and grows out of the noise inherent to the combustion process. An instability of this type can be expected to occur just after an engine has reached its normal operating conditions, because no perturbation is required for its occurrence. Variations in test conditions and the closeness to a stability boundary may sometimes delay the occurrence of a spontaneous instability.

Instability in a combustion chamber may also be induced by natural or artificial perturbations which may occur in the combustion process. Such perturbations are also known as spikes or pops, where a spike indicates a significant overpressure in the combustion chamber upon ignition of the engine, and a pop indicates a similar overpressure occurring spontaneously during engine operation at nominal pressure in the combustion chamber. For example, at high altitudes, some combinations of hypergolic bi-propellants may start with an extremely high spike of pressure in the combustion chamber. This spike has been attributed to the explosion or deflagration

of the propellants collected in the combustion chamber or accumulated on its walls during the period of ignition delay. This spike of pressure may be of sufficient magnitude to either cause destructive failure in the combustion chamber or adversely affect the guidance sensor systems. In addition, for small rocket engines used for intermittent operation, the resultant thrust or the total impulse is seriously altered from that of a smooth start. For large engines, the ignition spike can trigger resonance in the combustion process, with consequent hardware destruction [42].

In most cases, the combustion process in a rocket engine shows a non-linear behaviour, which requires some kind of trigger, be it natural or artificial, to cause pressure oscillations of high frequency and amplitude in the combustion chamber. Consequently, it is necessary to determine the types and the magnitudes of the triggers which may occur in an engine during flight. This done, it is also necessary to evaluate the stability of that engine with artificial triggers of the assumed types. However, as has been shown above, a pressure oscillation may in some cases grow out of combustion noise, in the absence of any observable trigger.

The dynamic stability of a rocket engine is concerned with the responses of the engine to transients occurring during its operation. A rocket engine must, to be dynamically stable, return to its normal operating conditions after transients of any type which may occur to it. In other words, in order for a rocket engine to be dynamically stable, the transients resulting from any type of operating conditions must die out, or the amplitudes of the subsequent sustained oscillations of pressure must be sufficiently small. In order to evaluate the dynamic stability of a rocket engine, the engine is driven by any means into pressure oscillations of high amplitude. If these oscillations subsequently decay to those proper to steady-state conditions, then there is sufficient assurance that no oscillations of high amplitude exist within the range of the given perturbations. A rocket engine, which has shown a dynamically stable behaviour within the range of the operating conditions expected in flight, should also remain stable in actual flight.

Another method which may be used to gain confidence in the stability of a rocket engine consists in conducting a large number of tests and flight. A confidence gained in this way is called statistical stability. This confidence indicates only that instability has rarely or never occurred in the operating condition tested, but not that instability can never occur.

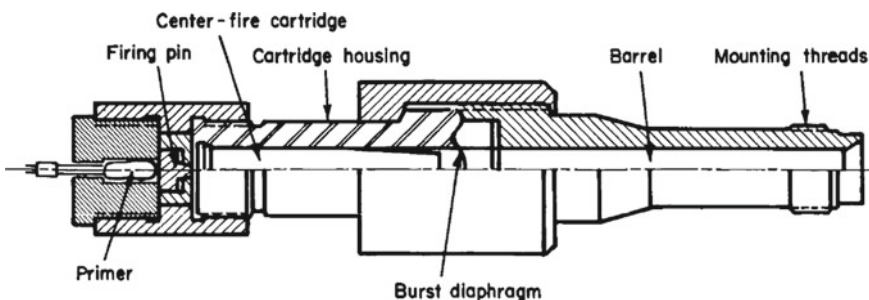
As will be shown at length in Chap. 2, Sect. 2.9, the problem of assuring a stable combustion in an existing rocket engine (without changing the dimensions of the combustion chamber, the hydraulic resistances of the propellant feed system, the type of injector, the heat flux in the combustion chamber, and the engine performance) can be solved by using baffles, which are simple damping devices. Baffles can be mounted on existing injectors, in order to solve the stability problem with minimum effort and time. The early injectors had baffles consisting of an even number of blades extending radially from a central hub. Later on, baffles have been used in conjunction with injectors having larger orifices in order to gain stability by modifying the combustion process [42].

Attempts made so far to induce artificial pressure perturbations in the combustion chamber of a rocket engine have used pulses of very short duration and sufficient

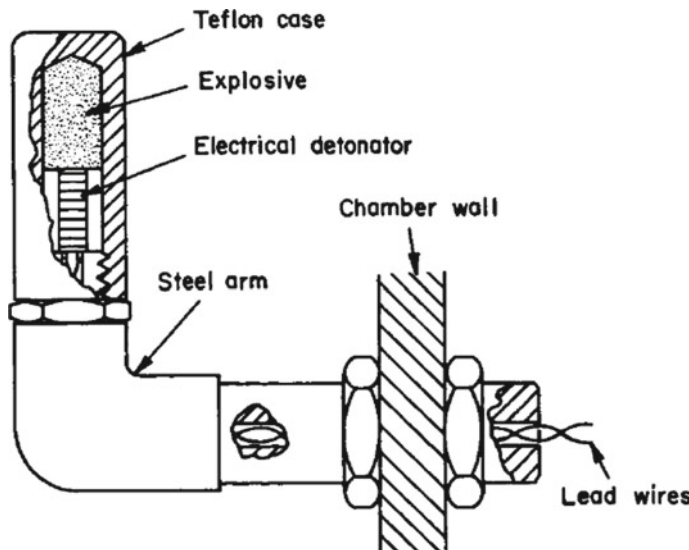
amplitude to excite the acoustic modes of the chamber. Sometimes, these pulses have been provided by explosive devices. Three types of techniques have been used to test the stability of combustion in a rocket engine. They are the inert gas (nitrogen or helium) pulse, the pulse gun, and the non-directional bomb.

The first technique acts as a velocity perturbation to the combustion process, whereas the pulse gun and the non-directional bomb generate perturbations in both pressure and velocity by using explosives. Therefore, the resulting perturbation is of the triggered (or induced) type. A gas pulse has been used in engines burning liquid oxygen and RP-1. For such engines, this technique has been found effective in producing perturbations triggering sustained instability. A gas pulse has also been used in engines burning nitrogen tetroxide and Aerozine 50 with negligible effects on the combustion.

A pulse gun is a device which resembles a gun. It consists of a breech into which an explosive charge is placed, usually in a cartridge case, a firing mechanism, a barrel, and often a diaphragm to protect the explosive charge from the environment of the combustion chamber of the engine. The barrel of a pulse gun is usually attached to the wall of the combustion chamber of the engine, in order for the pulse to be fired in the tangential direction or in the radial direction. A pulse gun is actuated by a command given to its firing mechanism, which is usually a mechanical detonator acting on the main charge. The explosive charge of a pulse gun contains a mass of gun powder ranging from 194.4 to 259.2 mg, but may also contain a mass as high as 6480 mg of high explosive. A typical pulse gun is shown in the following figure, due to the courtesy of NASA [42].



A non-directional bomb mounted on the wall of a combustion chamber is shown in the following figure, also due to the courtesy of NASA [42].



It consists of three principal parts, which are an explosive charge (for example, RDX), a detonator which may be commanded either by the rocket gases or by an electric signal, and a case which insulates the explosive charge and the detonator from the environment of the rocket engine and also contains the explosive charge. Unlike an inert gas pulse and a pulse gun, a non-directional bomb is usually mounted inside the combustion chamber and is not restricted to a location on the wall. Pulse guns and non-directional bombs can induce pressure perturbations ranging from 10 to 500% of the normal value in the combustion chamber. In the development of liquid-propellant rocket engines, non-directional bombs are the type of device most frequently used to induce pressure perturbations in the combustion chamber.

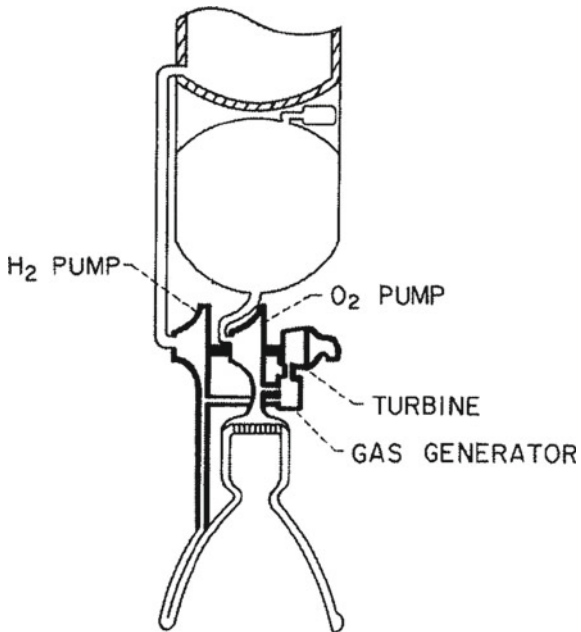
1.7 Principal Components of a Liquid-Propellant Rocket Engine

A liquid-propellant rocket vehicle is composed of the following essential parts:

- propulsion system;
- structure of the vehicle;
- guidance system;
- payload; and
- accessories.

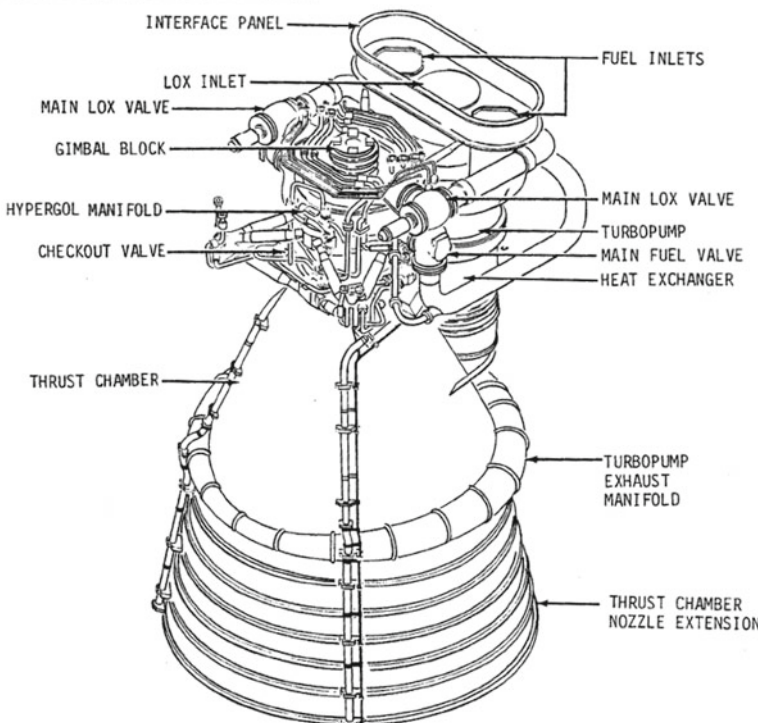
This book deals only with the propulsion system and its parts. The parts of the propulsion system considered here include only those which are strictly necessary to generate thrust and keep it in the desired direction. Therefore, the tanks and their

accessory parts are included in the number. The following figure, due to the courtesy of NASA [44], shows a scheme of the propulsion system of a typical liquid-bi-propellant engine fed by turbo-pumps.



The following figure, also due to the courtesy of NASA [45], shows the principal components of the F-1 engine, used in the first stage of the Saturn V.

F-1 ENGINE MAJOR COMPONENTS



The propulsion system of a liquid-propellant rocket vehicle is composed of the following principal parts:

- a thrust chamber assembly;
- a feed system for the propellants, including a gas pressurising system;
- valves and other systems of propellant control;
- tanks containing the fuel and the oxidiser; and
- interconnecting components and structures.

The design of each of these parts will be shown in a specific chapter.

References

1. NASA, Jet Propulsion Laboratory, California Institute of Technology, Basics of space flight. <http://www2.jpl.nasa.gov/basics/index.php>
2. Crown JC (1948, June) Supersonic nozzle design, NACA Technical Note No. 1651, NACA, Washington, D.C., 35pp. <https://ntrs.nasa.gov/archive/nasa/casi.ntrs.nasa.gov/19930082268.pdf>

3. Greene W (2012) J-2X progress: the next phase for E10001, NASA, 3 Feb 2012. <https://blogs.nasa.gov/J2X/tag/convergent-divergent-nozzle/>
4. Huzel DK, Huang DH (1967) Design of liquid propellant rocket engines. NASA SP-125, NASA, Washington, D.C., 472pp. <https://ntrs.nasa.gov/archive/nasa/casi.ntrs.nasa.gov/19710019929.pdf>
5. NASA, Glenn Research Centre, Bernoulli Equation. <https://www.grc.nasa.gov/www/k-12/airplane/bern.html>
6. Sutton GP, Biblarz O (2001) Rocket propulsion elements, 7th edn. Wiley, New York. ISBN 0-471-32642-9
7. Liepmann HF, Puckett AE (1947) Introduction to aerodynamics of a compressible fluid. Wiley, New York
8. Hill PG, Peterson CR (1992) Mechanics and thermodynamics of propulsion, 2nd edn. Addison-Wesley, Reading, Massachusetts. ISBN 0-201-14659-2
9. Braeunig RA Rocket and space technology—rocket propellants. <http://braeunig.us/space/propel.htm>
10. Braeunig RA Rocket and space technology—rocket propulsion. <http://braeunig.us/space/propuls.htm>
11. Aerojet Rocketdyne, RS-25 Engine. <https://www.rocket.com/rs-25-engine>
12. Aerojet Rocketdyne, RL10 engine. <http://www.rocket.com/rl10-engine>
13. NASA (1968, December) Saturn V news reference, J-2 engine fact sheet. https://www.nasa.gov/centers/marshall/pdf/499245main_J2_Engine_fs.pdf
14. Astronautix. <http://www.astronautix.com/f/f-1.html>
15. Nufer BM (2009, June) A summary of NASA and USAF hypergolic propellant related spill and fires. NASA/TP-2009-214769, 112pp. <https://ntrs.nasa.gov/archive/nasa/casi.ntrs.nasa.gov/20090029348.pdf>
16. IOK (Own work) [Public domain], via Wikimedia Commons. https://upload.wikimedia.org/wikipedia/commons/4/4c/Nozzle_de_Laval_diagram.svg
17. NASA/Tom Farrar, Scott Haun, Raphael Hernandez. https://www.nasa.gov/mission_pages/shuttle/flyout/multimedia/discovery/2007-10-23.html
18. Gerald CF, Wheatley PO (1984) Applied numerical analysis. Addison-Wesley, Reading. ISBN 0-201-11577-8
19. Buchheim RW et al (1959) Space handbook: astronautics and its applications. United States Government, Printing Office, Washington, D.C. <http://history.nasa.gov/conghand/propelnt.htm>
20. Lohner KA, Scherson YD, Lariviere BW, Cantwell BJ, Kenny TW (2008) Nitrous oxide mono-propellant gas generator development. Stanford University, 13pp. http://web.stanford.edu/~cantwell/Recent_publications/Lohner_Scherson_JANNAF_2008.pdf
21. Kitson BA, Oliaee SN (2016) Selective, catalytic decomposition of hydrazine, 29 Apr 2016. Honours Research Projects, 286, 25pp. http://ideaexchange.uakron.edu/honors_research_projects/286
22. Greene WD (2013) Inside the LEO doghouse, start me up! NASA, 19 Dec 2013. <https://blogs.nasa.gov/J2X/2013/12/19/inside-the-leo-doghouse-start-me-up/>
23. Spores RA, Masse R, Kimbrel S, McLean C (2013) GPIM AF-M315E propulsion system. In: 50th AIAA/ASME/SAE/ASEE joint propulsion conference & exhibit, 28–30 July 2013, Cleveland, Ohio, USA, 12pp. <https://ntrs.nasa.gov/archive/nasa/casi.ntrs.nasa.gov/20140012587.pdf>
24. Park J, Chakraborty D, Lin MC (1998) Thermal decomposition of gaseous ammonium dinitramide at low pressure: kinetic modelling of product formation with ab initio MO/cVRRKM calculations. In: Twenty seventh symposium (international) on combustion/The Combustion Institute, pp 2351–2357. <http://www.chemistry.emory.edu/faculty/lin/ref/adn.pdf>
25. Sjöberg P, Skifs H, Thormählen P, Anflo K (2009) A stable liquid mono-propellant based on ADN. In: Insensitive munitions and energetic materials technology symposium, Tucson, USA, 11–14 May 2009. <http://www.dtic.mil/cgi-bin/GetTRDoc?Location=U2&docname=GetTRDoc.pdf&docid=GetTRDoc/GetTRDoc.pdf&CategoryID=6&DocumentID=1>

26. Sanders JC, Wenzel LM (1962) Dynamics and control of chemical rockets. In: Proceedings of the NASA-university conference on the science and technology of space exploration, vol 2. NASA SP-11, Chicago, Illinois, USA, 1–3 November 1962, pp 53–56. <http://www.dtic.mil/dtic/tr/fulltext/u2/a396443.pdf>
27. Dougherty NS Jr, Rafferty CA (1969, February) Altitude developmental testing of the J-2 rocket engine. AEDC-TR-68-266, 261pp. <http://www.dtic.mil/get-tr-doc/pdf?AD=AD0848188>
28. NASA, Human space flight, Space Shuttle main engines. <https://spaceflight.nasa.gov/shuttle/reference/shutref/orbiter/prop/engines.html>
29. Varghese PL (1988, January) Investigation of energy transfer in a NASA standard initiator. NASA-CR-184673, 31pp. <https://ntrs.nasa.gov/archive/nasa/casi.ntrs.nasa.gov/19890005798.pdf>
30. Turner MJL (2006) Rocket and spacecraft propulsion, 2nd edn. Springer, Berlin. ISBN 3-540-22190-5
31. Anonymous (1994, December) DOE Handbook, Primer on spontaneous heating and pyrophoricity. DOE-HDBK-1081-94, U.S. Department of Energy, Washington, D.C., U.S.A. <http://www.hss.energy.gov/nuclearsafety/ns/techstds/standard/hdbk1081/hdbk1081.pdf>
32. Anonymous, Pyrophoric materials, handling Pyrophoric and other air/water reactive materials. University of Illinois. <https://www.drs.illinois.edu/SafetyLibrary/PyrophoricMaterials>
33. Jonash ER, Tomazic WA (1962) Current research and development on thrust chambers. In: Proceedings of the NASA-university conference on the science and technology of space exploration, vol 2. NASA SP-11, Chicago, Illinois, 1–3 Nov 1962, pp 43–52. <http://www.dtic.mil/dtic/tr/fulltext/u2/a396443.pdf>
34. Davis ML, Allgeier RK Jr, Rogers TG, Rysavy G (1970) The development of cryogenic storage systems for space flight. NASA SP-247, 132pp. <https://ntrs.nasa.gov/search.jsp?R=19710021434>
35. Aerojet Rocketdyne, Titan liquid rocket engine. <http://www.rocket.com/titan-liquid-rocket-engine>
36. Aerojet Rocketdyne, Delta II stage 2 engine. <http://www.rocket.com/delta-ii-stage-2-engine>
37. Technical University of Delft. https://blackboard.tudelft.nl/bbcswebdav/users/bzandbergen/LVC/Launch%20Vehicle%20Catalogue/Fiches/ARIANE_42_L.pdf
38. Spaceflight101, India's most-powerful rocket successfully reaches orbit. <https://spaceflight101.com/gslv-mk3-d1/gslv-mk-iii-first-orbital-launch-success/>
39. Clark JD (1972) Ignition!: an informal history of liquid rocket propellants. Rutgers University Press, New Brunswick, New Jersey. ISBN 0-8135-0725-1
40. Dickinson LA (1964) Technical problems in the production of solid and liquid propellants, Stanford Research Institute. In: Casci C (ed) Fuels and new propellants, pp 265–280, Proceedings of the conference held in Milan by Federazione Associazioni Scientifiche e Tecniche and sponsored by Consiglio Nazionale delle Ricerche, Elsevier. ISBN 978-1-4831-9829-3
41. Rapp DC (1990) High energy-density rocket fuel performance. NASA-CR-185279, 1st July 1990. <https://ntrs.nasa.gov/archive/nasa/casi.ntrs.nasa.gov/19900019426.pdf>
42. Harrje DT, Reardon FH (eds) (1972, January) Liquid propellant rocket combustion instability. NASA SP-194, 657pp. <https://ntrs.nasa.gov/archive/nasa/casi.ntrs.nasa.gov/19720026079.pdf>
43. Culick FE, Kuentzmann P (2006, December) Unsteady motions in combustion chambers for propulsion systems. NATO, RTO AGARDograph AG-AVT-039, 663pp. ISBN 978-92-837-0059-3. <https://apps.dtic.mil/dtic/tr/fulltext/u2/a466461.pdf>
44. Hartmann MJ, Ball CL (1962) New problems encountered with pumps and turbines. In: Proceedings of the NASA-university conference on the science and technology of space exploration, vol 2, NASA SP-11, Chicago, Illinois, USA, 1–3 Nov 1962, pp 23–35. <http://www.dtic.mil/dtic/tr/fulltext/u2/a396443.pdf>
45. Anonymous (1968, November) Saturn V flight manual SA 503, Technical Manual MSFC-MAN-503, NASA TM X-72151, 243pp. <https://ntrs.nasa.gov/archive/nasa/casi.ntrs.nasa.gov/19750063889.pdf>

Chapter 2

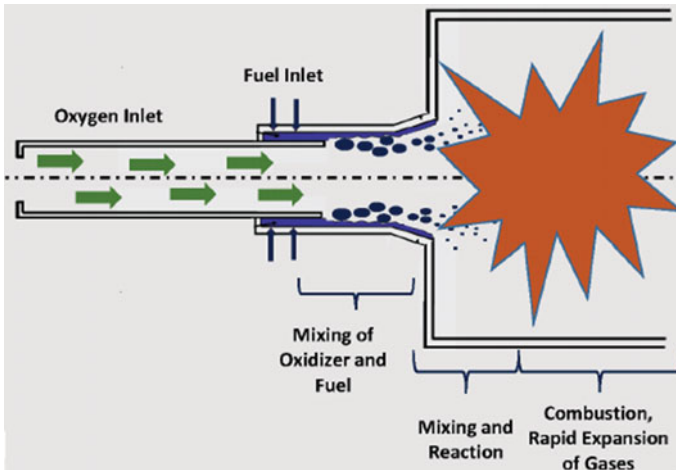
The Thrust Chamber Assembly



2.1 The Principal Components of a Thrust Chamber

The thrust chamber of a rocket engine comprises essentially a combustion chamber and a nozzle. This is the part of the engine in which the chemical energy of the propellants is converted into the kinetic energy of the combusted gas.

The following figure, due to the courtesy of NASA [1], is a simple scheme of the phenomena which take place in and near each element of an injector.



For a liquid bi-propellant rocket engine, the combustion process has been shown in Chap. 1, Sect. 1.5. It is summarised below for convenience of the reader.

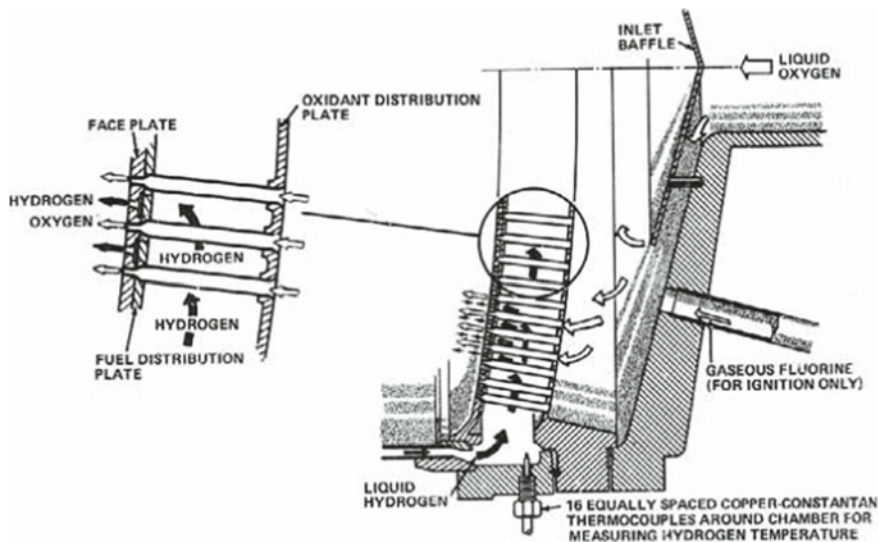
- (1) Firstly, the fuel and the oxidiser are injected, in the proper mixture ratio, into the combustion chamber through the elements of the injector, as shown in the preceding figure. The injection velocity ranges from about 7 to 60 m/s [2]. The droplets of the two propellants may either mix together in form of a spray or go separately into the combustion chamber.
- (2) Then, the high temperature existing in the combustion chamber causes the droplets to vaporise.
- (3) Then, the vaporised combination of fuel and oxidiser is further heated and burns at its stoichiometric mixture ratio, causing a continuous increase in mass flow rate in the combustion chamber. The combustion is aided by the high velocity of the molecules within the combustion chamber, and takes place completely upstream of the throat plane. Care must be taken by the designer in order for the combustion process to be stable, that is, free from shocks and detonation waves in the combustion front.
- (4) Finally, the combusted gas flows in the converging portion of the nozzle. The velocity of the gas increases in subsonic conditions ($M < 1$) and reaches the sonic value ($M = 1$) at the throat plane of the nozzle. The subsequent passage through the diverging portion of the nozzle causes the velocity of the gas molecules to increase further in supersonic conditions ($M > 1$). The combusted gas is then ejected from the thrust chamber through the exit plane of the nozzle.

The principal components of a thrust chamber are the injector including the propellant inlets and distributing manifolds, the ignition device (which is necessary in case of a rocket engine burning non-hypergolic propellants), the combustion chamber, the converging portion of the nozzle between the inlet plane and the throat, and the diverging portion of the nozzle between the throat and the exit plane. The following figure, due to the courtesy of NASA [3] shows a thrust chamber assembly comprising the injector (left) and the combustion chamber including the converging portion of the nozzle (right), for a rocket engine whose propellants are methane and liquid oxygen.



The combustion chamber illustrated in the preceding figure is a body of tubular shape. The cross-section narrows in the converging portion of the nozzle and reaches its minimum value at the throat. The diverging portion of the nozzle is usually bell-shaped, in order to allow the combusted gas to expand towards the exit section.

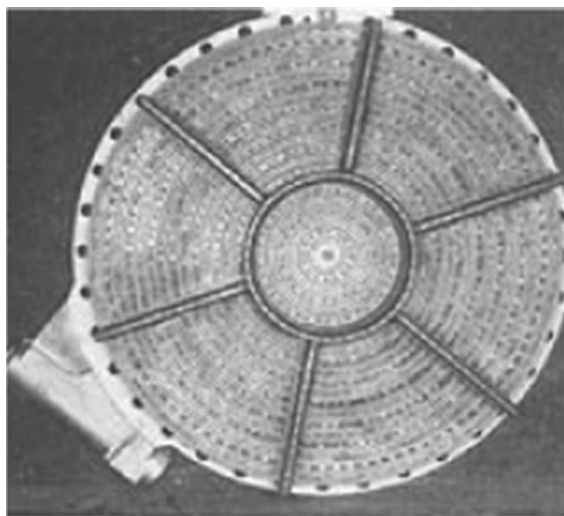
The injector has the purpose of distributing the propellants into the combustion chamber at the proper mixture ratio, pressure, and spray pattern, in order to initiate and sustain a stable combustion. A cutaway view of the injector used in the thrust chamber of a rocket engine burning liquid hydrogen and liquid oxygen (with gaseous fluorine for ignition only) is shown in the following figure, due to the courtesy of NASA [4].



The particular injector shown above is of the shower-head type (described in Sect. 2.6), where both the fuel and the oxidiser injection holes are drilled at angles which allow the convergent streams of the propellants to meet at a common point placed at a given distance from the injector face.

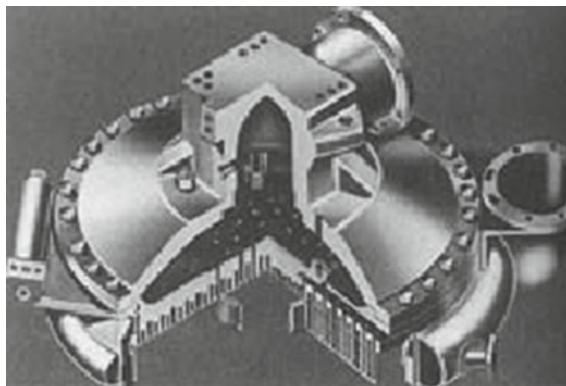
Generally speaking, an injector is a round plate, having a honeycomb structure, with circular and radial inner passages, leading to drilled orifices. It is usually made of steel with nickel-plated surfaces, and is held in position at the fuel manifold below the liquid oxygen dome by means of high-strength bolts [5].

The following figure, due to the courtesy of NASA [6], shows the injector plate used for the Rocketdyne H-1 engine, which was used for the S-I and S-IB first stages of the Saturn I and Saturn IB rockets.



The seals between the injector and the body of the thrust chamber are of the O-ring type, made of rubber selected for compatibility with the fuel. The H-1 engine cited above burns liquid oxygen and RP-1 (kerosene). A threaded hole is provided in the centre of the injector face to permit the installation of the igniter. The fuel and the oxidiser are kept separate by the distribution system. The injection orifices may be arranged at angles such that the impingement angles should be either equal (uni-planar impingement) or different (multi-planar impingement) for the two propellants.

The following figure, due to the courtesy of NASA [6], shows the liquid oxygen dome, which is bolted in position above the injector. This figure relates to the same H-1 engine indicated above.



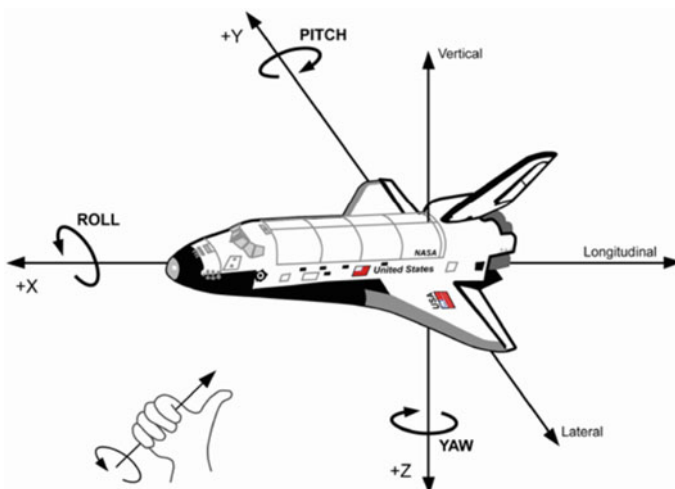
The liquid oxygen dome provides the inlet to the liquid oxygen, and is also the attachment interface between the thrust chamber and the vehicle. It is a single-piece, aluminium alloy die forging. The liquid oxygen dome and the injector have flanges

which are sealed by a spirally wound gasket made of stainless steel strips with non-asbestos fillers (aramid or graphite fibres). The type of gasket used depends on the range of temperature in working conditions. For thrust-vector-controlled engines, as is the case, for example, with the Rocketdyne J-2 engine, the liquid oxygen dome also serves as a mount for the gimbal bearing. The thrust vector control of rocket engines will be considered in Sect. 2.2.

Finally, the pyrotechnic igniter of an engine is fired electrically, and is fixed to the injector surface by means of a threaded joint. It is designed for a single start, and must therefore be replaced after each firing. Igniters of this and other types will be described and illustrated at length in Sect. 2.8.

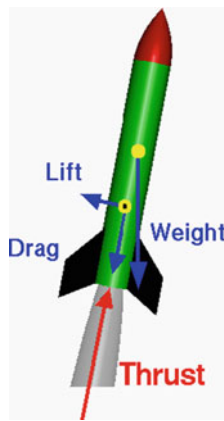
2.2 The Design of a Thrust Chamber for Thrust Vector Control

The present paragraph concerns the methods used to control the direction of the thrust vector in a rocket or spacecraft. These methods are considered here in view of their bearing on the design of a thrust chamber, as will be shown below. By thrust vector control we mean the ability of a space vehicle to deflect the direction of the thrust away (that is, at an angle, θ , other than zero) from the longitudinal axis of the vehicle. The following figure, due to the courtesy of NASA [7], shows the principal axes of inertia and the rotations in roll, pitch and yaw for the Space Shuttle.



The necessity of this control arises from several causes. First, an intentional change of the direction of the flight path followed by the centre of mass of the vehicle. Second, an intentional change of attitude (or rotation) of the vehicle about one or more of

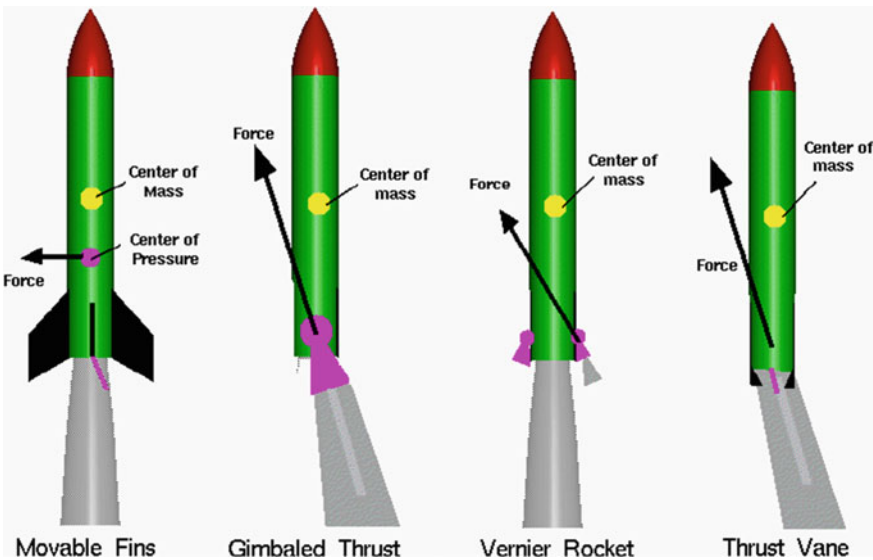
the principal axes of inertia passing through its centre of mass. Third, a correction of either the flight path or the attitude which becomes necessary in order for the vehicle to maintain the desired trajectory and orientation. Fourth, a correction of the misalignment between the thrust vector and the gravity force vector. As to the last issue, the thrust vector is applied to the nozzle of the vehicle, whereas the gravity force vector is applied to its centre of gravity, as shown in the following figure, due to the courtesy of NASA [8].



In order for the vehicle not to be subject to unwanted torques, the directions of the thrust and weight vectors must be aligned at π radians (180°). A rocket is also subject, when flying through the atmosphere, to aerodynamic forces (lift and drag), which are applied to its centre of pressure, not to its centre of gravity, as shown in the preceding figure.

These forces produce moments about the principal axes of inertia of the vehicle. These moments, in turn, cause the vehicle to rotate about its centre of gravity. For a stable flight, the centre of gravity of a rocket must be above its centre of pressure. The longitudinal axis of the rocket, or the line joining the tip of the nose with the centre of the exit section of the nozzle, is called the roll axis, and a motion of the rocket about the roll axis is called a rolling motion. The centre of gravity of the rocket lies along the roll axis. The pitch and yaw axes are mutually perpendicular and form a plane passing through the centre of gravity and perpendicular to the roll axis. Pitch moments tend to either lower or raise the nose of the rocket. Yaw moments cause the nose to move from side to side.

Both mechanical and aerodynamic methods can be used to re-direct the rocket thrust and provide the necessary steering forces. Some of such methods use static fins, movable fins, jet vanes, jetelevators, canards, gimballed (that is, swivelled) nozzles, Vernier rockets, fuel injectors, and attitude-control rockets, as shown in the following figure, due to the courtesy of NASA [9].

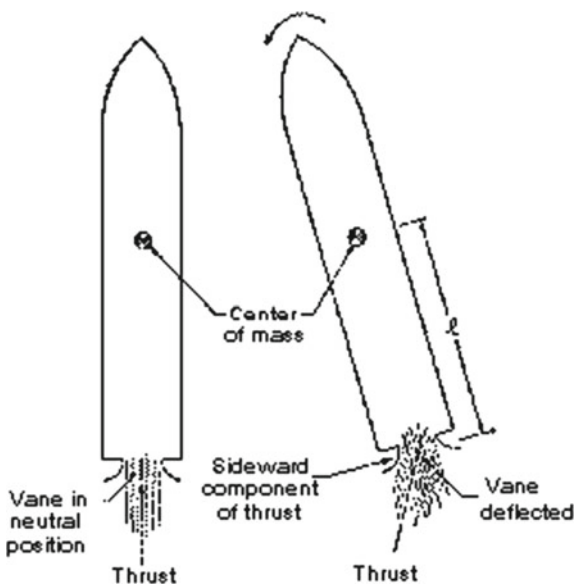


As long as a rocket travels in the atmosphere, static fins at the tail of the rocket can generate aerodynamic forces which act at the centre of pressure and generate moments about the centre of gravity. These moments oppose the deflection of the rocket in the directions of the pitch and yaw axes. Of course, the static fins must be so sized as to generate the amount of aerodynamic forces required to counteract the deviations. On the other hand, the fins generate further drag, in the direction opposed to the rocket velocity vector. In spite of that, aerodynamic fins, be they fixed or movable, are very effective for controlling a vehicle flying through the atmosphere. They continue to be used in weather rockets, anti-aircraft missiles, and air-to surface missiles.

Generally speaking, a thrust vector control system used in a rocket may be either passive or active. A passive control system is a fixed device meant to stabilise a rocket by its very presence on the outside of the rocket. An example of such a device is a cluster of fins mounted around the lower end of a rocket, near the nozzle. The purpose of the fins is to keep the centre of pressure below the centre of gravity of the rocket.

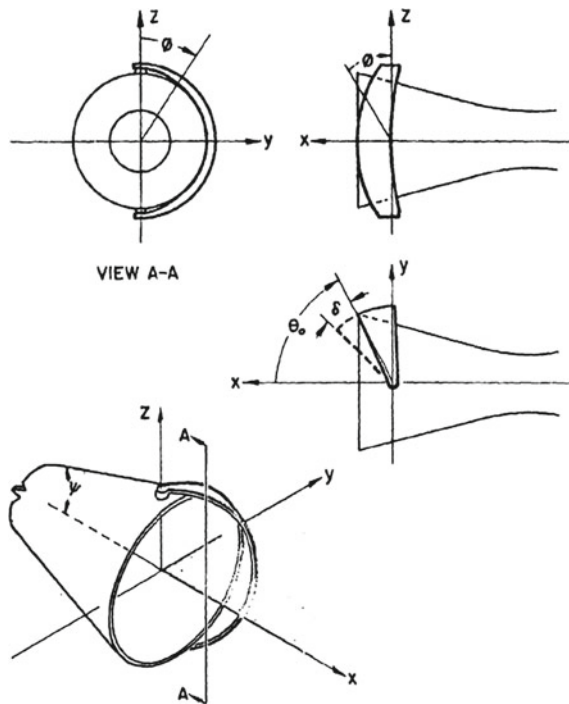
In order to overcome the disadvantages (higher drag and mass) of the fins, active control systems have been developed. They are described below.

Jet vanes and movable fins are planar surfaces, which are used in the jet stream of a rocket to deflect the exhaust gases. They are shown in the following figure, due to the courtesy of NASA [10].

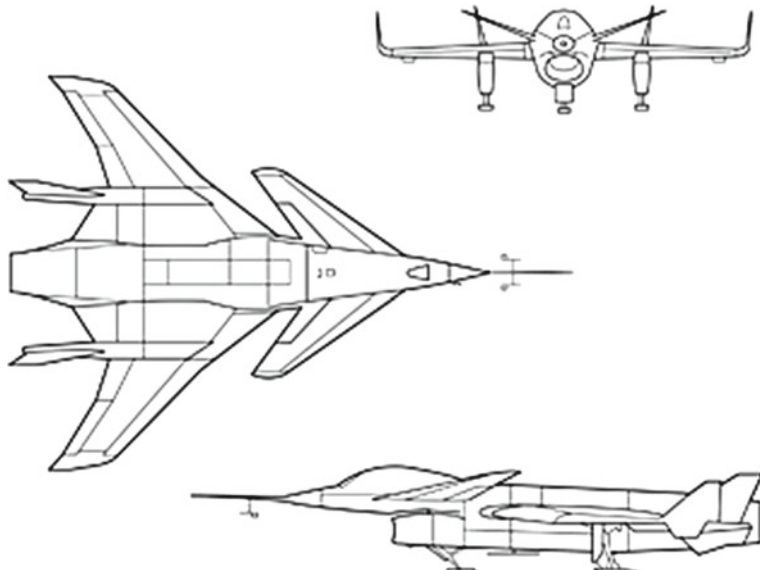


Thrust vanes have been employed on the V-2 and Redstone missiles to deflect the exhaust gas jet of the main propulsion motors by carbon vanes.

Jetelevators, which are shown in the following figure, due to the courtesy of Lockheed [11], are control surfaces which can be moved into or against the jet stream of a rocket, in order to change the direction of the jet flow. The jetelevator invented by Dr. Willy Fiedler is a solid ring with a spherical inside surface which is hinged over the rocket nozzle [12, page 52]. This device, which was used in the A1 version of the Polaris missile and then replaced by rotatable nozzles in the A2 version, deflects the flow when turned into the exhaust stream. It has the advantage of not causing propulsion losses when in the neutral position, since, unlike vanes, it does not interfere with the exhaust flow [10]. The same device has also been described by Edwards and Parker as a semi-spherical shell hinged to a rocket nozzle and rotated, at the command of a sensing unit, into the exhaust flow to produce a control force. Jetelevators have been most frequently applied to control the direction of thrust of solid-propellant rockets [10].

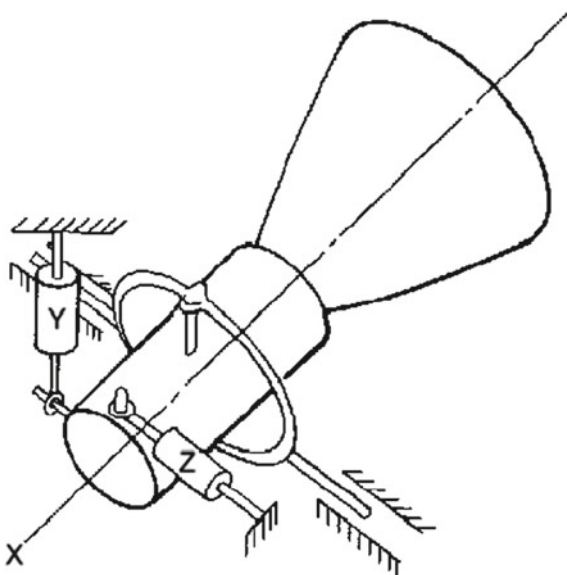


Canards are fore-plane surfaces mounted on the front end of a rocket or aircraft. The following figure, due to the courtesy of NASA [13], shows such surfaces.



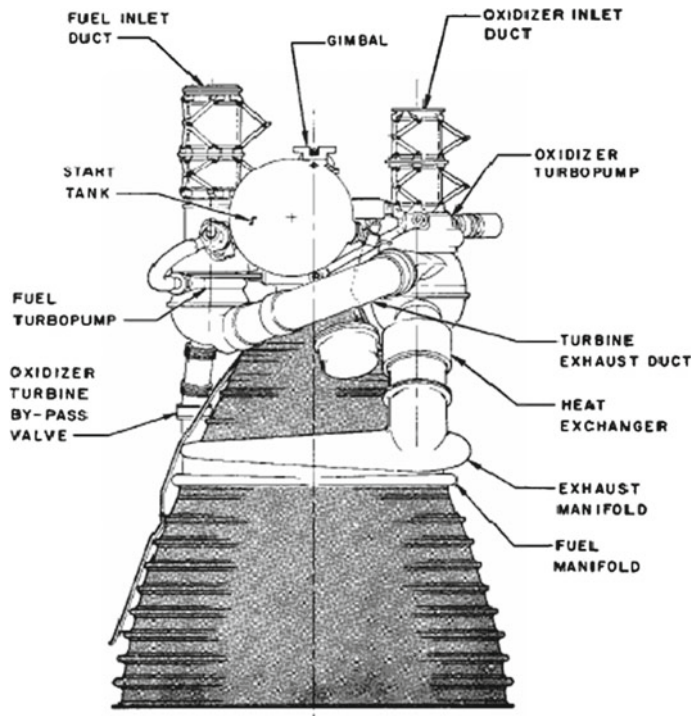
Movable fins and canards are quite similar to each other in appearance. The only real difference is their location on the rocket, because canards are mounted on the front end, whereas the movable fins are at the rear end. In flight, both of them tilt as rudders to deflect the air flow and cause the rocket to correct its course, in the event of unwanted directional changes being detected by motion sensors [14].

Another method for changing the direction of the exhaust gases, and hence the direction of the rocket, is to gimbal the nozzle. For this purpose, the engine can be mounted in a two-axis ring-suspension system, as shown in the following figure, due to the courtesy of NASA [15]. This figure, which relates to the engine gimbal system of the Viking Orbiter 1975, shows the two actuators mounted along directions parallel to, but not coincident with, respectively, the pitch axis (Y) and the yaw axis (Z) of the vehicle. This is because the origin of the roll, pitch, and yaw axes is the centre of mass of the vehicle.



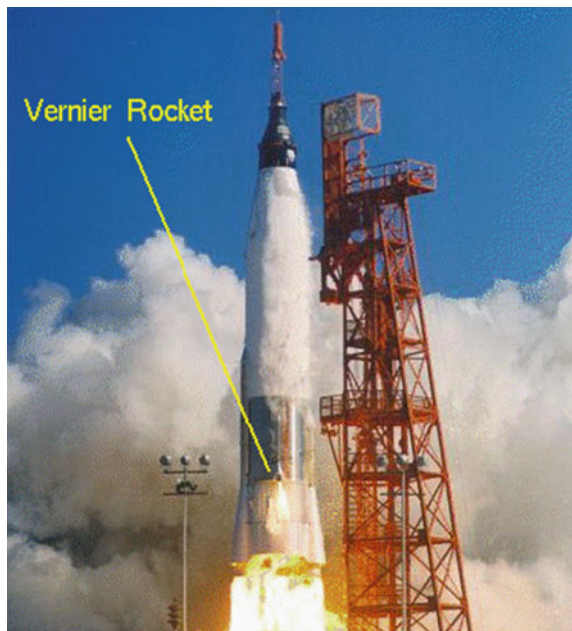
The Viking 1 orbiter (NSSDCA/COSPAR ID: 1975-075A) was launched from Cape Canaveral on the 20th of August 1975. The propulsion of the Viking 1 orbiter was furnished by a bi-propellant (monomethyl hydrazine, CH_3NHNH_2 , and nitrogen tetroxide, N_2O_4) liquid-fuelled rocket engine which could be tilted up to $\pi/20$ rad (9°). Attitude control during engine burns was provided in roll (X -axis) by the attitude control system (using 12 small compressed-nitrogen gas jets located at the solar panel tips), and in pitch and yaw by an autopilot which commanded the engine gimbal system shown above [16].

Another type of gimbal system, relating to the Rocketdyne J-2 engine, is shown at the top of the following figure, due to the courtesy of NASA [17].

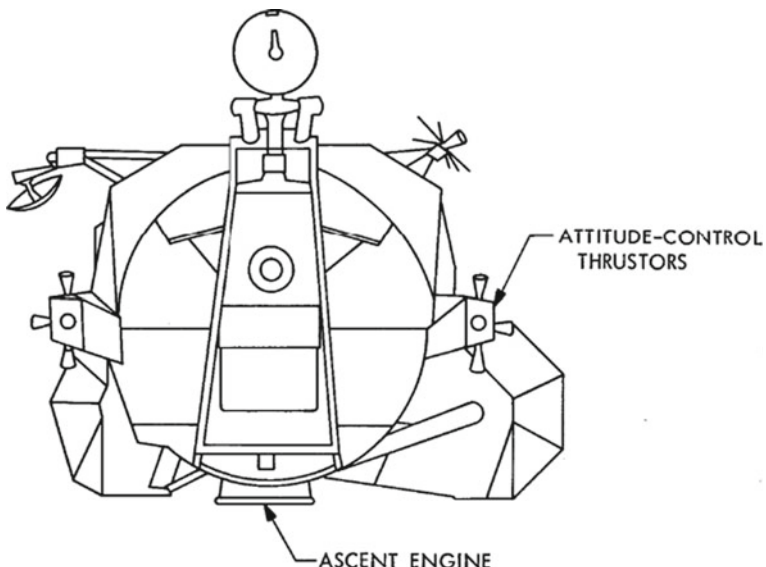


This type of gimbal system has a highly loaded ($1.38 \times 10^8 \text{ N/m}^2$) universal joint which is a spherical, socket-type bearing with a Teflon®/fibreglass composition coating which provides a dry, low friction bearing surface. It also has a lateral adjustment device for aligning the thrust chamber with the vehicle. This gimbal system transmits the thrust from the injector assembly to the thrust structure of the vehicle, and provides a pivot bearing for deflection of the thrust vector. As shown in the preceding figure, the gimbal is mounted on the top of the injector and liquid oxygen dome assembly [17]. This gimbal bearing system has been used in the Saturn V rocket and in the Space Shuttle [14]. In a gimballed thrust control system, the nozzle of the rocket can be swivelled from side to side. As the nozzle direction is deflected away from the axis of symmetry of the rocket, so does the direction of the thrust change with respect to the centre of gravity of the vehicle.

In a Vernier thrust control system, small rockets are mounted on the outside of the main thruster. In case of need, such rockets are fired in the proper direction, in order to produce the desired course change [14]. The following figure, due to the courtesy of NASA [18], shows a Vernier rocket mounted on the outside of the Atlas rocket.



Attitude-control rockets, shown below, are used to trim misalignments of the translational thruster, the basic attitude control with respect to the body principal axes being provided by a separate set of thrusters.



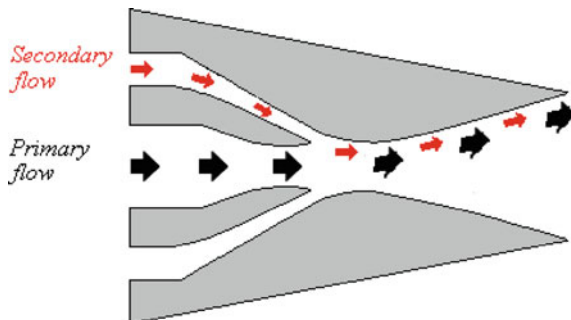
By so doing, the main engine is used only for the motion of the centre of mass of the vehicle. Attitude-control rockets are used in the coasting phase of flight. For this

purpose, clusters of small rockets are mounted all around a space vehicle. By firing these small rockets in the proper combination, it is possible to turn the vehicle in the desired direction. After the vehicle has been aimed as required, the main engine is fired, in order to send the vehicle in the new direction. For example, the ascent stage of the Apollo Lunar Module used a fixed, high-thrust engine for translation and a series of small liquid-propellant rockets for attitude control, as shown in the preceding figure, which is due to the courtesy of NASA [19].

The methods described above use, all of them, mechanical means to control the direction of the thrust vector. They require actuating components which must work efficiently in the high-temperature environment of the rocket exhaust and are invariably associated with a loss of axial thrust when performing manoeuvres of thrust vector control [20].

Other methods use fluidic means to perform the same function. These methods use a static nozzle and the injection (or the removal) of a secondary flow into (or from) the region between the primary flow and the nozzle, which generates the thrust, and the nozzle. They do not require any kinematic structure and mechanical actuators. There is a variety of methods based on fluidic thrust vectoring, which differ one from the other by the way in which the secondary flow is used for thrust vector control. They may be classified as follows.

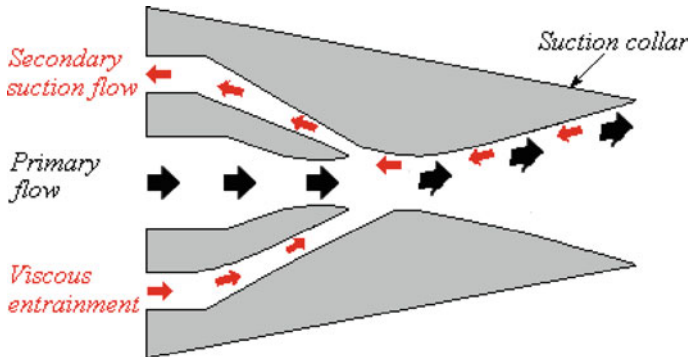
- Co-flow for fluidic thrust vectoring, which is based on the Coanda effect. The Coanda effect (so named after the Romanian engineer Henri-Marie Coanda) is the phenomenon in which a stream of fluid, ejected at high speed from a slot and coming in contact with a convexly curved surface, adheres to that surface along its curvature rather than continue to travel in a straight line.



In other words, the stream is deflected from the axis of flow and follows the slope (or curvature) of a divergent wall whilst increasing in velocity and in mass by entraining additional fluid [21]. This happens because of the increase in the flow velocity over the curved surface, which causes pressure to decrease. The low pressure causes not only the injected co-flow but also the primary flow to be deflected off the nozzle axis toward the divergent wall, as shown in the preceding figure, where the

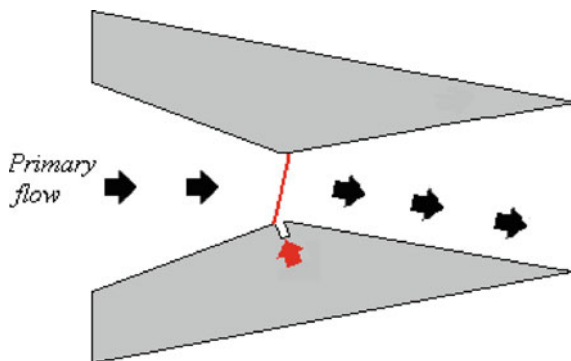
black arrows represent the primary flow, and the red arrows represent the injected co-flow. Of all the fluidic methods for controlling the thrust vector, the co-flow method has been found [22] to be the one which produces the smallest deflection angle.

- Counter-flow for fluidic thrust vectoring, which is also based on the Coanda effect to deflect the thrust vector, as shown in the following figure.

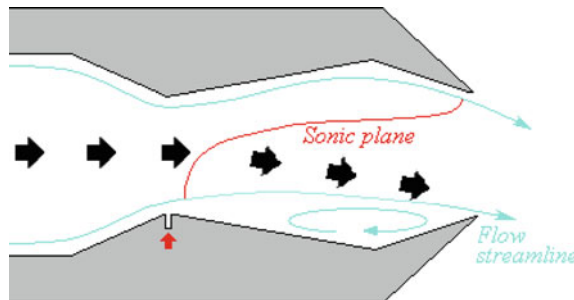


Strykowski et al [23] have shown that the thrust due to a jet stream can be continuously deflected to at least 0.2793 rad (16°) by creating a secondary counter-flowing stream between the primary jet and an adjacent curved surface. For this purpose, suction is applied asymmetrically between the trailing edge of a primary nozzle and an aft suction collar. This creates a low-pressure region along the suction collar, and causes the primary jet to turn [24]. The results found by Strykowski et al. [23] at Mach 2 show that the thrust loss is less than 4% and the required mass flow rates are less than approximately 2% of the primary jet. A co-flow, due to the viscous entrainment generated by the primary flow, takes place at the wall of the suction collar, and interferes with the primary flow. By activating asymmetrically this co-flow, the primary flow is deflected towards the side on which the suction flow is applied, due to the pressure drop which causes the thrust to turn [22].

- Throat-shifting for fluidic thrust vectoring, which is performed by injecting secondary flow at or just upstream of the throat, as shown in the following figure. By so doing, there is no formation of shock waves.

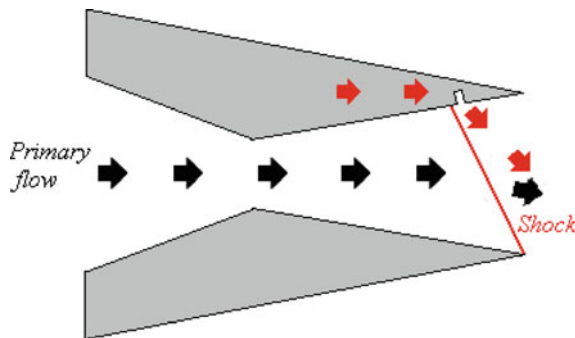


This injection skews the sonic plane and deflects the flow. Another version of this method uses variable recessed cavities, which deflect the primary flow by means of vortices in the cavities, as shown in the following figure.

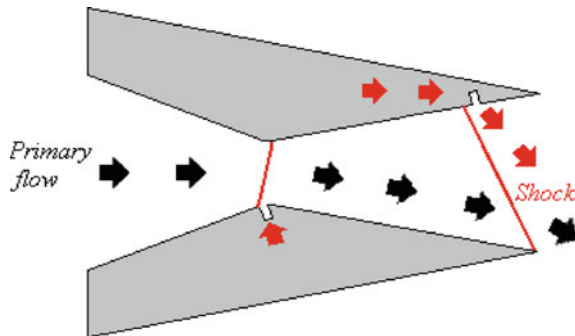


The recessed cavity portion of the nozzle shown above is located between the upstream minimum area and the downstream minimum area of the nozzle itself. The fluidic injection is performed at the upstream minimum area. A simulation study carried out by Deere et al. [25] has shown that substantial thrust-vector angles are obtainable without large penalties in thrust efficiency. This version is a combined method, because the recessed-cavity technique is used in addition to the throat-shifting technique in order to obtain greater performance.

- Shock vector control for fluidic thrust vectoring, which is performed by injecting secondary flow downstream of the throat, as shown in the following figure.



The secondary injected flow acts as a compression ramp in the direction of the primary supersonic flow. This compression induces an oblique shock wave in the diverging portion of the nozzle at some angle with respect to the direction of the primary flow. The primary flow, when interacting with the oblique shock wave, turns away from the axis of symmetry of the nozzle. This turn changes the direction of the thrust vector. By so doing, the direction of the primary flow does not change in the vicinity of the throat. The shock vector control may also be combined with the throat shifting, by using two ports instead of one to inject the secondary flow into the nozzle, as shown in the following figure.



The aerospace vehicles which use fluidic instead of mechanical thrust vectoring methods have the advantages of being lightweight, free from moving parts, less expensive, easy to integrate, and less detectable by radars, the last advantage being of particular interest in military applications. On the other hand, they must be designed from the outset as such, and existing vehicles currently in use cannot be retrofitted. In addition, their capability of directional change is often held to be lower than that of vehicles using mechanical thrust vectoring. On the last issue, Strykowski et alii [23] have obtained a thrust vector angle of 0.2793 rad (16°) by using the counter-flow technique described above, and Wing and Giuliano [26] have obtained a value of up to $\pi/10 \text{ rad}$ (18°) for this angle, by using the shock vector control technique. Such values are by no means small in comparison with those cited by Sutton and Biblarz [2, page 611], Table 16.1 for mechanical thrust vectoring systems. They are

lower only than the value of $\pi/9$ rad (20°), relating to the movable nozzle (rotary ball with gas seal). Another disadvantage of the fluidic thrust vectoring methods has been found in their need for a source of secondary flow. In the event of that source being the same as that of the primary flow which generates the thrust, it has been argued, the performance of the vehicle would decrease, at least in the phase of thrust vector control. As to the loss in performance, Strykowski et al. [23] have found, at Mach 2, a thrust loss lower than 4%, with the required mass flow rates being lower than approximately 2% of the primary jet. Consequently, the only strong disadvantage of the fluidic thrust vectoring methods seems to us to be the deficiency or insufficiency of data on their behaviour gathered by testing them in flight.

2.3 Performance of a Thrust Chamber

The performance of the thrust chamber of a rocket engine is measured by some indicators, which have been discussed at length in Chap. 1, Sect. 1.3. For convenience of the reader, a list of the principal performance indicators is also given below.

- (1) Specific impulse (I_s)_{tc} of the thrust chamber, which is measured in seconds and is defined by

$$(I_s)_{tc} = \frac{F}{\dot{W}_{tc}} = \frac{c^* C_F}{g_0}$$

where F (N) is the thrust, $\dot{W}_{tc} = g_0 \dot{m}_{tc}$ (N/s) is the weight flow rate of the propellant at the thrust chamber, c^* (m/s) is the characteristic velocity, C_F is the dimensionless thrust coefficient, and $g_0 = 9.80665$ m/s² is the acceleration of gravity of the Earth at the sea level.

- (2) Characteristic velocity c^* , which is measured in m/s and is defined by

$$c^* = \frac{[\gamma R(T_c)_{ns}]^{\frac{1}{2}}}{\gamma \left[\left(\frac{2}{\gamma+1} \right)^{\frac{\gamma+1}{\gamma-1}} \right]^{\frac{1}{2}}}$$

where $(T_c)_{ns} = T_i [1 + \frac{1}{2}(\gamma - 1)M_i^2]$ is the total temperature (K) of the combustion chamber at the nozzle inlet, M_i is the Mach number at the nozzle inlet, $\gamma \equiv c_p/c_v$ is the specific heat ratio of the combusted gas, and R is the constant of the specific gas, that is, the universal gas constant $R^* = 8314.460$ N m kmol⁻¹ K⁻¹ divided by the average molar mass \mathcal{M} (kg/kmol) of the combusted gas. When the propellant combination and its mixture ratio have been chosen, then the specific heat ratio γ

and the constant $R = R^*/\mathcal{M}$ of the combusted gas are also determined within known limits. In these limits, the characteristic velocity depends on the total temperature $(T_c)_{ns}$ of the gas in the combustion chamber at the nozzle inlet.

(3) Thrust coefficient C_F , which is dimensionless and is defined by

$$C_F = \left\{ \frac{2\gamma^2}{\gamma-1} \left(\frac{2}{\gamma+1} \right)^{\frac{\gamma+1}{\gamma-1}} \left[1 - \left(\frac{p_e}{(p_c)_{ns}} \right)^{\frac{\gamma-1}{\gamma}} \right] \right\}^{\frac{1}{2}} + \frac{A_e}{A_t} \left[\frac{p_e - p_0}{(p_c)_{ns}} \right]$$

where $\gamma \equiv c_p/c_v$ is the specific heat ratio of the combusted gas, p_e (N/m^2) is the pressure of the exhaust gas at the exit plane of the nozzle, $(p_c)_{ns}$ (N/m^2) is the total pressure in the combustion chamber at the nozzle inlet, p_0 (N/m^2) is the ambient pressure, and $\varepsilon \equiv A_e/A_t$ is the ratio of the area of the cross-section at the exit plane of the nozzle to the area of the cross-section at the throat. When the performance of the combustion process has been determined, then the value of the first addend on the right-hand side of the preceding equation is known. The value of the second addend depends on the geometric characteristics of the diverging portion of the nozzle, namely, on the expansion ratio $\varepsilon \equiv A_e/A_t$, which determines the pressure ratios $p_e/(p_c)_{ns}$ and $p_0/(p_c)_{ns}$.

As an example, it is required to determine the specific impulse of the thrust chamber, the characteristic velocity, and the thrust coefficient for a rocket, whose first stage has the properties indicated below. The propellant combination is liquid oxygen with RP-1 (kerosene), the oxidiser-to-fuel mixture ratio at the thrust chamber is $olf = 2.35$, the total absolute pressure in the combustion chamber at the nozzle inlet is $(p_c)_{ns} = 6.895 \times 10^6 \text{ N/m}^2$, the total temperature of the combustion chamber at the nozzle inlet is $(T_c)_{ns} = 3589 \text{ K}$, the molar mass of the combusted gas is $\mathcal{M} = 22.5 \text{ kg/kmol}$, the specific heat ratio of the combusted gas is $\gamma \equiv c_p/c_v = 1.222$, and the expansion area ratio of the nozzle is $A_e/A_t = 14$. The atmospheric pressure and the acceleration of gravity at sea level have the standard values $p_0 = 101325 \text{ N/m}^2$ and $g_0 = 9.80665 \text{ m/s}^2$.

The constant of the specific gas results from

$$R = \frac{R^*}{\mathcal{M}} = \frac{8314.460}{22.5} = 369.5 \text{ N m K}^{-1} \text{ kg}^{-1}$$

The static pressure p_e (N/m^2) at the exit section of the nozzle results from the following equation of Chap. 1, Sect. 1.2:

$$\frac{A_e}{A_t} = \frac{\left(\frac{2}{\gamma+1} \right)^{\frac{1}{\gamma-1}} \left(\frac{(p_c)_{ns}}{p_e} \right)^{\frac{1}{\gamma}}}{\left\{ \frac{\gamma+1}{\gamma-1} \left[1 - \left(\frac{p_e}{(p_c)_{ns}} \right)^{\frac{\gamma-1}{\gamma}} \right] \right\}^{\frac{1}{2}}}$$

where $A_e/A_t = 14$, $\gamma = 1.222$, and $(p_c)_{ns} = 6.895 \times 10^6 \text{ N/m}^2$. As has been shown in Chap. 1, Sect. 1.2, the value of p_e can be determined numerically by defining an auxiliary variable $z = p_e/(p_c)_{ns}$ and a function $f(z)$ such that

$$f(z) \equiv 14^2 - \frac{\left(\frac{2}{1.222+1}\right)^{\frac{2}{1.222-1}} \left(\frac{1}{z}\right)^{\frac{2}{1.222}}}{\frac{1.222+1}{1.222-1} \left(1 - z^{\frac{1.222-1}{1.222}}\right)}$$

We search a zero of the function $f(z)$ in the interval $0.007 \leq z \leq 0.008$, because $f(z)$ changes sign in this interval. By using the Müller method shown in Chap. 1, Sect. 1.2, we find, with four significant figures, $z = 0.007538$. Hence, we have $p_e = z(p_c)_{ns} = 0.007538 \times 6.895 \times 10^6 = 5.197 \times 10^4 \text{ N/m}^2$.

The theoretical value c^* of the characteristic velocity results from

$$c^* = \frac{\left[\gamma R(T_c)_{ns}\right]^{\frac{1}{2}}}{\gamma \left[\left(\frac{2}{\gamma+1}\right)^{\frac{\gamma+1}{\gamma-1}}\right]^{\frac{1}{2}}} = \frac{[1.222 \times 369.5 \times 3589]^{\frac{1}{2}}}{1.222 \times \left[\left(\frac{2}{1.222+1}\right)^{\frac{1.222+1}{1.222-1}}\right]^{\frac{1}{2}}} = 1764 \text{ m/s}$$

By introducing a correction factor $\eta_{c^*} = 0.975$, the design value \bar{c}^* of the characteristic velocity results from the theoretical value c^* as follows

$$\bar{c}^* = \eta_{c^*} c^* = 0.975 \times 1764 = 1720 \text{ m/s}$$

The theoretical value C_F of the thrust coefficient at sea level results from

$$C_F = \left\{ \frac{2\gamma^2}{\gamma-1} \left(\frac{2}{\gamma+1} \right)^{\frac{\gamma+1}{\gamma-1}} \left[1 - \left(\frac{p_e}{(p_c)_{ns}} \right)^{\frac{\gamma-1}{\gamma}} \right] \right\}^{\frac{1}{2}} + \frac{A_e}{A_t} \left[\frac{p_e - p_0}{(p_c)_{ns}} \right]$$

After substituting $\gamma = 1.222$, $p_e = 5.197 \times 10^4 \text{ N/m}^2$, $(p_c)_{ns} = 6.895 \times 10^6 \text{ N/m}^2$, $p_0 = 1.013 \times 10^5 \text{ N/m}^2$, and $A_e/A_t = 14$ into the preceding equation, we find $C_F = 1.561$.

By introducing a correction factor $\eta_F = 0.98$, the design value \bar{C}_F of the thrust coefficient at sea level can be computed from the corresponding theoretical value C_F as follows

$$\bar{C}_F = \eta_F C_F = 0.98 \times 1.561 = 1.530$$

By using the design values computed above of, respectively, the characteristic velocity and the thrust coefficient at the sea level, the design value of the specific impulse of the thrust chamber at sea level results from

$$(\bar{I}_s)_{tc} = \frac{\bar{c}^* \bar{C}_F}{g_0} = \frac{1720 \times 1.530}{9.807} = 268.3 \text{ s}$$

In the following example, we want to determine the specific impulse of the thrust chamber, the characteristic velocity, and the thrust coefficient for a rocket, whose second stage burns a combination of liquid oxygen with liquid hydrogen, and has the properties specified below. The oxidiser-to-fuel mixture ratio at the thrust chamber is $of = 5.22$, the total absolute pressure and the total temperature in the combustion chamber at the nozzle inlet are respectively $(p_c)_{ns} = 5.516 \times 10^6 \text{ N/m}^2$ and $(T_c)_{ns} = 3356 \text{ K}$, the molar mass of the combusted gas is $\mathcal{M} = 12 \text{ kg/kmol}$, the specific heat ratio of the combusted gas is $\gamma \equiv c_p/c_v = 1.213$, and the expansion area ratio of the nozzle is $A_e/A_t = 40$. The constant of the specific gas results from

$$R = \frac{R^*}{\mathcal{M}} = \frac{8314.460}{12} = 692.9 \text{ N m K}^{-1} \text{ kg}^{-1}$$

The static pressure p_e (N/m^2) at the exit section of the nozzle results from the following equation of Chap. 1, Sect. 1.2:

$$\frac{A_e}{A_t} = \frac{\left(\frac{2}{\gamma+1}\right)^{\frac{1}{\gamma-1}} \left(\frac{(p_c)_{ns}}{p_e}\right)^{\frac{1}{\gamma}}}{\left\{\frac{\gamma+1}{\gamma-1} \left[1 - \left(\frac{p_e}{(p_c)_{ns}}\right)^{\frac{\gamma-1}{\gamma}}\right]\right\}^{\frac{1}{2}}}$$

where $A_e/A_t = 40$, $\gamma = 1.213$, and $(p_c)_{ns} = 5.516 \times 10^6 \text{ N/m}^2$. By solving numerically the preceding equation for p_e as has been shown in the preceding example, we find $p_e = 1.094 \times 10^4 \text{ N/m}^2$.

The theoretical value c^* of the characteristic velocity results from

$$c^* = \frac{\left[\gamma R(T_c)_{ns}\right]^{\frac{1}{2}}}{\gamma \left[\left(\frac{2}{\gamma+1}\right)^{\frac{\gamma+1}{\gamma-1}}\right]^{\frac{1}{2}}} = \frac{\left[1.213 \times 692.9 \times 3356\right]^{\frac{1}{2}}}{1.213 \times \left[\left(\frac{2}{1.213+1}\right)^{\frac{1.213+1}{1.213-1}}\right]^{\frac{1}{2}}} = 2342 \text{ m/s}$$

By introducing a correction factor $\eta_{c^*} = 0.975$, the design value \bar{c}^* of the characteristic velocity results from the theoretical value c^* as follows

$$\bar{c}^* = \eta_{c^*} c^* = 0.975 \times 2342 = 2284 \text{ m/s}$$

The theoretical value C_F of the thrust coefficient in vacuo ($p_0 = 0$) results from

$$C_F = \left\{ \frac{2\gamma^2}{\gamma-1} \left(\frac{2}{\gamma+1}\right)^{\frac{\gamma+1}{\gamma-1}} \left[1 - \left(\frac{p_e}{(p_c)_{ns}}\right)^{\frac{\gamma-1}{\gamma}}\right] \right\}^{\frac{1}{2}} + \frac{A_e}{A_t} \left[\frac{p_e}{(p_c)_{ns}} \right]$$

After substituting $\gamma = 1.213$, $p_e = 1.094 \times 10^4 \text{ N/m}^2$, $(p_c)_{ns} = 5.516 \times 10^6 \text{ N/m}^2$, and $A_e/A_t = 40$ into the preceding equation, we find $C_F = 1.871$.

A value of 1.01 can be taken for the correction factor η_F of C_F . Therefore, the design value \bar{C}_F of the thrust coefficient in vacuo can be computed from the corresponding theoretical value C_F as follows

$$\bar{C}_F = \eta_F C_F = 1.01 \times 1.871 = 1.890$$

By using the design values computed above of, respectively, the characteristic velocity and the thrust coefficient in vacuo, the design value of the specific impulse of the thrust chamber in vacuo results from

$$(\bar{I}_s)_{tc} = \frac{\bar{c}^* \bar{C}_F}{g_0} = \frac{2284 \times 1.890}{9.807} = 440.2 \text{ s}$$

2.4 Configuration and Design of a Thrust Chamber

In the design of a combustion chamber, account must be taken of the so-called stay time t_s (measured in seconds), which is the time required by the fuel to mix with the oxidiser and burn completely before the combusted gas is expelled through the nozzle.

The volume V_c (m^3) occupied by a combustion chamber is also important for the combustion efficiency. This volume depends on the mass flow rate \dot{m}_{tc} (kg/s) of the propellant components, on their average density ρ (kg/m^3), and on the stay time t_s (s) defined above, as follows

$$V_c = \frac{\dot{m}_{tc} t_s}{\rho}$$

Of course, the same equality also holds when the mass flow rate and the average density are replaced by, respectively, the weight flow rate (N/s) of the propellant components and their average specific weight (N/m^3).

Another important quantity in the design of a combustion chamber is its characteristic length L^* (m), which is defined as the ratio of the volume V_c (m^3) of the combustion chamber to the area A_t (m^2) of the cross section of the nozzle at the throat, as follows

$$L^* = \frac{V_c}{A_t} = \frac{\dot{m}_{tc} t_s}{\rho A_t}$$

As shown by the preceding equation, the characteristic length of a combustion chamber depends on the stay time of the propellant in the combustion chamber.

The characteristic velocity c^* of a rocket engine increases with the characteristic length L^* of its combustion chamber, and approaches asymptotically a maximum

value. This value has been determined experimentally for each combination of propellants. Consequently, it is not advantageous to increase L^* beyond the value corresponding to the maximum value of c^* , because a higher characteristic length implies higher volume and mass, a higher surface to be cooled, and higher losses due to friction at the chamber walls.

Recommended values of the characteristic length L^* (m) of a combustion chamber for various combinations of propellants are given in the following table, which is due to the courtesy of NASA [5].

Propellant combination	L^* (m)
Chlorine trifluoride/hydrazine-base fuel	0.76–0.90
Liquid fluorine/hydrazine	0.61–0.71
Liquid fluorine/liquid hydrogen (GH ₂ injection)	0.56–0.66
Liquid fluorine/liquid hydrogen (LH ₂ injection)	0.64–0.76
Hydrogen peroxide/RP-1 (including catalyst bed)	1.6–1.8
Nitric acid/hydrazine-base fuel	0.76–0.90
Nitrogen tetroxide/hydrazine-base fuel	0.76–0.90
Liquid oxygen/ammonia	0.76–1.0
Liquid oxygen/liquid hydrogen (GH ₂ injection)	0.56–0.71
Liquid oxygen/liquid hydrogen (LH ₂ injection)	0.76–1.0
Liquid oxygen/RP-1	1.0–1.3

After selecting a combination of propellants, the cross section area A_t (m²) of the nozzle at the throat, and the minimum value of the characteristic length L^* (m), the volume V_c (m³) of a combustion chamber can be determined as follows

$$V_c = L^* A_t$$

The stay time t_s (s) of the propellant in the combustion chamber depends on the volume but not on the shape of the combustion chamber. This shape is chosen according to the following criteria.

A cylindrical combustion chamber having a small cross section and a high length is subject to high losses due to the friction of the combusted gas with the chamber walls. In addition, it is difficult to place the necessary number of orifices in a planar surface of small cross section. On the other hand, a cylindrical combustion chamber having a large cross section and a small length leaves a space sufficient for propellant mixing but insufficient for a complete combustion. Further considerations to be taken into account in choosing a shape concern heat transfer, stability of combustion, weight, and easiness of manufacturing.

The following figure, due to the courtesy of NASA [27], shows the two principal shapes, namely, spherical (or near-spherical) and cylindrical, which may be chosen for a combustion chamber. The spherical shape (left) was chosen for the combustion

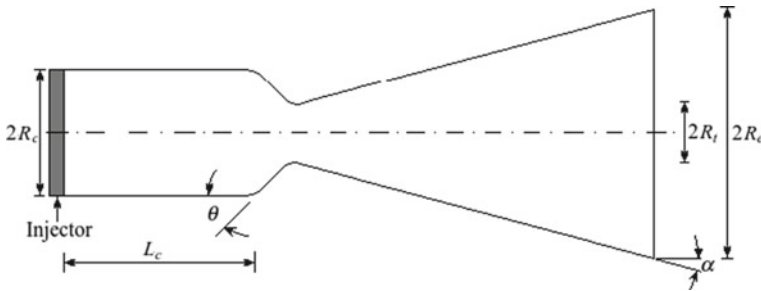
chamber of the V-2 missile, whereas the cylindrical shape (right) was chosen for the combustion chamber of the Navaho missile.



A spherical combustion chamber has, in comparison with a cylindrical one of the same volume, a smaller mass and a smaller surface to be cooled. In addition, for the same pressure and for the same strength of the materials used, the walls of a spherical combustion chamber can be less thick than those of a cylindrical combustion chamber. On the other hand, a spherical combustion chamber is more difficult to manufacture and offers a lower performance than is the case with a cylindrical combustion chamber. Therefore, a cylindrical combustion chamber is considered firstly, and other shapes will be discussed successively.

Let the cross-sectional area $A_t = \pi R_t^2$ of the throat and the characteristic length L^* of the combustion chamber be known for a cylindrical combustion chamber. The value to be given to the contraction area ratio $\varepsilon_c \equiv A_c/A_t$, where $A_c = \pi R_c^2$ is the cross-sectional area of the combustion chamber, depends on various factors connected with the performance of the process of combustion. However, on the basis of the experience gained so far, Huzel and Huang [5] suggest the following values for the contraction area ratio: 2–5 in case of pressurised-gas low-thrust engines, and 1.3–2.5 in case of turbo-pump high-thrust engines.

A simple scheme of a rocket engine is illustrated in the following figure, which shows, from left to right, the injector, the cylindrical combustion chamber, and the converging-diverging nozzle.



The length L_c of the combustion chamber is measured from the internal face of the injector to the inlet plane of the nozzle, as shown in the preceding figure.

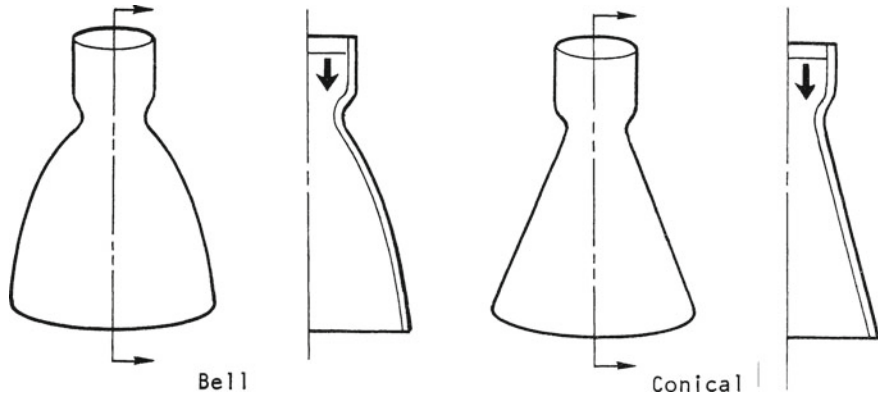
Let V_c and A_{tot} be respectively the volume (measured from the injector face to the throat plane of the nozzle) and the total area, minus the injector face, of the combustion chamber. Huzel and Huang [5] suggest to use the following approximate formulae to determine the volume V_c and the total area A_{tot} of the combustion chamber as functions of the quantities L_c , A_t , A_c/A_t , and θ :

$$V_c = A_t L_c \left(\frac{A_c}{A_t} \right) + \frac{A_t}{3} \left(\frac{A_t}{\pi} \right)^{\frac{1}{2}} (\cot \theta) \left[\left(\frac{A_c}{A_t} \right)^{\frac{1}{3}} - 1 \right]$$

$$A_{tot} = 2L_c \left[\pi \left(\frac{A_c}{A_t} \right) A_t \right]^{\frac{1}{2}} + (\csc \theta) \left[\left(\frac{A_c}{A_t} \right) - 1 \right] A_t$$

As has been shown in Chap. 1, Sect. 1.1, for the optimum performance of a rocket engine in terms of thrust, the gas pressure p_e at the exit plane of the nozzle should be exactly equal to the pressure p_0 due to the environment around it. Since a given expansion ratio $\varepsilon \equiv A_e/A_t$ results in the optimum expansion only at a specific altitude, then the design expansion ratio of a nozzle must be selected in such a way as to give the best average performance during powered flight.

The supersonic expansion of the combusted gas occurs in the diverging portion of the nozzle. The two principal types (bell-shaped and conical) of the diverging portion of a nozzle are shown in the following figure, due to the courtesy of NASA [28].



A bell-shaped nozzle (left) has the advantages, over a conical nozzle (right), of better performance and shorter length. The former has a radial-flow section in the initial divergent region. This fact generates a uniform flow directed along the symmetry axis at the exit cross-section of the nozzle. In addition, the gradual change of the wall angle with respect to the axis prevents oblique shocks.

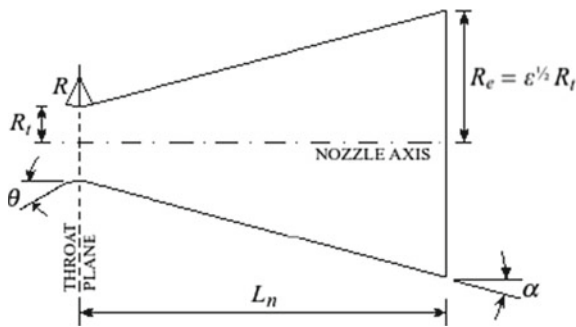
Some of the methods (in particular, those due to Prandtl-Busemann, Puckett, and Foelsch) to determine a nozzle contour have been described by Crown [29]. Rao [30] has applied the calculus of variations to determine the shape of a nozzle contour leading to the maximum thrust. For engineering purposes, near-optimum parabolic contours are suitable for many applications [28].

According to Huzel and Huang [5], the optimum shape of a nozzle having a given expansion ratio is chosen on the basis of the following considerations:

- uniform parallel axial flow of the combusted gas at the exit section of the nozzle for the maximum magnitude of the momentum vector;
- minimum losses due to separation and turbulence within the nozzle;
- shortest possible length of the nozzle for minimum requirements of space envelope, weight, losses due to friction at the walls, and cooling; and
- easiness of manufacturing.

In practice, the cone and the bell are the most frequently used of all shapes for the diverging portion of a rocket nozzle.

The advantages of a conical nozzle over a bell-shaped nozzle are easiness of manufacturing, and capability of increasing or decreasing its exit section, without the necessity of re-designing the full surface of the nozzle. The diverging portion of a conical nozzle is shown in the following figure.



On both sides of the throat plane, the contour of the nozzle is a circular arc, whose radius R ranges from 0.5 to 1.5 times the radius R_t of the throat [5]. In the converging portion (not shown in the preceding figure) of the nozzle, the angle θ of semi-aperture ranges from $\pi/9$ rad to $\pi/4$ rad (from 20 to 45°). The semi-aperture angle α of the diverging portion of the nozzle varies from about $\pi/15$ rad to $\pi/10$ rad (from 12 to 18°) [5]. The length L_n of the diverging portion of a conical nozzle is expressed by the following equation of [5]:

$$L_n = \frac{R_t \left[\left(\frac{A_e}{A_t} \right)^{\frac{1}{2}} - 1 \right] + R(\sec \alpha - 1)}{\tan \alpha}$$

In practice, $\pi/12$ rad (15°) is the most frequently chosen value for the divergence angle α of a conical nozzle, for reasons of weight, length, and performance. In case of a conical nozzle, the velocity vector v_e of the exhaust gas at the exit plane of the nozzle forms the divergence angle α with respect to the axis of symmetry of the nozzle. Therefore, not all the gas momentum is in the axial direction, there being a non-axial component of the exhaust gas velocity vector. This loss of axial momentum in a conical nozzle is taken into account by means of the factor

$$\lambda = \frac{1}{2}(1 + \cos \alpha)$$

where λ is the ratio between the momentum of the gases in a nozzle with a semi-aperture angle α and the momentum of an ideal nozzle with all gases flowing in the axial direction [2]. With this factor, the thrust of a rocket engine having a conical nozzle is [31]:

$$F = \lambda \dot{m} v_e + A_e(p_e - p_0)$$

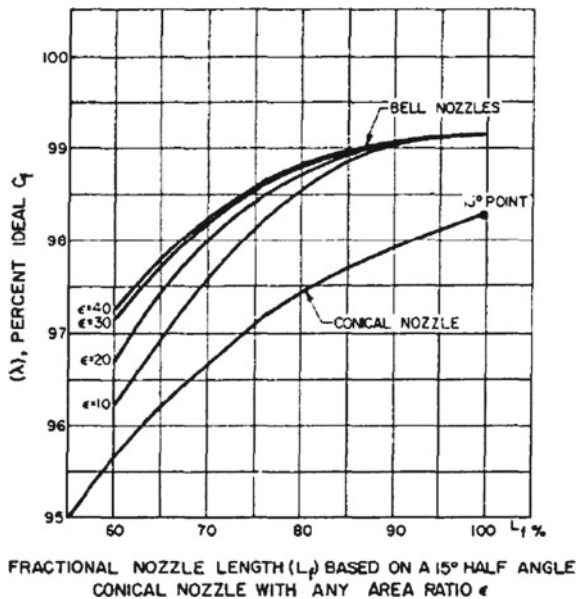
In the ideal case of all the gas momentum being in the axial direction at the exit plane of a nozzle, the factor λ is equal to unity. In the case of a conical nozzle having a semi-aperture angle $\alpha = \pi/12$ rad = 15°, there results $\lambda = 0.983$, and therefore

the velocity of the exhaust gas at the exit plane of a conical nozzle is in magnitude 98.3% of the velocity of the gas for an ideal nozzle.

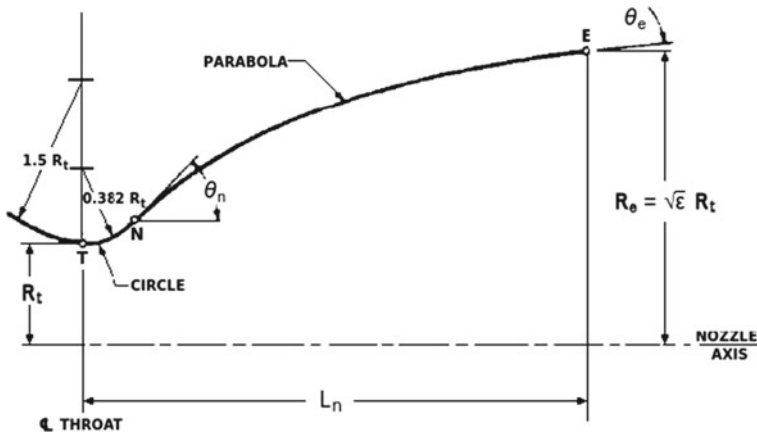
For the purposes of reducing the length L_n of the divergent portion of a nozzle and increasing the performance, a bell-shaped nozzle has been studied. This type of nozzle offers the advantages of decreasing the portion of nozzle where the gas flow expands, and changing gradually the local angle of semi-aperture, so as to have a uniform, nearly axially directed flow at the exit plane. In addition, since the slope of the wall contour changes continuously, then the formation of oblique shocks is avoided. The optimum contour for a bell-shaped nozzle which leads to the maximum magnitude of thrust has been determined in 1958 by Rao [30], by using the method of characteristics combined with the calculus of variations. Several computer programmes have subsequently been developed (see, for example, 32) in order to determine the optimum contour by applying the method described by Rao [30]. In practice, an equivalent conical nozzle having a semi-aperture angle $\alpha = \pi/12 \approx 0.2618 \text{ rad} = 15^\circ$ is used as a standard to specify the length of a bell-shaped nozzle. For example, a bell-shaped nozzle is said to have a fractional length $L_f = n\%$ when its true length L_n , measured from the throat plane to the exit plane, is

$$L_n = \frac{n}{100} \frac{R_t}{\tan 0.2618} \left[\varepsilon^{\frac{1}{2}} - 1 + 1.5 \left(\frac{1}{\cos 0.2618} - 1 \right) \right]$$

that is, when the true length L_n of that nozzle is $n/100$ times the length of a conical nozzle having a semi-aperture angle $\alpha = \pi/12 \text{ rad} = 15^\circ$, the same radius R_t at the throat plane, and the same expansion ratio $\varepsilon \equiv A_e/A_t$. It has been proved experimentally that a bell-shaped nozzle whose fractional length L_f is greater than about 85% does not offer substantial advantages for the purpose of increasing the nozzle correction factor λ , because an increase in length implies an increase in mass. This fact is shown in the following figure, due to the courtesy of NASA [5].



Rao [33] and other authors have found a convenient way to design a near-optimum bell contour by using a parabolic approximation to the optimum contour. This parabolic approximation is shown in the following figure, due to the courtesy of NASA [5]. In the converging portion of the nozzle, immediately upstream of the throat plane, the nozzle contour is a circular arc, whose radius is equal to 1.5 times R_t , where R_t is the radius of the throat. This arc terminates at the point T, where T is the point in which this arc intersects the throat plane. The angle which subtends this circular arc is to be chosen by the designer. In the diverging portion of the nozzle, immediately downstream of the throat plane, the nozzle contour is also a circular arc, whose radius is equal to 0.382 times R_t . This circular arc goes from the point T to the point of inflection N, where N is the point in which the parabolic segment begins. The parabolic segment goes from to the point of inflection N to the point E, where E is the point in which the parabolic segment intersects the exit plane of the nozzle.

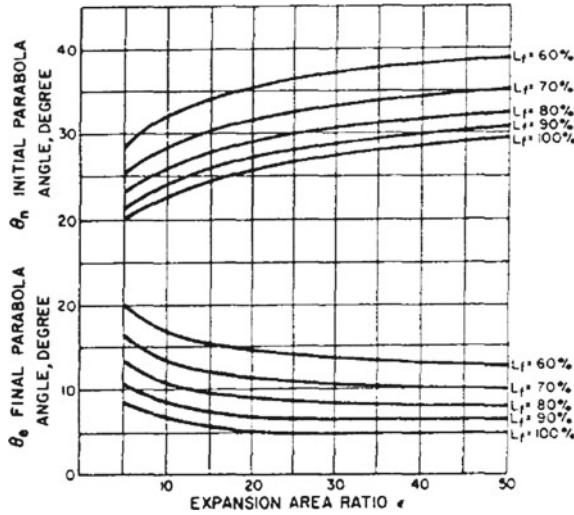


In order to design a specific bell-shaped nozzle, the following data must be known: the radius R_t of the throat, the true length L_n of the nozzle (measured from the throat plane to the exit plane along the axis of symmetry of the nozzle), the expansion area ratio $\varepsilon \equiv A_e/A_t$, the angle θ_n which the tangent in N to the parabola forms with the axis of symmetry, and the angle θ_e which the tangent in E to the parabola forms with the axis of symmetry.

Of course, the true length L_n of a bell-shaped nozzle may be expressed in terms of the fractional length L_f , with reference to an equivalent conical nozzle having a semi-aperture angle $\pi/12$ radians (15°).

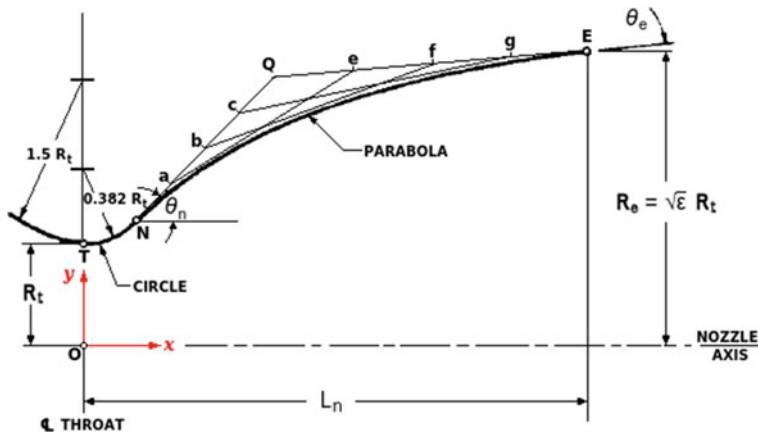
The values of the angles θ_n and θ_e are given in, respectively, the upper part and the lower part of the following figure, due to the courtesy of NASA [5], as functions of the expansion area ratio $\varepsilon \equiv A_e/A_t$. The values of the angles θ_n and θ_e are those of the optimal (maximum thrust) nozzle determined by Rao [30].

This figure shows that the value of the angle θ_e at the exit plane of the nozzle is never equal to zero. The same figure can also be found in [34, 35]. In particular, Newlands [35] has extrapolated the curves found by Rao [30] to values greater than 50 of the expansion area ratio $\varepsilon \equiv A_e/A_t$. Experience has shown that these curves are substantially the same for all the values of the specific heat ratio $\gamma \equiv c_p/c_v$ which are of practical interest.



In order to draw a parabola from the point of inflection N to the point of exit E, Newlands [35] has suggested to use an ancient geometrical method, which is briefly described below.

With reference to the following figure, adapted from [5], a straight line is drawn at an angle θ_n from N, and then another straight line is drawn back at an angle θ_e from E. Let Q be the point of intersection of these straight lines. Next, both of these lines are divided into an equal number of segments, which is four in the following figure. The terminal points of these segments are labelled a, b, c and e, f, g. A straight line is drawn from point a to point e, then another from b to f, and another from c to g. These straight lines form a mesh, whose edge gives the parabola outline. This parabola is also tangent to the straight lines QN and QE. By using many more divisions, for example by means of a CAD package, there results a sharper contour. A series of straight-line segments results from removing most of the mesh. By joining the midpoint of each segment with a smooth curve, such as a CAD spline, there results the nozzle contour.



For the same purpose, an analytical method based on Bézier curves has also been suggested by Newlands [35]. Without loss of generality, this method is described below by means of a numerical example. With reference to the preceding figure, we consider a nozzle having a radius $R_t = 13.8$ cm measured in the plane of the throat, an expansion area ratio $\varepsilon \equiv A_e/A_t = 70$, and a fractional length $L_f = 80\%$ of a $\pi/12$ -rad = 15° equivalent conical nozzle. We want to determine the equation of the parabolic segment of nozzle going from the inflexion point N to the exit point E, where the axes x and y and their origin O are shown in the preceding figure. For this value of fractional length, the Rao curves give the angles $\theta_n = 0.5760$ rad = 33° and $\theta_e = 0.1222$ rad = 7° which the tangents to the contour of the nozzle in the points respectively N and E form with the axis of symmetry (x -axis) of the nozzle. These wall angles result from extrapolating the graphs given above. By substituting $n = 80$, $R_t = 13.8$ cm, and $\varepsilon = 70$ in the following formula, the true length of the nozzle results

$$L_n = \frac{n}{100} \frac{R_t}{\tan 0.2618} \left[\varepsilon^{\frac{1}{2}} - 1 + 1.5 \left(\frac{1}{\cos 0.2618} - 1 \right) \right] = 305.70 \text{ cm}$$

We take 0.5760 rad for the value of the angle α subtending the circular arc TN of radius $0.382 R_t$, downstream of the throat. Therefore, the co-ordinates of N are

$$x_N = 0.382 R_t \sin \alpha = 0.382 \times 13.8 \times \sin 0.5760 = 2.8711 \text{ cm}$$

$$y_N = R_t [1 + 0.382(1 - \cos \alpha)] = 13.8 \times [1 + 0.382 \times (1 - \cos 0.576)] \\ = 14.650 \text{ cm}$$

The co-ordinates of the point E laying on the exit plane of the nozzle are

$$x_E = L_n = 305.70 \text{ cm}$$

$$y_E = R_E = \varepsilon^{\frac{1}{2}} R_t = 70^{\frac{1}{2}} \times 13.8 = 115.46 \text{ cm}$$

From the inflection point N, we produce the straight line NQ, which forms the angle θ_n with the x-axis. As is well known, the equation of NQ is

$$y - y_N = (x - x_N) \tan \theta_n$$

By substituting $y_N = 14.650$ cm, $x_N = 2.8711$ cm, and $\theta_n = 0.5760$ rad into the preceding equation, there results

$$y = 0.64941x + 12.785$$

Likewise, from the exit point E, we produce the straight line QE, which forms the angle θ_e with the x-axis. The equation of QE is

$$y - y_E = (x - x_E) \tan \theta_e$$

By substituting $y_E = 115.46$ cm, $x_E = 305.70$ cm, and $\theta_e = 0.1222$ rad into the preceding equation, there results

$$y = 0.12278x + 77.925$$

The straight line NQ (whose equation is $y = 0.64941x + 12.785$) intersects the straight line QE (whose equation is $y = 0.12278x + 77.925$) in the point Q, whose co-ordinates are easily found to be

$$\begin{aligned} x_Q &= 123.69 \text{ cm} \\ y_Q &= 93.112 \text{ cm} \end{aligned}$$

Since the co-ordinates of the points N, Q, and E are known, then the parabolic segment of nozzle going from N to E can be expressed by means of a Bézier quadratic curve having the following parametric equations

$$\begin{aligned} x(t) &= (1-t)^2 x_N + 2(1-t)t x_Q + t^2 x_E \quad (0 \leq t \leq 1) \\ y(t) &= (1-t)^2 y_N + 2(1-t)t y_Q + t^2 y_E \quad (0 \leq t \leq 1) \end{aligned}$$

The preceding equations specify the co-ordinates x and y of any point P of this curve corresponding to a value of t taken between 0 and 1. For example, the co-ordinates of three points P_1 , P_2 , and P_3 (other than N and E) of the curve can be determined by assigning the values 0.25, 0.50, and 0.75 to the parameter t .

In the present case, after substituting the values of (x_N, y_N) , (x_Q, y_Q) , and (x_E, y_E) computed above into the preceding equations, there results

$$\begin{aligned} x(t) &= 2.8711(1-t)^2 + 247.38(1-t)t + 305.70t^2 \quad (0 \leq t \leq 1) \\ y(t) &= 14.650(1-t)^2 + 186.22(1-t)t + 115.46t^2 \quad (0 \leq t \leq 1) \end{aligned}$$

The preceding equations express analytically the segment of nozzle going from the inflection point N to the exit point E in the reference system Oxy shown in the preceding figure. As has been shown above, the coefficients of these equations have been determined in such a way as to satisfy the four boundary conditions, which specify the co-ordinates of the endpoints N and E and the angles θ_n and θ_e which the tangents to the parabola in these points form with the x -axis.

In the general case, there may be no set of three coefficients a , b , and c whose values satisfy exactly the boundary conditions specified above, in order to express the contour of a nozzle by means of the equation $y(x) = ax^2 + bx + c$. Such is the case with the numerical example given above, since $x_Q \neq (x_N + x_E)/2$. This is because a parabola can be expressed by the equation $y = ax^2 + bx + c$ only when its axis of symmetry is parallel to the y -axis.

When the requirements posed to the designer of a bell nozzle are: (a) the continuity of its contour; (b) the continuity of its slope; and (c) the respect of the four boundary conditions specified above, independently of whether a parabola or any other smooth curve may be chosen, then the contour can be expressed by a cubic equation, as follows

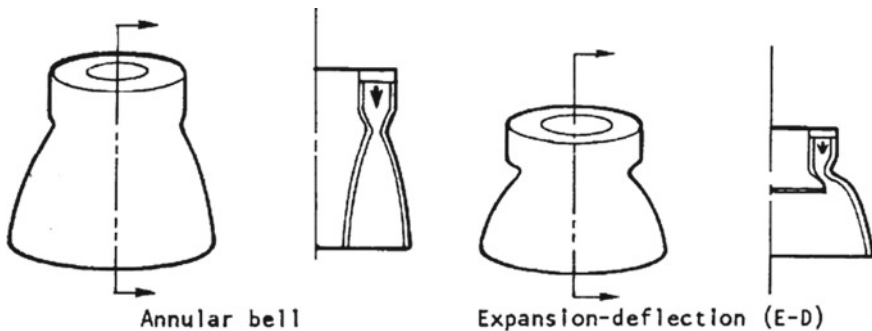
$$y(x) = ax^3 + bx^2 + cx + d$$

where the unknown values of the coefficients a , b , c , and d result from solving the following system of four linear equations

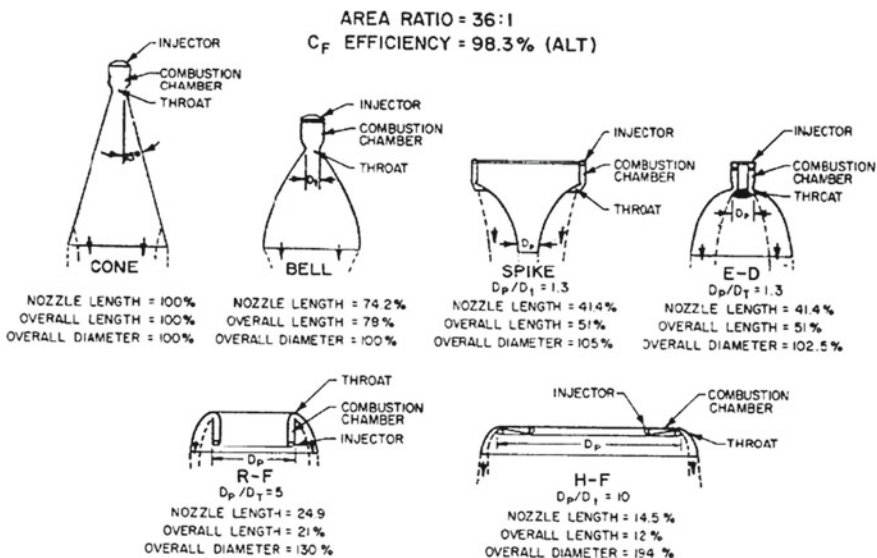
$$\begin{aligned} y_N &= ax_N^3 + bx_N^2 + cx_N + d \\ y_E &= ax_E^3 + bx_E^2 + cx_E + d \\ \tan \theta_n &= 3ax_N^2 + 2bx_N + c \\ \tan \theta_e &= 3ax_E^2 + 2bx_E + c \end{aligned}$$

In the numerical example given above, after substituting the known values of x_N , y_N , x_E , y_E , θ_n and θ_e in the four preceding equations, we find the following values: $a = 1.1602 \times 10^{-6}$, $b = -0.0014065$, $c = 0.65746$, and $d = 12.774$.

The exhaust gas generated within the combustion chamber need not flow along the axis of symmetry of the nozzle. Such is the case with the two annular nozzles illustrated in the following figure, due to the courtesy of NASA [28].



Annular (or plug or altitude-compensating) nozzles are so called because the propellant is combusted into a ring, also called an annulus, which is located around the base of the nozzle. They are shown in the following figure, due to the courtesy of NASA [5], which also illustrates a conical nozzle and a bell-shaped nozzle.



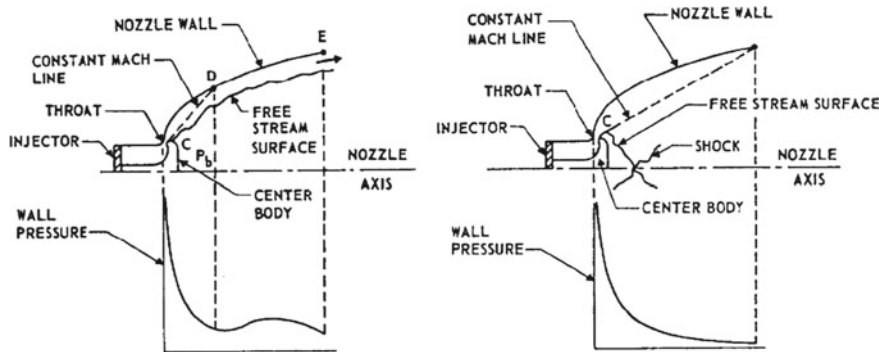
A central body, also called a plug, keeps the gas flow away from a central portion of the nozzle. There are two principal types of annular nozzles. They are the radial in-flow type (spike nozzle) and the radial out-flow type. The latter type, in turn, includes expansion-deflection or E-D, reverse-flow or R-F, and horizontal-flow or H-F nozzles. The nozzles shown above have, all of them, the same level of thrust, the same expansion area ratio, and the same theoretical thrust coefficient C_F (see Chap. 1, Sect. 1.3). Annular nozzles are shorter than conical or bell-shaped nozzles, and are therefore advantageous over the latter in terms of length and mass of the whole vehicle.

For an annular nozzle, the expansion area ratio ε is defined as the ratio of the projected area of the contoured nozzle wall to the area of the throat (A_t). The projected area of the contoured nozzle wall, in turn, is the area of the nozzle at the exit plane (A_e) minus the projected area of the central body (A_p). Therefore

$$\varepsilon \equiv \frac{A_e - A_p}{A_t}$$

The preceding figure indicates the values of the annular diameter ratio, D_p/D_t , where D_p is the diameter of the central body, and D_t is the diameter of the throat of an equivalent nozzle having a circular cross section. The value of annular diameter ratio makes it possible to compare an annular nozzle with a conventional (conical or bell-shaped) nozzle.

Annular nozzles are not subject to losses which affect nozzles of the bell or conical type. This is because, in nozzles of the latter type, the exhaust gas may expand to pressures which are considerably smaller than the ambient pressure before the gas flow detaches from the nozzle wall. This over-expansion results in thrust losses at high altitudes. The property of annular nozzles which avoids an over-expansion of the exhaust gas flow is shown in the following figure, due to the courtesy of NASA [5], for an E-D (expansion-deflection) nozzle.

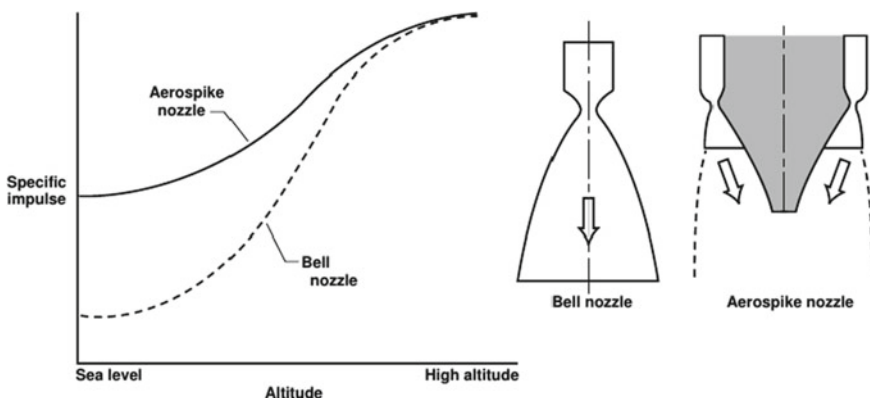


This figure illustrates an E-D nozzle operating at low altitudes (left) and at high altitudes (right). In this figure, p_b indicates the pressure at the back face of the central body of the nozzle. The value of p_b depends on the value of the ambient pressure p_0 , and is usually smaller than that of p_0 . The point C indicates the shoulder of the central body. The dashed line CD is a line of constant Mach number. Downstream of the throat, the exhaust gas expands unaffected around the shoulder C of the central body as long as its pressure at the wall is greater than p_b . After the gas expands from the throat to the point D along the line CD, the flow downstream of D depends on the nozzle contour DE, and also on the pressure p_b , whose value affects the free stream surface of the boundary of the inner jet. The gas flow is deflected by the contour of the curved wall, and therefore is subject to compression, which increases the pressure at the wall. This increase in wall pressure at low altitudes is shown on the left-hand

side of the preceding figure. At such altitudes, the exhaust gas remains attached to the wall, as is the case with a conical or bell-shaped nozzle.

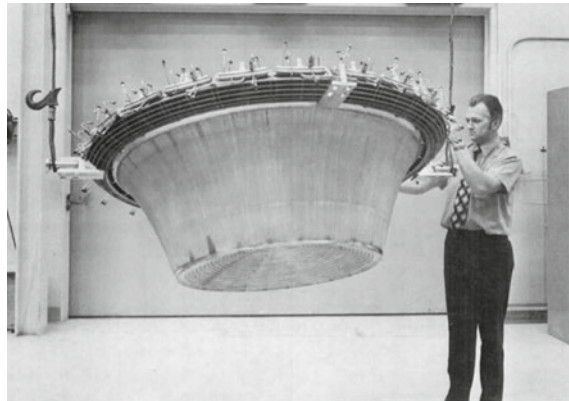
By contrast, at high altitudes, the value of p_b becomes so low, that the gas flow deviates towards the central body. This deviation is shown on the right-hand side of the preceding figure. In such conditions, a shock wave may occur, or the gas flow may continue unaffected up to the exit plane of the nozzle, depending on the flow conditions. This decrease in wall pressure at high altitudes is shown on the right-hand side of the same figure.

The following figure, due to the courtesy of NASA [36], illustrates a plug (or truncated aerodynamic spike) nozzle, which is an annular nozzle discharging exhaust gas having a radial inward component of velocity. This figure also shows the better performance of this aerospike nozzle in comparison with a bell nozzle in terms of specific impulse.



The advantage of the aerospike nozzle over the bell-shaped nozzle resides in its ability to adjust with altitude changes to the static pressure of the free stream. This results in a higher specific impulse than that of a bell-shaped nozzle at low altitudes, as shown in the preceding figure. This altitude compensation is due to the shape of the aerospike nozzle, which has a central ramp terminating either in a plug base or in a spike in the centre, and is open to the atmosphere on the sides.

An aerospike nozzle having a central ramp terminating in a plug base is shown in the following figure, which is due to the courtesy of NASA [36].



The central spike need not be a solid wall, because it can be aerodynamically formed by injecting gases from the engine base, as will be shown below. The exhaust gas is free to expand on the open sides of the nozzle, and to adjust its static pressure with the static pressure of the ambient, which decreases with altitude. Thus, a nozzle of very high area ratio (of high performance in vacuo) can also operate efficiently and safely at sea level.

By contrast, a bell-shaped nozzle can be designed to be optimum (that is, to operate at its maximum level of efficiency) at only one altitude. By maximum level of efficiency, we mean the optimal expansion of the combusted gas, which results in the maximum thrust. For example, the initial stage of the Saturn rocket, which carried the Apollo astronauts to the Moon, had a narrow bell-shaped nozzle to produce an ideal straight-edged column of exhaust gas at sea level. However, the command module, which orbited around the Moon, had a much wider bell-shaped nozzle, which was better suited than the nozzle of the initial stage to the expansion of the combusted gas in the vacuum of space.

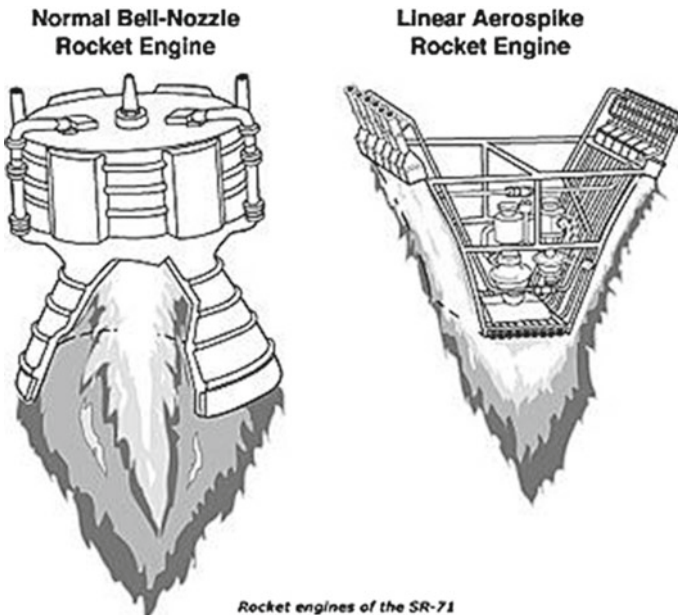
As shown above, in an aerospike nozzle, the static pressure (p_e) of the exhaust gas is the same as the static pressure (p_0) of the ambient, and therefore the term $A_e(p_e - p_0)$ in the equation of thrust (see Chap. 1, Sect. 1.1):

$$F = \dot{m}v_e + A_e(p_e - p_0)$$

reduces to zero. In addition, an aerospike engine may also be made of individual thruster segments, which can be turned on or off to provide thrust vector control in order to steer the vehicle [37], instead of using one of the techniques described in Sect. 2.2.

An aerospike rocket engine was developed by Rockwell Aerospace/Rocketdyne Division of Canoga Park, California. In the 1960s, Rocketdyne developed a rounded aerospike engine, whose thrust chamber consisted of a truncated annular spike nozzle, of the radial in-flow type, and a number of discrete combustion chambers arranged around the periphery of the nozzle, so as to discharge their gases along the surface of the nozzle. Subsequently, in 1972, this design gave rise to a linear aerospike engine,

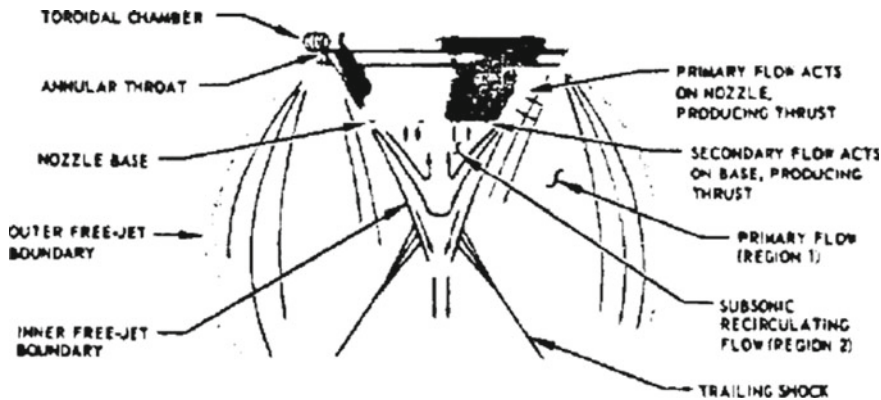
where the gases are discharged along the surface of a rectangular wedge rather than around a round spike-shape. The following figure, due to the courtesy of NASA [38], illustrates (left) a normal rocket engine having a bell-shaped nozzle, and (right) the linear aerospike rocket engine designed for the Lockheed-Martin X-33 wing-shaped vehicle, which was a technology demonstrator (cancelled on the 1st of March 2001) for NASA's "next-generation" of space launch vehicles [39].



Rocket engines of the SR-71

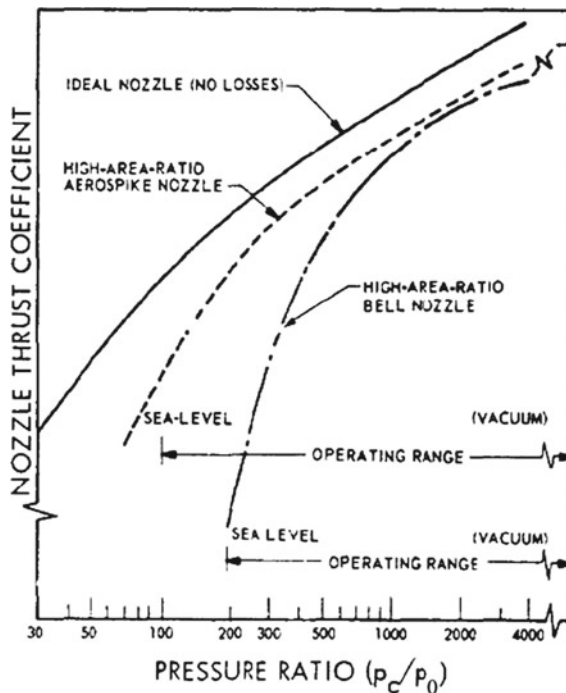
The performance of an aerospike nozzle depends on various factors, such as the shape of the nozzle, the amount of the secondary flow (about 1% of the primary flow), the manner of introducing the secondary flow, and the energy ratio of the secondary flow to the primary.

The working principle of an aerospike nozzle can be explained as follows. The following figure, due to the courtesy of NASA [5], illustrates the gas flow, under altitude conditions (that is, high value of the pressure ratio p_c/p_0), of a rocket engine having a toroidal combustion chamber, an annular throat, and a truncated spike nozzle ending in a circular base.



The primary flow of the exhaust gas expands along the wall of the nozzle, in the Region 1 of the preceding figure, and generates thrust. The primary flow continues to expand beyond the base of the nozzle, and gives rise to a subsonic recirculating flow in the Region 2 of the same figure. The pressure acting on the base generates additional thrust. By adding a small amount of secondary flow to the recirculating flow at the base of the nozzle, the pressure acting on the base is increased further. There is a limit to this increase in efficiency, which determines the optimum amount of secondary flow to be added for each given shape of the nozzle. The outer surface of the primary flow is the boundary of a free stream, and therefore depends on the ambient pressure. This fact provides the property of altitude compensation to the aerospike nozzle illustrated above.

The performance of the gas expansion in nozzles of various types can be expressed by means of a graph of the thrust coefficient C_F (defined in Chap. 1, Sect. 1.3) versus the pressure ratio p_c/p_0 of the static pressure in the combustion chamber p_c to the ambient pressure p_0 . In the following figure, due to the courtesy of NASA [5], we consider the thrust coefficient C_F for: (a) an ideal nozzle of variable expansion area ratio having the optimum expansion for any value of the pressure ratio p_c/p_0 , (b) an aerospike nozzle of high area ratio, and (c) a bell-shaped nozzle of high area ratio. This graph shows that the dashed line of the aerospike nozzle approximates the solid line of the ideal nozzle much better than does the dash-and-dot line of the bell-shaped nozzle.

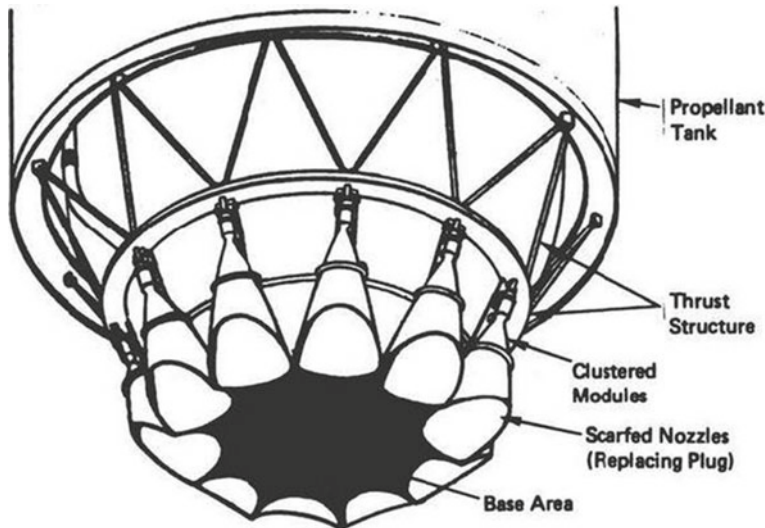


The same graph also shows that, for all the three types of nozzle indicated above, the value of the thrust coefficient C_F increases with the value of the pressure ratio p_c/p_0 .

The choice of an aerospike nozzle instead of a traditional nozzle has important consequences on the design of a rocket engine, particularly in case of multistage rockets. Huzel and Huang [5] have identified four advantages and three disadvantages of aerospike nozzles, in the following order:

- shorter length, and therefore reduced mass, for the same performance;
- better performance at sea level;
- possibility of using the stagnant region in the centre of the nozzle to install gas generators, turbo-pumps, tanks, auxiliary equipment, and turbine gas discharges;
- possibility of propelling a rocket vehicle by means of a cluster of engines around a contoured plug instead of a large single engine, as shown in the following figure, due to the courtesy of NASA [40];
- higher cooling requirements;
- heavier structures in some applications; and
- increased difficulty of manufacturing.

The following figure shows a cluster of bell nozzles of high expansion area ratio which have been scarfed for the external expansion of their exhaust gases.



By the way, according to the definition given by Shyne and Keith [41], a scuffed nozzle is a two-dimensional asymmetric nozzle whose lower end (the cowl) is terminated at the point where the last characteristic which emanates from the upper nozzle wall (the ramp) intersects the cowl.

According to Aukerman [36], there are two distinct applications for aerospike nozzles:

- the first stage of a rocket, where the external expansion of the exhaust gas makes it possible to increase the effective expansion area ratio of the engine, due to the property of altitude compensation; and
- the stages operating at high altitudes or in space, where the nozzle can be truncated to a very short length, with minimum detriment of performance.

According to O'Leary and Beck [42], during the 1960s, Pratt & Whitney Rock- etdyne tested numerous aerospike engines, ranging in size from subscale, cold-flow models to a 1.112×10^6 N thrust oxygen/hydrogen engine, which was tested at a test stand in Nevada.

A numerical example of design of a thrust chamber is given below. Let us consider a rocket whose first stage burns a combination of liquid oxygen with RP-1 (kerosene), and has the data given in Sect. 2.3. Let $F_{tc} = 3.323 \times 10^6$ N be the desired thrust of the first stage at sea level.

As has been shown in Sect. 2.3, the design value of the thrust coefficient at sea level is $\bar{C}_F = 1.530$, the total absolute pressure in the combustion chamber at the nozzle inlet is $(p_c)_{ns} = 6.895 \times 10^6$ N/m², and the expansion area ratio of the nozzle is $\varepsilon \equiv A_e/A_t = 14$. After substituting these values in the following equation of Chap. 1, Sect. 1.3

$$\bar{C}_F = \frac{F}{A_t(p_c)_{ns}}$$

and solving this equation for the area A_t of the cross section of the nozzle at the throat plane, there results

$$A_t = \frac{F}{\bar{C}_F(p_c)_{ns}} = \frac{3.323 \times 10^6}{1.530 \times 6.895 \times 10^6} = 0.3150 \text{ m}^2$$

The radius R_t of the cross section of the nozzle at the throat plane is

$$R_t = \left(\frac{A_t}{\pi} \right)^{\frac{1}{2}} = \left(\frac{0.3150}{3.1416} \right)^{\frac{1}{2}} = 0.3166 \text{ m}$$

Since the expansion area ratio of the nozzle is $\varepsilon \equiv A_e/A_t = 14$, then the radius of the cross section of the nozzle at the exit plane is

$$R_e = \varepsilon^{\frac{1}{2}} R_t = 14^{\frac{1}{2}} \times 0.3166 = 1.185 \text{ m}$$

The table of Sect. 2.4 gives recommended values of the characteristic length L^* of a combustion chamber for various combinations of propellants. In case of the combination of liquid oxygen with RP-1, this table indicates a value of L^* falling in the interval from 1.0 m to 1.3 m. We choose $L^* = 1.143$ m. This makes it possible to determine the volume V_c of the combustion chamber by means of the following equation of Sect. 2.4

$$V_c = L^* A_t$$

After substituting $L^* = 1.143$ m and $A_t = 0.3150 \text{ m}^2$ in the preceding equation, we find $V_c = 0.3600 \text{ m}^3$.

As has been shown in Sect. 2.4, the value of the angle θ of semi-aperture in the converging portion of the nozzle ranges from 0.3491 rad to 0.7854 rad. We take $\theta = 0.3491$ rad. We also take 1.6 for the contraction area ratio $\varepsilon_c \equiv A_c/A_t$, where $A_c = \pi R_c^2$ is the cross-sectional area of the combustion chamber.

As has also been shown in Sect. 2.4, the contour of the nozzle upstream of the throat plane is a circular arc, whose radius R ranges from 0.5 to 1.5 times the radius R_t of the throat. We take

$$R = 1.5 R_t = 1.5 \times 0.3166 = 0.4749 \text{ m}$$

Since 1.6 is the value chosen for the contraction area ratio A_c/A_t , then the radius R_c of the cross-section of the cylindrical combustion chamber is

$$R_c = \left(\frac{A_c}{A_t} \right)^{\frac{1}{2}} R_t = 1.6^{\frac{1}{2}} \times 0.3166 = 0.4005 \text{ m}$$

Since the converging portion of the nozzle is a cone, whose semi-aperture angle is $\theta = 0.3491$ rad, then the length L_{conv} of the converging portion of the nozzle results from the following formula of Sect. 2.4

$$L_{conv} = \frac{R_t \left[\left(\frac{A_c}{A_t} \right)^{\frac{1}{2}} - 1 \right] + R \left(\frac{1}{\cos \theta} - 1 \right)}{\tan \theta}$$

After substituting $R_t = 0.3166$ m, $A_c/A_t = 1.6$, $R = 0.4749$ m, and $\theta = 0.3491$ rad in the preceding equation, we find $L_{conv} = 0.3142$ m.

Since the volume of a frustum of a right circular cone is $\frac{1}{3}\pi h(R^2 + Rr + r^2)$, where R and r are the radii of the two circular bases and h is the height of the frustum, then the approximate volume V_{conv} of the converging portion of the nozzle is

$$V_{conv} = \frac{1}{3} \times 3.1416 \times 0.3142 \times (0.4005^2 + 0.4005 \times 0.3166 + 0.3166^2) = 0.1275 \text{ m}^3$$

This value is approximate, because the rounding at the throat plane and the rounding at the inlet plane of the nozzle are not taken into account.

The volume V_{cyl} of the cylindrical combustion chamber, whose length goes from the internal face of the injector to the inlet plane of the nozzle, is

$$V_{cyl} = V_c - V_{conv} = 0.3600 - 0.1275 = 0.2325 \text{ m}^3$$

The length L_{cyl} of this cylindrical combustion chamber is

$$L_{cyl} = \frac{V_{cyl}}{1.6A_t} = \frac{0.2325}{1.6 \times 0.3150} = 0.4613 \text{ m}$$

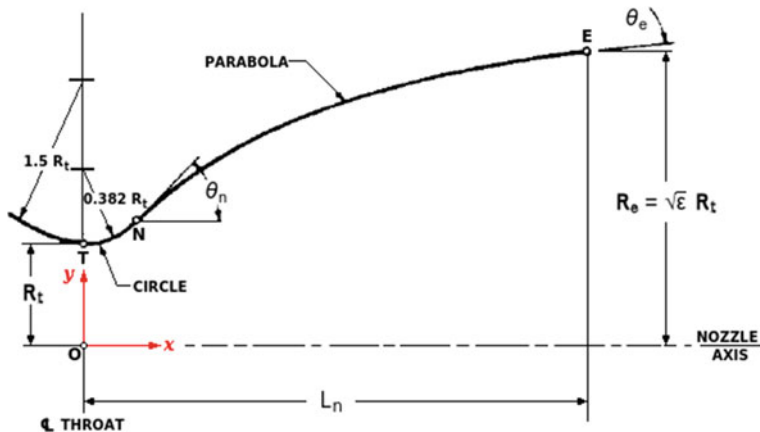
The total distance L_{total} from the internal face of the injector to the plane of the throat is

$$L_{total} = L_{cyl} + L_{conv} = 0.4613 + 0.3142 = 0.7755 \text{ m}$$

For the diverging portion of the nozzle, we choose a fractional length $L_f = 80\%$ of a $\pi/12$ rad equivalent conical nozzle. Therefore, the true length L_n of the diverging portion of the nozzle is

$$L_n = \frac{n}{100} \frac{R_t}{\tan 0.2618} \left[\varepsilon^{\frac{1}{2}} - 1 + 1.5 \left(\frac{1}{\cos 0.2618} - 1 \right) \right]$$

After substituting $n = 80$, $R_t = 0.3166$ m and $\varepsilon \equiv A_e/A_t = 14$ in the preceding equation, we find $L_n = 2.642$ m. Let us consider again the following figure, adapted from [5].



We take the optimum values of the wall angles θ_n and θ_e from the Rao curves for $L_n = 80\%$ and $\varepsilon = 14$. These curves indicate $\theta_n = 0.4782$ rad and $\theta_e = 0.1710$ rad.

Then, we take $\alpha = \theta_n = 0.4782$ rad for the value of the angle α which subtends the circular arc *TN* of radius $0.382 R_t$, where *N* is the inflexion point of the nozzle contour. We use again the system of reference *Oxy*, whose origin *O* is on the axis of symmetry of the nozzle, in the plane of the throat, whose *x*-axis is the axis of symmetry of the nozzle pointing downstream, and whose *y*-axis is perpendicular to the axis of symmetry and points upward. The co-ordinates *x* and *y* of the points *N* and *E* in the system of reference defined above are

$$x_N = 0.382 R_t \sin \alpha = 0.382 \times 0.3166 \times \sin 0.4782 = 0.05566 \text{ m}$$

$$\begin{aligned} y_N &= R_t [1 + 0.382(1 - \cos \alpha)] = 0.3166 \times [1 + 0.382 \times (1 - \cos 0.4782)] \\ &= 0.3302 \text{ m} \end{aligned}$$

$$x_E = L_n = 2.642 \text{ m}$$

$$y_E = R_E = \varepsilon^{\frac{1}{2}} R_t = 14^{\frac{1}{2}} \times 0.3166 = 1.185 \text{ m}$$

A parabola is chosen for the segment of nozzle going from the inflexion point *N* to the point *E* laying on the exit plane of the nozzle. In order to determine the co-ordinates *x* and *y* of each point of this parabola, we use again the analytical method suggested by Newlands [31], as will be shown below.

The equation of the straight line *NQ* tangent in *N* to the parabola is

$$y - y_N = (x - x_N) \tan \theta_n$$

In the present case, the equation of *NQ* is $y = 0.5183 x + 0.3014$.

The equation of the straight line *EQ* tangent in *E* to the parabola is

$$y - y_E = (x - x_E) \tan \theta_e$$

In the present case, the equation of EQ is $y = 0.1727 x + 0.7288$.

The straight line NQ (whose equation is $y = 0.5183 x + 0.3014$) intersects the straight line EQ (whose equation is $y = 0.1727 x + 0.7288$) in the point Q, whose co-ordinates are easily found to be

$$\begin{aligned}x_Q &= 1.237 \text{ m} \\y_Q &= 0.9424 \text{ m}\end{aligned}$$

Since the co-ordinates of the points N, Q, and E are known, then the parabolic segment of nozzle going from N to E can be expressed by means of a Bézier quadratic curve having the following parametric equations

$$\begin{aligned}x(t) &= (1-t)^2 x_N + 2(1-t)t x_Q + t^2 x_E \quad (0 \leq t \leq 1) \\y(t) &= (1-t)^2 y_N + 2(1-t)t y_Q + t^2 y_E \quad (0 \leq t \leq 1)\end{aligned}$$

In the present case, after substituting the values of (x_N, y_N) , (x_Q, y_Q) , and (x_E, y_E) computed above into the preceding equations, there results

$$\begin{aligned}x(t) &= 0.05566(1-t)^2 + 2.474(1-t)t + 2.642t^2 \quad (0 \leq t \leq 1) \\y(t) &= 0.3302(1-t)^2 + 1.885(1-t)t + 1.185t^2 \quad (0 \leq t \leq 1)\end{aligned}$$

Another numerical example is given below. It concerns the design of a thrust chamber for a rocket whose second stage burns a combination of liquid oxygen with liquid hydrogen, and has the properties specified in Sect. 2.3, which are also given here for convenience. The oxidiser-to-fuel mixture ratio at the thrust chamber is $o/f = 5.22$, the total absolute pressure and the total temperature in the combustion chamber at the nozzle inlet are respectively $(p_c)_{ns} = 5.516 \times 10^6 \text{ N/m}^2$ and $(T_c)_{ns} = 3356 \text{ K}$, the molar mass of the combusted gas is $\mathcal{M} = 12 \text{ kg/kmol}$, the specific heat ratio of the combusted gas is $\gamma = 1.213$, and the expansion area ratio of the nozzle is $A_e/A_t = 40$. Let $F_{tc} = 6.650 \times 10^5 \text{ N}$ be the desired thrust of the second stage in vacuo.

As has been shown in Sect. 2.3, the design value of the thrust coefficient in vacuo is $\bar{C}_F = 1.890$. By substituting this value and $(p_c)_{ns} = 5.516 \times 10^6 \text{ N/m}^2$ in the following equation of Chap. 1, Sect. 1.3

$$\bar{C}_F = \frac{F}{A_t(p_c)_{ns}}$$

and solving this equation for the area A_t of the cross section of the nozzle at the throat plane, there results

$$A_t = \frac{F}{\bar{C}_F(p_c)_{ns}} = \frac{6.650 \times 10^5}{1.890 \times 5.516 \times 10^6} = 0.06379 \text{ m}^2$$

The radius R_t of the cross section of the nozzle at the throat plane is

$$R_t = \left(\frac{A_t}{\pi} \right)^{\frac{1}{2}} = \left(\frac{0.06379}{3.1416} \right)^{\frac{1}{2}} = 0.1425 \text{ m}$$

Since the expansion area ratio of the nozzle is $\varepsilon \equiv A_e/A_t = 40$, then the radius of the cross section of the nozzle at the exit plane is

$$R_e = \varepsilon^{\frac{1}{2}} R_t = 40^{\frac{1}{2}} \times 0.1425 = 0.9012 \text{ m}$$

By using the values given in the table of Sect. 2.4, we choose $L^* = 0.6604 \text{ m}$ for the characteristic length of the combustion chamber.

The volume V_c of the combustion chamber results from the following equation of Sect. 2.4

$$V_c = L^* A_t$$

After substituting $L^* = 0.6604 \text{ m}$ and $A_t = 0.06379 \text{ m}^2$ in the preceding equation, we find $V_c = 0.6604 \times 0.06379 = 0.04213 \text{ m}^3$.

We take $\theta = 0.3491 \text{ rad}$ for the value of the angle of semi-aperture in the converging portion of the nozzle. We also take 1.6 for the contraction area ratio $\varepsilon_c \equiv A_c/A_t$, where $A_c = \pi R_c^2$ is the cross-sectional area of the combustion chamber.

The contour of the nozzle upstream of the throat plane is a circular arc, whose radius R ranges from 0.5 to 1.5 times the radius R_t of the throat. We take

$$R = 1.5 R_t = 1.5 \times 0.1425 = 0.2138 \text{ m}$$

Since 1.6 is the value chosen for the contraction area ratio A_c/A_t , then the radius R_c of the cross-section of the cylindrical combustion chamber is

$$R_c = \left(\frac{A_c}{A_t} \right)^{\frac{1}{2}} R_t = 1.6^{\frac{1}{2}} \times 0.1425 = 0.1802 \text{ m}$$

Since the converging portion of the nozzle is a cone, whose semi-aperture angle is $\theta = 0.3491 \text{ rad}$, then the length L_{conv} of the converging portion of the nozzle results from

$$L_{conv} = \frac{R_t \left[\left(\frac{A_c}{A_t} \right)^{\frac{1}{2}} - 1 \right] + R \left(\frac{1}{\cos \theta} - 1 \right)}{\tan \theta}$$

After substituting $R_t = 0.1425 \text{ m}$, $A_c/A_t = 1.6$, $R = 0.2138 \text{ m}$, and $\theta = 0.3491 \text{ rad}$ in the preceding equation, we find $L_{conv} = 0.1414 \text{ m}$.

The approximate volume V_{conv} of the converging portion of the nozzle is

$$V_{conv} = \frac{1}{3} \times 3.1416 \times 0.1414 \times (0.1802^2 + 0.1802 \times 0.1425 + 0.1425^2) = 0.01162 \text{ m}^3$$

The volume V_{cyl} of the cylindrical combustion chamber, whose length goes from the internal face of the injector to the inlet plane of the nozzle, is

$$V_{cyl} = V_c - V_{conv} = 0.04213 - 0.01162 = 0.03051 \text{ m}^3$$

The length L_{cyl} of the cylindrical combustion chamber is

$$L_{cyl} = \frac{V_{cyl}}{1.6A_t} = \frac{0.03051}{1.6 \times 0.06379} = 0.2989 \text{ m}$$

The total distance L_{total} from the internal face of the injector to the plane of the throat is

$$L_{total} = L_{cyl} + L_{conv} = 0.2989 + 0.1414 = 0.4403 \text{ m}$$

For the diverging portion of the nozzle, we choose a fractional length $L_f = 75\%$ of a $\pi/12$ rad equivalent conical nozzle. Therefore, the true length L_n of the diverging portion of the nozzle is

$$L_n = \frac{n}{100} \frac{R_t}{\tan 0.2618} \left[\varepsilon^{\frac{1}{2}} - 1 + 1.5 \left(\frac{1}{\cos 0.2618} - 1 \right) \right]$$

After substituting $n = 75$, $R_t = 0.1425 \text{ m}$ and $\varepsilon \equiv A_e/A_t = 40$ in the preceding equation, we find $L_n = 2.145 \text{ m}$.

We take the optimum values of the wall angles θ_n and θ_e from the Rao curves for $L_n = 75\%$ and $\varepsilon = 40$. These curves indicate $\theta_n = 0.5760 \text{ rad}$ and $\theta_e = 0.1614 \text{ rad}$.

We also take $\alpha = \theta_n = 0.5760 \text{ rad}$ for the value of the angle α which subtends the circular arc TN of radius $0.382 R_t$, where N is the inflexion point of the nozzle contour. The co-ordinates x and y of the points N and E in the system of reference defined above are

$$\begin{aligned} x_N &= 0.382 R_t \sin \alpha = 0.382 \times 0.1425 \times \sin 0.5760 = 0.02965 \text{ m} \\ y_N &= R_t [1 + 0.382(1 - \cos \alpha)] = 0.1425 \\ &\quad \times [1 + 0.382 \times (1 - \cos 0.5760)] = 0.1513 \text{ m} \\ x_E &= L_n = 2.145 \text{ m} \\ y_E &= R_E = \varepsilon^{\frac{1}{2}} R_t = 40^{\frac{1}{2}} \times 0.1425 = 0.9013 \text{ m} \end{aligned}$$

A parabola is chosen for the segment of nozzle going from the inflexion point N to the point E laying on the exit plane of the nozzle. We determine the co-ordinates x and y of each point of this parabola by using again the analytical method suggested by Newlands [31]. The equation of the straight line NQ tangent in N to the parabola is

$$y - y_N = (x - x_N) \tan \theta_n$$

In the present case, the equation of NQ is $y = 0.6495 x + 0.1320$.
The equation of the straight line EQ tangent in E to the parabola is

$$y - y_E = (x - x_E) \tan \theta_e$$

In the present case, the equation of EQ is $y = 0.1628 x + 0.5521$.

The straight line NQ (whose equation is $y = 0.6495 x + 0.1320$) intersects the straight line EQ (whose equation is $y = 0.1628 x + 0.5521$) in the point Q, whose co-ordinates are easily found to be

$$\begin{aligned}x_Q &= 0.8632 \text{ m} \\y_Q &= 0.6926 \text{ m}\end{aligned}$$

Since the co-ordinates of the points N, Q, and E are known, then the parabolic segment of nozzle going from N to E can be expressed by means of a Bézier quadratic curve having the following parametric equations

$$\begin{aligned}x(t) &= (1-t)^2 x_N + 2(1-t)t x_Q + t^2 x_E \quad (0 \leq t \leq 1) \\y(t) &= (1-t)^2 y_N + 2(1-t)t y_Q + t^2 y_E \quad (0 \leq t \leq 1)\end{aligned}$$

In the present case, after substituting the values of (x_N, y_N) , (x_Q, y_Q) , and (x_E, y_E) computed above into the preceding equations, there results

$$\begin{aligned}x(t) &= 0.02965(1-t)^2 + 1.726(1-t)t + 2.145t^2 \quad (0 \leq t \leq 1) \\y(t) &= 0.1513(1-t)^2 + 1.385(1-t)t + 0.9013t^2 \quad (0 \leq t \leq 1)\end{aligned}$$

2.5 Cooling of a Thrust Chamber

The walls of the thrust chamber of a liquid-propellant rocket engine must be protected from the high temperatures of combustion, which could melt the materials or seriously damage the walls. This is because the hot gases contained in a thrust chamber reach high temperatures, and also transfer high heat fluxes to the walls.

As to the values of temperatures and heat fluxes reached in a liquid-propellant rocket engine, the opinions of the authors are not unanimous. According to Huzel and Huang [5], the combustion temperatures range from 2500 to 3600 K and the heat fluxes range from 817 to 82000 kW/m². According to Wieseneck [43], the combustion temperatures in oxygen-hydrogen rocket engines (such as J-2, J-2S, and M-1) range from 3600 to 4700 K and the heat fluxes range from 28000 to

57000 kW/m². Wieseneck also cite the case of the engines of the Space Shuttle, where the maximum value of design for the heat flux was 118000 kW/m². According to Sutton and Biblarz [2], the combustion temperatures are well above the melting points of the materials of which the walls are made, and the heat fluxes range from 500 to 160000 kW/m². According to Turner [44], a typical temperature is 3000 K, but the melting point of most metals is below 2000 K.

There are several methods for maintaining the temperatures of the walls at levels of safety. Van Huff and Fairchild [45] cite the following methods:

- regenerative cooling, obtained by forcing one or both of the propellants to flow into tubes or channels running longitudinally along the outer surface of the wall to be cooled, before being discharged into a special gas generator or directly into the combustion chamber;
- transpiration cooling, obtained by cooling a porous inner wall by means of a cooling fluid which is forced to flow through the porous material;
- film cooling, obtained by maintaining a thin layer of cooling fluid over the inner surface of the wall; and
- coating, obtained by depositing a layer of low-conductivity material which acts as a thermal barrier on the inner side of the wall.

Huzel and Huang [5] add the following methods:

- dump cooling, obtained by feeding a small percentage of propellant (for example, hydrogen, in a liquid hydrogen-liquid oxygen engine) through passages in the wall of the thrust chamber for cooling, and subsequently dumping it overboard through openings at the rear end of the nozzle skirt;
- ablative cooling, obtained by intentional loss of the inner wall of the thrust chamber, whose material (usually fibre-reinforced organic material) is melted or vaporised away, in order to dissipate heat and save the material of which the outer wall is made; and
- radiation cooling, obtained by radiating heat away from the surface of the outer wall of the thrust chamber.

The choice of one of the methods indicated above depends on the design of the thrust chamber. Huzel and Huang [5] suggest some factors to be considered for a choice. They are indicated below.

- (a) Propellants used, because their combustion products have properties (such as temperature, specific heat ratio, density, viscosity, etc.) which determine the heat fluxes and therefore the cooling requirements.
- (b) Pressure in the combustion chamber, whose value also determines the heat flow rate. In case of high pressure in the combustion chamber, combined regenerative and film cooling methods are frequently used.
- (c) Propellant feed system, which determines the values of pressure in the combustion chamber. For example, in case of a rocket engine fed by turbo-pumps, a high amount of pressure is available for cooling. This amount can be used for regenerative cooling, in order to force the cooling propellant to flow into the

cooling tubes before reaching the injector. By contrast, a rocket engine fed by pressurised gas is limited by a low amount of pressure, and therefore works at a low pressure in the combustion chamber. In the latter case, film, ablative, or radiation cooling methods are to be used.

- (d) Shape of the combustion chamber, which determines the local mass flow rates of combusted gas and the areas of the wall to be cooled.
- (e) Materials used in the construction of a thrust chamber. This is because strength and heat conductivity at high temperatures are desirable properties in materials used for regeneratively cooled thrust chambers. In case of film cooled thrust chambers, materials allowing higher working temperatures are necessary for the purpose of reducing the heat flow rates and therefore the flow rates of the film coolant. The possibility of using radiative cooling depends on the availability of refractory alloys capable of resisting temperatures of 1922 K and more. Likewise, the possibility of using ablative cooling depends on the availability of reinforced plastic materials.

As a general rule, the choice of cooling method has a deep influence on the design of a thrust chamber, and vice versa.

An analysis is made below of the heat transfer from the combustion products contained in a thrust chamber and the walls of that chamber. Due to the high velocity of the hot gases, the heat transfer occurs through convection, and therefore the heat propagates because of the motion of gaseous masses in the thrust chamber. The heat passes from the moving gas firstly to the stagnant boundary layer along the wall, and then to the wall itself.

Let q (measured in W/m^2) be the quantity of heat per unit time per unit surface transferred across the boundary layer. Let h_g ($\text{W m}^{-2} \text{K}^{-1}$) be the heat transfer coefficient on the hot gas side. Let T_{aw} (K) be the temperature of the hot gas at the adiabatic wall. The temperature T_{aw} is assumed to be equal to the total (or stagnation) temperature in the thrust chamber multiplied by a recovery factor (whose value ranges from 0.90 to 0.98) of the turbulent boundary layer. Let T_{wg} (K) be the local temperature of the wall on the hot gas side. The heat transfer through convection is governed by the following equation

$$q = h_g(T_{aw} - T_{wg})$$

The value of the convective heat transfer coefficient h_g can be determined by using the Bartz equation [46, page 30, Eq. 50], as follows

$$h_g = \left[\frac{0.026}{D_t^{0.2}} \left(\frac{\mu^{0.2} c_p}{Pr^{0.6}} \right)_{ns} \left(\frac{(p_c)_{ns}}{\bar{c}^*} \right)^{0.8} \left(\frac{D_t}{\bar{R}} \right)^{0.1} \right] \left(\frac{A_t}{A} \right)^{0.9} \sigma$$

where D_t (m) is the diameter of the nozzle in the throat plane, μ (N s m^{-2}) is the coefficient of dynamic viscosity of the gas, c_p ($\text{J kg}^{-1} \text{K}^{-1}$) is the specific heat of the gas at constant pressure, $Pr = \mu c_p/k$ is the Prandtl number, k ($\text{W m}^{-1} \text{K}^{-1}$) is the thermal conductivity of the gas, $(p_c)_{ns}$ (N/m^2) is the total pressure of the

combustion chamber at the inlet plane of the nozzle, \bar{c}^* (m/s) is the design value of the characteristic velocity, \bar{R} (m) is the mean radius of curvature of the throat in a plane which contains the axis of symmetry of the nozzle, A_t (m^2) is the area of the cross-section of the nozzle in the throat plane, and A (m^2) is the area of the cross-section under consideration along the axis of symmetry of the nozzle.

The dimensionless factor σ of correction is [46, page 30, Eq. 49]:

$$\sigma = \frac{1}{\left[\frac{1}{2} \frac{T_{wg}}{(T_c)_{ns}} \left(1 + \frac{\gamma-1}{2} M^2 \right) + \frac{1}{2} \right]^{0.8-0.2\omega} \left[1 + \frac{\gamma-1}{2} M^2 \right]^{0.2\omega}}$$

where $(T_c)_{ns} = T [1 + \frac{1}{2}(\gamma - 1)M^2]$ is the total temperature (K) of the combustion chamber at the nozzle inlet, M is the local Mach number, $\gamma \equiv c_p/c_v$ is the specific heat ratio of the combusted gas, T_{wg} (K) is the local temperature of the wall on the hot gas side, and ω is the exponent of the temperature dependence of viscosity given below. The value of ω is equal to 0.6 for diatomic gases [47].

According to Wang et al. [48, page 911, Eqs. 4 and 5], in case of data on Pr and μ (N s m^{-2}) not being available for particular mixtures of combusted gas, it is possible to determine approximate values by means of the following equations

$$Pr = \frac{4\gamma}{9\gamma - 5}$$

$$\mu = \kappa T^\omega = (1.184 \times 10^{-7}) \mathcal{M}^{0.5} T^{0.6}$$

where \mathcal{M} (kg/kmol) is the molar mass, T (K) is the temperature of the mixture of combusted gas, and the exponent ω of T has been taken equal to 0.6.

The preceding equations give approximate values of the convective heat transfer coefficient h_g on the hot gas side. The calculated value of h_g may be lower than the real value, because a substantial part of combusted gases may transfer heat through radiation, or because a substantial part of gaseous molecules dissociate and then recombine near the wall of the thrust chamber, or because the gas flow is unstable. Conversely, the calculated value of h_g may be higher than the real value, because the chemical reactions occurring in the combustion process may be incomplete in the combustion chamber, or because the combusted gases may deposit solid particles, which in turn create insulating layers on the wall of the chamber. These solid particles are made of carbon, in case of a combination of liquid oxygen with RP-1 (kerosene). This carbon layer increases the thermal insulation of the wall on the hot gas side.

In order to take account of the solid deposit of carbon on the chamber walls in the computation of the heat transfer, the following equation may be used

$$q = h_{gc} (T_{aw} - T_{wg})$$

where h_{gc} ($\text{W m}^{-2} \text{ K}^{-1}$), which is the overall heat transfer coefficient on the hot gas side, has the following expression

$$h_{gc} = \frac{1}{\frac{1}{h_g} + R_d}$$

where R_d ($\text{m}^2 \text{ K W}^{-1}$) is the thermal resistance caused by the solid deposit. This thermal resistance vanishes ($R_d = 0$) in the absence of deposit.

As an application, taken from [5], we want to compute the approximate value of the overall heat transfer coefficient h_{gc} on the hot gas side in the combustion chamber, at the throat plane, and at the exit plane, for a nozzle whose area expansion ratio is $\varepsilon \equiv A_e/A_t = 5$, for a regeneratively cooled thrust chamber of a rocket engine which burns a combination of liquid oxygen with RP-1 (kerosene), and has the data given in Sect. 2.3. These data are also given below for convenience: the oxidiser-to-fuel mixture ratio at the thrust chamber is $o/f = 2.35$, and the total absolute pressure in the combustion chamber at the nozzle inlet is $(p_c)_{ns} = 6.895 \times 10^6 \text{ N/m}^2$. The chemical reactions in the combustion chamber are assumed to be homogeneous and complete.

As has been shown in Sect. 2.3, the total temperature of the combustion chamber at the nozzle inlet is $(T_c)_{ns} = 3589 \text{ K}$, the molar mass of the combusted gas is $\mathcal{M} = 22.5 \text{ kg/kmol}$, and the specific heat ratio of the combusted gas is $\gamma \equiv c_p/c_v = 1.222$.

The design value $(\bar{T}_c)_{ns}$ of the total temperature of the combustion chamber at the nozzle inlet is equal to the theoretical value $(T_c)_{ns}$ given above multiplied by the square of the correction factor η_{c^*} of the characteristic velocity c^* . Since we have taken $\eta_{c^*} = 0.975$ in Sect. 2.3, then

$$(\bar{T}_c)_{ns} = (T_c)_{ns} \eta_{c^*}^2 = 3589 \times 0.975^2 = 3412 \text{ K}$$

As has been found in Sect. 2.3, the design value of the characteristic velocity is

$$\bar{c}^* = \eta_{c^*} c^* = 0.975 \times 1764 = 1720 \text{ m/s}$$

As has been found in Sect. 2.4, the diameter of the cross section of the nozzle at the throat plane is

$$D_t = 2R_t = 2 \times 0.3166 \text{ m} = 0.6332 \text{ m}$$

The radius of curvature R_{us} of the nozzle contour upstream of the throat plane is

$$R_{us} = 1.5R_t = 1.5 \times 0.3166 \text{ m} = 0.4749 \text{ m}$$

The radius of curvature R_{ds} of the nozzle contour downstream of the throat plane is

$$R_{ds} = 0.382R_t = 0.382 \times 0.3166 \text{ m} = 0.1209 \text{ m}$$

The mean radius \bar{R} of curvature of the nozzle contour at the throat is

$$\bar{R} = \frac{1}{2}(R_{us} + R_{ds}) = 0.5 \times (0.4749 + 0.1209) = 0.2979 \text{ m}$$

In Sect. 2.3, the value of the constant R of the specific gas has been found to be

$$R = \frac{R^*}{\mathcal{M}} = \frac{8314.460}{22.5} = 369.5 \text{ J K}^{-1} \text{ kg}^{-1}$$

Since $\gamma \equiv c_p/c_v = 1.222$ and $c_p - c_v = R = 369.5 \text{ J K}^{-1} \text{ kg}^{-1}$, then

$$c_p = \frac{\gamma}{\gamma - 1} R = \frac{1.222}{1.222 - 1} \times 369.5 = 2034 \text{ J K}^{-1} \text{ kg}^{-1}$$

The Prandtl number is computed as follows

$$Pr = \frac{4\gamma}{9\gamma - 5} = \frac{4 \times 1.222}{9 \times 1.222 - 5} = 0.8149$$

The coefficient of dynamic viscosity of the gas is computed as follows

$$\begin{aligned} \mu &= (1.184 \times 10^{-7}) \mathcal{M}^{0.5} T^{0.6} = (1.184 \times 10^{-7}) \times (22.5)^{0.5} \times (3412)^{0.6} \\ &= 7.400 \times 10^{-5} \text{ N s m}^{-2} \end{aligned}$$

By using the Bartz equation, the convective heat transfer coefficient is computed as follows

$$h_g = \left[\frac{0.026}{D_t^{0.2}} \left(\frac{\mu^{0.2} c_p}{Pr^{0.6}} \right)_{ns} \left(\frac{(p_c)_{ns}}{\bar{c}^*} \right)^{0.8} \left(\frac{D_t}{\bar{R}} \right)^{0.1} \right] \left(\frac{A_t}{A} \right)^{0.9} \sigma$$

After substituting $D_t = 0.6332 \text{ m}$, $\mu = 7.400 \times 10^{-5} \text{ N s m}^{-2}$, $c_p = 2034 \text{ J K}^{-1} \text{ kg}^{-1}$, $Pr = 0.8149$, $(p_c)_{ns} = 6.895 \times 10^6 \text{ N m}^{-2}$, $\bar{c}^* = 1720 \text{ m s}^{-1}$, and $\bar{R} = 0.2979 \text{ m}$ in the preceding equation, we find

$$h_g = 8042 \left(\frac{A_t}{A} \right)^{0.9} \sigma \text{ W m}^{-2} \text{ K}^{-1}$$

In order to determine the value of the correction factor σ at the exit plane of the nozzle, we compute the static pressure p_e of the combusted gas at the exit plane, as will be shown below. The static pressure p_e at the exit section of area $A_e = 5A_t$ results from the following equation

$$\frac{A_e}{A_t} = \frac{\left(\frac{2}{\gamma+1}\right)^{\frac{1}{\gamma-1}} \left(\frac{(p_c)_{ns}}{p_e}\right)^{\frac{1}{\gamma}}}{\left\{\frac{\gamma+1}{\gamma-1} \left[1 - \left(\frac{p_e}{(p_c)_{ns}}\right)^{\frac{\gamma-1}{\gamma}}\right]\right\}^{\frac{1}{2}}}$$

The unknown value of p_e can be computed numerically. For this purpose, we define $z \equiv p_e/(p_c)_{ns}$, where z is an auxiliary variable. In the present case ($A_e/A_t = 5$ and $\gamma = 1.222$), we define a function $f(z)$ such that

$$f(z) \equiv 5^2 - \frac{\left(\frac{2}{1.222+1}\right)^{\frac{2}{1.222-1}} \left(\frac{1}{z}\right)^{\frac{2}{1.222}}}{\frac{1.222+1}{1.222-1} \left(1 - z^{\frac{1.222-1}{1.222}}\right)}$$

We search the unknown value of z in the interval $0.025 \leq z \leq 0.035$, because the value of the function $f(z)$ changes sign in this interval.

By applying repeatedly Müller's method (see Chap. 1, Sect. 1.2), we find, with four significant figures, $z = 0.03044$. Therefore, remembering the definition of the auxiliary variable z , we have

$$p_e = z(p_c)_{ns} = 0.03044 \times 6.895 \times 10^6 = 2.099 \times 10^5 \text{ N/m}^2$$

Now, we compute the flow temperature at the exit plane of the nozzle (T_e). In case of an isentropic flow ($\rho/\rho^\gamma = \text{constant}$), the energy equation, written for any two points 1 and 2 placed along the axis of symmetry of the nozzle, yields

$$\frac{T_1}{T_2} = \left(\frac{p_1}{p_2}\right)^{\frac{\gamma-1}{\gamma}}$$

Since $(\bar{T}_c)_{ns} = 3412 \text{ K}$ and $(p_c)_{ns} = 6.895 \times 10^6 \text{ N/m}^2$ are respectively the total temperature and the total pressure of the combustion chamber at the inlet plane of the nozzle, then the preceding equation, solved for the flow temperature T_e at the exit plane of the nozzle, yields

$$T_e = (\bar{T}_c)_{ns} \left[\frac{p_e}{(p_c)_{ns}} \right]^{\frac{\gamma-1}{\gamma}} = 3412 \times \left(\frac{2.099 \times 10^5}{6.895 \times 10^6} \right)^{\frac{1.222-1}{1.222}} = 1809 \text{ K}$$

Now we compute the flow velocity v_e at the exit plane of the nozzle. The flow velocity at the exit plane of the nozzle, where the static pressure of the combusted gas is $p_e = 2.099 \times 10^5 \text{ N/m}^2$, is expressed by the following equation

$$v_e = \left\{ \frac{2\gamma}{\gamma-1} R (\bar{T}_c)_{ns} \left[1 - \left(\frac{p_e}{(p_c)_{ns}} \right)^{\frac{\gamma-1}{\gamma}} \right] \right\}^{\frac{1}{2}}$$

After substituting $p_e = 2.099 \times 10^5 \text{ N/m}^2$ into the preceding equation, there results

$$v_e = \left\{ \frac{2 \times 1.222}{1.222 - 1} \times 369.5 \times 3412 \times \left[1 - \left(\frac{2.099 \times 10^5}{6.895 \times 10^6} \right)^{\frac{1.222-1}{1.222}} \right] \right\}^{\frac{1}{2}} = 2553 \text{ m/s}$$

Finally, we compute the Mach number M_e of the gas flow at the exit plane of the nozzle. The sonic velocity a_e of the gas flow at the exit plane of the nozzle is

$$a_e = (\gamma RT_e)^{\frac{1}{2}} = (1.222 \times 369.5 \times 1809)^{\frac{1}{2}} = 903.8 \text{ m/s}$$

Therefore, the Mach number of the gas flow at the exit plane of the nozzle is

$$M_e = \frac{v_e}{a_e} = \frac{2553}{903.8} = 2.825$$

Since the temperature T_{wg} of the carbon deposit approaches the temperature $(T_c)_{ns}$ of the combusted gas, then we take 0.8 as the value of the ratio $T_{wg}/(T_c)_{ns}$. We have also taken 0.4 as the value of the Mach number M at the inlet plane of the nozzle. After introducing these values in the following equation

$$\sigma = \frac{1}{\left[\frac{1}{2} \frac{T_{wg}}{(T_c)_{ns}} \left(1 + \frac{\gamma-1}{2} M^2 \right) + \frac{1}{2} \right]^{0.68} \left[1 + \frac{\gamma-1}{2} M^2 \right]^{0.12}}$$

where the exponent ω has been set equal to 0.6, we find $\sigma = 1.066$ at the inlet plane of the nozzle.

We take 1.6 (see Sect. 2.4) for the value of the contraction area ratio A_t/A_i of the nozzle, and find at the inlet plane of the nozzle

$$\left(\frac{A_t}{A} \right)^{0.9} = \left(\frac{1}{1.6} \right)^{0.9} = 0.6551$$

Therefore, the heat transfer coefficient at the inlet plane of the nozzle is

$$h_g = 8042 \left(\frac{A_t}{A} \right)^{0.9} \sigma = 8042 \times 0.6551 \times 1.066 = 5016 \text{ W m}^{-2} \text{ K}^{-1}$$

At the throat plane of the nozzle, there results $M = 1$, $(A_t/A)^{0.9} = 1$, and $\sigma = 1.027$. Therefore, the heat transfer coefficient at the throat plane is

$$h_g = 8042 \times 1 \times 1.027 = 8259 \text{ W m}^{-2} \text{ K}^{-1}$$

At the exit plane of the nozzle, there results

$$\left(\frac{A_t}{A}\right)^{0.9} = \left(\frac{1}{5}\right)^{0.9} = 0.2349$$

and the Mach number has been found to be $M_e = 2.825$. After introducing this value in the following equation

$$\sigma = \frac{1}{\left[\frac{1}{2} \frac{T_{wg}}{(T_e)_{ns}} \left(1 + \frac{\gamma-1}{2} M^2\right) + \frac{1}{2}\right]^{0.68} \left[1 + \frac{\gamma-1}{2} M^2\right]^{0.12}}$$

we find $\sigma = 0.7944$.

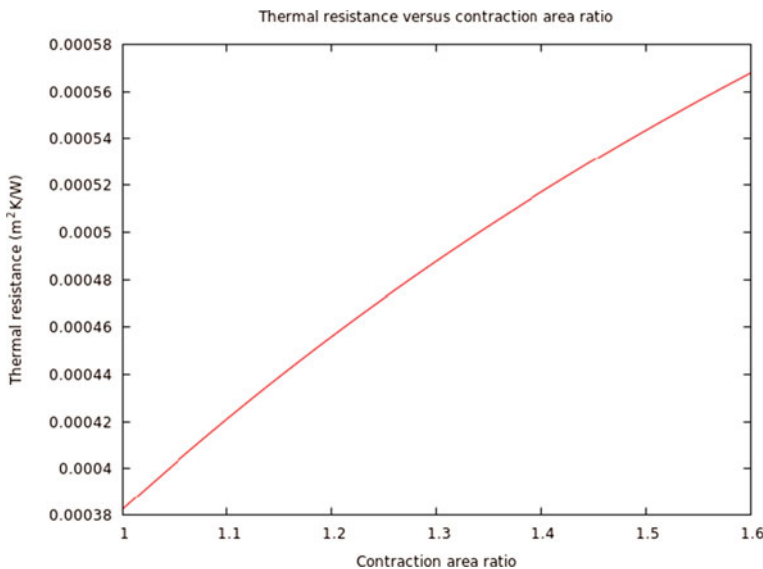
Therefore, the heat transfer coefficient at the exit plane is

$$h_g = 8042 \times 0.2349 \times 0.7944 = 1501 \text{ W m}^{-2} \text{ K}^{-1}$$

Experimental data have been given graphically by NASA [5] on the thermal resistance R_d of carbon deposit on thrust chamber walls, for a rocket engine which burns liquid oxygen and RP-1, at a mixture ratio $o/f = 2.35$, and at a total absolute pressure at the nozzle inlet plane $(p_c)_{ns} = 6.895 \times 10^6 \text{ N/m}^2$, as is the case with the present calculation. The same data can also be expressed numerically by using the following equations.

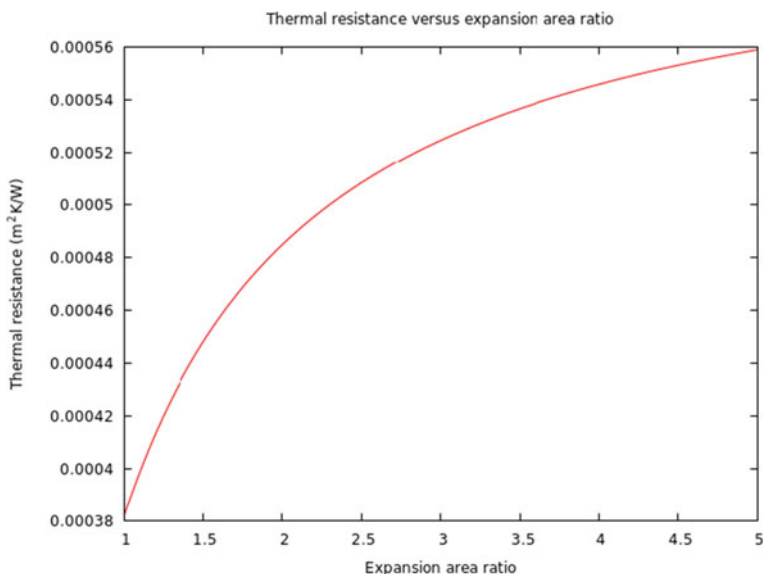
- (1) For the portion of nozzle going from the throat plane to the inlet plane, where the contraction area ratio ε_c is equal to 1.6:

$$R_d = 3.397 \times 10^{-7} \times \left[\exp\left(8.079 - \frac{1.053}{\varepsilon_c}\right) \right]$$



- (2) For the portion of nozzle going from the throat plane to the exit plane, where the expansion area ratio ε is equal to 5.0:

$$R_d = 3.397 \times 10^{-7} \times \left[\exp\left(7.5 - \frac{0.4749}{\varepsilon}\right) \right]$$



By substituting $\varepsilon_c = 1.6$, $\varepsilon = 1.0$, and $\varepsilon = 5.0$ in the two equations written above, the resulting values of thermal resistance R_d are

$$R_d = 0.0005675 \text{ m}^2\text{K/W} \text{ at the inlet plane}$$

$$R_d = 0.0003823 \text{ m}^2\text{K/W} \text{ at the throat plane}$$

$$R_d = 0.0005585 \text{ m}^2\text{K/W} \text{ at the exit plane}$$

The values of the overall heat transfer coefficient h_{gc} on the hot gas side result from substituting the values of h_g and of R_d determined above in the following equation

$$h_{gc} = \frac{1}{\frac{1}{h_g} + R_d}$$

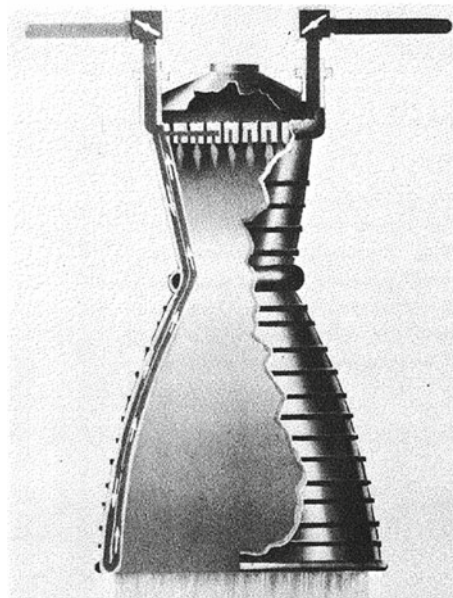
By so doing, we find

$$h_{gc} = 1341 \text{ W m}^{-2} \text{ K}^{-1} \text{ at the inlet plane}$$

$$h_{gc} = 1987 \text{ W m}^{-2} \text{ K}^{-1} \text{ at the throat plane}$$

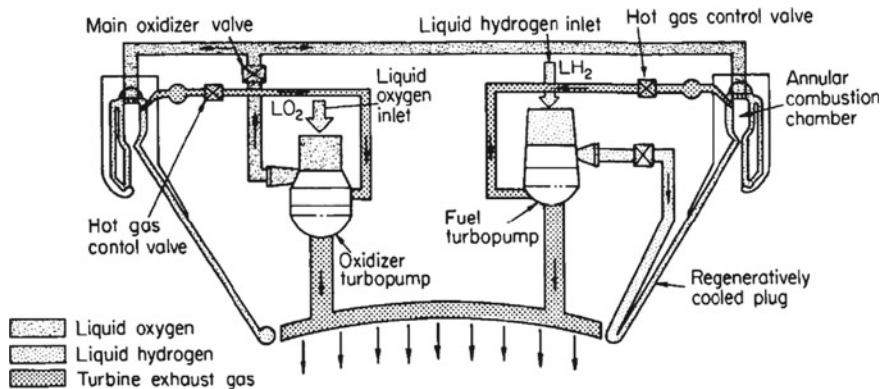
$$h_{gc} = 816.5 \text{ W m}^{-2} \text{ K}^{-1} \text{ at the exit plane}$$

We describe first the regenerative cooling method, because it is the most widely used of all cooling methods, due to its advantages in terms of reliability, durability, and high performance. The following figure, due to the courtesy of NASA [43], illustrates a regeneratively cooled thrust chamber for a bell nozzle.



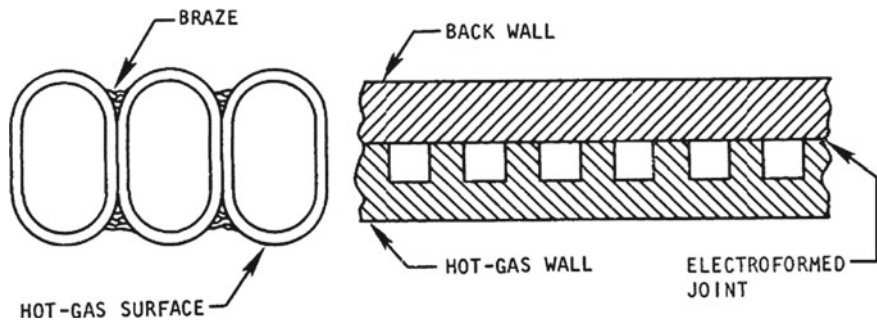
The cooling tubes or channels run longitudinally along the wall and carry cryogenic fuel, which is liquid hydrogen for the main engines of the Space Shuttle. The cryogenic fuel coming from the fuel pump passes through the fuel valve, and then flows downward, that is, toward the exit plane of the nozzle, as indicated by the white arrows in the preceding figure. At this plane, the fuel reverses the direction of its motion, and therefore flows upward in a parallel tube, is mixed with liquid oxygen at the top, and is then ignited inside the combustion chamber. The cryogenic fuel removes, by heat convection, the heat due to the burned gas in the combustion chamber and in the nozzle.

The following figure, due to the courtesy of NASA [49], illustrates the regeneratively cooled plug and combustion chamber for an aerospike engine.



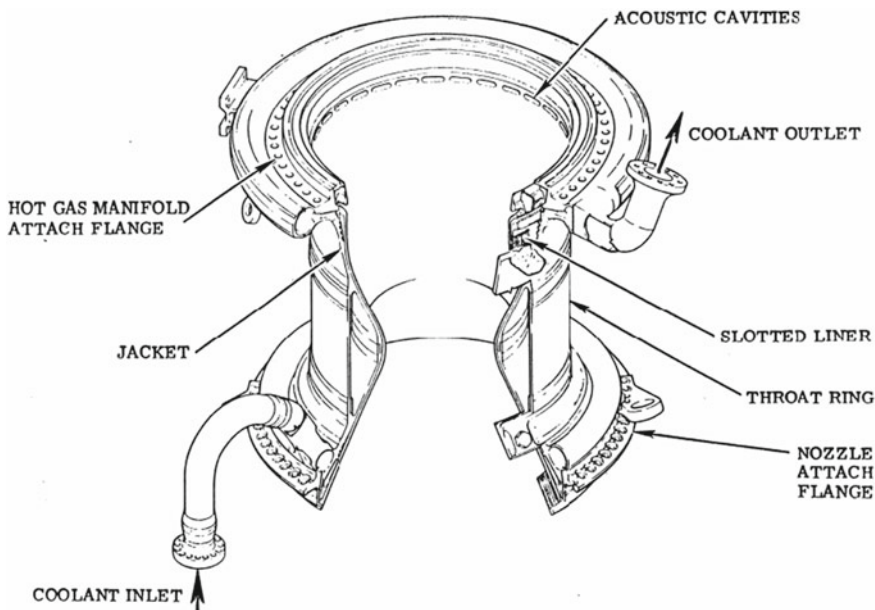
Usually, the fuel is used as the cooling fluid rather than the oxidiser, because of its higher heat capacity, that is, because of its higher capability of removing heat from the nozzle without vaporising. In addition, the fuel, when heated, requires a smaller supply of energy, acquired through ignition, in order to be burned in the presence of the oxidiser. The heat removal for the Saturn V F-1 engines was slightly different from that described above, because these engines burned kerosene, which is not a cryogenic fuel, but is still capable of cooling a nozzle. The kerosene came down from the top to the bottom in one tube, turned around, and came back up in the parallel tube.

The following figure, also due to the courtesy of NASA [43], illustrates a cross-section of the wall of a thrust chamber, having tubes (left) or rectangular channels (right).



Additional information (taken from [50]) is given below on the regenerative cooling system used for each of the three liquid hydrogen-liquid oxygen main engines of the Space Shuttle. The same method has also been successfully used for the Thor, Jupiter, Atlas, H-1, J-2, F-1, RS-27, and several other US Air Force and NASA rocket engines.

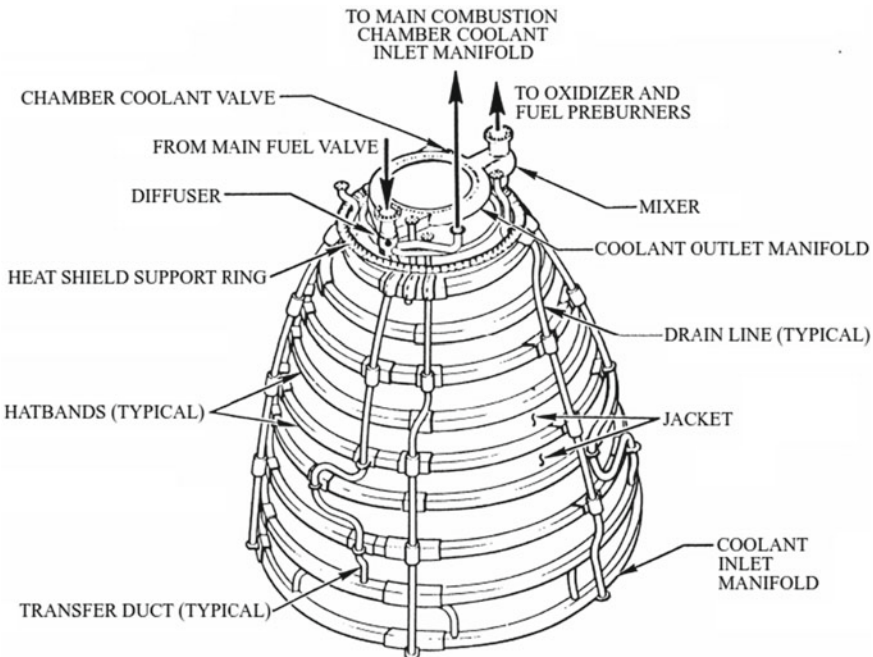
The main combustion chamber of the RS-25 engine of the Space Shuttle is shown in the following figure, due to the courtesy of NASA [51].



This combustion chamber includes a liner, a jacket, a throat ring, a coolant inlet manifold, and a coolant outlet manifold. The outer surface of the liner has 430 milled slots, which are closed out by electro-deposited nickel. The jacket halves are placed around the liner and welded. The coolant manifolds are welded to the jacket and the liner. The throat ring is welded to the jacket to add strength to the main combustion chamber. This creates a regeneratively-cooled combustion chamber, in which the

cooling fuel makes a single up-pass through the milled slots of the liner. The liner is made of NARloy Z (North American Rockwell alloy Z), which is mostly copper, with silver and zirconium added.

The nozzle of the same engine is shown in the following figure, also due to the courtesy of NASA [51]. This nozzle consists of 1800 stainless steel tubes brazed to themselves and to a structural jacket. Nine hatbands are welded around the jacket for hoop strength. Coolant manifolds are welded to the top and to the bottom of the nozzle, along with three fuel transfer ducts and six drain lines.

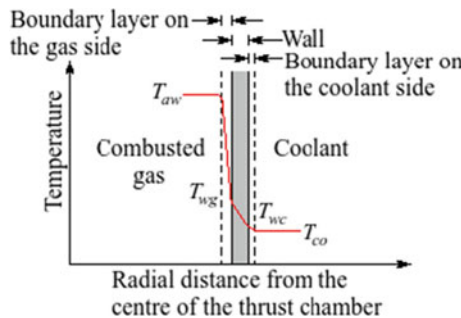


This nozzle is cooled by the fuel, which enters the diffuser and splits to flow to the main combustion chamber, to the three fuel transfer ducts, and through the chamber coolant valve to the mixer. Fuel flowing through each transfer duct splits at each steer-horn to enter the nozzle coolant inlet manifolds at six points.

The fuel then makes a single up-pass through the 1080 tubes to the outlet manifold, and then to the mixer, to join the bypass flow from the chamber coolant valve. The flow recirculation inhibitor is a porous rope-like barrier, which prevents a recirculating flow of hot exhaust gas from reaching and damaging the bellows seal located at the joint between the main combustion chamber and the nozzle. This flow recirculation inhibitor is a sleeve of braided Nextel® 321 filled with Saffil® batting. Both materials, which are composed of silica-glass ceramic fibre, can withstand working temperatures of up to 1700 K. The materials provide the required resistance to flow.

By the way, the thermal protection system used in the nozzle is an insulation system which protects the nozzle from high temperatures during launch and re-entry. During the ascent phase, the three nozzles are subject to plume radiation and convection from the three main engines and to plume radiation from the solid rocket boosters. During the re-entry phase, two of the nozzles are exposed to high heat loads due to convective aerodynamic heating.

In the following part of this paragraph, we consider in further depth the heat transfer through convection between the hot gas which moves on one side of the thrust chamber and the coolant fluid which moves on the other side. This heat passes through a series of contiguous layers, including the boundary layer along the wall on the side of the combusted gas, the thickness of the wall, and the boundary layer along the wall on the side of the coolant fluid, as shown in the following figure. Let h_{gc} ($\text{W m}^{-2} \text{K}^{-1}$) be the heat transfer coefficient on the hot gas side, h_c ($\text{W m}^{-2} \text{K}^{-1}$) be the heat coefficient on the coolant side, q (W/m^2) be the heat flux, T_{aw} , T_{wg} , T_{wc} , and T_{co} (K) be the temperatures of respectively the hot gas at the adiabatic wall, the wall on the hot gas side, the wall on the coolant side, and the coolant, k ($\text{W m}^{-1} \text{K}^{-1}$) be the thermal conductivity of the wall, t (m) be the thickness of the wall, and H ($\text{W m}^{-2} \text{K}^{-1}$) be the overall heat transfer coefficient. In the absence of deposits on the hot gas side, h_{gc} and h_g have the same value.



In the steady state, the heat transfer equations can be expressed as follows

$$q = h_{gc}(T_{aw} - T_{wg}) = \frac{k}{t}(T_{wg} - T_{wc}) = h_c(T_{wc} - T_{co}) = H(T_{aw} - T_{co})$$

where the overall heat transfer coefficient H results from

$$H = \left(\frac{1}{h_{gc}} + \frac{t}{k} + \frac{1}{h_c} \right)^{-1}$$

The coolant increases its temperature from its point of entry into to its point of exit from the cooling channel, depending on the heat absorbed and its rate of flow. The metals commonly used for the walls of combustion chambers are stainless steel,

nickel, and Inconel®, the last of them being a high-performance austenitic nickel-chromium-based alloy. According to Huzel and Huang [5], the temperature of the wall on the hot gas side is about 1089–1255 K, and the difference of temperature between the combusted gas and the wall ranges from 1644 to 3589 K. The equations written above show that the heat flux q is the same for the three layers and depends on the temperatures and on the overall heat transfer coefficient H . The value of H , in turn, depends on the individual heat transfer coefficients relating to the boundary layers and to the wall.

Since $q = H(T_{aw} - T_{co})$, then a small value of H implies a small value of q . It is a primary objective for a designer to keep the value of h_{gc} lower than the values of h_c and t/k . By so doing, there will be a higher temperature drop $T_{aw} - T_{wg}$ in the boundary layer on the hot gas side, as shown in the preceding figure, than the temperature drops ($T_{wg} - T_{wc}$ and $T_{wc} - T_{co}$) in, respectively, the wall and the boundary layer on the coolant side.

The value of the heat transfer coefficient h_c on the coolant side depends on several factors, such as possible chemical reactions of dissociation occurring in the coolant, its pressure, and its bulk temperature. It also depends on a possible formation of bubbles due to a coolant boiling near the wall. In order to achieve a good heat-absorbing capacity of the coolant, the pressure and the velocity of the coolant in its flow are selected so that a boiling is permitted locally, but the bulk of the coolant does not reach the boiling condition [2]. In the absence of boiling, at subcritical temperatures, and in transitional or turbulent regime (in the interval $3000 \leq Re \leq 10^6$), the relation between the wall temperature and the heat flux, which depends on the heat transfer coefficient h_c , can be expressed approximately by using one of the following three equations due to Taler [52, page 4, Eqs. 18, 19, and 20]. The value of the Prandtl number indicates which of these equations is to be used.

$$Nu = 0.02155 Re^{0.8018} Pr^{0.7095} (0.1 \leq Pr \leq 1)$$

$$Nu = 0.01253 Re^{0.8413} Pr^{0.6179} (1 < Pr \leq 3)$$

$$Nu = 0.00881 Re^{0.8991} Pr^{0.3911} (3 < Pr \leq 1000)$$

where $Nu = h_c d/k$ is the Nusselt number, h_c ($\text{W m}^{-2} \text{ K}^{-1}$) is the heat transfer coefficient on the coolant side, d (m) is the hydraulic diameter (defined below) of each coolant duct at the section of interest, k ($\text{W m}^{-1} \text{ K}^{-1}$) is the thermal conductivity of the coolant at the bulk temperature T_{co} , $Re = \rho v d / \mu$ is the Reynolds number, ρ (kg/m^3) is the density of the coolant at the bulk temperature T_{co} , v (m/s) is the velocity of the coolant, μ (Ns/m^2) is the coefficient of dynamic viscosity of the coolant at the bulk temperature T_{co} , $Pr = \mu c_p / k$ is the Prandtl number, and c_p ($\text{J kg}^{-1} \text{ K}^{-1}$) is the specific heat of the coolant at constant pressure at the bulk temperature T_{co} .

In the conditions specified above and in turbulent or transitional regime (in the interval $3000 \leq Re \leq 5 \times 10^6$), it is also possible to use the following relation due to Gnielinski [53, page 11, Eq. 11]:

$$Nu = \frac{0.125 f_D (Re - 1000) Pr}{1 + 12.7(0.125 f_D)^{\frac{1}{2}} (Pr^{\frac{2}{3}} - 1)}$$

where Nu , Re , and Pr are defined above, and f_D is the Darcy friction factor (see below) of the cooling tubes. Some authors (see, for example, [54], Table 12, and [55], Table 8) have proposed other equations, which also express the relation between the wall temperature and the heat flux.

By hydraulic diameter of a duct, we mean the quantity $d = 4A/P$, where A (m^2) is the cross-sectional area of the duct, and P (m) is the perimeter of the wetted portion of its cross section.

When the heat is transferred through a vapour-film boundary layer, for example, when the coolant is hydrogen in supercritical conditions of pressure and temperature, then the value of h_c ($\text{W m}^{-2} \text{ K}^{-1}$) can be estimated by means of the following correlation due to McCarthy and Wolf [56, page 95, Eq. 2]:

$$h_c = 0.025 \left(\frac{c_p \mu^{0.2}}{Pr^{0.6}} \right)_{co} \frac{G^{0.8}}{d^{0.2}} \left(\frac{T_{co}}{T_{wc}} \right)^{0.55}$$

where c_p ($\text{J kg}^{-1} \text{ K}^{-1}$) is the isobaric specific heat of the coolant, μ (N s m^{-2}) is the coefficient of dynamic viscosity of the coolant, Pr is the Prandtl number defined above, G ($\text{kg s}^{-1} \text{ m}^{-2}$) is the mass flow rate of the coolant per unit area to be cooled, d (m) is the diameter of the coolant passage, T_{co} (K) is the bulk temperature of the coolant, T_{wc} (K) is the temperature of the wall on the coolant side, and the subscript co indicates the bulk temperature of the coolant.

In the conditions specified above, the value of h_c ($\text{W m}^{-2} \text{ K}^{-1}$) can also be estimated by using the following correlation due to Taylor [56, page 95, Eq. 8]:

$$h_c = 0.023 \left(\frac{c_p \mu^{0.2}}{Pr^{0.6}} \right)_{co} \frac{G^{0.8}}{d^{0.2}} \left(\frac{T_{co}}{T_{wc}} \right)^{0.57 - \frac{1.59d}{x}}$$

where d (m) is the inner diameter of each cooling tube, and x (m) is the axial distance downstream of the section of entrance of the coolant.

As mentioned above, the bulk temperature of the coolant should be kept below the critical value, because the value of the heat transfer coefficient of the vapour-film boundary layer would be too low to cool effectively the wall.

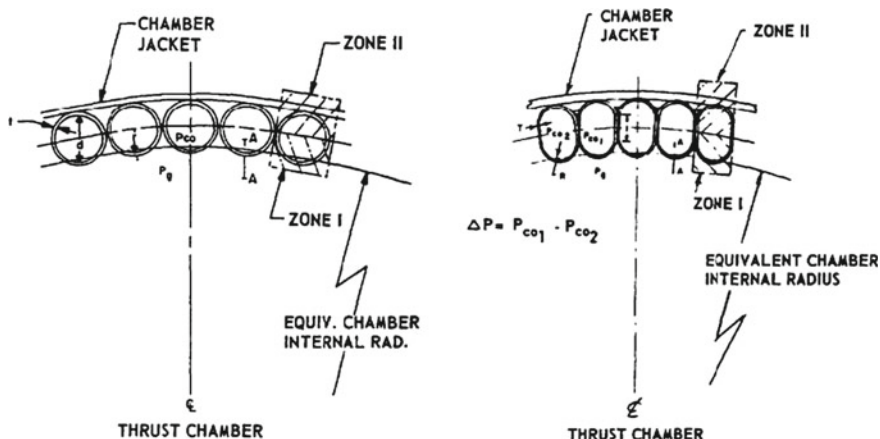
The cooling capacity Q_c (W) of a liquid coolant used in a regenerative cooling system can be estimated by means of the following equation [5]:

$$Q_c = \dot{m}_c c_p (T_{cc} - T_{ci})$$

where \dot{m}_c (kg/s) is the mass flow rate of the coolant, c_p ($\text{J kg}^{-1} \text{ K}^{-1}$) is the specific heat of the coolant at constant pressure, T_{cc} (K) is the critical temperature of the coolant, and T_{ci} (K) is the temperature of the coolant at the inlet. The allowed value of the total heat transfer rate Q (W) from the hot gas to the wall must be less than the

cooling capacity Q_c (that is, $Q < Q_c$) of the coolant by a margin imposed by safety. This limitation does not affect hydrogen when used as a coolant fluid, because of its high transfer coefficient even in supercritical conditions of pressure and temperature. Hydrogen enters the coolant passage of the thrust chamber at supercritical pressure and reaches its supercritical temperature at a short distance from the inlet section. The cross-section areas of the coolant passage at various points along the wall of the thrust chamber must be designed to maintain the coolant velocity imposed by the heat transfer coefficient determined by the calculation. Possible design choices for the cooling jacket include longitudinal tubes (for engines whose thrust is equal to or greater than 13,400 N) and coaxial shells separated by helical ribs or wires (for engines of smaller thrust). In the latter case, the coolant passage is the rectangular area limited by the inner shell, the outer shell, and two adjacent ribs. The ribs are wrapped helically around the inner shell.

In case of thrust chambers of tubular shape, such as those described in Sect. 2.4, the number of tubes for the coolant fluid depends on factors such as the size of the thrust chamber, the mass flow rate of the coolant for unit area of the tubes, the maximum allowable stress for the material of which the tubes are made, and manufacturing considerations. The region of a thrust chamber which needs the maximum cooling is the throat, because there the heat flux q is also maximum. Therefore, the cooling requirements at the throat determine the number of cooling tubes for a given flow rate of the coolant used. The cross section of the cooling tubes is often circular, for easiness of manufacturing and lower stress. The mechanical and thermal stresses acting on the cooling tubes are induced by the pressure exerted by the coolant, and by the difference of temperature between the tubes and the wall. In addition, since two adjacent tubes may be subject to different pressures, then distorting stresses may also arise. As has been shown above, the region of a thrust chamber subject to the maximum stress is the throat.



In order to evaluate the maximum combined tensile stress σ_t (N/m^2) acting on the cross section A-A of a circular cooling tube, as shown on the left-hand side of

the preceding figure, due to the courtesy of NASA [5], Huzel and Huang [5] indicate the following formula

$$\sigma_t = \frac{(p_{co} - p_g)r}{t} + \frac{E\lambda qt}{2(1-\nu)k} + \frac{6M_A}{t^2}$$

where p_{co} (N/m^2) is the pressure of the coolant, p_g (N/m^2) is the pressure of the combusted gas, r (m) is the radius of the cross section of the cooling tubes, t (m) is the thickness of the cooling tubes, E (N/m^2) is the modulus of elasticity of the material of which the cooling tubes are made, λ ($\text{m m}^{-1} \text{K}^{-1}$) is the coefficient of thermal expansion of the same material, q (W/m^2) is the quantity of heat per unit time per unit surface, ν is the Poisson ratio of the same material, k ($\text{W m}^{-1} \text{K}^{-1}$) is the thermal conductivity of the same material, and M_A (Nm/m) is the bending moment per unit length acting at the section A-A due to the distortion induced by difference of pressure between adjacent cooling tubes or by other effects, such as discontinuities. In case of tubes of circular cross section, the bending moment per unit length M_A is caused only by discontinuity, because there is no effect of difference of pressure between adjacent tubes [5].

With reference to the preceding figure, the mean temperature in the zone I (which is on the side of the combusted gas) of each cooling tube is much higher than the mean temperature in the zone II (which is on the side of the outer shell). Therefore, the thermal expansion of the cooling tube in zone I is restrained by the low temperature in zone II. Since the mass in zone II is greater than the mass in zone I, then thermal inelastic buckling can arise in zone I in the longitudinal direction. The thermal stress σ (N/m^2) in the longitudinal direction and the critical stress σ_c (N/m^2) relating to the longitudinal inelastic buckling may be evaluated by using the following equations [5]:

$$\sigma = E\lambda\Delta T$$

$$\sigma_c = \frac{4E_t E_c t}{(E_t^{\frac{1}{2}} E_c^{\frac{1}{2}})^2 [3(1 - \nu^2)]^{\frac{1}{2}} r}$$

where ΔT (K) is the mean difference of temperature between zone I and zone II, E_t (N/m^2) is the tangential modulus of elasticity at the wall temperature, and E_c (N/m^2) is the tangential modulus of elasticity from the compression stress-strain curve at the wall temperature. The thermal stress σ should not be higher than $0.9\sigma_c$. The preceding figure also shows, on the right-hand side, cooling tubes of elongated cross section. The equations written above can also be applied for the purpose of computing the stresses in such tubes. The maximum combined stress acts in the section A-A. The bending moment per unit length M'_A (Nm/m) acting at this section should be computed by taking into account not only the effect of discontinuities, but also the difference of pressure between adjacent tubes, as follows

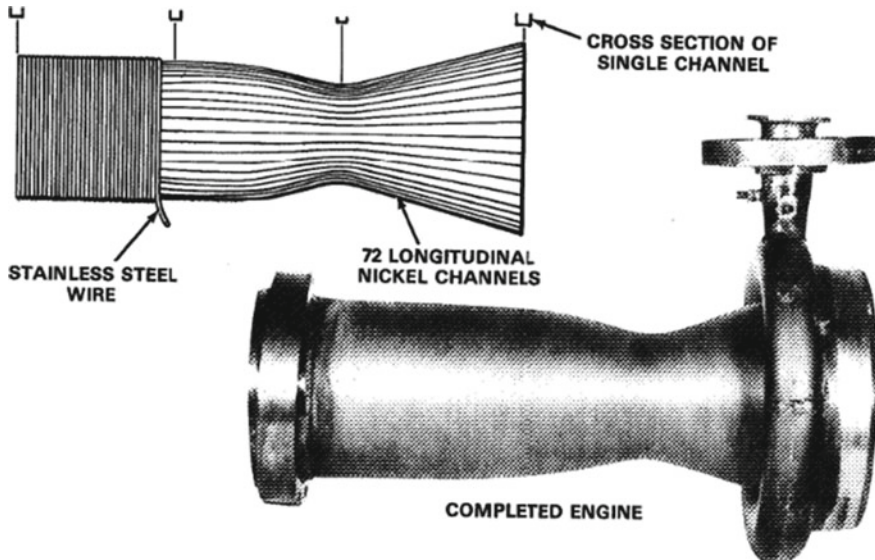
$$M'_A = M_A + K_A \frac{\ell \Delta p}{2}$$

where M_A (Nm/m) is the bending moment per unit length acting on the section A-A due only to discontinuity, K_A is a dimensionless constant whose value is in the range 0.3–0.5, ℓ (m) is the length of the flat portion on the cross-section of each tube, and Δp (N/m²) is the difference of pressure between adjacent tubes. The value of M'_A , determined as specified above, is to be inserted (instead of M_A) in the preceding equation

$$\sigma_t = \frac{(p_{co} - p_g)r}{t} + \frac{E\lambda qt}{2(1-\nu)k} + \frac{6M_A}{t^2}$$

in order to evaluate the maximum combined tensile stress σ_t (N/m²) acting on the cross section A-A of an elongated tube. The loads due to the pressure acting on a regeneratively cooled thrust chamber of tubular shape are borne by the chamber jacket or by tension bands wrapped around the chamber.

The following figure, due to the courtesy of NASA [57] shows a regeneratively cooled thrust chamber of the coaxial shell type, relating to an experimental rocket developing a thrust of 22,000 N.



This thrust chamber, which was designed in 1957 by Edward Baehr, consists of a number of longitudinal channels of varying depth according to the velocity required for the coolant. These channels are bonded together to make up the chamber and bound by stainless steel wire wrapping which is brazed to make a fluid-tight and strong outer skin. In a thrust chamber of this type, the outer skin (the brazed wire) is

subject only to the hoop stress due to the pressure exerted by the coolant. The inner shell is subject to the mechanical stress is due to the difference of pressure existing between the combusted gas and the coolant, and also to the thermal stress due to the heat transfer across the wall.

The combined maximum compressive stress σ_c (N/m^2) occurs at the inner surface of the inner shell and can be computed as follows [5]:

$$\sigma_c = \frac{(p_{co} - p_g)R}{t} + \frac{E\lambda qt}{2(1-\nu)k}$$

where p_{co} and p_g (N/m^2) are the pressures of respectively the coolant and the combusted gas, R (m) is the radius of the inner shell, t (m) is the thickness of the inner shell, E (N/m^2) is the modulus of elasticity of the material of which the inner shell is made, λ ($\text{m m}^{-1} \text{K}^{-1}$) is the coefficient of thermal expansion of the same material, q (W/m^2) is the quantity of heat per unit time per unit surface, ν is the Poisson ratio of the same material, and k ($\text{W m}^{-1} \text{K}^{-1}$) is the thermal conductivity of the same material.

Since the heat transfer in a rocket engine occurs mainly through convection, it is desirable to reduce the pressure drop of the coolant fluid to the minimum possible value. For this purpose, it is necessary to avoid abrupt changes in the direction of the coolant fluid and also in the hydraulic diameter of the tubes. In addition, the inner surfaces of these tubes should be smooth and clean. The pressure drop Δp (N/m^2) in a tube of length L (m) and hydraulic diameter d (m) is expressed as a function of the Darcy friction factor f_D (dimensionless) of the tube by means of the Darcy-Weisbach equation, as follows

$$\Delta p = f_D \frac{L}{d} \left(\frac{1}{2} \rho v^2 \right)$$

where ρ (kg/m^3) and v are respectively the density and the average velocity of the coolant flowing in the tube. The Darcy friction factor f_D depends on the Reynolds number Re defined above and also on the shape and smoothness of the tubes.

The value of f_D is determined experimentally. In practice, in laminar flow regime ($Re < 2300$), $f_D = 64/Re$. In transitional flow regime ($2300 \leq Re \leq 4000$), there are large uncertainties as to the value of f_D . In turbulent flow regime ($Re > 4000$) and in rough tubes, the value of f_D can be determined by means of the Colebrook-White relation [58], as follows

$$\frac{1}{f_D^{\frac{1}{2}}} = -2 \log_{10} \left(\frac{\varepsilon}{3.7d} + \frac{2.51}{Re f_D^{\frac{1}{2}}} \right)$$

where ε (m), called absolute roughness, is the average height of the irregularities existing on the inner surface of a tube, and d (m) is the hydraulic diameter of the tube. The dimensionless ratio ε/d is called relative roughness.

The relation written above is implicit, because the unknown f_D is on both sides of the relation. It can be solved numerically, for given values of ε/d and Re , by defining an interval of search $a \leq f_D \leq b$ and a function $g(f_D)$ such that

$$g(f_D) \equiv \frac{1}{f_D^{\frac{1}{2}}} + 2 \log_{10} \left(\frac{\varepsilon}{3.7d} + \frac{2.51}{Re f_D^{\frac{1}{2}}} \right)$$

with $g(a)g(b) < 0$, and then searching the value of f_D which satisfies the condition $g(f_D) = 0$ to some acceptable degree of tolerance, as has been shown in Chap. 1, Sect. 1.2. The following table, taken from [59], gives values of absolute roughness ε for some piping materials.

Material	$\varepsilon \times 10^{-3}$ (m)
Copper, lead, brass, aluminium (new)	0.001–0.002
Stainless steel	0.0015
Steel commercial pipe	0.045–0.09
Weld steel	0.045
Carbon steel (new)	0.02–0.05
Carbon steel (slightly corroded)	0.05–0.15
Carbon steel (moderately corroded)	0.15–1
Carbon steel (badly corroded)	1–3

Calculators are also available through the Internet to solve numerically the Colebrook-White relation. For example, after inserting $\varepsilon = 0.0015$ mm, $d = 18$ mm, and $Re = 10000$ in the calculator of [60], there results $f_D = 0.03101157$.

After substituting this value in the function $g(f_D)$ defined above, there results $g(0.03101157) = 3.5 \times 10^{-7}$.

As an application of the concepts given above, it is required to design the cooling tubes at the throat (which is the most stressed section) of the thrust chamber of a rocket, whose first stage burns a combination of liquid oxygen with RP-1 (kerosene), and has the data given in Sects. 2.3 and 2.4. The coolant fluid is the fuel (RP-1). The material chosen for the cooling tubes is a high-strength alloy, namely, Inconel® 718. As a result of the carbon deposits on the wall of the thrust chamber, the design temperature of the wall is assumed to be less than or equal to 811 K. In particular, in the throat region of the thrust chamber, the temperature of the wall on the hot gas side is assumed to be $T_{wg} = 660$ K.

The design value $(T_c)_{ns}$ of the total temperature of the combustion chamber at the nozzle inlet has been found above to be

$$(\bar{T}_c)_{ns} = (T_c)_{ns} \eta_{c^*}^2 = 3589 \times 0.975^2 = 3412 \text{ K}$$

where $(T_c)_{ns}$ is the theoretical value of the total temperature of the combustion chamber at the same section, and η_c^* is the correction factor of the characteristic velocity. The design value $(\bar{T}_c)_{ns}$, multiplied by an estimated value 0.923 of the stagnation recovery factor, is used to determine the temperature T_{aw} at the adiabatic wall, as follows

$$T_{aw} = 3412 \times 0.923 = 3149 \text{ K}$$

The overall heat transfer coefficient on the hot gas side at the throat plane has also been found above to be $h_{gc} = 1987 \text{ W m}^{-2} \text{ K}^{-1}$. By substituting this value in the following equation, the heat flux q at the throat results

$$q = h_{gc}(T_{aw} - T_{wg}) = 1987 \times (3149 - 660) = 4.946 \times 10^6 \text{ W/m}^2$$

By interpolating the data of [61], we find the following data for Inconel® 718 at $T = 555 \text{ K}$: coefficient of thermal expansion $\lambda = 13.8 \times 10^{-6} \text{ m m}^{-1} \text{ K}^{-1}$, modulus of elasticity $E = 1.86 \times 10^{11} \text{ N/m}^2$, thermal conductivity $k = 15.5 \text{ W m}^{-1} \text{ K}^{-1}$, and Poisson's ratio $\nu = 0.274$. We use circular cooling tubes of inner diameter d , whose value is to be determined. The thickness t of the cooling tubes ranges usually from 0.254 to 1.02 mm [45], depending on the combination of propellants and on the material used. We take initially $t = 0.329 \text{ mm} = 3.29 \times 10^{-4} \text{ m}$. This value will be checked against the results of the following heat transfer and mechanical stress calculations. Remembering the preceding equation

$$q = h_{gc}(T_{aw} - T_{wg}) = \frac{k}{t}(T_{wg} - T_{wc}) = h_c(T_{wc} - T_{co}) = H(T_{aw} - T_{co})$$

the temperature T_{wc} of the wall on the coolant side can be determined as follows

$$T_{wc} = T_{wg} - \frac{tq}{k} = 660 - \frac{3.29 \times 10^{-4} \times 4.946 \times 10^6}{15.5} = 555 \text{ K}$$

A cooling system based on a double pass is used, such that the coolant flows downward through alternating tubes and upward through adjacent tubes.

For each tube through which the coolant flows upward, we assume the bulk temperature of the coolant at the throat to be $T_{co} = 333 \text{ K}$, which is a conservative estimate, since the coolant has previously flown through the throat region on its way downward. This temperature is much less than the critical temperature of RP-1, which is 666 K [54], Table 4, and can be expected to remain nearly constant in the remaining portion of the passage. The increase in total temperature for a typical thrust chamber is about 311 K between the inlet and the outlet of a cooling jacket [5]. The value of the heat transfer coefficient h_c on the coolant side, which is necessary to permit the heat flux $q = 4.946 \times 10^6 \text{ W/m}^2$ with the difference of temperature $T_{wc} - T_{co} = 555 - 333 \text{ K}$, can be computed by using the following equation

$$q = h_c(T_{wc} - T_{co})$$

This equation, solved for h_c , yields

$$h_c = \frac{q}{T_{wc} - T_{co}} = \frac{4.946 \times 10^6}{555 - 333} = 2.228 \times 10^4 \text{ W m}^{-2} \text{ K}^{-1}$$

According to Huzel and Huang [5], the number N of cooling tubes can be determined as follows

$$N = \frac{\pi[D_t + 0.8(d + 2t)]}{d + 2t}$$

where, for the engine considered here, $D_t = 0.6332 \text{ m}$ (see Sect. 2.4) is the diameter of the throat, $d (\text{m})$ is the unknown inner diameter of each tube, $t = 3.29 \times 10^{-4} \text{ m}$ is the thickness of each tube, and 0.8 is a factor which takes account of the fact that the centres of the tubes are located on a circle, not on a straight line. After substitution of these values, the preceding equation becomes

$$N = \frac{\pi(0.8d + 0.6337)}{d + 0.000658}$$

For a double-pass cooling system, the velocity $v (\text{m/s})$ of the coolant in the tubes results from [5]:

$$v = \frac{\dot{m}}{\rho} \frac{1}{\frac{1}{2}N\left(\frac{1}{4}\pi d^2\right)}$$

where $\dot{m} (\text{kg/s})$ is the mass flow rate of the coolant, $\rho (\text{kg/m}^3)$ is the local value of the density of the coolant, N is the number of the cooling tubes, and $d (\text{m})$ is the inner diameter of each cooling tube. After taking the value 375 kg/s for the mass flow rate of the coolant and substituting this value in the preceding equation, we find

$$v = \frac{375 \times 8}{\pi N d^2 \rho} = \frac{3000}{\pi N d^2 \rho}$$

We compute the density ρ , the thermal conductivity k , the dynamic viscosity μ , and the specific heat c_p at constant pressure of RP-1 at the temperature $T_{co} = 333 \text{ K}$ by interpolating the data tabulated by Giovanetti et al. [54, Table 4].

By so doing, we find $\rho = 776 \text{ kg/m}^3$, $k = 0.0920 \text{ W/(mK)}$, $\mu = 0.0009652 \text{ Ns/m}^2$, and $c_p = 2130 \text{ J/(kgK)}$ at $T_{co} = 333 \text{ K}$.

We use the following correlation due to Gnielinski [53, page 11, Eq. 11]:

$$Nu = \frac{0.125 f_D (Re - 1000) Pr}{1 + 12.7(0.125 f_D)^{\frac{1}{2}} (Pr^{\frac{2}{3}} - 1)}$$

where the Darcy friction factor f_D of the cooling tubes is computed by using the following equation due to Filonenko [53, page 11, Eq. 9]:

$$f_D = [1.82 \log_{10}(Re) - 1.64]^{-2}$$

By substituting the interpolated data indicated above, $v = 3000/(\pi N d^2 \rho)$, and $N = \pi(0.8 d + 0.6337)/(d + 0.000658)$ into $Re = \rho v d / \mu$, there results

$$Re = \frac{3000(d + 0.000658)}{0.0009652\pi^2 d(0.8d + 0.6337)}$$

Substituting this expression of Re into $f_D = [1.82 \log_{10}(Re) - 1.64]^{-2}$ yields

$$\begin{aligned} f_D &= [1.82 \log_{10}(Re) - 1.64]^{-2} \\ &= \left\{ 1.82 \log_{10} \left[\frac{3000(d + 0.000658)}{0.0009652\pi^2 d(0.8d + 0.6337)} \right] - 1.64 \right\}^{-2} \\ Pr &= \frac{\mu c_p}{k} = \frac{0.0009652 \times 2130}{0.092} \\ Nu &= \frac{h_c d}{k} = \frac{2.228 \times 10^4 d}{0.092} \end{aligned}$$

The quantities Re , f_D , and Nu are functions of the unknown value of d . These functions and the constant value $Pr = 0.0009652 \times 2130/0.092$ are substituted into the Gnielinski correlation

$$Nu = \frac{0.125 f_D (Re - 1000) Pr}{1 + 12.7(0.125 f_D)^{1/2} (Pr^{2/3} - 1)}$$

which is solved numerically for d . By so doing, we find $d = 0.01671$ m.

For comparison, by using the Taler correlation $Nu = 0.00881 Re^{0.8991} Pr^{0.3911}$ [52, page 4, Eq. 20], we find $d = 0.01689$ m.

Substituting $d = 0.01671$ m into

$$N = \frac{\pi(0.8d + 0.6337)}{d + 0.000658}$$

yields $N = 117$. Since the number of tubes for a double-pass cooling system must be not only whole but also even, then we take $N = 118$.

By substituting $N = 118$ into the following equation

$$N = \frac{\pi(0.8d + 0.6337)}{d + 0.000658}$$

we find $d = 0.01657$ m. Therefore, the cooling system at the throat consists of 118 tubes (59 tubes for the coolant flowing downward plus 59 tubes for the coolant flowing upward), each of which is 16.57 mm in diameter and 0.329 mm in thickness. As has been found above, the density of the coolant at the temperature $T_{co} = 333$ K is $\rho = 776$ kg/m³. By substituting this value, $d = 0.01657$ m, and $N = 118$ in the following equation

$$v = \frac{3000}{\pi N d^2 \rho}$$

the velocity of the coolant results

$$v = 37.98 \text{ m/s}$$

The Gnielinski correlation used above is valid for

$$\begin{aligned} 0.5 &\leq Pr \leq 2000 \\ 3000 &\leq Re \leq 5 \times 10^6 \end{aligned}$$

In the present case, there results

$$\begin{aligned} Pr &= \frac{\mu c_p}{k} = \frac{0.0009652 \times 2130}{0.092} = 22.35 \\ Re &= \frac{\rho v d}{\mu} = \frac{776 \times 37.98 \times 0.01657}{0.0009652} = 5.06 \times 10^5 \end{aligned}$$

The pressure of the coolant at the throat is $p_{co} = 1.034 \times 10^7$ N/m², which value results from an interpolation between the pressure at the outlet of the fuel pump and the pressure at the injector manifold. The static pressure p_t (N/m²) of the combusted gas at the throat can be computed by using the following equation of Chap. 1, Sect. 1.2:

$$(p_c)_{ns} = p_i \left(1 + \frac{\gamma - 1}{2} M_i^2 \right)^{\frac{\gamma}{\gamma - 1}}$$

where $(p_c)_{ns} = 6.895 \times 10^6$ N/m² is the total pressure of the combustion chamber at the inlet plane of the nozzle, M_i is the Mach number at the section of interest, and $\gamma \equiv c_p/c_v = 1.222$ is the specific heat ratio. In particular, at the throat ($M_t = 1$), the preceding equation, solved for p_t , yields

$$p_t = (p_c)_{ns} \left(\frac{2}{\gamma + 1} \right)^{\frac{\gamma}{\gamma - 1}} = 6.895 \times 10^6 \times \left(\frac{2}{1.222 + 1} \right)^{\frac{1.222}{1.222 - 1}} = 3.863 \times 10^6 \text{ N/m}^2$$

The maximum combined tensile stress σ_t (N/m²) acting on the cross section A-A of a circular cooling tube can be computed by using the following equation

$$\sigma_t = \frac{(p_{co} - p_g)r}{t} + \frac{E\lambda qt}{2(1-\nu)k} + \frac{6M_A}{t^2}$$

where $p_{co} = 1.034 \times 10^7 \text{ N/m}^2$ is the pressure of the coolant at the throat, $p_g = p_t = 3.863 \times 10^6 \text{ N/m}^2$ is the static pressure of the combusted gas at the throat, $r = d/2 = 0.008285 \text{ m}$ is the radius of the cross section of the tubes, $t = 3.29 \times 10^{-4} \text{ m}$ is the thickness of the tubes, $E = 1.86 \times 10^{11} \text{ N/m}^2$ is the modulus of elasticity of Inconel® 718 at $T = 555 \text{ K}$, $\lambda = 13.8 \times 10^{-6} \text{ m m}^{-1} \text{ K}^{-1}$ is the coefficient of thermal expansion of the same alloy at the same temperature, $q = 4.946 \times 10^6 \text{ W/m}^2$ is the quantity of heat per unit time per unit surface at the throat, $\nu = 0.274$ is the Poisson ratio of the same alloy at the same temperature, $k = 15.5 \text{ W m}^{-1} \text{ K}^{-1}$ is the thermal conductivity of the same alloy at the same temperature, and $M_A (\text{Nm/m})$ is the bending moment per unit length acting on the section A-A due to the distortion induced by discontinuity.

After substituting these values in the preceding equation, we find

$$\sigma_t = 1.631 \times 10^8 + 1.856 \times 10^8 + 0.5543 \times 10^8 M_A$$

By keeping σ_t less than or equal to the 0.2% offset tensile yield strength, which is $\sigma_{ty} = 9.34 \times 10^8 \text{ N/m}^2$ at the temperature $T = 555 \text{ K}$, as recommended by the manufacturer of Inconel® 718 [61], the maximum allowable bending moment per unit length due to discontinuity results

$$(M_A)_{\max} = \frac{(9.34 - 1.631 - 1.856) \times 10^8}{0.5543 \times 10^8} = 10.56 \text{ Nm/m}$$

According to Huzel and Huang [5], the value of the bending moment per unit length due to discontinuity is, in the present case, smaller than 8.36 Nm/m, as shown by experience. Therefore, the results found above (at the throat plane, 118 cooling tubes, each of which is 16.57 mm in diameter and 0.329 mm in thickness) are confirmed.

As a further example of application of these concepts, it is required to design the cooling tubes at the throat of the thrust chamber of a rocket, whose second stage burns a combination of liquid oxygen with liquid hydrogen, and has the properties specified below. The coolant fluid is the fuel (liquid hydrogen). The oxidiser-to-fuel mixture ratio at the thrust chamber is $o/f = 5.22$, the total absolute pressure and the total temperature in the combustion chamber at the nozzle inlet are respectively $(p_c)_{ns} = 5.516 \times 10^6 \text{ N/m}^2$ and $(T_c)_{ns} = 3356 \text{ K}$, the molar mass of the combusted gas is $\mathcal{M} = 12 \text{ kg/kmol}$, and the specific heat ratio of the combusted gas is $\gamma \equiv c_p/c_v = 1.213$. The pressure at which the fuel is discharged at the turbine outlet is $p = 9.653 \times 10^6 \text{ N/m}^2$, and the mass flow rate of the fuel is $\dot{m}_f = 24.72 \text{ kg/s}$.

As has been found in Sects. 2.3 and 2.4 for this engine, the design value \bar{c}^* of the characteristic velocity is

$$\bar{c}^* = \eta_{c^*} c^* = 0.975 \times 2342 = 2284 \text{ m/s}$$

where $c^* = 2342 \text{ m/s}$ and $\eta_{c^*} = 0.975$ are respectively the theoretical value and the correction factor of the characteristic velocity. In addition, the diameter D_t of the thrust chamber at the throat plane and the diameter D_e of the thrust chamber at the exit plane of the nozzle have been found to be respectively $D_t = 2R_t = 2 \times 0.1425 = 0.2850 \text{ m}$ and $D_e = 2R_e = 2 \times 0.9012 = 1.802 \text{ m}$.

The design value $(\bar{T}_c)_{ns}$ of the total temperature in the combustion chamber at the nozzle inlet results from the corresponding theoretical value $(T_c)_{ns}$ as follows

$$(\bar{T}_c)_{ns} = \eta_{c^*}^2 (T_c)_{ns} = 0.975^2 \times 3356 = 3190 \text{ K}$$

The temperature T_{aw} of the gas at the adiabatic wall is determined by multiplying $(\bar{T}_c)_{ns}$ by a recovery factor equal to 0.92, as follows

$$T_{aw} = 3190 \times 0.92 = 2935 \text{ K}$$

The radius of curvature R_{us} of the nozzle contour upstream of the throat plane is

$$R_{us} = 1.5R_t = 1.5 \times 0.1425 \text{ m} = 0.2138 \text{ m}$$

The radius of curvature R_{ds} of the nozzle contour downstream of the throat plane is

$$R_{ds} = 0.382R_t = 0.382 \times 0.1425 \text{ m} = 0.05444 \text{ m}$$

The mean radius \bar{R} of curvature of the nozzle contour at the throat is

$$\bar{R} = \frac{1}{2} \times (R_{us} + R_{ds}) = 0.5 \times (0.2138 + 0.05444) = 0.1341 \text{ m}$$

The value of the constant R of the specific gas is

$$R = \frac{R^*}{\mathcal{M}} = \frac{8314.460}{12} = 692.9 \text{ J K}^{-1} \text{ kg}^{-1}$$

Since $\gamma \equiv c_p/c_v = 1.213$ and $c_p - c_v = R = 692.9 \text{ J K}^{-1} \text{ kg}^{-1}$, then

$$c_p = \frac{\gamma}{\gamma - 1} R = \frac{1.213}{1.213 - 1} \times 692.9 = 3946 \text{ J K}^{-1} \text{ kg}^{-1}$$

The Prandtl number is computed as follows

$$Pr = \frac{4\gamma}{9\gamma - 5} = \frac{4 \times 1.213}{9 \times 1.213 - 5} = 0.82$$

The coefficient of dynamic viscosity is computed as follows

$$\begin{aligned}\mu &= (1.184 \times 10^{-7}) \mathcal{M}^{0.5} T^{0.6} = (1.184 \times 10^{-7}) \times (12)^{0.5} \times (3190)^{0.6} \\ &= 5.191 \times 10^{-5} \text{ N s m}^{-2}\end{aligned}$$

The convective heat transfer coefficient h_g is computed by using the Bartz equation written below

$$h_g = \left[\frac{0.026}{D_t^{0.2}} \left(\frac{\mu^{0.2} c_p}{Pr^{0.6}} \right)_{ns} \left(\frac{(p_c)_{ns}}{\bar{c}^*} \right)^{0.8} \left(\frac{D_t}{\bar{R}} \right)^{0.1} \right] \left(\frac{A_t}{A} \right)^{0.9} \sigma$$

After substituting $D_t = 0.2850$ m, $\mu = 5.191 \times 10^{-5}$ N s m $^{-2}$, $c_p = 3946$ J K $^{-1}$ kg $^{-1}$, $Pr = 0.82$, $(p_c)_{ns} = 5.516 \times 10^6$ N m $^{-2}$, $\bar{c}^* = 2284$ m s $^{-1}$, and $\bar{R} = 0.1341$ m in the preceding equation, we find

$$h_g = 1.132 \times 10^4 \left(\frac{A_t}{A} \right)^{0.9} \sigma \text{ W m}^{-2} \text{ K}^{-1}$$

The value of σ is determined by means of the following equation

$$\sigma = \frac{1}{\left[\frac{1}{2} \frac{T_{wg}}{(\bar{T}_c)_{ns}} \left(1 + \frac{\gamma-1}{2} M^2 \right) + \frac{1}{2} \right]^{0.68} \left[1 + \frac{\gamma-1}{2} M^2 \right]^{0.12}}$$

Since there is no solid deposit on the walls of the thrust chamber, we assume an average temperature $T_{wg} = 833$ K on the hot gas side of the wall. This yields

$$\frac{T_{wg}}{(\bar{T}_c)_{ns}} = \frac{833}{3190} \approx 0.26$$

By substituting this value, $M = 1$, and $\gamma = 1.213$ into the expression of σ , we find at the throat plane

$$\sigma \approx 1.33$$

Therefore, at the throat plane, where $\sigma = 1.33$ and $A_t/A = 1$, there results

$$h_g = 1.132 \times 10^4 (A_t/A)^{0.9} \sigma = 1.132 \times 10^4 \times 1^{0.9} \times 1.33 = 1.506 \times 10^4 \text{ W m}^{-2} \text{ K}^{-1}$$

In order to avoid excessive thermal stresses in the material to be used, we want to keep the mean temperature of the tube wall below 811 K. By substituting this value of h_g in the following equation, the heat flux q at the throat results

$$q = h_g (T_{aw} - T_{wg}) = 1.506 \times 10^4 \times (2935 - 833) = 3.166 \times 10^7 \text{ W/m}^2$$

where 833 K is the value (see above) used for the temperature T_{wg} of the wall on the hot gas side. The material chosen for the cooling tubes is again Inconel® 718. By interpolating the data of [61], we find the following data for this material at $T = 833$ K: coefficient of thermal expansion $\lambda = 14.6 \times 10^{-6} \text{ m m}^{-1} \text{ K}^{-1}$, modulus of elasticity $E = 1.70 \times 10^{11} \text{ N/m}^2$, thermal conductivity $k = 20.0 \text{ W m}^{-1} \text{ K}^{-1}$, and Poisson's ratio $\nu = 0.272$. We use cooling tubes of circular cross-section, having an internal diameter d , whose value is to be determined, and a thickness $t = 0.2 \text{ mm} = 0.0002 \text{ m}$. By solving the following equation

$$q = h_{gc}(T_{aw} - T_{wg}) = \frac{k}{t}(T_{wg} - T_{wc}) = h_c(T_{wc} - T_{co}) = H(T_{aw} - T_{co})$$

for T_{wc} , the temperature of the wall on the coolant side results

$$T_{wc} = T_{wg} - \frac{qt}{k} = 833 - \frac{3.166 \times 10^7 \times 0.0002}{20.0} = 516.4 \text{ K}$$

The mean value of the temperature of the wall on the coolant side is the mean between the temperature computed above ($T_{wc} = 516.4 \text{ K}$) and the temperature ($T_{wg} = 833 \text{ K}$) of the wall on the hot gas side at the throat plane, as follows

$$\frac{516.4 + 833.0}{2} = 674.7 \text{ K}$$

This value is lower than the maximum allowed value (811 K).

We assume the bulk temperature of the coolant at the throat to be $T_{co} = 75 \text{ K}$.

By solving the following equation

$$q = h_{gc}(T_{aw} - T_{wg}) = \frac{k}{t}(T_{wg} - T_{wc}) = h_c(T_{wc} - T_{co}) = H(T_{aw} - T_{co})$$

for h_c , there results at the throat

$$h_c = \frac{q}{T_{wc} - T_{co}} = \frac{3.166 \times 10^7}{516.4 - 75} = 7.173 \times 10^4 \text{ W m}^{-2} \text{ K}^{-1}$$

We use the following correlation due to McCarthy and Wolf [56, page 95, Eq. 2]:

$$h_c = 0.025 \left(\frac{c_p \mu^{0.2}}{Pr^{0.6}} \right)_{co} \frac{G^{0.8}}{d^{0.2}} \left(\frac{T_{co}}{T_{wc}} \right)^{0.55}$$

where c_p ($\text{J kg}^{-1} \text{ K}^{-1}$) is the specific heat of the coolant (hydrogen) at constant pressure, μ (N s m^{-2}) is the coefficient of dynamic viscosity of the coolant, $Pr = c_p \mu / k$ is the Prandtl number, k ($\text{W m}^{-1} \text{ K}^{-1}$) is the thermal conductivity of the coolant, G ($\text{kg s}^{-1} \text{ m}^{-2}$) is the mass flow rate of the coolant per unit area to be cooled, d (m) is the diameter of the coolant passage, T_{co} (K) is the bulk temperature of the

coolant, T_{wc} (K) is the temperature of the wall on the coolant side, and the subscript co indicates the bulk temperature of the coolant.

According to NIST [62], at $T_{co} = 75$ K and $p = 9.653 \times 10^6$ N/m², the coolant has the following properties: $c_p = 14890$ J kg⁻¹ K⁻¹, $\mu = 4.9949 \times 10^{-6}$ N s m⁻², and $k = 0.090639$ W m⁻¹ K⁻¹. Therefore, the Prandtl number in such conditions is

$$Pr = \frac{c_p \mu}{k} = \frac{14890 \times 4.9949 \times 10^{-6}}{0.090639} = 0.82055$$

which confirms the value $Pr = 0.82$ found above. A sesqui-pass (literally one-and-a-half-pass) type of design is chosen here for the cooling tubes. This term actually means a partial pass starting below the throat. This type of pass is used with coolants (such as liquid hydrogen) which must previously be heated in order to become effective, that is, in order to absorb the high heat fluxes at the throat. The extent of the partial pass results from a trade-off between thermal and gimbaling requirements, since it is desirable to keep the inlet manifold forward [45].

As has been shown above, the number N of cooling tubes can be determined as follows

$$\begin{aligned} N &= \frac{\pi[D_t + 0.8(d + 2t)]}{d + 2t} = \frac{\pi[0.2850 + 0.8 \times (d + 2 \times 0.0002)]}{d + 2 \times 0.0002} \\ &= \frac{\pi(0.8d + 0.2853)}{d + 0.0004} \end{aligned}$$

where d (whose value is to be determined) and $t = 0.0002$ m are respectively the inner diameter and the thickness of each cooling tube.

The mass flow rate of the coolant per unit area to be cooled is

$$G = \frac{\dot{m}_f}{N\pi\left(\frac{d}{2}\right)^2} = \frac{24.72 \times 4}{\pi Nd^2} = \frac{24.72 \times 4 \times (d + 0.0004)}{\pi^2 d^2 (0.8d + 0.2853)}$$

After substituting the values determined above into the McCarthy-Wolf correlation, there results

$$\begin{aligned} 7.173 \times 10^4 &= 0.025 \times \left(\frac{14890 \times 0.000004995^{0.2}}{0.820550.6} \right) \times \left[\frac{24.72 \times 4 \times (d + 0.0004)}{\pi^2 d^2 (0.8d + 0.2853)} \right]^{0.8} \\ &\quad \times \left(\frac{1}{d^{0.2}} \right) \times \left(\frac{75}{516.4} \right)^{0.55} \end{aligned}$$

The preceding equation, solved numerically for d , yields $d = 0.0033$ m. By substituting $d = 0.0033$ into the following equation

$$N = \frac{\pi(0.8d + 0.2853)}{d + 0.0004}$$

we find $N = 244.5$. We take $N = 244$. By substituting this value of N into the preceding equation, there results $d = 0.003307$ m.

Therefore, the cooling system at the throat consists of 244 tubes, each of which is 3.307 mm in diameter and 0.2 mm in thickness.

The estimated pressure of the coolant at the throat is $p_{co} = 8.274 \times 10^6$ N/m². The static pressure p_t (N/m²) of the combusted gas at the throat can be computed by using the general equation of Chap. 1, Sect. 1.2:

$$(p_c)_{ns} = p_i \left(1 + \frac{\gamma - 1}{2} M_i^2 \right)^{\frac{\gamma}{\gamma - 1}}$$

where $(p_c)_{ns} = 5.516 \times 10^6$ N/m² is the total pressure of the combustion chamber at the inlet plane of the nozzle, M_i is the Mach number at the section of interest, and $\gamma \equiv c_p/c_v = 1.213$ is the specific heat ratio. In particular, at the throat ($M_t = 1$), the preceding equation, solved for p_t , yields

$$p_t = (p_c)_{ns} \left(\frac{2}{\gamma + 1} \right)^{\frac{\gamma}{\gamma - 1}} = 5.516 \times 10^6 \times \left(\frac{2}{1.213 + 1} \right)^{\frac{1.213}{1.213 - 1}} = 3.1 \times 10^6 \text{ N/m}^2$$

The maximum combined tensile stress σ_t (N/m²) acting on the cross section A-A of a circular cooling tube can be computed by using the following equation

$$\sigma_t = \frac{(p_{co} - p_g)r}{t} + \frac{E\lambda qt}{2(1-\nu)k} + \frac{6M_A}{t^2}$$

where $p_{co} = 8.274 \times 10^6$ N/m² is the pressure of the coolant at the throat, $p_g = p_t = 3.1 \times 10^6$ N/m² is the pressure of the combusted gas at the throat, $r = d/2 = 0.001654$ m is the radius of the cross section of the tubes, $t = 2.0 \times 10^{-4}$ m is the thickness of the tubes, $E = 1.70 \times 10^{11}$ N/m² is the modulus of elasticity of Inconel® 718 at $T = 833$ K, $\lambda = 14.6 \times 10^{-6}$ m m⁻¹ K⁻¹ is the coefficient of thermal expansion of the same alloy at the same temperature, $q = 3.166 \times 10^7$ W/m² is the quantity of heat per unit time per unit surface at the throat, $\nu = 0.272$ is the Poisson ratio of the same alloy at the same temperature, $k = 20.0$ W m⁻¹ K⁻¹ is the thermal conductivity of the same alloy at the same temperature, and M_A (Nm/m) is the bending moment per unit length acting on the section A-A due to the distortion induced by discontinuity.

After substituting these values in the preceding equation, we find

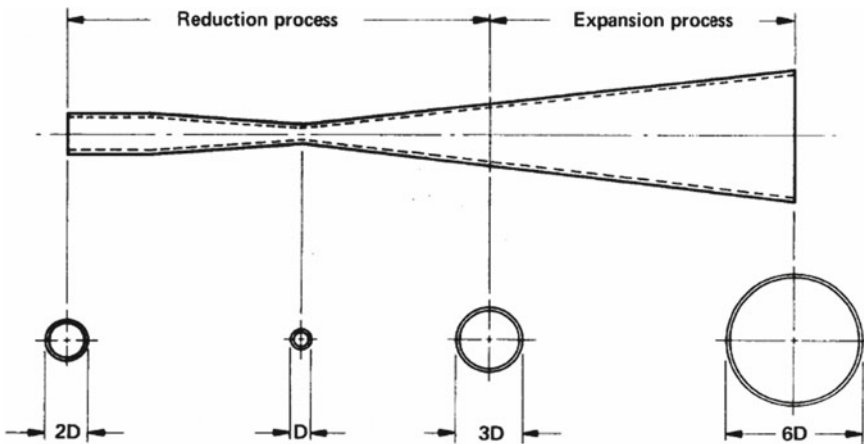
$$\sigma_t = 0.4279 \times 10^8 + 5.397 \times 10^8 + 1.500 \times 10^8 M_A$$

By keeping σ_t less than or equal to the 0.2% offset tensile yield strength, which is $\sigma_{ty} = 1.06 \times 10^9$ N/m² at the temperature $T = 675$ K, as recommended by the manufacturer of Inconel® 718 [61], the maximum allowable bending moment per unit length due to discontinuity results

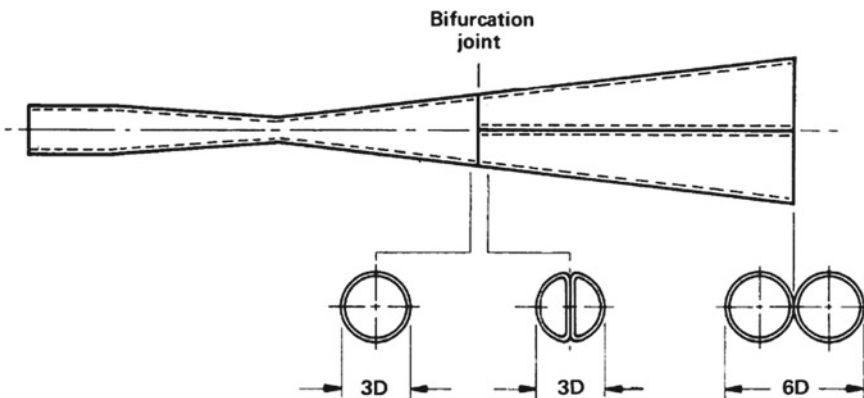
$$(M_A)_{\max} = \frac{(10.6 - 0.4279 - 5.397) \times 10^8}{1.500 \times 10^8} = 3.183 \text{ Nm/m}$$

According to Huzel and Huang [5], the value of the bending moment due to discontinuity is, in the present case, smaller than 0.583 Nm/m, as shown by experience. Therefore, the results found above (at the throat plane, 244 tubes, each of which is 3.183 mm in diameter and 0.2 mm in thickness) are confirmed.

The results found in the two preceding examples concern the size of the cooling tubes at the throat, which is narrowest section of a thrust chamber. The size of the tubes changes along the longitudinal axis of a thrust chamber. The following figure, due to the courtesy of NASA [45], shows a cooling tube having a circular cross section of variable size with 6:1 maximum taper.

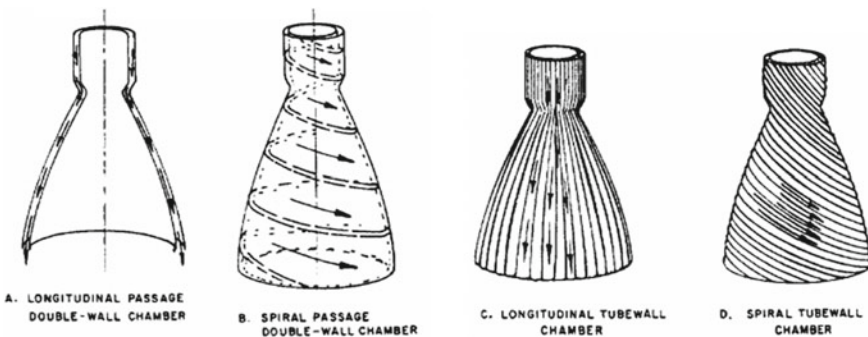


Another option consists in bifurcating the tubes by means of joints, as shown in the following figure, which is also due to the courtesy of NASA [45].

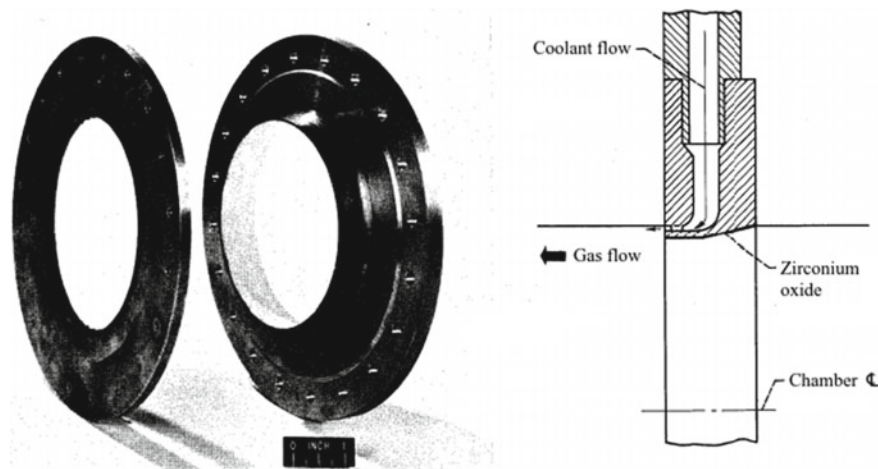


The cooling tubes are brazed to each other and to a metal shell or to hatbands for stiffening. To this end, furnace brazing is usually applied. In order to avoid the necessity of tapering, Volvo Aero Corporation has used tubes of square cross-section, which are wrapped in a spiral pattern around the inner wall of the nozzle. They are joined by gas-tungsten arc fillet welds [63]. Volvo Aero Corporation has also used a manufacturing process which consists in laser welding a close-out cover sheet on to an inner wall with milled cooling channels. When the outer sheet is laser welded to the inner sheet, the part has the form of a straight cone. Successively, the forming of a bell-shaped contour is done by expansion in a conventional expander [64].

As has been shown above, the dump cooling method is similar to the regenerative cooling, because the coolant flows, for both of these methods, through small passages on the outer side of the thrust chamber. However, in the case of dump cooling, the coolant is discharged overboard through openings at the end plane of the divergent portion of the nozzle, instead of flowing back to be discharged into the injector. This method is used in rocket engines fuelled by hydrogen at low pressures ($p_c < 689500 \text{ N/m}^2$, where p_c is the static absolute pressure in the combustion chamber). The heated hydrogen dumped overboard gives a contribution to the total thrust. The coolant, if flowing longitudinally from the injector plane to the exit plane, can pass either in the interstice between a double wall (case A) or in tubes running along a single wall (case C). The coolant, if flowing spirally from the injector plane to the exit plane, can pass either in spiral passages existing between a double wall (case B) or in tubes wound around a single wall (case D), before being dumped overboard in the axial direction. The four cases described above are illustrated in the following figure, which is due to the courtesy of NASA [5].



As has been shown above, film cooling method consists in the protection of a given surface from the harmful effects of a stream of hot gas by interposing a continuous protective film between the surface and the stream. In a liquid-propellant engine, a liquid or gaseous coolant, which is usually the fuel, is injected tangentially or at low angles into the combustion chamber along the hot gas side of the wall by means of a row of slots or orifices, as shown in the following figure, due to the courtesy of NASA [65].



Due to phenomena of heat and mass transfer between the coolant film and the combusted gas, the thickness of the coolant film decreases in the direction of the hot stream. Therefore, in case of need, further coolant is injected through additional holes placed downstream of those placed along the first row. Film cooling is sometimes used in conjunction with regenerative cooling, for the purpose of reducing the heat transfer through the wall and, therefore, the thermal stress of the materials.

The coolant is often in the liquid state at the moment of injection, in order to absorb heat from the combusted gas by evaporating and diffusing into the main stream. This injection gives rise to a liquid film placed around the wall of the combustion chamber and containing the gaseous stream. The cooling efficiency of the injected fuel is subject to losses, due to disturbance waves on the surface of the liquid film adjacent to the combusted gas.

Zucrow and Sellers [66] indicate the following equation to be used for the design a thrust chamber cooled by a liquid film:

$$\frac{G_c}{G_g} = \frac{1}{\eta_c} \frac{H}{a(1+b^c)}$$

where G_c ($\text{kg s}^{-1} \text{ m}^{-2}$) is the mass flow rate of the film coolant per unit area of the wall of the thrust chamber to be cooled, G_g ($\text{kg s}^{-1} \text{ m}^{-2}$) is the mass flow rate of the combusted gas per unit area of the cross section of the thrust chamber in the direction perpendicular to the flow, η_c is the efficiency of the film cooling, H (J/kg) is the enthalpy per unit mass of the film coolant, resulting from

$$H = \frac{c_{pvc}(T_{aw} - T_{wg})}{c_{plc}(T_{wg} - T_{co}) + \Delta H_{vc}}$$

c_{pvc} ($\text{J kg}^{-1} \text{ K}^{-1}$) is the average specific heat at constant pressure of the coolant in the vapour phase, c_{plc} ($\text{J kg}^{-1} \text{ K}^{-1}$) is the average specific heat at constant pressure

of the coolant in the liquid phase, T_{aw} (K) is the temperature of the gas at the adiabatic wall, T_{wg} (K) is the temperature of the wall on the hot gas side and also the temperature of the coolant film, T_{co} (K) is the bulk temperature of the coolant at the manifold, ΔH_{vc} (J/kg) is the vaporisation heat of the coolant, $a = 2V_d/(V_m f)$, V_d (m/s) is the velocity of the stream of combusted gas in the axial direction at the edge of the boundary layer, V_m (m/s) is the average velocity of the stream of combusted gas in the axial direction, f is the friction coefficient for the two-phase flow between the combusted gas and the liquid film, $b = V_g/V_d - 1$, V_g (m/s) is the velocity of the velocity of the stream of combusted gas in the axial direction at the central line of the thrust chamber, $c = c_{pvc}/c_{pg}$, and c_{pg} ($\text{J kg}^{-1} \text{ K}^{-1}$) is the average specific heat at constant pressure of the combusted gas.

The losses mentioned above can be taken into account by means of the coefficient η_c , whose values range from 0.3 to 0.7 [5]. These values are to be determined experimentally. Hydrocarbon fuels have proven to be effective when used as coolants, because of the heat insulation properties of the carbon deposits generated by them on the walls of a thrust chamber.

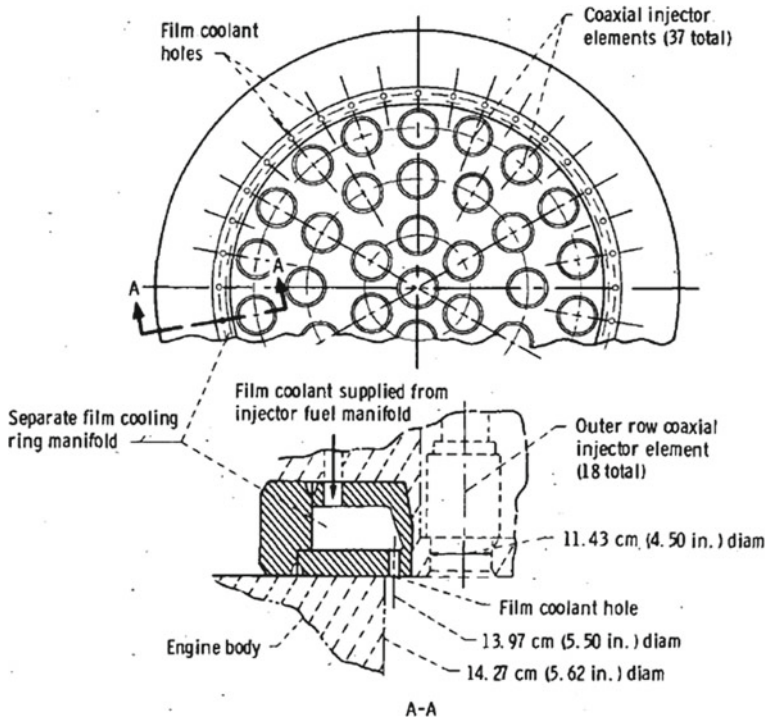
When liquid hydrogen is used as a fuel, the very low critical temperature of hydrogen ($T_c = 33.18$ K, according to [62]) causes the initially liquid film to evaporate at a short distance from the point of injection.

Hatch and Papell [67] indicate the following equation to be used for the design a thrust chamber cooled by a gaseous film:

$$\frac{T_{aw} - T_{wg}}{T_{aw} - T_{co}} = \exp\left(\frac{-h_g}{G_c c_{pvc} \eta_c}\right)$$

where T_{aw} (K) is the temperature of the gas at the adiabatic wall, T_{wg} (K) is the maximum allowable temperature of the wall on the hot gas side, T_{co} (K) is the initial temperature of the coolant, h_g ($\text{W m}^{-2} \text{ K}^{-1}$) is the heat transfer coefficient on the hot gas side, G_c ($\text{kg s}^{-1} \text{ m}^{-2}$) is the mass flow rate of the film coolant per unit area of the wall of the thrust chamber to be cooled, c_{pvc} ($\text{J kg}^{-1} \text{ K}^{-1}$) is the average specific heat at constant pressure of the gaseous coolant, and η_c is the efficiency of the film cooling. By means of the efficiency η_c , whose values range from about 0.25 to 0.65 [5], account is taken of the coolant which is lost into the main stream of combusted gas without producing the desired effect.

The following figure, due to the courtesy of NASA [68] shows a 37-element injector with removable film coolant ring manifold used in a small hydrogen-oxygen thrust chamber cooled by means of a hydrogen film.



The Hatch-Papell equation written above is based on the assumption of a balance between the heat coming from the wall of the combustion chamber and the heat absorbed by the coolant. The heat coming from the wall depends on the heat transfer h_g coefficient on the hot gas side and also on the difference between the temperature T_{aw} of the gas at the adiabatic wall and the initial temperature T_{co} of the coolant. The heat absorbed by the coolant depends on the heat capacity of the coolant in the interval from the initial temperature to the final temperature. When the two amounts of heat are in equilibrium, no heat is transferred through the wall. In such conditions, the inner surface of the thrust chamber reaches the temperature of the coolant corresponding to the particular location along the flow axis. Therefore, the temperature of the inner surface of the thrust chamber increases from the initial temperature of the coolant at the point of injection to the maximum allowable value of the temperature, at which point a further injection of coolant becomes necessary.

As an example of application, it is required to determine the mass flow rate G_c ($\text{kg s}^{-1} \text{ m}^{-2}$) of film coolant per unit area of the wall of the thrust chamber to be cooled, for a rocket engine burning a combination of liquid hydrogen (fuel) with liquid fluorine (oxidiser). At the throat plane, the following quantities are known: heat transfer coefficient on the hot gas side $h_g = 3238 \text{ W m}^{-2} \text{ K}^{-1}$, temperature of the gas at the adiabatic wall $T_{aw} = 2911 \text{ K}$, maximum allowable temperature of the wall on the hot gas side $T_{wg} = 1056 \text{ K}$, initial temperature of the coolant $T_{co} = 28 \text{ K}$,

average specific heat at constant pressure of the gaseous coolant $C_{pvc} = 1.507 \times 10^4 \text{ J kg}^{-1} \text{ K}^{-1}$, and efficiency of the film cooling $\eta_c = 0.3$.

By substituting these data into the Hatch-Papell equation

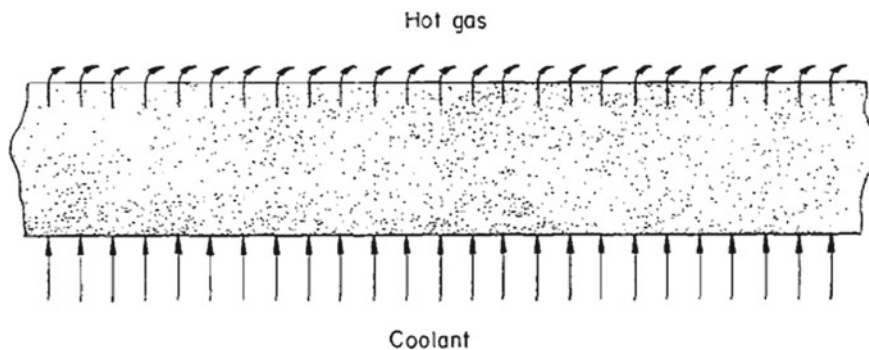
$$\frac{T_{aw} - T_{wg}}{T_{aw} - T_{co}} = \exp\left(\frac{-h_g}{G_c C_{pvc} \eta_c}\right)$$

and solving for G_c , there results

$$G_c = \frac{-3238}{1.507 \times 10^4 \times 0.3 \times \ln\left(\frac{2911-1056}{2911-28}\right)} = 1.624 \text{ kg s}^{-1} \text{ m}^{-2}$$

When the heat flux q (W/m^2), that is, the quantity of heat transferred per unit time per unit surface, is computed for a regeneratively cooled engine with added film cooling, then it is necessary to modify the value of the temperature T_{aw} (K) of the adiabatic wall, before using this value in the equation $q = h_g(T_{aw}-T_{wg})$ or in the equation $q = h_{gc}(T_{aw}-T_{wg})$. The modified value of T_{aw} must be determined experimentally. By contrast, it is not necessary to modify the value of the heat transfer coefficient h_g or h_{gc} ($\text{W m}^{-2} \text{ K}^{-1}$) on the hot gas side.

As has been shown at the beginning of this paragraph, in case of transpiration cooling, the wall to be cooled has drilled holes or is made of a porous material, in order for the coolant to pass through the wall into the gas flow. A protective layer builds up on the hot gas side of the wall and insulates it from the heat carried by the stream of combusted gas, as shown in the following figure, due to the courtesy of NASA [69].



Since the coolant is directed away from the surface when leaving the wall, then a counterflow is generated between the heat carried away from the surface with the coolant stream and the heat transferred from the stream of combusted gas toward the wall. This counterflow reduces the overall heat transfer between the hot gas and the surface of the wall [69]. The permeable inner liner of the thrust chamber is enclosed into an outer shell, and forms a jacket from which the coolant comes.

The cooling efficiency $(T_g - T_w)/(T_g - T_c)$ can be evaluated by using the Rannie equation [70], as follows

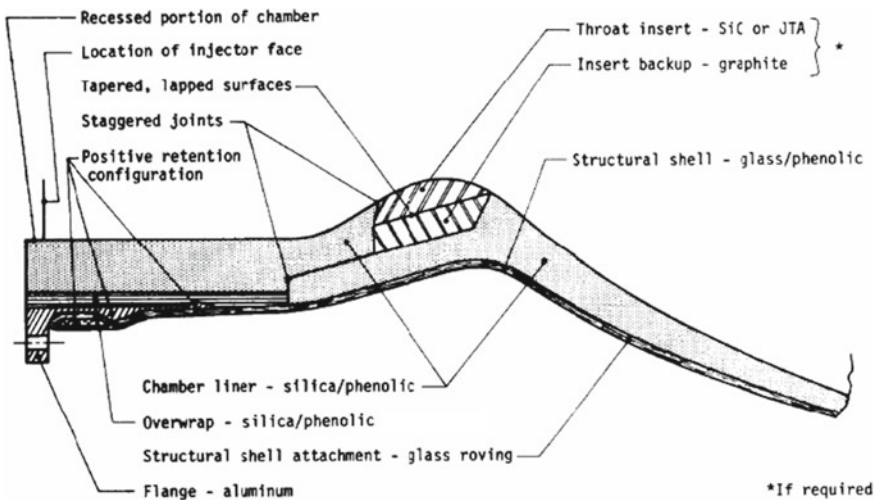
$$\frac{T_g - T_w}{T_g - T_{co}} = 1 - \frac{\exp(-36.9 Pr_g Re_d^{0.1} f)}{1 + \frac{c_{pc}}{c_{pg}} (1.18 Re_d^{0.1} - 1) [1 - \exp(-36.9 Pr_g Re_d^{0.1} f)]}$$

where T_g (K) is the recovery temperature of the hot gas, T_w (K) is the temperature of the wall, T_{co} (K) is the temperature of the coolant reservoir, $Pr_g = \mu_g c_{pg}/k_g$ is the Prandtl number of the hot gas, μ_g ($N s m^{-2}$) is the coefficient of dynamic viscosity of the hot gas, c_{pg} ($J kg^{-1} K^{-1}$) is the specific heat at constant pressure of the hot gas, k_g ($W m^{-1} K^{-1}$) is the thermal conductivity of the hot gas, $Re_d = \rho v d / \mu$ is the Reynolds number of the coolant based on the hydraulic diameter d (m), ρ (kg/m^3) is the density of the coolant at bulk temperature, v (m/s) is the velocity of the coolant, μ ($N s m^{-2}$) is the coefficient of dynamic viscosity of the coolant at bulk temperature, c_{pc} ($J kg^{-1} K^{-1}$) is the specific heat at constant pressure of the coolant at bulk temperature, $f = G_c/G_g$ is the blowing ratio, G_c ($kg s^{-1} m^{-2}$) is the mass flow rate of the coolant per unit area of the wall of the thrust chamber to be cooled, and G_g ($kg s^{-1} m^{-2}$) is the mass flow rate of the hot gas per unit area of the cross section of the thrust chamber in the direction perpendicular to the flow.

Since the Rannie equation written above indicates coolant flows slightly lower than those found necessary in experiments, then Huzel and Huang [5] recommend to use a cooling efficiency value of about 0.85. The porous material used for the walls of transpiration-cooled thrust chambers must, of course, withstand the mechanical and thermal stresses acting on such walls.

As has been shown above, ablative cooling is performed by using a protective material which covers the inner surface of a wall to be cooled. This material is made of either epoxy or, more often, phenolic resins reinforced by fibres. The protective material thermally degrades, and the products of this degradation (an endothermal pyrolysis of the resin, which leaves a pure carbon solid, called char, and releases oxygen and hydrogen) are carried away by the main stream of hot gas. The process of ablation blocks the heat flux to the outer surface of the wall. The reinforcement of the resin consists of either fibre-woven fabrics or chopped fibres of materials such as silica, graphite, or carbon.

With reference to the following figure, adapted from [71], an ablatively-cooled thrust chamber consists of a flame liner (made of a reinforced phenolic resin), a thin layer (made of silica impregnated with a phenolic resin) used for insulation, and a high-strength structural shell. In rocket engines subject to erosion at the throat, inserts (made of either silicon carbide or JTA graphite, the latter being made of 48% graphite, 35% zirconium, 9% silicon, and 8% boron) are incorporated in the throat region.



The thickness of the ablative materials varies as a function of the cross section considered. When several liner components are used, especially for the throat inserts, then joints are staggered axially to prevent a direct leak path to the outer structural shell. Such joints are located where they are not likely to open up under the action of thermal or mechanical loads. A differential thermal expansion of the components is taken into account by using materials having compatible elastic moduli or by inserting crushable or flexible materials which can expand without excessive stresses induced by strain [71].

The structural shell is made of either fibreglass or aluminium alloy or stainless steel. The thermal resistance of the inner layers keeps the outer shell at moderate temperatures.

For the design of a thrust chamber cooled by ablative materials, Huzel and Huang [5] indicate the following equation found experimentally, which expresses the char depth a (m) as a function of the heat absorbed:

$$a = c \left\{ \frac{2kt}{R_r R_v c_p \rho} \ln \left[1 + \frac{R_r R_v c_p (T_{aw} - T_d)}{L_p} \right] \right\}^{0.5} \left[\frac{(p_c)_{ns}}{6.895 \times 10^5} \right]^{0.4}$$

where c is a factor whose value is determined experimentally at the throat section and for a nozzle stagnation absolute pressure of $6.895 \times 10^5 \text{ N/m}^2$, R_r is the weight fraction of resin content in the ablative material used, R_v is the weight fraction of the pyrolysed resin versus the total resin content R_r , c_p ($\text{J kg}^{-1} \text{ K}^{-1}$) is the specific heat at constant pressure of the pyrolysis gases, ρ (kg/m^3) is the density of the ablative material used, k ($\text{W m}^{-1} \text{ K}^{-1} \text{ m}^{-1}$) is the thermal conductivity per metre of char, t (s) is the duration of firing in the thrust chamber, L_p (J/kg) is the latent heat of pyrolysis, T_{aw} (K) is the temperature of the gas at the adiabatic wall, T_d (K) is the decomposition temperature of the resin, and $(p_c)_{ns}$ (N/m^2) is the total pressure in the combustion chamber at the nozzle inlet.

The results obtained by using the preceding equation have been found to be in good agreement with the char depths measured in thrust chambers protected with Refrasil®, which is an amorphous silica woven fabric.

However, the char depths measured in sections placed downstream of the throat plane have been found to be greater than those computed by means of this equation. Therefore, Huzel and Huang [5] indicate the following equation to compute the char depth a (m) in sections downstream of the throat:

$$a = bt^{\frac{1}{2}} \exp(-0.0247\varepsilon)$$

where b ($\text{m}/\text{s}^{1/2}$) is a constant whose value is determined experimentally and depends on the ablative material used, t (s) is the duration of firing in the thrust chamber, $\varepsilon \equiv A_x/A_t$ is the expansion area ratio of the nozzle at the section x of interest, A_x (m^2) is the area of the section of interest, and A_t (m^2) is the area of the throat section. As an application of the concepts discussed above, it is required to determine the char depth at: (a) the combustion chamber and the throat, and (b) the cross-section of the nozzle whose area is five times the area of the throat (that is, $\varepsilon = 5$), for a rocket engine fired for a time $t = 410$ s and having the following properties: total pressure in the combustion chamber at the nozzle inlet $(p_c)_{ns} = 6.895 \times 10^5 \text{ N/m}^2$, constant factor $c = 1.05$, weight fraction of resin content in the ablative material $R_r = 0.3$, weight fraction of the pyrolysed resin versus total resin content $R_v = 0.41$, specific heat at constant pressure of the pyrolysis gases $c_p = 1591 \text{ J kg}^{-1} \text{ K}^{-1}$, density of the ablative material $\rho = 1688 \text{ kg/m}^3$, thermal conductivity per metre of char $k = 0.7327 \text{ W m}^{-1} \text{ K}^{-1} \text{ m}^{-1}$, latent heat of pyrolysis $L_p = 1.596 \times 10^6 \text{ J/kg}$, temperature of the gas at the adiabatic wall $T_{aw} = 2811 \text{ K}$, decomposition temperature of the resin $T_d = 811 \text{ K}$, and constant factor $b = 0.0008509 \text{ m/s}^{1/2}$.

By inserting these data in the following equation

$$a = c \left\{ \frac{2kt}{R_r R_v c_p \rho} \ln \left[1 + \frac{R_r R_v c_p (T_{aw} - T_d)}{L_p} \right] \right\}^{0.5} \left[\frac{(p_c)_{ns}}{6.895 \times 10^5} \right]^{0.4}$$

we find $a = 0.021 \text{ m} = 2.10 \text{ cm}$.

Likewise, by inserting $b = 0.0008509 \text{ m/s}^{1/2}$ and $\varepsilon = 5$ in the following equation

$$a = bt^{\frac{1}{2}} \exp(-0.0247\varepsilon)$$

we find $a = 0.0152 \text{ m} = 1.52 \text{ cm}$.

Radiation cooling occurs in a combustion chamber having a thin wall which is heated by the combusted gas to a temperature of thermal equilibrium. At this temperature, the heat from the wall to space equals the heat from the combusted gas to the wall. In order to prevent the inner surface of the wall from being overheated by the combusted gas, materials having high thermal conductivity are necessary.

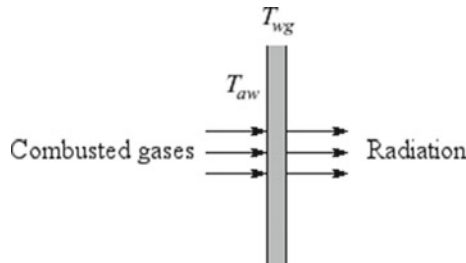
The limits of application of radiation cooling depend on the maximum temperature which the available materials can withstand. The temperature of the combusted gas

in a combustion chamber depends on such factors as the thrust level, the burning time, the pressure in the chamber, the combination of propellants, and their mixture ratios. Most portions of radiation cooled engines are subject to temperatures greater than 1500 K, with the exception of extension skirts of nozzles.

The heat-blocking properties of graphites resulting from pyrolysis of phenolic resins have been described above. Apart from these graphites, the only materials capable of meeting the requirements of a radiation cooled engine at temperatures above 1500 K are refractory materials, such as tungsten, molybdenum, and niobium. These materials are subject to oxidation caused by exhaust gases containing water vapour, carbon dioxide, and free oxygen. Therefore, refractory materials to be used in rocket engines must be protected by suitable coatings.

So far, radiation-cooled rocket engines have used a niobium alloy (C-103) with a fused silica coating (R512E). Since this coating has a limitation in temperature of 1643 K, then fuel film cooling has been necessary in rocket engines using this niobium alloy to maintain this temperature limit. Reed et alii [72] have described a material made of a rhenium substrate with an iridium oxidation-resistant coating, whose operating temperature is as high as 2473 K.

Assuming negligible difference of temperature between the alloy and the coating, a scheme of heat transfer by radiation cooling in steady state for a wall is illustrated in the following figure.



Let q (W/m^2), T_{aw} (K), and T_{wg} (K) be respectively the quantity of heat transferred per unit time per unit surface of the wall, the temperature of the combusted gases at the adiabatic wall, and the temperature of the wall on the gas side. As has been shown at the beginning of this section, the heat flux q from the combusted gases is proportional to the difference of temperature $T_{aw} - T_{wg}$, as follows

$$q = h_{gc}(T_{aw} - T_{wg})$$

where h_{gc} ($\text{W m}^{-2} \text{ K}^{-1}$) is the overall heat transfer coefficient on the hot gas side.

The heat flux q , due to the radiant energy emitted from the surface of the wall, is expressed by the Stefan-Boltzmann law, as follows

$$q = \varepsilon\sigma T_{wg}^4$$

where ε ($0 < \varepsilon < 1$) is the emissivity of the outer surface of the material of which the wall is made, and $\sigma = 5.670367 \times 10^{-8} \text{ W m}^{-2} \text{ K}^{-4}$ [73] is the Stefan-Boltzmann constant.

In conditions of thermal equilibrium, the following equation holds

$$h_{gc}(T_{aw} - T_{wg}) = \varepsilon\sigma T_{wg}^4$$

The design of a radiation cooling system consists in determining a value of the temperature T_{wg} of the combusted gases at the adiabatic wall which satisfies the equation written above and meets the requirements posed by the material in the operating conditions.

As an application of the concepts discussed above, it is required to determine the temperature T_{wg} of the wall on the hot gas side for a nozzle extension of a rocket engine such that the overall heat transfer coefficient on the hot gas side is $h_{gc} = 206.6 \text{ W/(m}^2 \text{ K)}$, the temperature of the combusted gases at the adiabatic wall is $T_{aw} = 2722 \text{ K}$, and the emissivity of the outer surface of the wall is $\varepsilon = 0.95$.

By substituting these data in the following equation

$$h_{gc}(T_{aw} - T_{wg}) = \varepsilon\sigma T_{wg}^4$$

there results

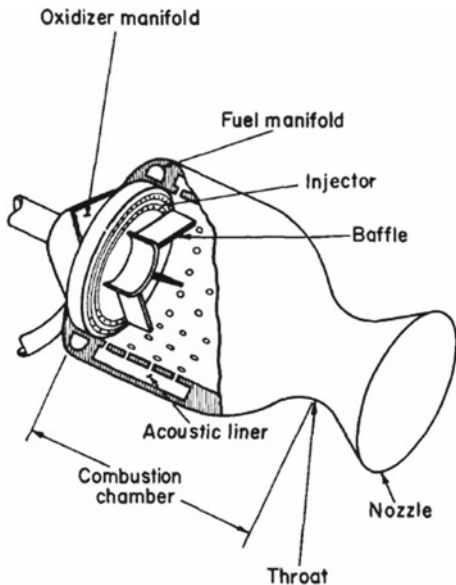
$$206.6 \times (2722 - T_{wg}) = 0.95 \times 5.67 \times 10^{-8} \times T_{wg}^4$$

This equation can be solved numerically for T_{wg} . The result, with four significant figures, is $T_{wg} = 1478 \text{ K}$. Consequently, the heat flux on the hot gas side of the wall is

$$q = h_{gc}(T_{aw} - T_{wg}) = 206.6 \times (2722 - 1478) = 2.57 \times 10^5 \text{ W/m}^2$$

2.6 Injectors

The position of a typical injector in the combustion chamber of a rocket engine is shown in the following figure, due to the courtesy of NASA [49].



As has been shown in Sect. 2.1, the injector is the part of a rocket engine in which the liquid fuel and the liquid oxidiser are admitted in the combustion chamber, broken up into particles or droplets in order to increase the areas of their contact surfaces, mixed one with the other, and left to vaporise before reacting in the combustion process. An injector terminates with a perforated plate which marks the beginning of the combustion chamber.

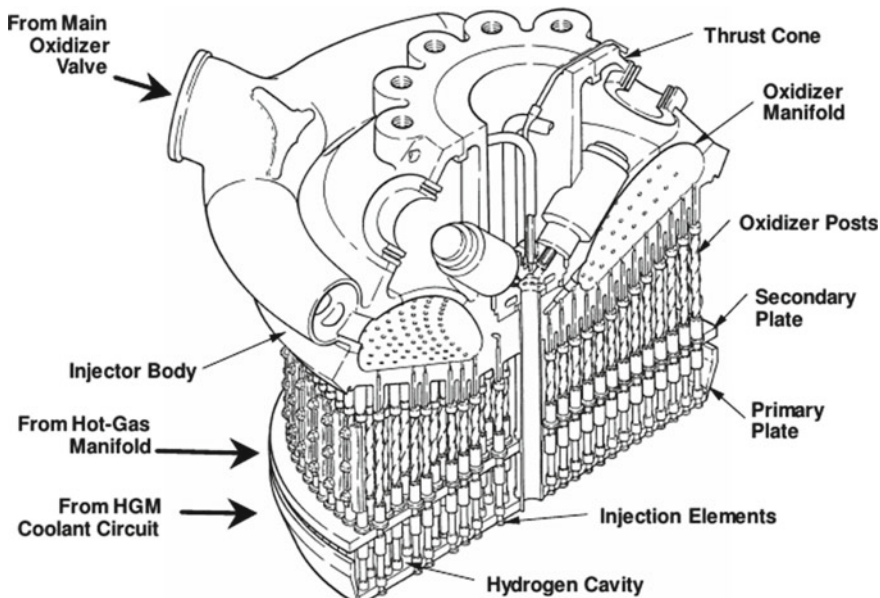
Huzel and Huang [5] have identified some requirements to be taken into account in the design of an injector. They are indicated below.

- Stability in the combustion process, meaning by that a smooth combustion not only during the steady state operation but also in the start and stop transients. For this purpose, it is necessary to prevent unburned propellants from accumulating in the combustion chamber before ignition, in order to avoid an excess of pressure. It is also necessary to maintain a mixture of propellants rich in fuel at the moment of shutting the engine off, in order to avoid overheating. The propagation of local detonations due to combustion instabilities can be prevented by using damping devices placed either on the injector face (baffles) or along the wall of the combustion chamber (acoustic liners). Full details on baffles, acoustic absorbers, and other stabilisation devices are given in Sect. 2.9 and also in [74]. The correct amount and mixture ratio of propellants are maintained by means of valves.
- Performance of an injector in the combustion process, which depends on factors such as distribution of the mass of propellants, local value of the mixture ratio, mixing of the propellants, size and vaporisation of the droplets, heat flow, and velocity of the chemical reactions. Experience has shown that droplets of small size vaporise at high rates, and therefore injectors having a large number of

injecting elements have also a better performance, for the same volume of the combustion chamber, than those having a small number.

- Thermal and structural integrity of the injector, meaning by that its capability of withstanding the thermal and mechanical loads to which it is subject during the various phases of operation of the engine. In particular, an adequate system of cooling it is necessary to protect the injector from overheating.
- Proper sizing of the orifices, in order to obtain desired values of droplet size and also of pressure drops at specific flow rates.
- Protection of the whole combustion chamber from heat, meaning by that a complete mixing of the propellants, in order to avoid the formation of hot spots near the wall. To this end, the value of the mixture ratio α/β is kept low near the wall by placing a set of fuel holes around the periphery of the injector.
- Capability of operating in special conditions, for example, at low thrust levels during throttling, or at values of the mixture ratio which differ from the nominal values.

The working principle of an injector is illustrated in the following figure, due to the courtesy of Boeing-Rocketdyne [50], which shows the main injector of the Space Shuttle main engine.



This injector admits into the main combustion chamber a combination of hot, fuel-rich gas from the two pre-burners, cold gaseous hydrogen from the cooling circuits, and cold liquid oxygen from the high-pressure oxidiser turbo-pump. Passageways are formed for these fluids to enter the proper cavities in the injector, by welding the injector into the centre of the hot-gas manifold (HGM). The injector consists

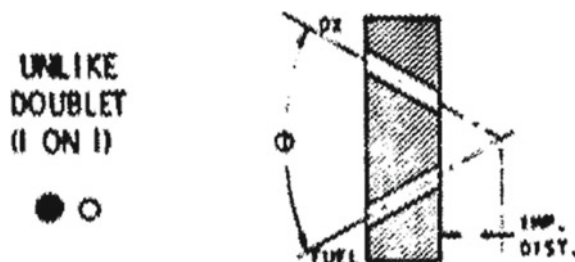
of 600 coaxial elements, which inject liquid oxygen from the oxidiser manifold through their centre posts. Each element also injects, through its annulus, the hot, fuel-rich gas entering the cavity between the heat shield and the secondary plate. Cold gaseous hydrogen, which had previously migrated through the double walls of the hot-gas manifold, enters the slot between the secondary plate and the lip of the primary plate. Both of these plates are porous and are transpiration-cooled by the cold gaseous hydrogen which flows through them. The flow shields are bolted to the outer row of elements and protect them from damage and erosion caused by the high-velocity gas. An augmented spark ignition (ASI) system chamber is located in the centre of the injector. Small quantities of hydrogen and oxygen are continuously injected into this chamber and initially ignited by two spark igniters located therein. This flame then ignites the propellants flowing through the injector elements into the combustion chamber. The thrust cone is a mounting pad for the gimbal bearing, which in turn attaches the engine to the vehicle [50].

The elements of the injector described above are of the coaxial type, which has been chosen because the combination of propellants is liquid oxygen and hydrogen. In order to meet the requirements posed by other combinations of propellants, elements of different types can be chosen, as will be shown below.

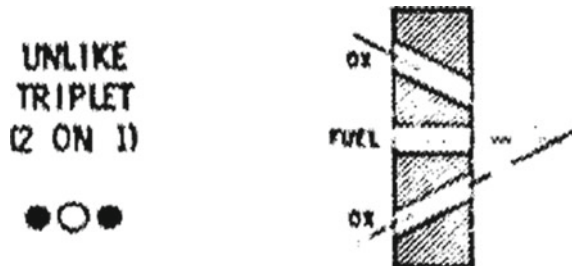
In many cases, the injected streams of propellants are made to impinge at a predetermined distance from the injector face, in order to obtain a good mixture. The impingement distance depends on the heat transfer conditions. The type of elements in which all impingement points are at the same distance from the injector face is called uni-planar impingement. The types of elements in which the impingement points are at two and at more than two distances from the injector face are called respectively bi-planar and multi-planar impingement. The angles between impinging streams are usually chosen in the range from 0.3491 rad to 0.7854 rad.

The following figures, due to the courtesy of NASA [75], show some types of injector elements used for liquid/liquid injection.

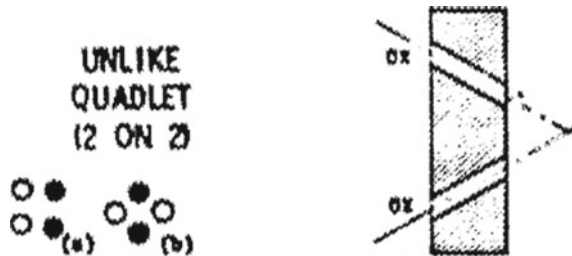
- (a) Unlike doublet, in which each stream of oxidiser is made to impinge on each stream of fuel in a pair. In this arrangement, the angle Φ between the two streams is variable within the range indicated above. It provides a good mixing, but its performance is sensitive to continuous throttling.



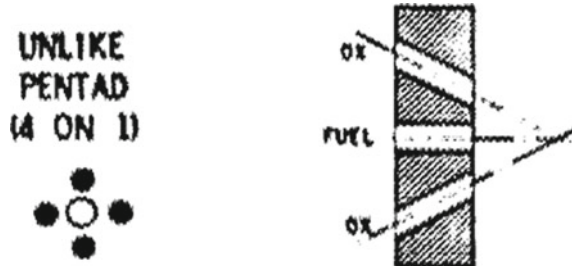
- (b) Unlike triplet, in which two streams of one propellant impinge symmetrically on one stream of the other propellant. It provides a good mixing, but its performance is sensitive to continuous throttling.



- (c) Unlike quadruplet, in which two streams of one propellant impinge symmetrically on two streams of the other propellant. It can be used near the wall of the combustion chamber, but is difficult to manifold.

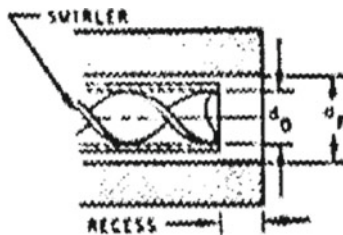


- (d) Unlike quintuplet, in which four streams of one propellant impinge symmetrically on one stream of the other propellant. It provides a good mixing, but is difficult to manifold.



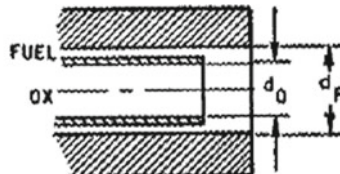
- (e) Concentric tube with swirling, in which two concentric tubes are used to inject coaxially the two propellants, in the presence of a swirling device. It provides a good mixing, but is unstable when throttled.

**CONCENTRIC
TUBE
(WITH
SWIRLER)**



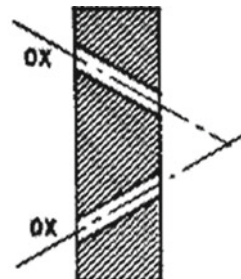
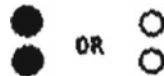
- (f) Concentric tube without swirling, in which two concentric tubes are used to inject coaxially the two propellants, without swirling devices. It has a very good compatibility with the wall of the combustion chamber, but provides a poor mixing.

**CONCENTRIC
TUBE
(WITHOUT
SWIRLER)**

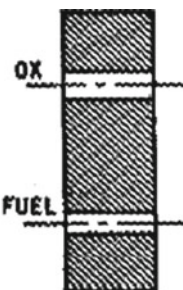


- (g) Like doublet, in which two streams of one propellant are made to impinge on two streams of the other propellant. It provides a good mixing, but requires an increased axial distance to mix the fuel with the oxidiser.

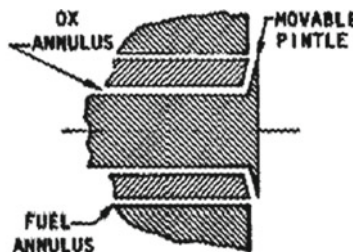
**LIKE
DOUBLET
(1 ON 1)**



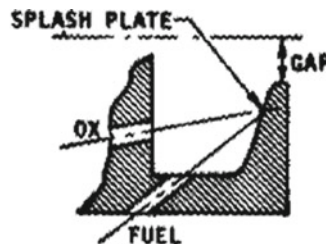
- (h) Shower head, in which non-impinging streams of oxidiser and fuel enter the combustion chamber perpendicularly to the injector face. In this arrangement, the mixing of one propellant with the other is due exclusively to the turbulence in the combustion chamber. It is excellent for boundary layer cooling, but provides a poor mixing.

SHOWERHEAD

- (i) Variable area (movable pinte). It can be throttled and is simple to manufacture, but poses problems of compatibility with the wall of the combustion chamber.

**VARIABLE
AREA
(PINTLE)**

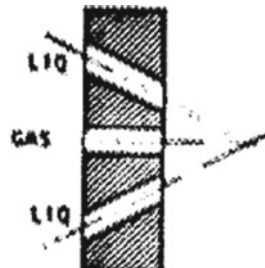
- (j) Splash plate, in which the streams of the injected propellants are deflected by splash plates. These plates are kept cool by the impinging liquid propellants, which ignite only after leaving the plates. It can be throttled, but poses problems of compatibility with the wall of the combustion chamber.

**SPLASH
PLATE**

The following figures, also due to the courtesy of NASA [75], show some types of injector elements used for gas/liquid injection.

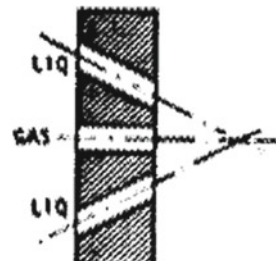
- (a) Unlike triplet, in which two streams of the liquid propellant impinge symmetrically on one stream of the gaseous propellant. It provides a good mixing, but its performance is sensitive to continuous throttling.

**UNLIKE
TRIPLET
(2 ON 1)**



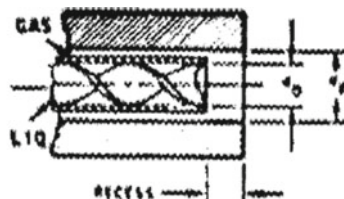
- (b) Unlike quintuplet, in which four streams of the liquid propellant impinge symmetrically on one stream of the gaseous propellant. It provides a good mixing, but its performance is sensitive to continuous throttling.

**UNLIKE
PENTAD
(4 ON 1)**



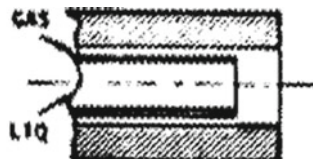
- (c) Concentric tube with swirling, in which two concentric tubes are used to inject coaxially the two propellants, in the presence of a swirling device. It provides an excellent mixing, but tends to become unstable when throttled.

**CONCENTRIC
TUBE
(WITH
SWIRLER)**

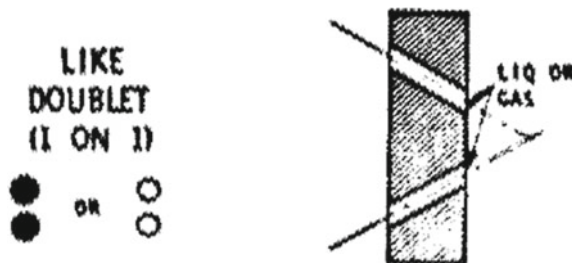


- (d) Concentric tube without swirling, in which two concentric tubes are used to inject coaxially the two propellants, without swirling devices. It has a very good compatibility with the wall of the combustion chamber, but tends to become unstable when throttled.

**CONCENTRIC
TUBE
(WITHOUT
SWIRLER)**

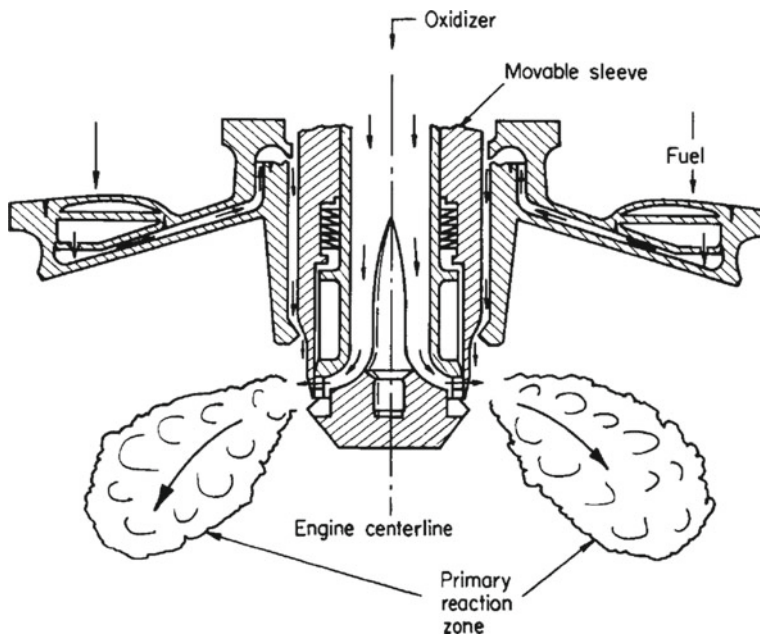


- (e) Like doublet, in which two streams of the gaseous (or liquid) propellant are made to impinge on two streams of the same propellant. It provides a good mixing, but requires an increased axial distance to mix the fuel with the oxidiser.

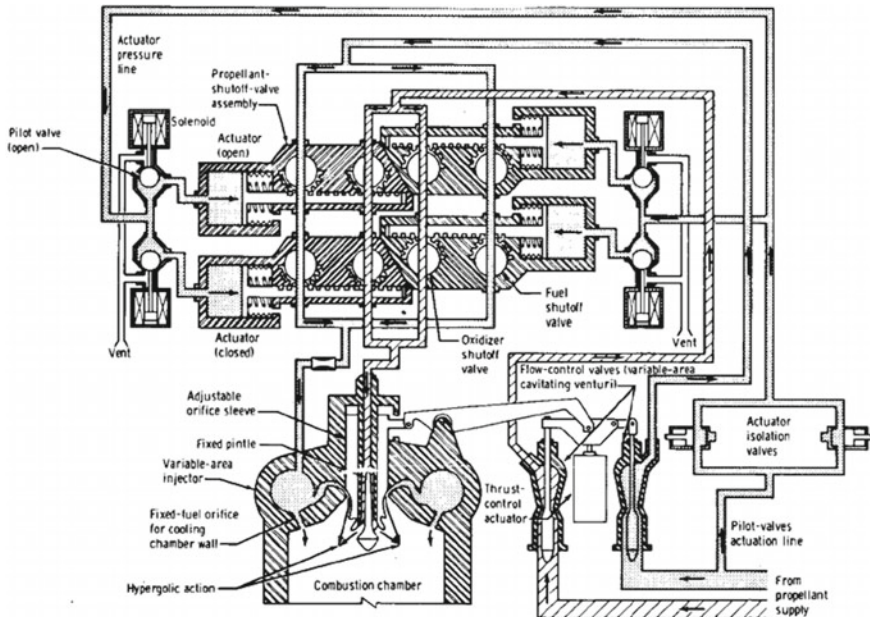


By throttling of a liquid-propellant rocket engine we mean a the variation of the thrust of that engine with respect to the 100% rated power level.

For example, the main engine of the Space Shuttle has a rated power level (100%) of thrust amounting to 2094223 N in vacuo and 1675200 N at the sea level. This thrust can be varied from 1408307 N (67%) to 2281493 N (109%) in increments of approximately 20907 N (1%). These three levels of thrust are called respectively rated power level, minimum power level, and full power level. Throttling is obtained by varying the output of the pre-burners, thus varying the speed of the high-pressure turbo-pumps, and therefore the mass flow rates of the propellants [50]. Throttling can also be obtained by using a variable-area injector. In particular, a pintle injector has a single central pintle, which can be moved to vary the area of the orifices of the injector, as shown in the following figure, due to the courtesy of NASA [49].



The maximum thrust of the engine is obtained by fully opening the orifices. When the area of the orifices is reduced with respect to its maximum value, the pressure in the combustion chamber and the thrust of the engine are also reduced. A pintle injector has been used in the Apollo Lunar Module Descent Engine [76], a scheme of which is shown in the following figure, due to the courtesy of NASA [77].



A pintle injector has also been used in the Merlin rocket engine, which burns liquid oxygen and RP-1 as propellants in a gas-generator power cycle. The Merlin engine has been developed by Space Exploration Technologies Corp. (SpaceX) for its Falcon rocket family [78].

In order to design an injector, it is necessary to take account of some factors. One of them is the injection velocity v (m/s), which is the velocity at which the oxidiser, or the fuel, is injected into the combustion chamber. The injection velocity can be determined as follows

$$v = \frac{\dot{m}}{A\rho}$$

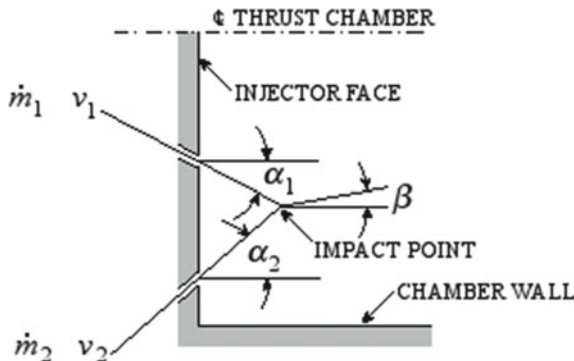
where \dot{m} (kg/s) is the mass flow rate of the propellant, A (m^2) is the area of the orifices of the injector, and ρ (kg/m^3) is the density of the propellant.

Another factor is the drop of injection pressure Δp_i (N/m^2), which can be calculated as follows

$$\Delta p_i = \frac{1}{2} \rho \left(\frac{v}{C_d} \right)^2 = \frac{1}{2\rho} \left(\frac{\dot{m}}{AC_d} \right)^2$$

where C_d is a dimensionless coefficient of discharge, whose value (usually in the range $0.5 \leq C_d \leq 0.92$) is determined experimentally by means of water flow tests. An orifice having a well-round entrance and a smooth bore has also a high value of C_d , and gives rise to a low value of drop of injection pressure, for the same value of injection velocity v .

Another factor is the resultant angle β of two impinging streams of propellant. With reference to the following figure, let \dot{m}_1 and \dot{m}_2 (kg/s) be the mass flow rates of two impinging streams. Let α_1 and α_2 be the angles which these streams form with the axis of symmetry of the thrust chamber. Let v_1 and v_2 (m/s) be the injection velocities of the two streams, determined as has been shown above.



The resultant angle β of these impinging streams is defined by Huzel and Huang [5] by means of the following equation

$$\beta = \arctan\left(\frac{\dot{m}_1 v_1 \sin \alpha_1 - \dot{m}_2 v_2 \sin \alpha_2}{\dot{m}_1 v_1 \cos \alpha_1 + \dot{m}_2 v_2 \cos \alpha_2}\right)$$

The resultant angle β is defined in such a way as to be positive when the resulting stream after the impact is directed toward the chamber wall, and negative when the stream is directed toward the axis of symmetry of the thrust chamber.

In case of an engine burning a combination of hypergolic propellants, a small positive value (ranging from 0.03491 rad to 0.08727 rad) of the β angle is advantageous for the purpose of mixing the liquid propellants along the wall of the combustion chamber.

In case of an engine burning a combination of cryogenic propellants, their mixing occurs principally in the gaseous state. In these conditions, a positive value of the β angle can generate hot streaks on the wall of the combustion chamber. A negative value of the β angle should be chosen to avoid this undesirable effect.

Another factor is the injection momentum ratio, which is defined as follows

$$R_m = \frac{\dot{m}_o v_o}{\dot{m}_f v_f}$$

where \dot{m}_o (kg/s) and \dot{m}_f (kg/s) are the mass flow rates of respectively the oxidiser and the fuel, and v_o (m/s) and v_f (m/s) are their respective injection velocities. The injection momentum ratio is an index of performance. For the design of oxygen-hydrogen injectors, Huzel and Huang [5] indicate the following values of injection

momentum ratio: $1.5 \leq R_m \leq 3.5$ when liquid hydrogen is injected, and $0.5 \leq R_m \leq 0.9$ when gaseous hydrogen is injected.

Still another factor is the structural load, which is due to the pressures (measured in N/m²) exerted by the propellants behind the face of the injector (p_f) and in the injector manifolds (p_m).

In the steady state, the pressure p_f behind the face of the injector is equal to the drop of injection pressure Δp_i , defined above, as follows

$$p_f = \Delta p_i$$

The pressure p_m in the injector manifolds results from summing the pressure ($p_c)_i$ of the combustion chamber at the injector end to the drop Δp_i of injection pressure, as follows

$$p_m = (p_c)_i + \Delta p_i$$

At the start of the engine, the pressure behind the face of the injector may be much greater than the corresponding pressure in the steady state. When the valves of the propellants are opened rapidly, the pressure of the propellant can cause a hydraulic ram. Let p_p (N/m²) be the pressure of the propellant at the moment of opening the valves. Huzel and Huang [5] indicate the following empirical formula to estimate the pressure load:

$$p_f = p_m = 4p_p$$

As an example of application, it is required to determine the size of the orifices of the injector for the two propellants, the injection velocity, and the injection momentum ratio for a rocket engine of given properties.

Let us consider again the rocket engine described in Sects. 2.3, 2.4, and 2.5. This engine burns a combination of liquid oxygen (oxidiser) with RP-1 (fuel). The density of the oxidiser is $\rho_o = 1141 \text{ kg/m}^3$ and its mass flow rate in the thrust chamber is $\dot{m}_o = 880.4 \text{ kg/s}$. The density of the fuel is $\rho_f = 808.1 \text{ kg/m}^3$ and its mass flow rate in the thrust chamber is $\dot{m}_f = 375.1 \text{ kg/s}$. The drop of injection pressure is $\Delta p_i = 1.379 \times 10^6 \text{ N/m}^2$ for both of the propellants. A coefficient of discharge $C_d = 0.75$ is taken for both of them.

The total area A_o of the orifices for the oxidiser in the injector results from the following equation

$$\Delta p_i = \frac{1}{2\rho_o} \left(\frac{\dot{m}_o}{A_o C_d} \right)^2$$

which, solved for A_o , yields

$$A_o = \frac{\dot{m}_o}{C_d(2\rho_o\Delta p_i)^{\frac{1}{2}}} = \frac{880.4}{0.75 \times (2 \times 1141 \times 1.379 \times 10^6)^{\frac{1}{2}}} = 0.02093 \text{ m}^2$$

Likewise, the total area A_f of the orifices for the fuel in the injector results from

$$A_f = \frac{\dot{m}_f}{C_d(2\rho_f\Delta p_i)^{\frac{1}{2}}} = \frac{375.1}{0.75 \times (2 \times 808.1 \times 1.379 \times 10^6)^{\frac{1}{2}}} = 0.01059 \text{ m}^2$$

In the present case (liquid/liquid injection), an injector of the like-doublet type can be used, in which oxidiser and fuel jets are made to impinge in pairs, as has been shown above.

In case of using 700 doublets for the oxidiser and 700 doublets for the fuel, the area of each orifice for the oxidiser is

$$a_o = \frac{A_o}{2 \times 700} = \frac{0.02093}{1400} = 0.1495 \times 10^{-4} \text{ m}^2 = 0.1495 \text{ cm}^2$$

Hence, the diameter of each orifice for the oxidiser is

$$d_o = \left(\frac{4a_o}{\pi} \right)^{\frac{1}{2}} = \left(\frac{4 \times 0.1495 \times 10^{-4}}{3.1416} \right)^{\frac{1}{2}} = 0.004362 \text{ m} = 4.362 \text{ mm}$$

Likewise, the area of each orifice for the fuel is

$$a_f = \frac{A_f}{2 \times 700} = \frac{0.01059}{1400} = 7.564 \times 10^{-6} \text{ m}^2$$

Hence, the diameter of each orifice for the fuel is

$$d_f = \left(\frac{4a_f}{\pi} \right)^{\frac{1}{2}} = \left(\frac{4 \times 7.564 \times 10^{-6}}{3.1416} \right)^{\frac{1}{2}} = 0.003103 \text{ m} = 3.103 \text{ mm}$$

The mean velocities of injection for respectively the oxidiser (v_o) and the fuel (v_f) result from the following equation

$$v = \frac{\dot{m}}{A\rho}$$

For the oxidiser, we find

$$v_o = \frac{\dot{m}_o}{A_o\rho_o} = \frac{880.4}{0.02093 \times 1141} = 36.87 \text{ m/s}$$

For the fuel, we find

$$v_f = \frac{\dot{m}_f}{A_f \rho_f} = \frac{375.1}{0.01059 \times 808.1} = 43.83 \text{ m/s}$$

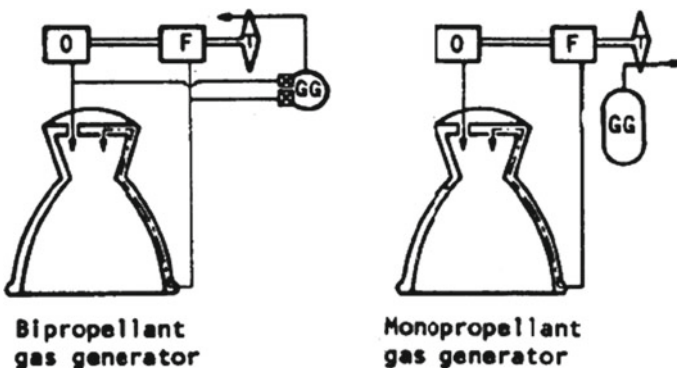
The injection momentum ratio results from

$$R_m = \frac{\dot{m}_o v_o}{\dot{m}_f v_f} = \frac{880.4 \times 36.87}{375.1 \times 43.83} = 1.974$$

2.7 Gas-generator and Other Engine Cycles

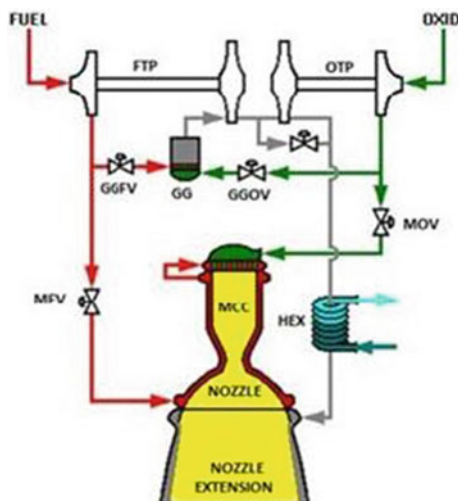
A gas generator is the part of a liquid-propellant rocket engine which supplies energy to drive the turbo-pumps. A turbo-pump is a rotating machine which takes one of the liquid propellants at low pressure from a tank and supplies it to the combustion chamber at the required mass flow rate and injection pressure. The energy absorbed by the turbine is provided by the expansion of compressed gases, which are usually mixtures of the propellants burned in the engine [79]. There are several ways to use the propellants for this purpose. Therefore, there are several arrangements of components, which are called rocket engine cycles. Some of these cycles are briefly described below.

The gas-generator cycle is shown in the following figure, due to the courtesy of NASA [80].



In the bi-propellant gas-generator cycle (left), the working fluid for the turbine (T) is derived by combustion of the oxidiser (O) with the fuel (F) in the gas generator (GG) at a temperature below the turbine temperature limits. A gas generator consists of a propellant valve, an injector, and a combustion chamber. The propellants for the gas generator are tapped from the turbo-pump discharge lines, injected into the combustor through the gas-generator injector, burned, and converted to gas. This gas is expanded through the turbine which drives the pumps. Since the operating temperature limit of

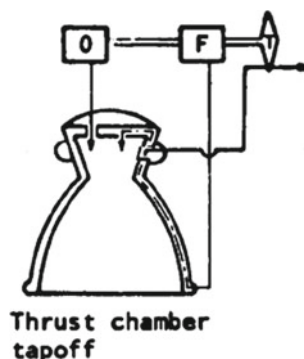
the current turbine materials is about 1090 K, the gas generator is operated with excess fuel, in order for the temperature to remain within this limit. A small amount (about 3% in the J-2X engine) of the propellants is used to keep the engine running, whereas the remaining part of the propellants is used to generate thrust. A gas generator (GG) is a separate, small combustion chamber which produces gases. These gases are used to drive the turbines connected to the pumps. The following figure, due to the courtesy of NASA [81], shows a scheme of the J-2X engine, which is based on the gas-generator cycle. This engine uses liquid hydrogen and liquid oxygen as, respectively, fuel and oxidiser (OXID).



These propellants go immediately from their tanks into their turbo-pumps, which are the fuel turbo-pump (FTP) and the oxidiser turbo-pump (OTP). There, the mechanical energy of the rotating pumps is used to put the liquid propellants under pressure. At the exit from the pumps, a small amount of each propellant is tapped off to supply the gas generator (GG), which is substantially a small engine included into the principal engine. This small engine generates hot combustion products (which are, in the present case, steam and gaseous hydrogen) at high pressure. These gases are used to drive first the turbine connected to the fuel pump and then the turbine connected to the oxidiser pump. After driving the two turbines, the hot gases are used to warm the helium flowing through the heat exchanger (HEX), which is used to pressurise the oxygen tank of the stage, and are then dumped along the walls of the nozzle extension, to keep them cool. The remaining liquid oxygen, which does not go to the gas generator, is directed to the main injector. The hydrogen coming from the fuel pump is used to regeneratively cool the walls of the nozzle and the walls of the main combustion chamber (MCC), and is then directed to the injector of the main combustion chamber. A very small amount of the warm gaseous hydrogen is tapped off before entering the main injector, and is routed back to pressurise the hydrogen tank, as is the case with the helium flowing through the heat exchanger.

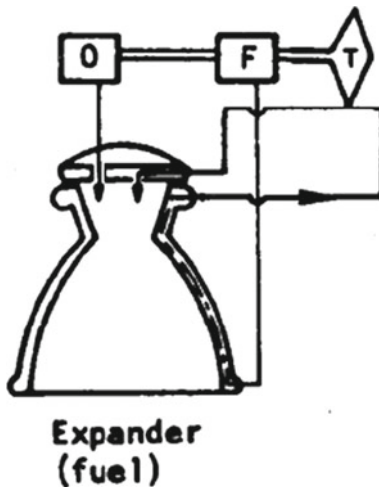
on the oxygen side. The exhaust gases coming from the turbines are dumped along the nozzle extension. These gases generate some thrust, but not as efficiently as the gases which are accelerated by flowing through the throat and the nozzle. The loss of effectiveness is the price paid for this simple engine cycle. On the other hand, the turbines of an engine using a gas-generator cycle are not subject to counter-pressure which would arise if the exhaust gases were injected into the combustion chamber. This fact makes it easy to design the turbines and the pipes. The other items shown in the preceding scheme are the main fuel valve (MFV), the main oxidiser valve (MOV), the gas-generator fuel valve (GGFV), and the gas-generator oxidiser valve (GGOV). These and other minor valves are used to control the engine during the start and shutdown transients [81]. The gas-generator cycle is used in the Vulcain, HM7B, Merlin, RS-68, RS-27A, J-2X, J-2, F-1, RD-107, and CE-20 engines.

The thrust chamber tap-off cycle is shown in the following figure, due to the courtesy of NASA [80].



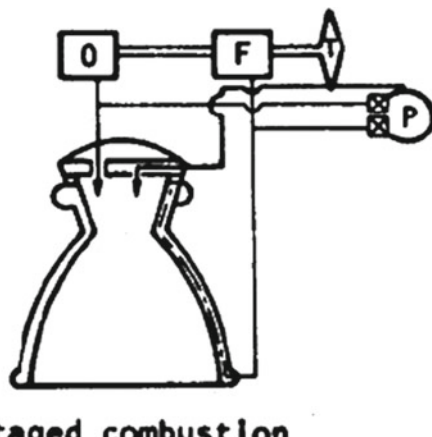
In the tap-off cycle, the working fluid for the turbine is tapped off near the face of the injector at a location in which a sufficiently cool gas is available [82]. The thrust chamber tap-off cycle is used in the J-2S engine.

The following figure, due to the courtesy of NASA [80], shows the expander cycle, which is used in the RL10, Vinci, RD-0146, YF-75D, LE-5A/5B (expander bleed cycle), LE-9, and MB-60 engines.



In the expander cycle, also called hot-fuel tap-off cycle, hydrogen (F) is evaporated and heated in the jacket of the thrust chamber, and is then used to drive the turbines. The exhaust gas coming from the turbines is fed to the combustion chamber [82].

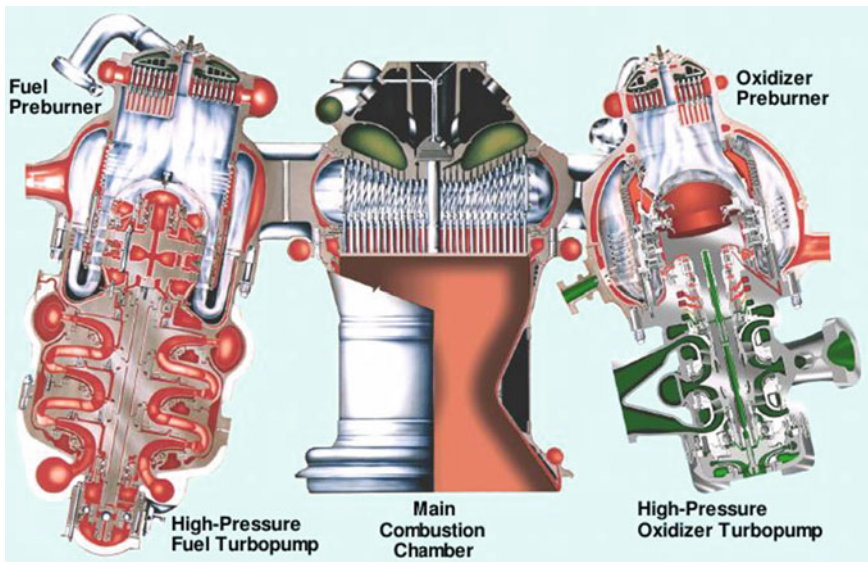
The following figure, due to the courtesy of NASA [80], shows the staged-combustion cycle.



Staged combustion

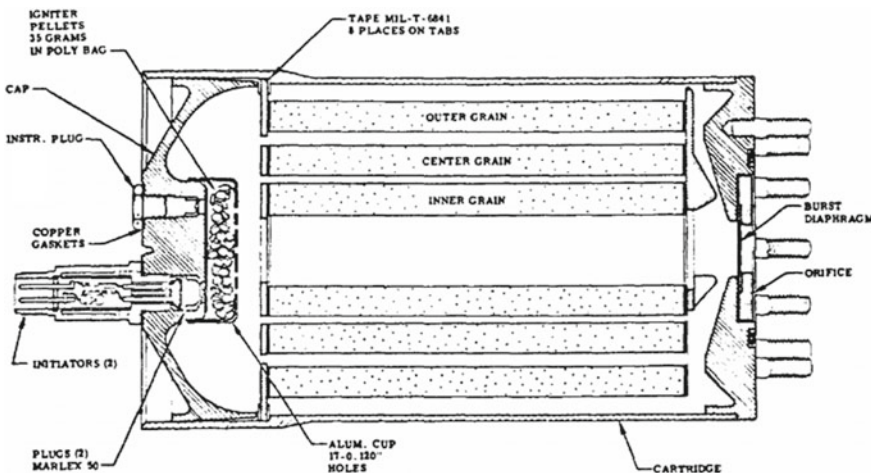
In the staged-combustion cycle, most of the fuel (F), except a small quantity used as coolant, and a small amount of the oxidiser (O) are pre-burned in a pre-burner (P) at an extremely fuel-rich mixture. The resulting fuel-rich hot gas is used to drive the turbo-pump turbine, and is then injected into the main combustion chamber together with the remaining oxidiser and the coolant fuel, where all of them are finally burned.

The following figure, due to the courtesy of Boeing-Rocketdyne [50], shows the staged-combustion cycle, used in the RS-25 engine (which is the main engine of the Space Shuttle) and in the RS-170/180 engine.

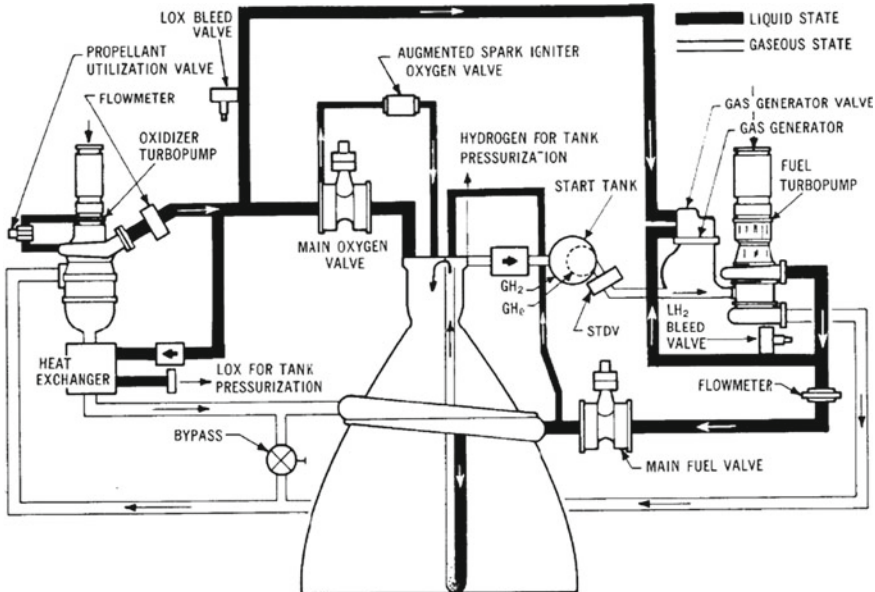


Liquid-propellant rocket engines may also use solid-propellant gas generators for turbine spinners at the engine start or for other applications of brief duration. This is because the temperature of the gases generated by solid-propellant gas generators is usually above 1366 K, which fact makes them unfit for non-cooled components over long times. These gas generators are only used to start, but the pressure and the gas flow should continue after the burnout of the solid propellant and the takeover of the liquid propellants.

The following figure, due to the courtesy of NASA [5] shows one of such devices, which is a disposable solid-propellant gas generator used to drive the turbines at the engine start. This device is a cartridge bolted to a flange at a liquid-propellant gas generator, as will be shown below. This particular cartridge can be used only once.



A rocket engine may also be started by using a start tank containing a gas (for example, hydrogen or helium) stored under high pressure. This device, also known as start bottle, is shown in the following figure, due to the courtesy of NASA [17], where the J-2 engine is illustrated.



The J-2 engine was used for the Saturn IB and Saturn V launch vehicles for the NASA Apollo programme. When the engine is started, the gas is allowed to leave the start tank and impinge on the blades of the turbines which drive the pumps.

Solid propellants are mixtures of fuels with oxidisers. Their exposed surfaces burn uniformly at rates depending on the temperature and on the pressure of the combusted gases. According to Huzel and Huang [5], the combustion rate R (m/s) of a given solid propellant can be expressed as follows

$$R = k_1 \left(\frac{p_c}{6.895 \times 10^6} \right)^n$$

where k_1 (m/s) is a constant quantity, which expresses the constant burning rate of a given propellant, at a given initial temperature, and at a pressure of 6.895×10^6 N/m² in the combustion chamber, p_c (N/m²) is the pressure in the combustion chamber, and n is a constant quantity, whose value depends on the sensitivity of the burning rate of the propellant to changes of pressure, at a given temperature.

The mass flow rate \dot{m}_g (kg/s) through a solid-propellant gas generator can be calculated by means of the following equation of [5]:

$$\dot{m}_g = A_b R \rho_p$$

where A_b (m^2) is the burning area of the propellant, R (m/s) is the combustion rate, and ρ_p (kg/m^3) is the density of the propellant.

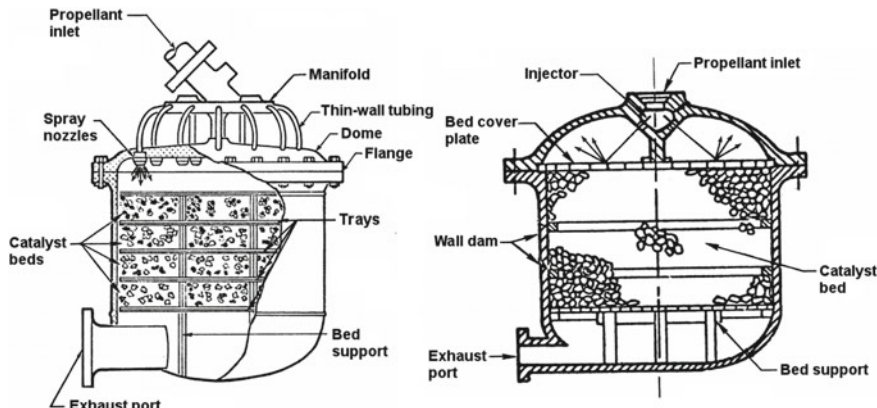
In order for the mass flow rate of a solid-propellant gas generator to be constant, the burning area of the propellant must also be constant.

The total area A_o (m^2) of the orifices of a solid-propellant gas generator must be such as to satisfy the following equation of [5]:

$$p_c = k_2 \left(\frac{A_b}{A_o} \right)^{\frac{1}{1-n}}$$

where p_c (N/m^2) is the pressure in the combustion chamber, k_2 (N/m^2) is a constant quantity for a given propellant at a given temperature, A_b (m^2) is the burning area of the propellant, and n is the constant quantity mentioned above.

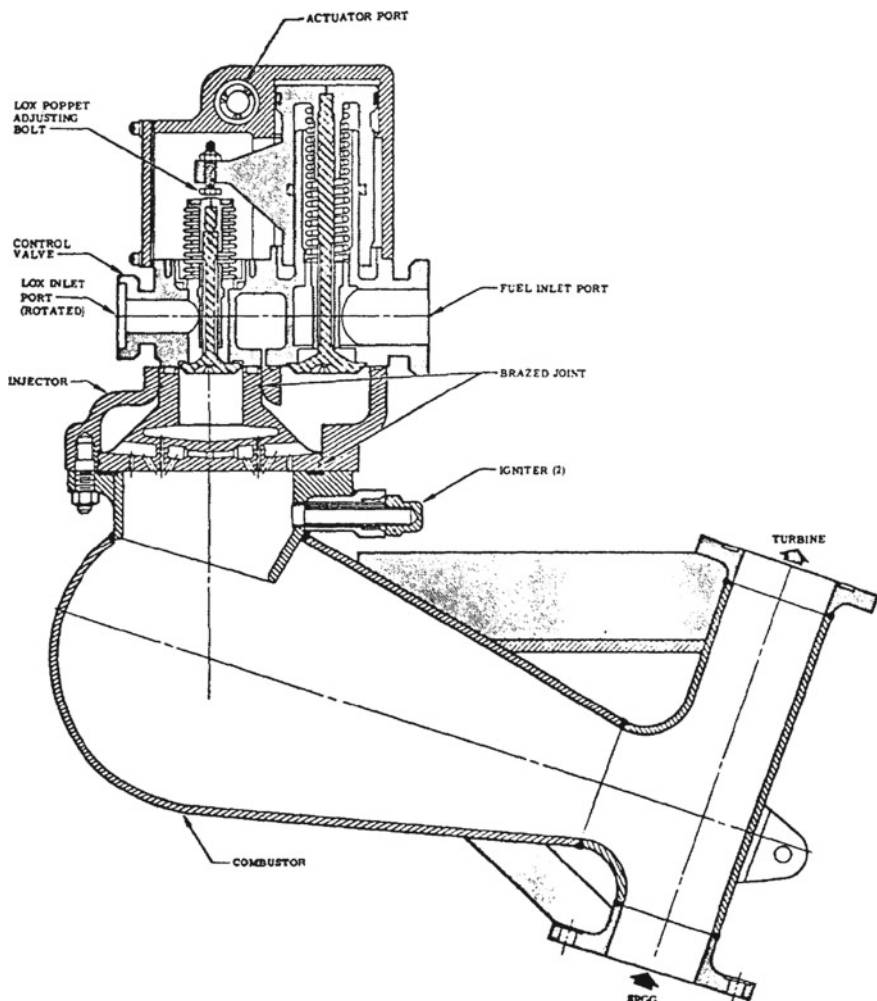
Liquid mono-propellants may also be used to generate gases. The following figure, due to the courtesy of NASA [83], shows two of these gas generators using (left) hydrazine and (right) hydrogen peroxide.



Gas generators using mono-propellants are simple and easy to control. They require a separate tank, unless the gas-generating mono-propellant is also used to feed the main engine.

Liquid-propellant gas generators are frequently chosen for liquid-propellant rocket engines, because the same propellants are used in the gas generators and in such engines. The liquid-propellant gas generator used in the H-1 rocket engine is shown in the following figure, due to the courtesy of NASA [5]. The H-1 engine was developed by Rocketdyne for use in the S-I and S-IB first stages of respectively the Saturn I and the Saturn I-B rockets, which were used for the NASA Apollo programme. The propellants used in this engine are liquid oxygen and RP-1 (kerosene). The liquid-propellant gas generator of the H-1 engine produces combusted gases during steady-state operation to drive the two-stage turbine.

The turbine supplies power through a gear reduction train to drive the propellant pumps. The liquid-propellant gas generator of the H-1 engine consists of a gas generator control valve, an injector assembly, a combustor, and two squib-less igniters. These components are briefly described below. The propellants entering the liquid-propellant gas generator are ignited by a solid-propellant gas generator (SPGG in the following figure) and by the two squib-less igniters during engine start. The hot gases from the solid-propellant gas generator ignite the squib-less igniters before the liquid propellants enter the liquid-propellant gas generator. The igniters burn for 2.5–3 s to ensure the ignition of the liquid propellants. The control valve of the liquid-propellant gas generator is a normally closed valve containing two poppets, which admit the bootstrap propellants into the combustor of the gas generator during engine operation.



The combustion pressure in the thrust chamber actuates the control valve by means of a piston, which opens the fuel poppet first. A yoke integral with the piston opens the oxidiser poppet. The cracking pressures relative to the atmosphere are $(7.239 \pm 1.379) \times 10^5$ N/m² for the fuel poppet and $(13.79 \pm 1.379) \times 10^5$ N/m² for the oxidiser poppet. The fully-open operating pressure relative to the atmosphere is $(18.96 \pm 1.724) \times 10^5$ N/m² for the control valve. The bootstrap propellant mass flow rates are 6.133 kg/s for the fuel and 2.091 kg/s for the oxidiser. A bellows assembly enclosing the liquid oxygen poppet stem and the closure spring, and the seals on the actuator piston prevent leakage of fuel and oxidiser into the control valve actuator. A drain line directs any fuel leakage into the valve actuator to the fuel drain manifold, where it is dumped overboard into the engine exhaust stream. The control valve is designed to ensure a fuel-rich cut-off to prevent an excessive increase in temperature in the combustor with consequent turbine burning. The spring pressure closes the control valve at engine cut-off, when the pressure in the thrust chamber decreases.

The fuel and the oxidiser from the gas generator control valve enter the injector and flow through passages which provide a uniform mixture ratio *of* = 0.3409. The injector cavity is designed to permit an oxidiser lead into the combustor during start to prevent detonation. From the injector, two fuel streams impinge on a single oxidiser stream. The injector has 44 impingement points. The fuel which enters the combustor through 36 holes around the periphery of the impingements provides film coolant for the injector. During countdown, the oxidiser injector of the gas generator receives a purge with ambient gaseous nitrogen to prevent entrance of contaminants from the solid-propellant gas generator into the injector.

The bootstrap propellants burn in the combustor and exit to the gas turbine. Two squib-less igniters installed in the combustor just below the injector of the gas generator assure propellant ignition during start. The combustor is a welded assembly with flanges for installation of the solid-propellant gas generator and for attachment to the gas turbine. The operating temperature is 920.9 ± 264.3 K, and the operating absolute pressure is $(4.456 \pm 0.03378) \times 10^6$ N/m².

Two squib-less igniters installed in the injector mounting flange on the combustor burn for 2.5–3 s after their ignition by the solid-propellant gas generator. They ensure ignition of fuel and oxidiser if the solid-propellant gas generator should have expired before bootstrap propellant entry into the combustor.

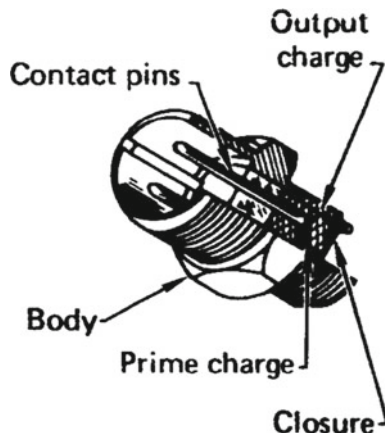
A gas generator burns the propellants just as the main engine does, the only difference being the capability possessed by the former of varying the mixture ratio *of*, whose value is adjusted in order for the combusted gas to have the desired temperature and chemical properties.

The guidelines for designing a gas generator for a liquid bi-propellant rocket engine are the same as those relating to the thrust chamber of the main engine. When the characteristic length *L** is calculated, the volume to be taken into account goes from the injector to the throat of the nozzle of the turbine. Account is also taken of the maximum temperature which the materials of which the turbine is made can withstand. Consequently, the design temperature of the turbine is usually kept under 1255 K [5].

2.8 Igniters

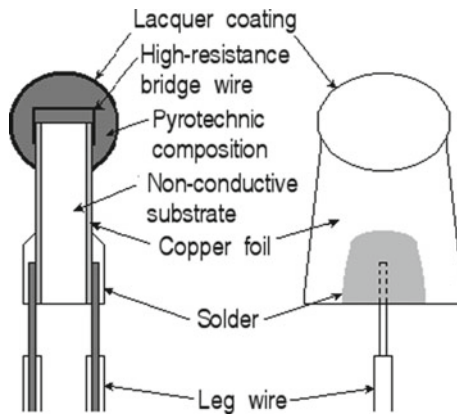
An igniter is a device which releases energy (usually in form of heat) in a rocket engine, for the purpose of initiating the combustion of the main propellants. This combustion, after initiation, is capable of sustaining itself without the necessity of receiving heat. The source of energy which stimulates an igniter to release heat is either inside (as is the case with a solid propellant) or outside (as is the case with a spark arrangement) the igniter itself. The principal types of igniters used in rocket engines are described below.

Pyrotechnic igniters are devices containing mixtures of fuels, oxidants, and often other materials. These devices are used in rocket engines (thrust chambers and gas generators) to release energy in form of heat. Pyrotechnic mixtures are in a state of meta-stability, meaning by this term, stability and non-reactivity under some conditions, and release of thermal energy originally stored in chemical form after receiving an external stimulus, which is usually given to such mixtures by addition of heat. The amount of energy required to stimulate this release of heat is called activation energy. The net amount of thermal energy released in a pyrotechnic reaction is called heat of reaction. The heats of reaction for some binary pyrotechnic compositions are given in [84]. The following figure, due to the courtesy of NASA [85], shows an electrically-triggered initiator, or squib, used to ignite a rocket engine.

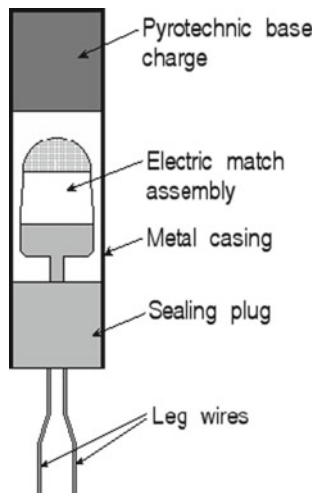


The initiator shown in the preceding figure is a body of metal containing a prime charge, an output charge, and two contact pins used as electrodes. The prime charge is the head of an electric match, which contains a short wire (a bridge wire), 0.0127–0.127 mm in diameter, made of a material (usually nichrome, which is an alloy 80% nickel and 20% chromium, by mass). This wire glows red-hot when a voltage is applied to its ends. The bridge wire is placed between the two electrodes, and is surrounded by a pyrotechnic composition (materials used for this purpose include

lead styphnate, lead azide, diazodinitrophenol, and zirconium-ammonium perchlorate) which is sensitive to heat. A scheme of an electric match is shown in the following figure (re-drawn from [86]).



The pyrotechnic composition specified above may be surrounded by a second, less sensitive composition, which protects the first. The second composition, in turn, is covered by a nitrocellulose lacquer. A scheme of a squib, including an electric match, is shown in the following figure (re-drawn from [86]).



When a small voltage (28 V or less) is applied to the electrodes, the heating of the bridge wire causes the deflagration of the pyrotechnic material in contact with it. The output charge is also made of pyrotechnic material, as will be shown below. The addition of the output charge to the prime charge greatly magnifies the ignition effect.

The initiator supplies the energy, in form of heat, which is necessary to ignite the propellants. The solid-propellant charge burns with a hot flame within the combustion chamber. The igniter can be designed to fit directly onto the injector. This method of ignition can only be used once. Therefore, a rocket engine having a pyrotechnic igniter cannot be restarted, as has been shown in Sect. 2.1.

The most effective materials used for output charges in initiators are metal-oxidant pyrotechnic formulations. Some examples of these formulations are shown in the following table, due to the courtesy of NASA [85].

Application /Designation	Fuel	Oxidants	Binders
Mk 247, Mk 265 (igniters)	Boron, 23.7%	KNO ₃ , 70.7%	Laminac, 5.6%
XM-6 & XM-8 (EBW)			
MB-1 (500-V initiator)	Zirconium, 66.3%	NH ₄ ClO ₄ , 32.7%	Nitrocellulose, 1.0%
FA-878	Zirconium, 40%	BaNO ₃ , 20%	
(ign. elements Mk 10,		PbO ₂ , 20%	
Mk 11, Mk 13, Mk 17)		PETN, 20%	
M2 squib	Pb(SCN) ₂ , 32% Charcoal, 18%	KClO ₃ , 40%	Egyptian lacquer, 10%
NOTS Model 39	Magnesium, 60%	Polytetrafluoro-ethylene, 40%	

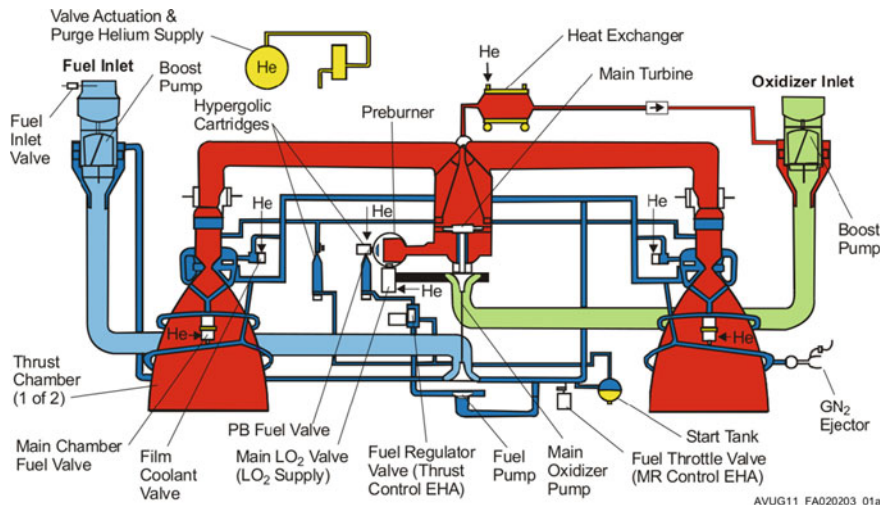
Pyrotechnic igniters can be mounted in recesses as plugs of the screw-in type, in case of gas generators and small thrust chambers.

Hypergolic igniters are based on the property of some bi-propellant combinations which ignite spontaneously at room temperature when the two components (the fuel and the oxidiser) of a combination get in touch one with the other. Therefore, hypergolic combinations do not require an external source of ignition. They need only a valve to mix the fluids for the purpose of initiating the combustion. This method of ignition reduces the components of an ignition system, and therefore its chances of failure.

As has been shown in Chap. 1, Sect. 1.2, the most common fuels used in a combination of hypergolic propellants are hydrazine (H_2NNH_2), monomethyl hydrazine ($CH_3(NH)NH_2$), unsymmetrical dimethyl hydrazine ($H_2NN(CH_3)_2$), and Aerozine 50, the last being an equal mixture of hydrazine and unsymmetrical dimethyl hydrazine. The oxidisers used in combination with these fuels are usually nitrogen tetroxide (N_2O_4) and various blends of nitrogen tetroxide with nitric oxide (NO).

Hypergolic igniters have been used in liquid bi-propellant engines. An example has been cited in Sect. 2.1, which describes a mixture of gaseous fluorine with liquid oxygen used to start an engine which burns liquid hydrogen and liquid oxygen. Two

further examples are cited below. The RD-180 engine of the Atlas V rocket burns a mixture of kerosene with liquid oxygen. This engine has a device, placed in the fuel line, for hypergolic ignition. This device consists of two cartridges which contain a mixture of 15% triethylaluminium ($\text{Al}_2(\text{C}_2\text{H}_5)_6$, also known as TEA, which is a pyrophoric substance) with 85% triethylborane ($(\text{C}_2\text{H}_5)_3\text{B}$, also known as TEB). A scheme of the RD-180 engine is shown in the following figure, which is due to the courtesy of the United Launch Alliance [87].



As shown in the preceding figure, the TEA-TEB mixture is stored in two closed cylindrical cartridges, one of which is in the fuel line directly ahead of the pre-burner, and the other is in either of the main fuel inlet to the two main combustion chambers. The cartridges have burst diaphragms to prevent this mixture from coming in contact with atmospheric oxygen. The pre-burner illustrated above is the gas generator which drives the main turbine.

In order to start the engine, a start tank of spherical shape, shown in the lower part of the preceding figure, is connected to both of the fuel lines by means of tubes and associated valves. The start tank is filled with fuel and put under pressure by using gas. When the valves to the fuel lines and the cartridges are opened, the high pressure of the fuel drives pistons which are in the cartridges. This causes the TEA-TEB mixture to be released into the gas generator and into the main combustion chambers, which in turn have been filled with oxygen after the liquid oxygen valves are opened, and the tank pressure causes oxygen to enter the engine. The TEA-TEB mixture comes in touch with oxygen, and therefore self-ignites and starts the combustion inside the gas generator and the main combustion chambers. The combustion is sustained by the fuel entering the gas generator and the main combustion chambers just after the TEA-TEB mixture. Now, the gas generator is running, and therefore the main turbine drives the boost pumps (shown on the two sides of the preceding figure), which in

turn discharge the propellants under pressure to the gas generator and to the main combustion chambers.

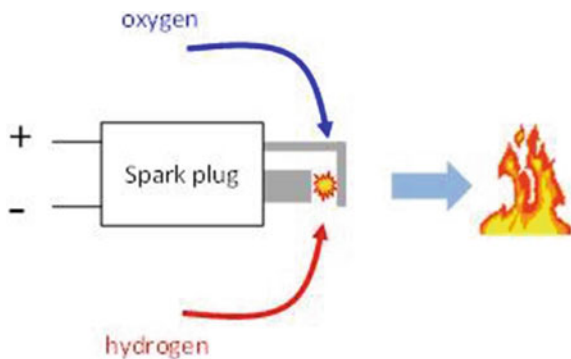
The F-1 engine of the Saturn V rocket burns a mixture of RP-1 (kerosene) with liquid oxygen. This engine also has an igniter containing a cartridge of hypergolic fluid (which is, again, a mixture of 85% triethylborane with 15% triethylaluminium) with burst diaphragms at either end. This igniter is in the fuel line, and the hypergolic fluid has its own orifices in the injector of the main combustion chamber. The hypergolic fluid, followed by the fuel, enters the main combustion chamber. There, this fluid ignites spontaneously in contact with the liquid oxygen already injected into the main combustion chamber. This method of ignition is also known as hypergolic starting slug [88].

The hypergolic igniters described in the examples cited above can only be used once, and therefore the rocket engines using them cannot be restarted. However, Hulka et al [89] have described a modified version of the Russian NK-33 rocket engine, called AJ26-59, which has the capability of being restarted. This engine burns liquid oxygen and kerosene, which of course are not hypergolic propellants, and also uses the TEA-TEB mixture for hypergolic ignition. Its capability of being restarted is obtained by carrying on board further cartridges of the TEA-TEB mixture than those necessary to the first start.

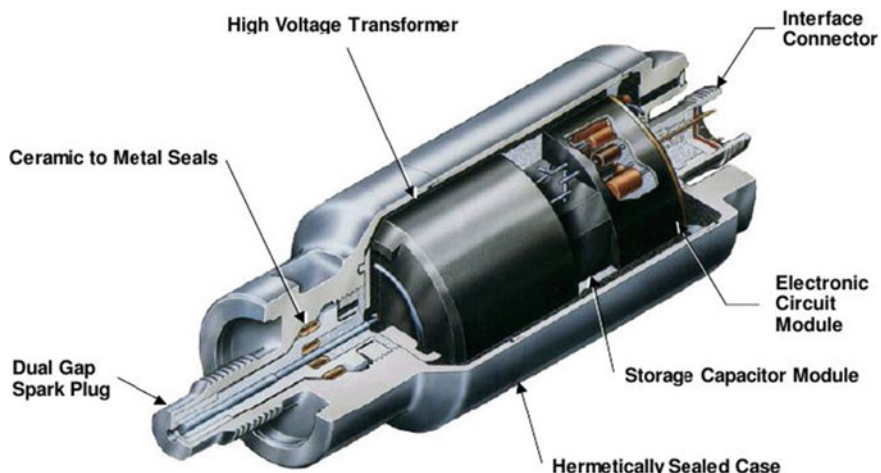
A rocket engine designed to burn exclusively hypergolic propellants does not require any special apparatus to be restarted as many times as necessary, because its propellants ignite spontaneously when coming in mutual contact. Such is the case, for example, with the AJ10-190 engine (whose fuel and oxidiser are respectively monomethyl hydrazine and nitrogen tetroxide) used in the orbital manoeuvring system of the Space Shuttle. An engine using other propellants than those of hypergolic type requires a re-usable igniter (a spark plug, for example) and a system of valves in order to be started and stopped when necessary.

Electric spark igniters based on spark plugs are often used in liquid-propellant rockets when multiple starts are necessary. They are efficient and reliable, and can be used in either direct spark igniters or augmented spark igniters.

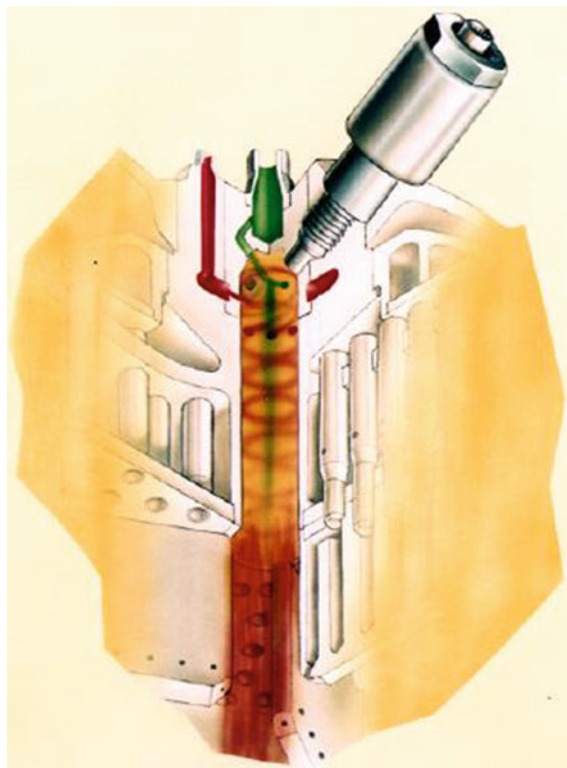
In case of a direct spark igniter, a high-voltage electric circuit is used to generate a spark across a gap, in order to expose the vaporised propellants in the combustion chamber to a ionising electric discharge, as shown in the following scheme, due to the courtesy of NASA [90].



Direct spark igniters are used in small combustion chambers, because the electric discharge is confined to a very small zone. One of the six spark plugs used in the main engine of the Space Shuttle is shown in the following figure, due to the courtesy of Boeing-Rocketdyne [50].

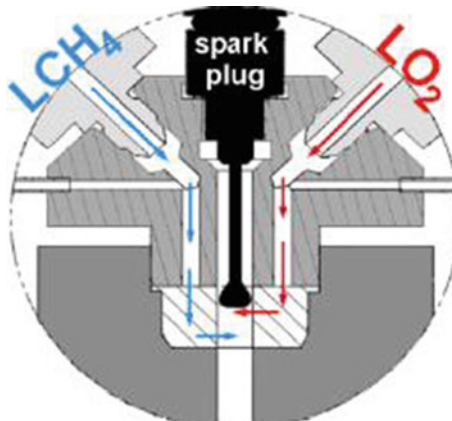


In the main engine of the Space Shuttle, an augmented spark igniter (also known as torch igniter), is used. In this type of igniter, a small quantity of propellants (in the present case, hydrogen and oxygen) is swirled into a very small zone, where a spark plug generates an electric discharge. This causes the ionisation of the gasified propellants, which become very hot and generate a flame front which propagates toward the combustion zone, just when the rest of the propellants reaches the injector. The following figure, due to the courtesy of Boeing-Rocketdyne [50], illustrates an augmented spark igniter used in the main engine of the Space Shuttle.



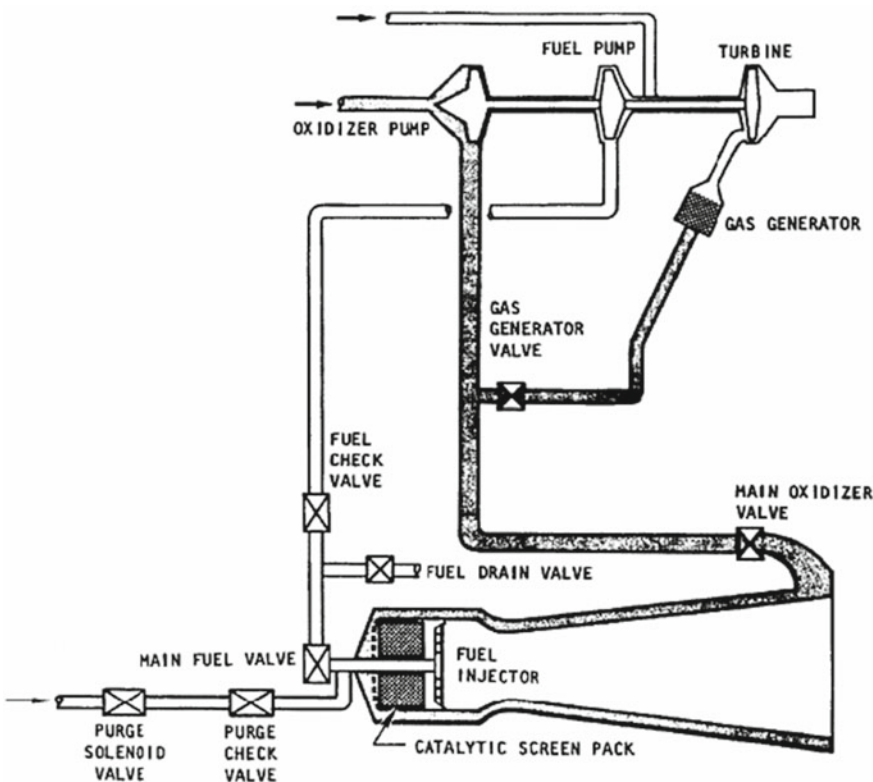
The J-2 rocket engine, which was used for the Saturn IB and Saturn V launch vehicles for the NASA Apollo programme, had an augmented spark igniter. Each of the main engines of the Space Shuttle had three augmented spark igniters, one for the main combustion chamber and two for the pre-burners. The chamber of each augmented spark igniter was located in the centre of the injector, as shown in the preceding figure. Two spark plugs were used, for redundancy, in each augmented spark igniter.

A further scheme of this type of igniter is shown in the following figure, due to the courtesy of NASA [91], which illustrates an augmented spark igniter used in a 445 N reaction control engine burning a mixture of liquid oxygen (LO_2) with liquid methane (LCH_4).



In case of rocket engines using liquid mono-propellants (for example, hydrogen peroxide), catalysts are used to initiate and sustain the reaction of decomposition of the mono-propellant. Liquid catalysts, if used for this purpose, require complex systems of valves and interlocking devices. This can be avoided by using solid catalysts. These catalysts have also been used in liquid bi-propellant rocket engines. One of such engines is the AR2-3, which was developed by Rocketdyne in the 1950s, and is briefly described below. The AR2-3 is one of the family of AR engines, where AR stands for aircraft rocket. The first engine of this family was the AR-1, which operated at a fixed thrust of 25577 N. It was proven in flight on the FJ-4 aircraft. The AR2 series of engines includes the AR-2, the AR2-1, the AR2-2, and the AR2-3. All the engines of the AR2 series have a main-stage thrust of 29358 N and are variable down to 14679 N of thrust. These engines use 90% hydrogen peroxide and kerosene. They have been used on the FJ-4, F-86, and NF104A aircraft. They are liquid-propellant pump-fed engines designed to provide aircraft thrust augmentation. The AR2-3 rocket engine supplies hydrogen peroxide and kerosene propellants to the thrust chamber by means of two centrifugal pumps (one for the oxidiser and one for the fuel). These pumps are directly driven by a single turbine. The pumps and the turbine are mounted on the same shaft. The oxidiser flows from the pump outlet through the pressure-actuated oxidiser valve, through the thrust chamber cooling jacket, and into the main thrust chamber, through the silver-plated catalytic screen pack, where it is decomposed into super-heated steam and oxygen. The fuel flows from the pump outlet through the chamber-pressure-actuated fuel valve, into the concentric annular-ring type fuel injector, and is injected into the hot, oxygen-rich gases, where it burns and is exhausted through the 12:1 area ratio nozzle. The auto-ignition of the fuel eliminates the necessity of an ignition system. A small oxidiser flow, of about 3% from the oxidiser pump discharge, is delivered and metered through the thrust control valve into a catalytic gas generator, where it is decomposed into super-heated steam and oxygen to drive the turbine.

A scheme of the engine flow described above is shown in the following figure, due to the courtesy of NASA [92].



Under emergency conditions, the engine may be operated as a mono-propellant engine using the oxidiser. The engine operates at a moderate chamber pressure and provides 29358 N of thrust in vacuo and 246 s specific impulse.

A timely ignition of the propellants is essential to the safe accomplishment of a mission. This holds in particular in case of manned missions. For this purpose, a safety device is required to control the supply of fuel or oxidiser or both to a liquid-propellant engine. A delayed ignition in the combustion chamber causes an accumulation of fuel within the chamber. This accumulation can cause an explosion and consequently the destruction of the engine or even of the whole vehicle on which the engine is mounted. These destructive effects can be avoided by interrupting or reducing the flow of either fuel, or oxidiser, or both to the combustion chamber when the combustion does not take place within a proper period of time. When a malfunction is detected, the control system switches the engine to a safe lock-up mode or shuts the engine down.

In order to assure a timely and even ignition of propellants and a smooth and quick increase in their flow to the rated value, the initial values of flow and mixture ratio are different from the corresponding operational values. A low initial value of flow prevents an excessive quantity of unburned fuel from accumulating in the combustion chamber. An initial value of mixture ratio close to the stoichiometric

value results in a high release of heat per unit mass of propellant. This fact, in turn, makes it possible to the hot gases in the combustion chamber to reach an equilibrium more rapidly than would be the case with other values of mixture ratio. By contrast, as has been shown in Chap. 1, Sect. 1.4, the mixture ratio in operating conditions is usually fuel-rich, in order to obtain a high value of specific impulse.

According to Sutton and Biblarz [2], the total time required to start a liquid-propellant rocket engine comprises ideally the following times:

- (1) time (from 0.002 s to more than 1 s) taken by the valves, which control the admittance of the propellants in the combustion chamber, to move from the closed position to the fully open position;
- (2) time taken by the propellants to go from the valves to the injector face;
- (3) time taken by the propellants to form and mix discrete streams of droplets into the combustion chamber;
- (4) time (from 0.02 to 0.05 s) taken by the droplets of propellant to vaporise and ignite;
- (5) time taken by the flame front to propagate downstream of the ignition section along the axis of the combustion chamber; and
- (6) time taken by the ignited propellant to raise the temperature and the pressure within the combustion chamber to values so high as to make the combustion self-sustaining.

There are overlaps in these intervals of time, because some of them may occur simultaneously. Apart from interval (4), the length of these intervals increases with the diameter of the combustion chamber.

The propellant valves are designed in such a way as to operate in a desired sequence, in order to admit one of the propellant before the other in the combustion chamber, and to also control the flow and the mixture ratio. Such valves are often partially opened at the ignition time, for the purpose of avoiding the accumulation of unburned propellants in the combustion chamber. After a signal indicating a successful ignition has been received by the controller, the valves are moved to the fully open position and the full flow of propellants arrives at the combustion chamber.

The signal of successful ignition can be generated by using several devices. Some of such devices are indicated below. They are:

- (a) Photocells for visual detection.
- (b) Optical detectors, such as cells, mounted inside the combustion chamber, which are sensitive to the visible or infrared radiation which is emitted by the combusted gases.
- (c) Pyrometers, which determine the temperature of the combusted gases by measuring the wavelength of the emitted radiation.
- (d) Fusible wire links, which are based on a fusible wire strung between two parallel conductors placed near the exit section of the thrust chamber, downstream of the throat. This wire is also a conductor, which is fused by the ignition flame, when the combustion reaction has been initiated correctly. The control system is substantially an electric motor, which is connected to a source of electric

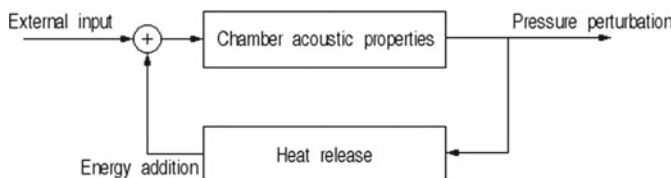
current (for example, to an accumulator). When the wire is melted, due to the heat generated by a correct ignition, then the motor circuit is interrupted and the propellant valves reach the fully open position. By contrast, when the wire is not melted, because the combustion reaction has not been initiated correctly, then the electric motor continues to operate, and moves the propellant valves to the closed position. Before the rocket engine is started, the propellant valves are in the closed position and the electric circuit carries no current. At the starting moment, the closure of a switch causes the electric motor to be fed by current, and therefore the propellant valves are moved toward the open position. A device like this was invented in 1952 by Prentiss [93].

- (e) Pressure-sensing devices, apt to detect the pressure rise in the combustion chamber due to a correct ignition of the propellants. Such devices, if capable of withstanding very high pressures, can also be used for multi-start engines.
- (f) Resistance wires, capable of measuring different values of electric resistance depending on whether a correct ignition has, or has not, taken place in the combustion chamber. Such devices, if capable of withstanding high temperatures without melting, can also be used for multi-start engines.
- (g) Electric devices used in spark plugs. Such devices detect the correct operation of spark plugs by sensing the ionisation near the electrodes.

2.9 Combustion Instability

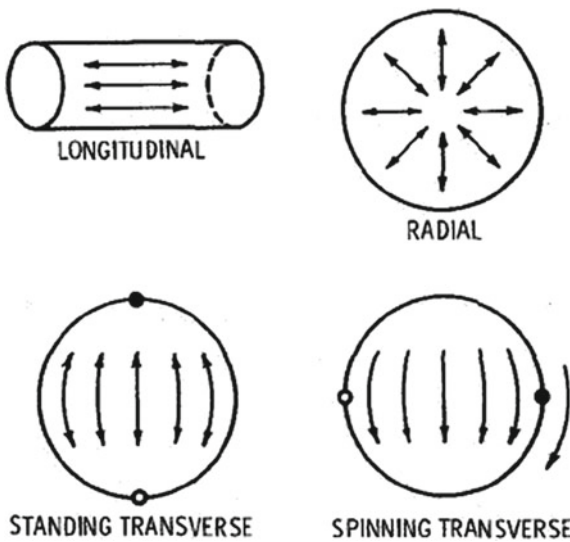
As has been shown in Chap. 1, Sect. 1.6, by combustion instability we mean the presence of self-sustaining pressure oscillations in the combustion chamber of a rocket engine. This phenomenon can appear in thermal devices when an unsteady release of heat is coupled with pressure oscillations. In a rocket engine, the heat released by the substances which react chemically is coupled with acoustic fluctuations. When the unsteady heat release and the acoustic fluctuations are in phase, then even a small perturbation will amplify according to the criterion enunciated by Lord Rayleigh. This criterion states that “If heat be given to the air at the moment of greatest condensation, or be taken from it at the moment of greatest rarefaction, the vibration is encouraged. On the other hand, if heat be given at the moment of greatest rarefaction, or abstracted at the moment of greatest condensation, the vibration is discouraged”. In addition, “When the transfer of heat takes place at the moment of greatest condensation or of greatest rarefaction, the pitch is not affected … the pitch is raised if heat be communicated to the air a quarter period before the phase of greatest condensation; and the pitch is lowered if heat be communicated a quarter period after the phase of greatest condensation” [94]. In other terms, the oscillations in a combustor are self-sustained when the rate of heat release and the pressure fluctuations are in phase. When this happens, pressure oscillations of large amplitude occur in a combustion chamber at frequencies of hundreds of hertz. Acoustic waves cause unsteadiness in a combustion process. An unsteady combustion process,

in turn, generates new acoustic waves. This fact can be represented graphically by means of the following feedback scheme.



An unsteady release of heat adds energy to the acoustic waves in the combustion chamber, when the unsteady heat release rate is in phase with the pressure oscillations at the location of the heat source, in accordance with the criterion of Lord Rayleigh. Consequently, the flame in the chamber may be extinguished or may come back to the injector face and burn part of the injection system. The amplitude of these oscillations can become so large as to damage the structure of the combustion chamber or destroy the engine.

These pressure waves can travel at sonic velocities up and down the length of the combustion chamber, around it, across it, or radially in and out. The following figure, due to the courtesy of NASA [95], shows the fundamental modes of acoustic combustion instability.



The F-1 engine, which was designed in the 1950s for the Saturn V rocket, was subject to combustion instability. This instability was observed for more than seven years during the development of the engine. Twenty of the forty-four tests of the first F-1 engine showed pressure oscillations due to combustion instability with peak amplitudes greater than or comparable to the average pressure in the combustor. The

pressure oscillations caused erosion and burning of the injector face, as a result of large radial and tangential motions of the gas.

In order to solve the instability problems, a programme called Project First was created to develop a stable F-1 engine. This programme lasted for four years: from 1962 to 1965. During this time, the engine was subject to more than 2000 full-scale tests [96]. Copper baffles were added to the injector plate to restrain the propagation of the pressure waves. The recovered injector plate of an F-1 engine (on display at the Museum of Flight in Seattle, Washington, U.S.A.) is shown in the following figure, due to the courtesy of Wikipedia [97].



Another example of passive control is the Pratt & Whitney FT8 gas turbine, which uses 13 Helmholtz resonators. These devices act as vibration absorbers, whose shape is chosen so that the absorption is tuned to a particular frequency, as the sequel will show.

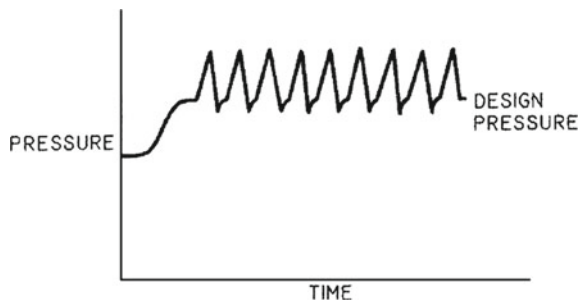
As has been shown above, the symmetry of the combustion chamber lends itself to certain natural acoustic modes which are driven into resonance because of their coupling with the rate of heat release. Several methods of breaking the symmetry of the chamber have been proven effective in quenching the combustion instabilities.

Combustion instabilities have been classified according to their respective frequency ranges, even though there are no sharp limiting lines to separate the so-called low, intermediate, and high frequency ranges.

The low-frequency (also called chugging) class includes pressure waves whose frequencies are less than 180 hertz [5]. In other terms, the low-frequency class includes waves whose lengths are much larger than the characteristic length (defined

in Sect. 2.4) of the combustion chamber. The instabilities belonging to this class begin with a sinusoidal wave, whose amplitude grows linearly with time. Such instabilities result from a coupling between the combustion process and the feed system [47]. They are usually eliminated by increasing the pressure drop in the injector, or by increasing the length-to-diameter ratio in the injector, or by decreasing the volume of the combustion chamber [49].

The high-frequency (also called screaming) class includes pressure waves whose frequencies are equal to or greater than 1000 hertz [5]. The following figure, due to the courtesy of NASA [98], shows pressure oscillation in a combustion chamber of a rocket engine in the presence of a high-frequency instability.

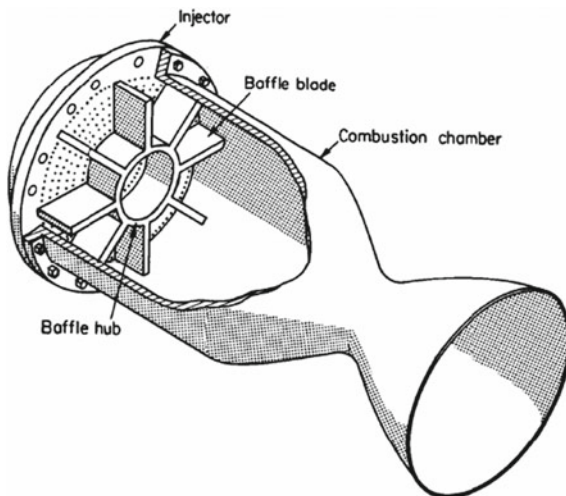


This is type of combustion instability which causes the most destructive effects. An oscillatory source of energy is required to sustain this particular instability. This energy comes from the combustion of the propellants, and is supplied according to the manner in which the combustion takes place. Each pressure wave interacts with the burning gases so strongly as to receive the sustaining energy directly from them, which means within a time interval no longer than the semi-period of the wave itself. Some of the means by which the combustion process supplies energy to the pressure waves are loss of ignition, delays due to chemical preparation or other causes, detonations, anomalous behaviour of droplets heated above their critical temperature and pressure, et c.

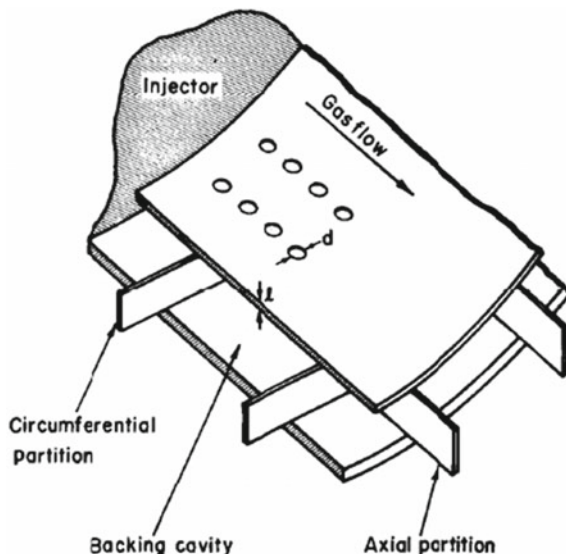
The two principal methods used to eliminate the combustion instability of the high-frequency class are the following: (1) changing the environment in which the combustion process takes place, by changing either the geometric properties of the combustion chamber or the manner (pattern of the injection holes, or size of the injector holes, or pressure drop) in which the propellants are injected into the combustion chamber; and (2) increasing the damping characteristics of the combustion chamber. Some means of passive control, which can be classified in the second of these methods, are baffles, acoustic liners, and resonators installed in the combustion chamber. They are briefly described below.

Baffles are mechanical devices meant to regulate or restrain the gas flow in the vicinity of the injector face, as shown in the following figure, due to the courtesy of NASA [49]. Baffles have been used successfully to prevent transverse acoustic modes of combustion instability. The transverse (that is, tangential and radial) modes

are characterised by oscillatory pressure waves and gas particle motion parallel to the injector face [74].

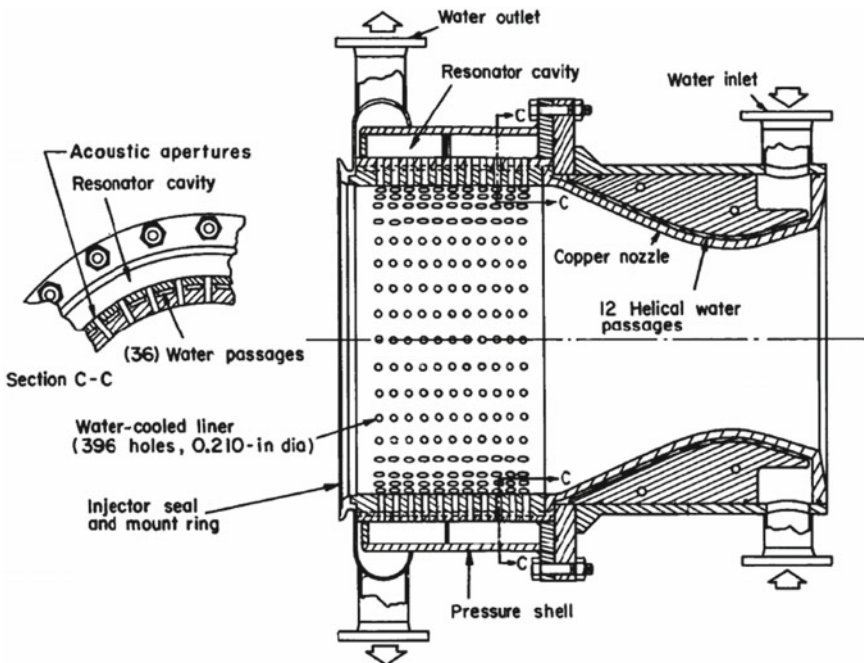


Another device for passive control is an acoustic liner installed within the combustion chamber. An acoustic liner consists of a number of cavities, each of which has a narrow opening or neck, as shown in the following figure, due to the courtesy of NASA [49].



In acoustic liners, energy is dissipated because of jet formation in the flow of gas through their orifices. The following figure, due to the courtesy of NASA [49],

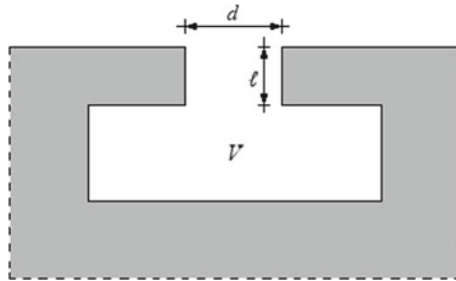
shows a water-cooled acoustic liner having an array of resonator cavities and used as a combustion stabiliser for a 66723 N thrust throttleable engine burning nitrogen tetroxide (oxidiser) and Aerozine 50 (fuel).



This combustion chamber consists of a composite cylindrical brazed shell with integral coolant passages. The liner apertures are drilled in spaces between the rectangular passages. The resonator cavities have a damping effect, because they allow a normal velocity at the wall which has a component in phase with the pressure oscillation. This means that work is done over each cycle in moving the fluid back and forth at the boundary. This work is equal to the energy dissipated due to jet formation and friction [49].

Two common types of acoustic resonators are Helmholtz resonators and quarter-wavelength tubes.

A Helmholtz resonator is a rigid-walled cavity of volume V (m^3), which is connected through a circular orifice of diameter d (m) and length ℓ (m) to the combustion chamber, where undesirable pressure oscillations are expected to occur. A Helmholtz resonator is shown in the following figure.



For the frequencies of interest, the wavelength λ of the pressure oscillations is assumed to be much greater than the dimensions of the resonator, that is,

$$\lambda \gg \ell$$

$$\lambda \gg d$$

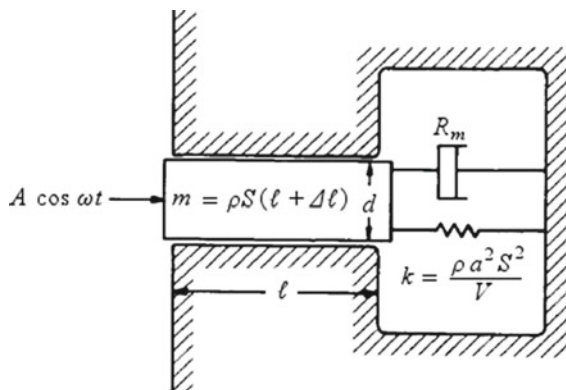
$$\lambda \gg V^{\frac{1}{3}}$$

By choosing properly the values of these dimensions, this device can be made resonant at any desired frequency. The resonance frequency f_0 (Hz) of a Helmholtz resonator is [99]:

$$f_0 = \frac{a}{2\pi} \left[\frac{S}{V(\ell + \Delta\ell)} \right]^{\frac{1}{2}} = \frac{a}{2\pi} \left[\frac{\pi d^2}{4V(\ell + \Delta\ell)} \right]^{\frac{1}{2}}$$

where $a = (\gamma RT)^{1/2}$ (m/s) is the speed of sound, $S = \pi d^2/4$ (m^2) is the area of the orifice, and $\Delta\ell = 0.85d$ (m) is the length correction, which takes account of the flow effects in the vicinity of the orifice ends.

As has been shown by several authors (see, for example, [100]), a Helmholtz resonator is analogous to a mechanical system comprising a body of mass m , a spring of elastic constant k , and a dashpot of mechanical resistance R_m , which is subject to a force $F(t) = A \cos \omega t$. This system is shown in the following figure, which is due to the courtesy of NASA (adapted from [49]).



In this mechanical system, the elastic constant k of the spring corresponds to $\rho a^2 S^2/V$, and the mass m of the body corresponds to $\rho S(\ell + \Delta\ell)$, where ρ is the density of the unperturbed gas. The differential equation governing the motion of the body of mass m in the direction x of the driving force $F(t) = A \cos \omega t$ is

$$m \frac{d^2x}{dt^2} + R_m \frac{dx}{dt} + kx = A \cos \omega t$$

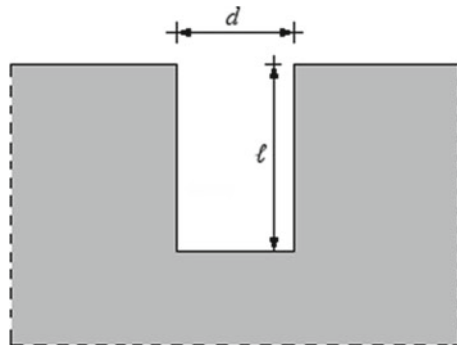
As is well known, the resonance frequency of this mechanical system is

$$f_0 = \frac{1}{2\pi} \left(\frac{k}{m} \right)^{\frac{1}{2}}$$

This equation accounts for the expression $f_0 = [a/(2\pi)] \{S/[V(\ell + \Delta\ell)]\}^{1/2}$ written above for the resonance frequency of a Helmholtz resonator.

A Helmholtz resonator can be tuned to a resonant frequency which corresponds to one of the natural frequencies of vibration of the combustion chamber. These natural frequencies can be determined as will be shown below.

Another type of acoustic resonator commonly used to damp pressure oscillations in a combustion chamber is a quarter-wavelength tube. It is similar to a Helmholtz resonator, but has no cavity, as shown in the following figure.



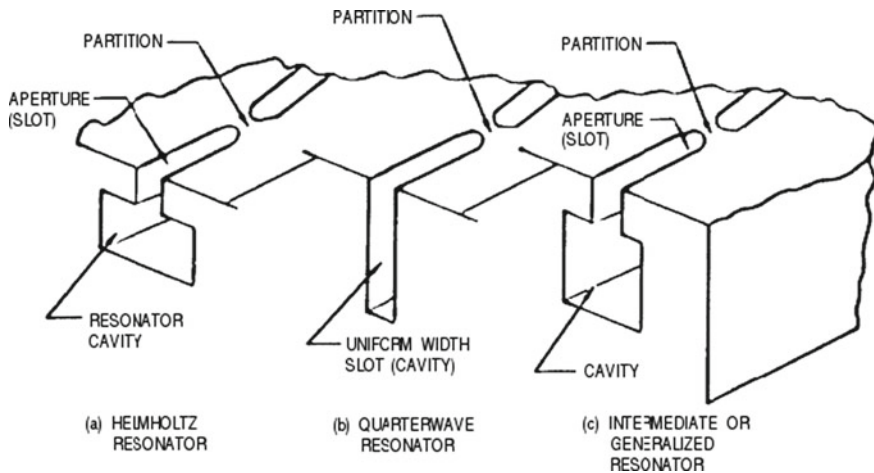
The resonance frequency f_0 (Hz) of a quarter-wavelength tube is [99]:

$$f_0 = \frac{a}{4(\ell + \Delta\ell)}$$

where $a = (\gamma RT)^{1/2}$ (m/s) is the speed of sound, ℓ (m) is the length of the quarter-wavelength tube, and $\Delta\ell = 0.85d$ (m) is the correction of the tube length ℓ .

In order to determine the natural modes of vibration for a given combustion chamber, Frendi et al [99] placed a loudspeaker at the centre of the inlet boundary of their combustion chamber. The loudspeaker emitted plane harmonic or random acoustic waves. A random acoustic disturbance was generated by the loudspeaker, and the sound pressure level (dB) was determined as a function of frequency at several points in the combustion chamber. By so doing, several peaks corresponding to the various vibration modes of the combustion chamber were determined. In order to determine the mode shapes, the individual modes were excited by introducing a plane, harmonic acoustic wave at the given frequency. After determining the natural frequencies (512 and 1880 Hz) of their combustion chamber, Frendi et al [99] selected the frequency of 1880 Hz, corresponding to one of the natural frequencies found by them, for extensive tests. Consequently, the resonant frequency f_0 of the acoustic devices indicated above was tuned to 1880 Hz.

Other types of acoustic resonators than those described above have slots instead of circular orifices, as shown in the following figure, due to the courtesy of NASA [74].

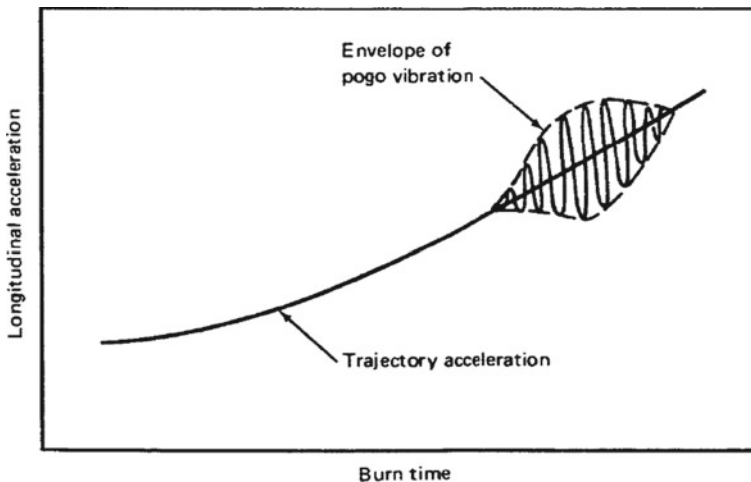


They are said to be of the Helmholtz, quarter-wavelength, or intermediate type, according to whether the width of their cavities is much larger, or equal, or slightly larger in comparison with the width of their slots.

The medium-frequency (also called buzzing) class includes pressure waves whose frequencies are in the range 180–1000 hertz [5]. The beginning of a medium-frequency instability usually shows a growing coherence of the combustion noise at a particular frequency with slowly increasing amplitude. There is usually wave motion in the propellant feed system. There may also be wave motion in the combustion chamber, but this motion does not usually correspond in phase and frequency to a natural mode of the chamber itself. The shape of the pressure wave is very nearly sinusoidal, and one or both of the propellant feed system may be highly coupled. Buzzing-type instabilities are not particularly damaging if they remain at low amplitudes, but may degrade performance, total impulse, or thrust vector. In some cases, the amplitude increases to such an extent as to triggering a high-frequency mode [49]. This type of instability occurs more frequently in medium-size engines (whose thrust is in the range 2000–250,000 N) than in large engines [2].

Finally, many rocket vehicles propelled by engines burning liquid propellants are subject to longitudinal vibrations, because of an instability arising from interaction of the vehicle structure with the propulsion system. This phenomenon has been nicknamed pogo instability, because of its analogy with the motion of a pogo jumping stick. Pogo instabilities can occur in the propellant feed lines of large vehicles, such as space launch vehicles or ballistic missiles [2].

The oscillations due to the pogo instability occur principally in the first longitudinal mode of the structure during operation of the first stage (burning liquid propellants) of a launch vehicle. The effects of this instability are shown in the following figure, due to the courtesy of NASA [101].

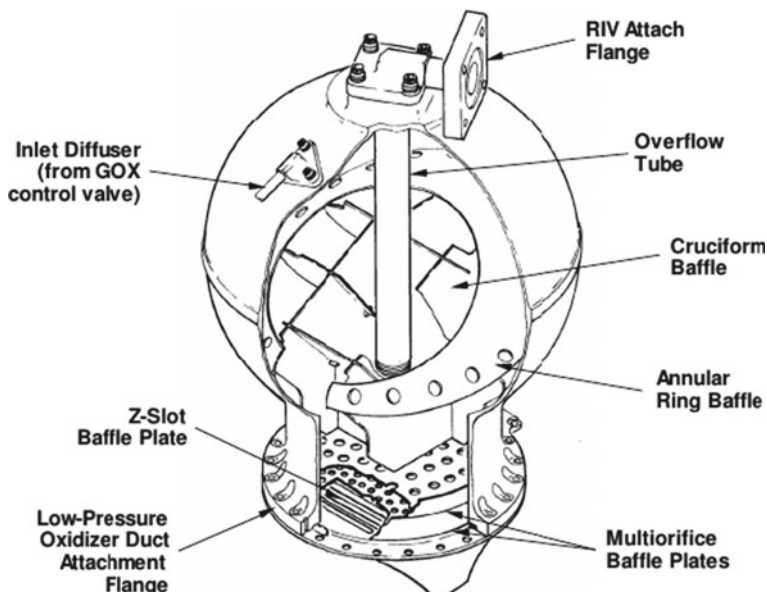


The pogo vibrations begin spontaneously, then intensify, and finally die away in a period of time ranging from 10 to 40 s. The frequency of vibration follows the frequency of the first structural mode, which increases with the consumption of propellants. Pogo vibrations have also occurred, but less often, in higher modes of longitudinal oscillation. More periods than one of instability have also been observed, each of which with its own mode of vibration, during operation of a single stage of a rocket vehicle. Vibrations have occurred in the range from 5 to 60 Hz, and vibration amplitudes (from zero to the peak values) have reached $17 g_0$ at the input to the payload and $34 g_0$ at the engine [101], where $g_0 = 9.80665 \text{ m/s}^2$ is the acceleration of gravity at the surface of the Earth.

The pogo vibrations can damage the crew and the equipment, and can also overload the structure of a rocket vehicle. In addition, they impair the propulsion performance of the vehicle.

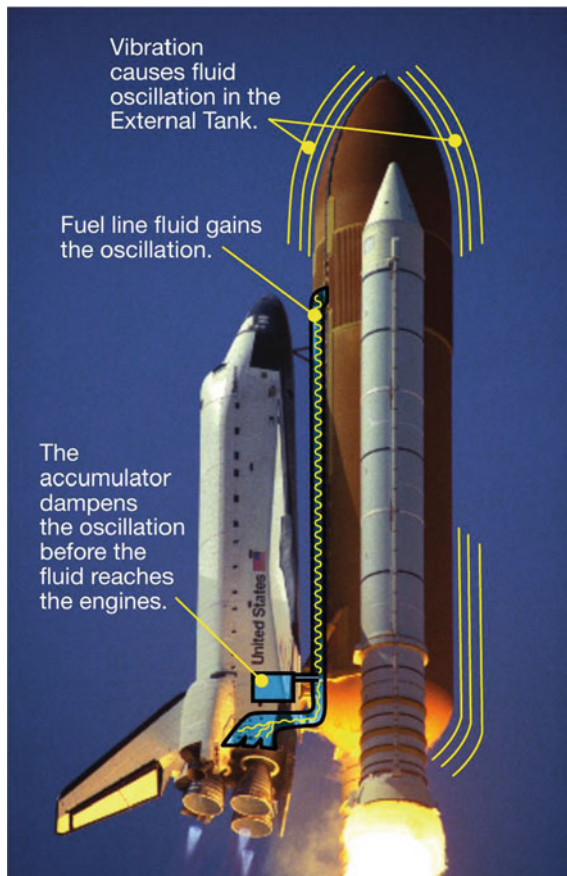
In order to suppress these vibrations, hydraulic accumulators have been installed in the propulsion systems of launch vehicles such as the Saturn V and the Space Shuttle.

As an example, each of the three main engines of the Space Shuttle has a pogo suppression system accumulator, which is attached to the low-pressure oxidiser duct. The accumulator, when pressurised with gaseous oxygen coming from the heat exchanger coil, dampens the pressure oscillations due to the oxidiser feed system. This accumulator is shown in the following figure, due to the courtesy of Boeing-Rocketdyne [50].



It is a hollow metallic sphere, 32 cm in diameter, which is mounted by a flange to the low-pressure oxidiser duct. During engine operation, the accumulator is pressurised with gaseous oxygen. The gaseous oxygen is a compliant medium in direct contact with the liquid oxygen, and is therefore capable of smoothing the oxidiser flow by absorbing the pressure oscillations. The pressure in the accumulator is maintained by a constant flow of gaseous oxygen into, through, and out of the accumulator. The gaseous oxygen comes from the heat exchanger coil, flows through the gaseous oxygen control valve into the accumulator, exits through the bottom of the inverted standpipe (overflow tube), and returns to the oxidiser feed system to be re-condensed in the liquid state [50].

The following figure, due to the courtesy of NASA [102], shows schematically how the accumulator described above is used to suppress the pogo vibrations in the Space Shuttle.



References

1. West J, Westra D, Richardson BR, Tucker PK (2014) Designing liquid rocket engine injectors for performance, stability, and cost. In: Conference paper. NASA Marshall Space Flight Centre, 16 Nov 2014, 13 p. <https://ntrs.nasa.gov/archive/nasa/casi.ntrs.nasa.gov/20150002585.pdf>
2. Sutton GP, Biblarz O (2001) Rocket propulsion elements. 7th edn, Wiley, New York. ISBN 0-471-32642-9
3. NASA (2015) Space Travel, NASA Tests Methane-Powered Engine Components for Next Generation Landers. Marshall Space Flight Centre, 28 Oct 2015. https://www.nasa.gov/sites/default/files/thumbnails/image/img_3190.jpg
4. Tomazic WA, Bartoo ER, Rollbuhler RJ (1960) Experiments with hydrogen and oxygen in regenerative engines at chamber pressures from 100 to 300 pounds per square inch absolute. NASA TM X-253, 1st Apr 1960, 37 p. <https://ntrs.nasa.gov/archive/nasa/casi.ntrs.nasa.gov/19660024054.pdf>

5. Huzel DK, Huang DH (1967) Design of liquid propellant rocket engines. NASA SP-125, NASA. 2nd edn Washington, D.C., 472 p. <https://ntrs.nasa.gov/archive/nasa/casi.ntrs.nasa.gov/19710019929.pdf>
6. Bilstein RE (1996) Stages to Saturn. NASA SP-4206. <https://ia802605.us.archive.org/19/items/stagesatosaturne00bilsrich/stagesatosaturne00bilsrich.pdf>
7. NASA, Math and science at work, space shuttle roll maneuver student edition. http://www.nasa.gov/pdf/519348main_AP_ST_Phys_RollManeuver.pdf
8. NASA. <https://spaceflightsystems.grc.nasa.gov/education/rocket/rktth1.html>
9. NASA. <http://exploration.grc.nasa.gov/education/rocket/rktctrl.html>
10. NASA. <http://www.hq.nasa.gov/office/pao/History/congand/orient.htm>
11. Edwards SS, Parker GH (1958) An investigation of the jet elevator as a means of thrust vector control. LMSD-2630, Lockheed, Sunnyvale, California, USA, Feb 1958, 44 p. <http://www.dtic.mil/cgi-bin/GetTRDoc?Location=U2&docName=a950112.pdf>
12. Spinardi G (1994) From Polaris to trident: the development of US fleet ballistic missile technology. Cambridge University Press. ISBN 0-521-41357-5
13. NASA dryden fact sheet—highly manoeuvrable aircraft technology. http://www.nasa.gov/sites/default/files/images/110536main_HiMAT_3-view.jpg
14. Benson T (ed) Practical rocketry, NASA, Glenn research centre. http://exploration.grc.nasa.gov/education/rocket/TRCRocket/practical_rocketry.html
15. McGlinchey LF (1974) Viking orbiter 1975 thrust vector control system accuracy. NASA-CR-140705, JPL Technical Memorandum 33–703, 15 Oct 1974. <https://ntrs.nasa.gov/archive/nasa/casi.ntrs.nasa.gov/19750002097.pdf>
16. NASA Space Science Data Coordinated Archive, Viking 1 Orbiter. <https://nssdc.gsfc.nasa.gov/nmc/spacecraftDisplay.do?id=1975-075A>
17. NASA (1968) Saturn V news reference, J-2 engine fact sheet, Dec 1968. https://www.nasa.gov/centers/marshall/pdf/499245main_J2_Engine_fs.pdf
18. NASA. Beginner's guide to rockets, guidance system. <https://spaceflightsystems.grc.nasa.gov/education/rocket/guidance.html>
19. Noll RB, Zvara J, Deyst JJ (1971) Spacecraft attitude control during thrusting manoeuvres, NASA SP-8059, Feb 1971, 51 p. <https://ntrs.nasa.gov/archive/nasa/casi.ntrs.nasa.gov/19710016722.pdf>
20. Shammas MS, Balakrishnan SR, Balaji S (2013) Effects of secondary injection in rocket nozzle at various conditions. Int J Eng Res Technol (IJERT) 2(6):373–379
21. Anonymous (1946) Augmented flow—an interesting method of fluid-flow augmentation with attractive possibilities. Flight, 15 Aug 1946, pp 174–175
22. Blake BA (2009) Numerical investigation of fluidic injection as a means of thrust modulation. Final thesis report, 2009, School of Engineering and Information Technology, University of New South Wales at the Australian Defence Force Academy, Canberra, Australia, 29 p. Article available at the <http://seit.unsw.adfa.edu.au/ojs/index.php/juer/article/viewFile/256/155>
23. Strykowski PJ, Krothapalli A, Forliti DJ (1996) Counterflow thrust vectoring of supersonic jets. AIAA J 34(11):2306–2314
24. Hunter CA, Deere KA (1999) Computational investigation of fluidic counterflow thrust vectoring, AIAA 99-2669. In: 35th AIAA/ASME/SAE/ASEE joint propulsion conference & exhibit, Los Angeles, CA, 20–23 June 1999, 13 p
25. Deere KA, Berrier BL, Flamm JD, Johnson SK (2003) Computational study of fluidic thrust vectoring using separation control in a nozzle, AIAA-2003-3803. In: 21st AIAA applied aerodynamics conference, 23–26 June 2003, Orlando, Florida, USA, 11 p
26. Wing DJ, Giuliano VJ (1997) Fluidic thrust vectoring of an axisymmetric exhaust nozzle at static conditions, FEDSM97-3228. In: 1997 ASME fluids engineering division summer meeting, 22–26 June 1997, 6 p
27. Heppenheimer TA (1999) The space shuttle decision: NASA search for a reusable space vehicle. NASA SP-4221. 1999, 554 p. <https://ntrs.nasa.gov/archive/nasa/casi.ntrs.nasa.gov/19990056590.pdf>

28. Hyde JC, Gill GS (1976) Liquid rocket engine nozzles, NASA SP-8120. NASA, Washington, D.C., July 1976, 123 p. <https://ntrs.nasa.gov/archive/nasa/casi.ntrs.nasa.gov/19770009165.pdf>
29. Crown JC (1948) Supersonic nozzle design. NACA Technical Note No. 1651, NACA, Washington, D.C., June 1948, 35 p <https://ntrs.nasa.gov/archive/nasa/casi.ntrs.nasa.gov/19930082268.pdf>
30. Rao GVR (1958) Exhaust nozzle contour for optimum thrust. *J Jet Propul* 28(6):377–382
31. Kuo KK, Acharya R (2012) Applications of turbulent and multiphase combustion. Wiley, Hoboken, New Jersey. ISBN 978-1-118-12756-8
32. Ahlberg JH, Hamilton S, Migdal D, Nilson EN (1961) Truncated perfect nozzles in optimum nozzle design. *ARS J* 31(5):614–620
33. Rao GVR (1960) Approximation of optimum thrust nozzle contour. *ARS J* 30(6):581
34. Braeunig RA, Rocket and space technology—rocket propulsion. http://braeunig.us/space/pro_puls.htm
35. Newlands R (2017) The thrust optimised parabolic nozzle. Aspirespace, 18 Apr 2017. <http://www.aspirespace.org.uk/downloads/Thrust%20optimised%20parabolic%20nozzle.pdf>
36. Aukerman CA (1991) Plug nozzles—the ultimate customer driven propulsion system. NASA-CR-187169, Aug 1991, 27 p. <https://ntrs.nasa.gov/archive/nasa/casi.ntrs.nasa.gov/19920013861.pdf>
37. Corda S, Neal BA, Moes TR, Cox TH, Monaghan RC, Voelker LS, Corpenering GP, Larson RR, Powers BG (1998) Flight testing the linear aerospike SR-71 experiment (LASRE), NASA/TM-1998-206567. NASA Dryden Space Research Centre, Sept 1998, 26 p. https://www.nasa.gov/centers/dryden/pdf/88598main_H-2280.pdf
38. NASA. Linear aerospike SR-71 experiment (LASRE) Project. <https://www.nasa.gov/centers/armstrong/news/FactSheets/FS-043-DFRC.html>
39. NASA. <https://www.hq.nasa.gov/pao/History/x-33/xrs2200.htm>
40. Anonymous (1981) Liquid rocket propulsion technology: an evaluation of NASA's program, NASA-CR-164550, Jan 1981, 67 p. <https://ntrs.nasa.gov/archive/nasa/casi.ntrs.nasa.gov/19810018653.pdf>
41. Shyne RJ, Keith Th G Jr (1990) Analysis and design of optimised truncated scarfed nozzles subject to external flow field effects. NASA Technical Memorandum 105175, Jan 1990, 12 p. <https://ntrs.nasa.gov/archive/nasa/casi.ntrs.nasa.gov/19900015790.pdf>
42. O'Leary RA, Beck JE (1992) Nozzle design, Threshold, Pratt & Whitney Rocketdyne's engineering journal of power technology. Spring 1992. <http://www.rocket-propulsion.info/resources/articles/NozzleDesign.pdf>
43. Wieseneck HC (1970) Regenerative cooling of the space shuttle engine. NASA, July 1970, 32 p. <https://ntrs.nasa.gov/archive/nasa/casi.ntrs.nasa.gov/19700030313.pdf>
44. Turner MJL (2006) Rocket and spacecraft propulsion, 2nd edn. Springer, Berlin. ISBN 3-540-22190-5
45. Van Huff NE, Fairchild DA (1972) Liquid rocket engine fluid-cooled combustion chambers. NASA SP-8087, Apr 1972, 120 p. <https://ntrs.nasa.gov/archive/nasa/casi.ntrs.nasa.gov/19730022965.pdf>
46. Bartz DR (1963) Turbulent boundary-layer heat transfer from rapidly accelerating flow of rocket combustion gases and of heated air, NASA CR-62615. Jet Propulsion Laboratory, California Institute of Technology, Pasadena, California. USA, Dec 1963, 128 p. <https://ntrs.nasa.gov/archive/nasa/casi.ntrs.nasa.gov/19650013685.pdf>
47. Hill PhG, Peterson CR (1965) Mechanics and thermodynamics of propulsion, addison-wesley, reading, USA, Massachusetts
48. Wang Q, Wu F, Zeng M, Luo L, Sun, J (2006) Numerical simulation and optimization on heat transfer and fluid flow in cooling channel of liquid rocket engine thrust chamber. *Eng Comput* 23(8):907–921
49. Harrje DT, Reardon FH (ed) (1972) Liquid propellant rocket combustion instability. NASA SP-194, Jan 1972, 657 p. <https://ntrs.nasa.gov/archive/nasa/casi.ntrs.nasa.gov/19720026079.pdf>

50. Anonymous (1998) Space Shuttle main engine orientation. Boeing-Rocketdyne Propulsion & Power, Presentation BC98-04, June 1998, 105 p. http://large.stanford.edu/courses/2011/ph240/nguyen1/docs/SSME_PRESENTATION.pdf
51. Anonymous (1993) Heat transfer in rocket engine combustion chambers and regeneratively cooled nozzles. NASA-CR-193949, 16 Nov 1993, 169 p. <https://ntrs.nasa.gov/archive/nasa/casi.ntrs.nasa.gov/19940019998.pdf>
52. Taler D, Taler J (2017) Simple heat transfer correlations for turbulent tube flow. In: E3S Web of conferences 13, 02008 (2017), 7 pages. https://www.e3s-conferences.org/articles/e3sconf/pdf/2017/01/e3sconf_wtue2017_02008.pdf
53. Gnielinski V (1975) Neue Gleichungen für den Wärme- und den Stoffübergang in turbulent durchströmten Rohren und Kanälen. *Forsch Ingenieurwes* 41:8–16
54. Giovanetti AJ, Spadaccini LJ, Szetela EJ (1983) Deposit formation and heat transfer in hydrocarbon rocket fuels. NASA-CR-168277, 1983, 168 p. <https://ntrs.nasa.gov/archive/nasa/casi.ntrs.nasa.gov/19840004157.pdf>
55. Haidn OJ (2008) Advanced rocket engines. In: Advances on propulsion technology for high-speed aircraft, NATO RTO-EN-AVT-150, 2008, Neuilly-sur-Seine (France), 40 p. Available at the <http://www.macro-inc.com/NASADocs/AdvanceRocketEnginesEN-AVT-150-06.pdf>
56. Locke JM, Landrum DB (2008) Study of heat transfer correlations for supercritical hydrogen in regenerative cooling channels. *J Propul Power* 24(1):94–103
57. Sloop JL (1978) Liquid hydrogen as a propulsion fuel. 1945-1959, NASA SP-4404, Jan 1978, 341 p. Available at the <https://ntrs.nasa.gov/archive/nasa/casi.ntrs.nasa.gov/19790008823.pdf>
58. Colebrook CF (1939) Turbulent flow in pipes, with particular reference to the transition region between smooth and rough pipe laws. *J Inst Civil Eng* 11(4):133–156
59. Nuclear Power, Darcy Friction Factor, Relative Roughness of Pipe. <http://www.nuclear-power.net/nuclear-engineering/fluid-dynamics/major-head-loss-friction-loss/relative-roughness-of-pipe/>
60. AJ Design Software, Colebrook Equations Formulas Calculator. https://www.ajdesigner.com/php_colebrook/colebrook_equation.php
61. Special Metals Corporation, Inconel® alloy 718, Pub. No. SMC-045. http://www.specialmetals.com/assets/smcc/documents/inconel_alloy_718.pdf
62. National Institute of Standards and Technology (NIST), NIST Chemistry WebBook, SRD 69, Hydrogen. <http://webbook.nist.gov/cgi/cbook.cgi?ID=C1333740&Mask=4>, see also Thermophysical Properties of Fluid Systems. <https://webbook.nist.gov/chemistry/fluid/>
63. Stenholm T, Pekkari LO, Andersson T (1988) The development of the Vulcain nozzle extension. In: 34th AIAA/ASME/SAE/ASEE joint propulsion conference & exhibit, 13–15 July 1988, Cleveland, Ohio, USA
64. Rydén R, Johansson L, Palmnäs U (2004) The Volvo Aero laser welded sandwich nozzle for booster engines. In: 55th International Astronautical Congress 2004—Vancouver, Canada, Paper number IAC-04-S.3.07. <https://iafastro.directory/iac/archive/browse/IAC-04/S/3/1259/>
65. Lucas JG, Golladay RL (1963) An experimental investigation of gaseous-film cooling of a rocket motor. NASA TN D-1988, Oct 1963, 24 p. <https://ntrs.nasa.gov/archive/nasa/casi.ntrs.nasa.gov/19630012015.pdf>
66. Zucrow MJ, Sellers JP (1961) Experimental investigation of rocket motor film cooling. *ARS J* 668
67. Hatch JE, Papell SS (1959) Use of a theoretical flow model to correlate data for film cooling or heating an adiabatic wall by tangential injection of gases of different fluid properties. NASA TN D-130, Nov 1959, 44 p. <https://ntrs.nasa.gov/archive/nasa/casi.ntrs.nasa.gov/19890068390.pdf>
68. Hannum N, Roberts WE, Russell LM (1977) Hydrogen film cooling of a small hydrogen-oxygen thrust chamber and its effect on erosion rates of various ablative materials. NASA-TP-1098, Dec 1977, 29 p. <https://ntrs.nasa.gov/archive/nasa/casi.ntrs.nasa.gov/19780005181.pdf>
69. Eckert ERG, Livingood JNB (1954) Comparison and effectiveness of convection-, transpiration-, and film-cooling methods with air as a coolant. NACA-TR-1182, Jan 1954, 17 p. <https://ntrs.nasa.gov/archive/nasa/casi.ntrs.nasa.gov/19930092205.pdf>

70. Rannie W (1947) A simplified theory for porous wall cooling. Progress Report No. 4-50, Jet Propulsion Laboratory, Pasadena, California, USA., 25 Nov 1947, 24 p. <https://trs.jpl.nasa.gov/bitstream/handle/2014/45706/17-0944.pdf?sequence=1&isAllowed=y>
71. Ewen RL, Evensen HM (1977) Liquid rocket engine self-cooled combustion chambers. NASA SP-8124, Sept 1977, 130 p. <https://ntrs.nasa.gov/archive/nasa/casi.ntrs.nasa.gov/19780013268.pdf>
72. Reed BD, Biaglow JA, Schneider SJ (1997) Iridium-coated rhenium radiation-cooled rockets, NASA TM-107453, July 1997, 14 p. <https://ntrs.nasa.gov/archive/nasa/casi.ntrs.nasa.gov/19970036365.pdf>
73. National Institute of Standards and Technology (NIST). <https://physics.nist.gov/cgi-bin/cuu/Value?sigma>
74. Combs LP et al (1974) Liquid rocket engine combustion stabilisation devices. NASA SP-8113, Nov 1974, 127 p. <https://ntrs.nasa.gov/archive/nasa/casi.ntrs.nasa.gov/19750020175.pdf>
75. Gill GS, Nurick WH, Keller RB Jr (ed) Liquid rocket engine injectors. NASA SP-8089, Mar 1976, 130 p. <https://ntrs.nasa.gov/archive/nasa/casi.ntrs.nasa.gov/19760023196.pdf>
76. Casiano MJ, Hulka JR, Yang V (2010) Liquid-propellant rocket engine throttling: a comprehensive review. J Propu Power 26(5):897–923. [http://www.yang.gatech.edu/publications/Journal/JPP%20\(2010,%20Casiano\).pdf](http://www.yang.gatech.edu/publications/Journal/JPP%20(2010,%20Casiano).pdf)
77. Hammock WR Jr, Currie EC, Fisher AE (1973) Apollo experience report—descent propulsion system. NASA TN D-7143, Mar 1973, 36 p. <https://ntrs.nasa.gov/archive/nasa/casi.ntrs.nasa.gov/19730011150.pdf>
78. Wikipedia, SpaceX rocket engines. https://en.wikipedia.org/wiki/SpaceX_rocket_engines
79. Stangeland ML (1988) Turbopumps for liquid rocket engines, Threshold, Pratt & Whitney Rocketdyne's engineering journal of power technology, Summer 1988. <http://www.pwrengineering.com/articles/turbopump.htm>
80. Macaluso SB, Keller RB Jr (ed) (1974) Liquid rocket engine turbines. NASA SP-8110, Jan 1974, 160 p. <https://ntrs.nasa.gov/archive/nasa/casi.ntrs.nasa.gov/19740026132.pdf>
81. Greene WD, Inside the J-2X doghouse: the gas-generator cycle engine. NASA. <https://blogs.nasa.gov/J2X/tag/gas-generator/>
82. Sabin AJ, Bissell WR, Keller RB Jr (ed) (1974) Turbopump systems for liquid rocket engines. NASA SP-8107, Aug 1974, 168 p. <https://ntrs.nasa.gov/archive/nasa/casi.ntrs.nasa.gov/19750012398.pdf>
83. Zehetner HW, Keller RB Jr. (ed) Liquid propellant gas generators. NASA SP-8081, Mar 1972, 110 p. <https://ntrs.nasa.gov/archive/nasa/casi.ntrs.nasa.gov/19730018978.pdf>
84. Kosanke KL, Kosanke BJ, Pyrotechnic ignition and propagation: a review. In: Kosanke KL, Kosanke BJ (eds) Selected pyrotechnic publications of, pp 420–431. <http://www.jpyro.com/wp-content/uploads/2012/08/Kos-420-431.pdf>
85. Barrett DH, Keller RB Jr (ed) (1971) Solid rocket motor igniters. NASA SP-8051, Mar 1971, 112 p. <https://ntrs.nasa.gov/archive/nasa/casi.ntrs.nasa.gov/19710020870.pdf>
86. Kosanke KL, Kosanke BJ (2012) Electric matches and squibs. In: KL Kosanke, BJ Kosanke (eds) Selected pyrotechnic publications of, pp. 257–259. <http://www.jpyro.com/wp-content/uploads/2012/08/Kos-257-259.pdf>
87. United Launch Alliance. <http://www.ulalaunch.com/uploads/docs/AtlasVUsersGuide2010.pdf>, Public Domain. <https://commons.wikimedia.org/w/index.php?curid=48196878>
88. Clark JD (1972) Ignition!: an informal history of liquid rocket propellants. Rutgers University Press, New Brunswick, New Jersey. ISBN 0-8135-0725-1
89. Hulka J, Forde JS, Werling RE, Anisimov VS, Kozlow VA, Kositsin IP (1998) Modification and verification testing of a Russian NK-33 rocket engine for reusable and restartable applications. AIAA 98-3361, 1998, 26 p. <http://lpre.de/resources/articles/AIAA-1998-3361.pdf>
90. Greene WD (2014) Inside the LEO doghouse: light my fire!. NASA, 24 Feb 2014. <https://blogs.nasa.gov/J2X/tag/ignition/>

91. Kleinhenz J, Sarmiento Ch, Marshall W (2012) Experimental investigation of augmented spark ignition of a LO₂/LCH₄ reaction control engine at altitude conditions. NASA/TM-2012-217611, June 2012, 43 p. <https://ntrs.nasa.gov/archive/nasa/casi.ntrs.nasa.gov/20120011145.pdf>
92. Anderson WE, Butler K, Crocket D, Lewis T, McNeal C (2000) Peroxide propulsion at the turn of the century, 13 Mar 2000, 59 p. <https://ntrs.nasa.gov/archive/nasa/casi.ntrs.nasa.gov/20000033615.pdf>
93. Prentiss SS (1956) Safety device, including fusible member for rocket engine starting control, U.S. patent No. 2,741,085 granted on the 10th of Apr 1956. <https://patents.google.com/patent/US2741085>
94. Rayleigh L (1878) The theory of sound, vol 2. Macmillan & Co., London. <http://gallica.bnf.fr/ark:/12148/bpt6k95131k.image>
95. Burrows MC, Exploring in aerospace rocketry, 4—Thermodynamics, NASA TM X-52391, Jan 1968, 21 p. <https://ntrs.nasa.gov/archive/nasa/casi.ntrs.nasa.gov/19680010371.pdf>
96. Ellison LR, Moser MD, Combustion instability analysis and the effect of drop size on acoustic driving rocket flow, 13 May 2004, 6 p. <https://ntrs.nasa.gov/archive/nasa/casi.ntrs.nasa.gov/20040075603.pdf>
97. Wikipedia, by Loungeflyz (CC BY-SA 4.0. <https://creativecommons.org/licenses/by-sa/4.0>) from Wikimedia Commons
98. Jonash ER, Tomazic WA (1962) Current research and development on thrust chambers. In: Proceedings of the NASA-university conference on the science and technology of space exploration, vol 2. NASA SP-11, Chicago, Illinois, 1–3 Nov 1962, pp. 43–52. <http://www.dtic.mil/cgi-bin/GetTRDoc?Location=U2&docName=a396443.pdf>
99. Frendi A, Nesman T, Canabal F (2005) Control of combustion instabilities through various passive devices, NASA, 25 p. <https://ntrs.nasa.gov/archive/nasa/casi.ntrs.nasa.gov/20050182054.pdf>
100. Kinsler LE, Frey AR, Coppens AB, Sanders JV (2000) Fundamentals of acoustics. 4th edn, Wiley, New York. ISBN 0-471-84789-5
101. Rubin S, Prevention of coupled structure-propulsion instability (pogo). NASA SP-8055, Oct 1970, 52 p. <https://ntrs.nasa.gov/archive/nasa/casi.ntrs.nasa.gov/19710016604.pdf>
102. Modlin T, Space Shuttle pogo—NASA eliminates “bad vibrations”. Eng Innov Struct Des 270–285 https://www.nasa.gov/centers/johnson/pdf/584733main_Wings-ch4g-pgs270-285.pdf

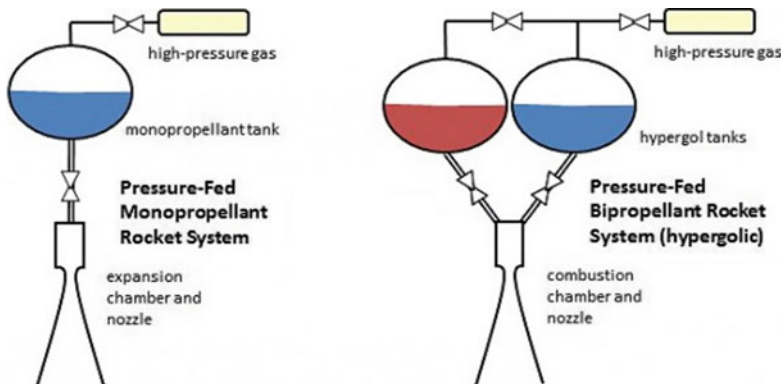
Chapter 3

Feed Systems Using Gases Under Pressure



3.1 Fundamental Concepts

As has been shown in Chap. 1, Sect. 1.4, a feed system is necessary to transfer either a mono-propellant or an oxidiser and a fuel from their respective tanks to the thrust chamber of a rocket engine. This chapter describes feed systems using gases stored at high pressures for this purpose. A scheme of such systems is shown in the following figure, due to the courtesy of NASA [1].



A gas stored under pressure makes it possible to control the pressure in the ullage space in the tanks of propellant. By ullage space we mean the volume by which a container or a tank falls short of being full of liquid.

In a rocket engine fed by a gas stored under pressure, the pressure in the ullage space is used to force the propellants through the lines of the feed system and into the combustion chamber at the required pressures and flow rates.

In a rocket engine fed by pumps, the pressure in the ullage space is used to supply the propellants to the inlet section of the pumps at the required pressures, and the pumps in turn deliver the propellants to the combustion chamber at the required pressures and flow rates.

As a general rule, the choice of a feed system, independently of whether it uses gases under pressure or pumps, depends on several factors, which are principally the mission which the rocket vehicle is meant to accomplish, the size and the mass of this vehicle, the intensity and the duration of the thrust, the space available to the engine, the degree of reliability of the propulsion system, and so on. In practice, according to Lee et al. [2], a pump-fed propulsion system is chosen when:

- the engine must produce more than 4500 N of thrust, or
- the total mass exceeds 9100 kg.

In contrast, a pressure-fed propulsion system, which may be either a mono-propellant or a bi-propellant system, is chosen when:

- the mission duty cycle is a pulse mode, or
- the propellant mass is less than 3600 kg.

For those cases in which the choice of the feed system is not obvious, a weight-and-cost trade-off study is made to determine the better system.

The types of gas used in the feed systems described here are the following:

- gases stored for bi-propellants;
- gases obtained by evaporation of two propellants;
- gases stored for mono-propellants; and
- gases obtained as combustion products.

Some criteria for choosing one or another of these types are briefly presented below. A gas under pressure must be chemically compatible with the propellants and also with the materials of which the tanks and the lines are made, at the temperatures of operation. The feed system using this gas must be simple and reliable. The gas used in the feed system must have a low molar mass, in order for the value of the mass ratio m_0/m_u (where m_0 is the mass of the rocket vehicle at launch, and m_u is its mass at burnout) to be low. The materials used for the feed system must have a low specific mass, for the same reason. These requirements will be discussed in the following paragraphs.

3.2 Requirements for Gases Stored Under Pressure

When the time of operation of a rocket engine is short, or when the temperature of the gas stored under pressure is less than or equal to the temperature of the propellants, then the required mass m_g (kg) of that gas can be computed by means of the law of perfect gases, as follows

$$m_g = \frac{p_T V_T}{R_g T_g}$$

where p_T (N/m²) is the pressure of the gas in the tank, V_T (m³) is the total volume of the empty tank, R_g (N m kg⁻¹ K⁻¹) is the constant of the specific gas used, and T_g (K) is the mean temperature of that gas. As has been shown in Chap. 1, Sect. 1.1, the constant R_g of a specific gas is equal to the universal gas constant $R^* = 8314.460$ N m kmol⁻¹ K⁻¹ divided by the molar mass \mathcal{M} (kg/kmol) of that gas, as follows

$$R_g = \frac{R^*}{\mathcal{M}}$$

When the conditions indicated above are not satisfied, the required mass m_g of the gas under pressure can be computed as follows.

We consider first a rocket engine which is started only once, and assume the heat transfer from the tank walls to be negligible. In such conditions, the total heat Q (J) transferred from the gas under pressure to the vaporised propellant is [3]:

$$Q = H A t (T_u - T_e)$$

where H (W m⁻² K⁻¹) is the total heat transfer coefficient, whose value is determined experimentally, at the interface between liquid and gas, A (m²) is the area of the interface between liquid and gas, t (s) the duration of operation, T_u (K) is the temperature of the gases at burnout, and T_e (K) is the temperature of the propellant. The temperatures T_e and T_u are assumed to have constant values at the interface between liquid and gas.

The total heat Q defined above is assumed to have heated and vaporised the propellant, as indicated by the following equation

$$Q = m_v [c_{pl}(T_v - T_e) + h_v + c_{pv}(T_u - T_v)]$$

where m_v (kg) is the total mass of vaporised propellant, c_{pl} and c_{pv} (J kg⁻¹ K⁻¹) are the specific heats at constant pressure of respectively the liquid propellant and the vaporised propellant, h_v (J/kg) is the heat of vaporisation per unit mass of the propellant, and T_v (K) is the temperature of vaporisation of the liquid propellant.

The equations $Q = H A t (T_u - T_e)$ and $Q = m_v [c_{pl}(T_v - T_e) + h_v + c_{pv}(T_u - T_v)]$ make it possible to compute the value of m_v for an assumed value of T_u .

The partial volume V_v (m³) occupied by vaporised propellant is [3]:

$$V_v = \frac{m_v Z R_p T_u}{p_T}$$

where m_v (kg) is the total mass of vaporised propellant, Z is the compressibility factor evaluated at the total pressure p_T (N/m²) and at the temperature T_u (K) of the

gaseous mixture at burnout, and R_p ($\text{N m kg}^{-1} \text{ K}^{-1}$) is the constant of the specific propellant vapour.

The remaining volume V_g (m^3) of the tank at burnout, in the absence of residual propellants, can be assumed to be occupied by the gas under pressure, as follows

$$V_g = V_T - V_v$$

where V_T (m^3) is the total volume of the empty tank.

The mass m_g (kg) of the gas under pressure can be computed by means of the law of perfect gases, as follows

$$m_g = \frac{p_T V_g}{R_g T_u}$$

In order for the heat balance to be maintained, the total heat Q (J) must be such that

$$Q = m_g c_{pg} (T_g - T_u)$$

where c_{pg} ($\text{J kg}^{-1} \text{ K}^{-1}$) is the specific heat at constant pressure of the gas under pressure. The preceding equation makes it possible to determine the mean value T_g (K) of the gas under pressure for the assumed value T_u (K) of the gases at burnout.

In case of the value of T_g being predetermined, m_g , m_v , and T_u must have values such that

$$m_g c_{pg} (T_g - T_u) = m_v [c_{pl}(T_v - T_e) + h_v + c_{pv}(T_u - T_v)]$$

The preceding discussion has neglected the heat transfer through the tank walls. On the contrary, when the gas under pressure, the propellants, and the tank walls have a considerable difference of temperature, then the total heat transferred from one to another of them must be taken into account for the purpose of determining the propellants vaporised at burnout. In these conditions, the preceding equation

$$Q = m_v [c_{pl}(T_v - T_e) + h_v + c_{pv}(T_u - T_v)]$$

can be re-written as follows

$$Q \pm Q_{w1} = m_v [c_{pl}(T_v - T_e) + h_v + c_{py}(T_u - T_v)]$$

where Q_{w1} (J) is the total heat transferred between the tank walls and the liquid or gaseous propellants during a given mission. The sign (plus or minus) in front of Q_{w1} indicates whether the tank walls add or subtract heat.

Likewise, the preceding equation

$$Q = m_g c_{pg} (T_g - T_u)$$

can be re-written as follows

$$Q = m_g c_{pg} (T_g - T_u) \pm Q_{w2}$$

where Q_{w2} (J) is the total heat transferred between the gas under pressure and the tank walls during a given mission. The sign (plus or minus) in front of Q_{w2} indicates whether the tank walls add or subtract heat.

Consequently, the equation expressing the heat balance when the gas under pressure, the propellants, and the tank walls have a considerable difference of temperature can be written as follows

$$m_g c_{pg} (T_g - T_u) \pm Q_{w2} = m_v [c_{pl}(T_v - T_e) + h_v + c_{pv}(T_u - T_v)] - (\pm Q_{w1})$$

When the mission to be accomplished by a space vehicle includes periods of propelled flight and periods of coasting, then the heat transfer across the gas-liquid interface must be determined by considering the total time of the mission. Therefore, the preceding equation

$$Q = H A t (T_u - T_e)$$

must be re-written as follows

$$Q = H A t_m (T_m - T_e)$$

where t_m (s) is the total time of the mission including periods of propelled flight and periods of coasting, and T_m (K) is the mean temperature of the gas under pressure during the total time of the mission. The temperature T_m depends on several factors, which are the duration of the coasting periods, the heat transfer between the gas and the walls, etc.

Other effects (vapour condensation, stability of the gas under pressure in the propellants, and chemical reactions between this gas and the propellants) can be taken into account, in case of availability of experimental data.

As an application of the concepts discussed above, we consider a rocket engine whose oxidiser and fuel are respectively nitrogen tetroxide (N_2O_4) and hydrazine (N_2H_4). These propellants are fed to the thrust chamber by using helium (He) as the gas under pressure. Let $V_T = 3.37 \text{ m}^3$ be the total volume of the empty tank of nitrogen tetroxide, $A = 1.86 \text{ m}^2$ be the area of the average cross section of the tank, $p_T = 1.14 \times 10^6 \text{ N/m}^2$ be the absolute pressure in the tank, and $T_e = 289 \text{ K}$ be the temperature of the oxidiser. As a first case, we want to calculate the total mass m_g (kg) of the gas under pressure and its temperature T_g (K) at the inlet section of the tank, knowing that the duration of operation is $t = 500 \text{ s}$, and that the heat transfer coefficient, determined experimentally, at the liquid-gas interface is $H = 40.9 \text{ W}/(\text{m}^2\text{K})$. We assume the temperature of the gas at burnout to be $T_u = 389 \text{ K}$, in the absence of heat transfer at the walls of the tanks.

The following data are available for nitrogen tetroxide (N_2O_4) at the pressure indicated above ($p_T = 1.14 \times 10^6 \text{ N/m}^2$): vaporisation temperature $T_v = 357 \text{ K}$, heat of vaporisation $h_v = 414000 \text{ J/kg}$, mean value of specific heat at constant pressure in liquid state $c_{pl} = 1760 \text{ J/(kg K)}$, mean value of specific heat at constant pressure in vapour state $c_{pv} = 754 \text{ J/(kg K)}$, compressibility factor $Z = 0.95$, and molar mass $\mathcal{M} = 2 \times 14 + 4 \times 16 = 92 \text{ kg/kmol}$. The specific heat at constant pressure of helium (He) at 293 K and atmospheric pressure is $c_{pg} = 5190 \text{ J/(kg K)}$ [4] and its molar mass is $\mathcal{M} = 4 \text{ kg/kmol}$.

The total heat transferred at the gas-liquid interface results from

$$Q = HAt(T_u - T_e) = 40.9 \times 1.86 \times 500 \times (389 - 289) = 3.804 \times 10^6 \text{ J}$$

This value of Q and the values of the quantities c_{pl} , c_{pv} , h_v , T_v , T_e , and T_u are substituted into the following equation

$$Q = m_v [c_{pl}(T_v - T_e) + h_v + c_{pv}(T_u - T_v)]$$

This yields

$$3.804 \times 10^6 = m_v [1760 \times (357 - 289) + 414000 + 754 \times (389 - 357)]$$

The preceding equation, solved for the total mass m_v of vaporised propellant, yields

$$m_v = \frac{3.804 \times 10^6}{1760 \times (357 - 289) + 414000 + 754 \times (389 - 357)} = 6.820 \text{ kg}$$

The partial volume occupied by vaporised propellant (N_2O_4 , whose molar mass is $\mathcal{M} = 92 \text{ kg/kmol}$) results from

$$V_v = \frac{m_v Z R_p T_u}{p_T} = \frac{6.820 \times 0.95 \times 8314.46 \times 389}{92 \times 1.14 \times 10^6} = 0.1998 \approx 0.2 \text{ m}^3$$

The partial volume V_g occupied by the gas under pressure (helium) results from the difference between the total volume V_T of the empty tank and the partial volume V_v computed above, as follows

$$V_g = V_T - V_v = 3.37 - 0.2 = 3.17 \text{ m}^3$$

The required mass m_g of the gas under pressure (helium, whose molar mass is $\mathcal{M} = 4 \text{ kg/kmol}$) results from the equation of perfect gases, as follows

$$m_g = \frac{p_T V_g}{R_g T_u} = \frac{1.14 \times 10^6 \times 3.17 \times 4}{8314.46 \times 389} = 4.469 \text{ kg}$$

In order for the heat balance to be maintained, the total heat Q must be such that

$$Q = m_g c_{pg} (T_g - T_u)$$

The preceding equation, solved for T_g , yields the required temperature of the gas under pressure at the inlet section of the tank, as follows

$$T_g = T_u + \frac{Q}{m_g c_{pg}} = 389 + \frac{3.804 \times 10^6}{4.469 \times 5190} = 553 \text{ K}$$

Now, as a second case, we want to calculate the total mass m_g (kg) of the gas under pressure and its temperature T_g (K) at the inlet section of the tank, for a mission which includes periods of propelled flight and periods of coasting, and has a total duration $t_m = 18000$ s. The mean temperature of the gas under pressure during this mission is $T_m = 292$ K. The total heat transferred between the tank walls and the propellant is $Q_{w1} = -2.11 \times 10^6$ J, where the minus sign indicates that the tank walls subtract heat from the propellant. The total heat transferred between the gas under pressure and the tank walls is $Q_{w2} = -0.633 \times 10^6$ J, where the minus sign indicate that the tank walls subtract heat from the gas under pressure. The temperature of the gases at burnout is $T_u = 367$ K.

The total heat Q transferred from the gas under pressure to the vaporised propellant at the gas-liquid interface is

$$Q = H A t_m (T_m - T_e) = 40.9 \times 1.86 \times 18000 \times (292 - 289) = 4.108 \times 10^6 \text{ J}$$

This value of Q and the values of the quantities Q_{w1} , c_{pl} , c_{pv} , h_v , T_v , T_e , and T_u are substituted into the following equation

$$Q \pm Q_{w1} = m_v [c_{pl}(T_v - T_e) + h_v + c_{pv}(T_u - T_v)]$$

Consequently, the total mass m_v of vaporised propellant is

$$m_v = \frac{4.108 \times 10^6 - 2.11 \times 10^6}{1760 \times (357 - 289) + 414000 + 754 \times (367 - 357)} = 3.692 \text{ kg}$$

The partial volume occupied by vaporised propellant (N_2O_4 , whose molar mass is $\mathcal{M} = 92$ kg/kmol) results from

$$V_v = \frac{m_v Z R_p T_u}{p_T} = \frac{3.692 \times 0.95 \times 8314.46 \times 367}{92 \times 1.14 \times 10^6} = 0.102 \text{ m}^3$$

The partial volume V_g occupied by the gas under pressure (helium) results from the difference between the total volume V_T of the empty tank and the partial volume V_v computed above, as follows

$$V_g = V_T - V_v = 3.37 - 0.102 = 3.268 \text{ m}^3$$

The mass m_g of the required gas under pressure (helium, whose molar mass is $\mathcal{M} = 4 \text{ kg/kmol}$) results from the equation of perfect gases, as follows

$$m_g = \frac{p_T V_g}{R_g T_u} = \frac{1.14 \times 10^6 \times 3.268 \times 4}{8314.46 \times 367} = 4.884 \text{ kg}$$

By substituting this value of m_g into the following equation

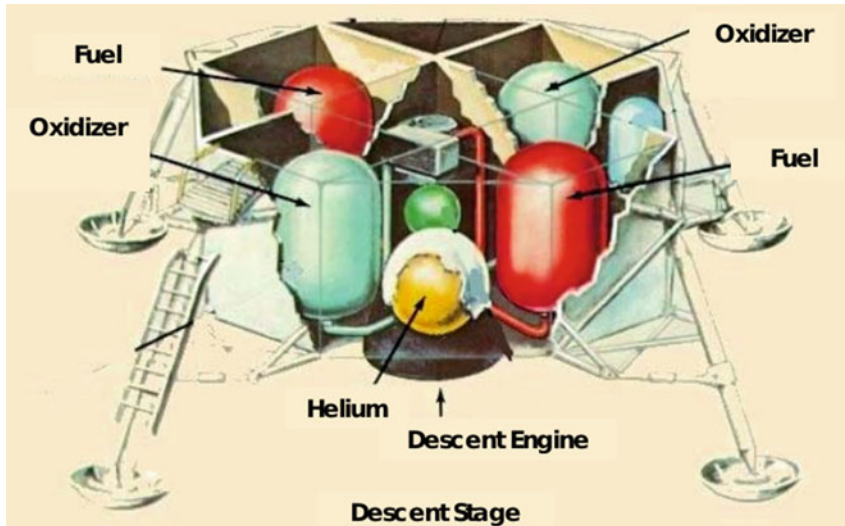
$$Q = m_g c_{pg} (T_g - T_u) \pm Q_{w2}$$

and solving for T_g , the required temperature of the gas under pressure at the inlet section of the tank results

$$T_g = T_u + \frac{Q - Q_{w2}}{m_g c_{pg}} = 367 + \frac{(4.108 + 0.633) \times 10^6}{4.884 \times 5190} = 554 \text{ K}$$

3.3 Feed Systems Using Gases Stored for Bi-Propellants

The gas used in these systems, which is usually nitrogen or helium, is stored in a vessel at a pressure going from 2.1×10^7 to $3.4 \times 10^7 \text{ N/m}^2$ [3]. The following figure, due to the courtesy of NASA [5], shows the position of the spherical vessel of helium in the descent stage of the Apollo lunar module.



Helium is preferred to other gases for the following reasons:

- low molar mass ($\mathcal{M} = 4 \text{ kg/kmol}$) and therefore low total mass;
- low boiling point (4.22 K at atmospheric pressure); and
- absence of chemical reactivity.

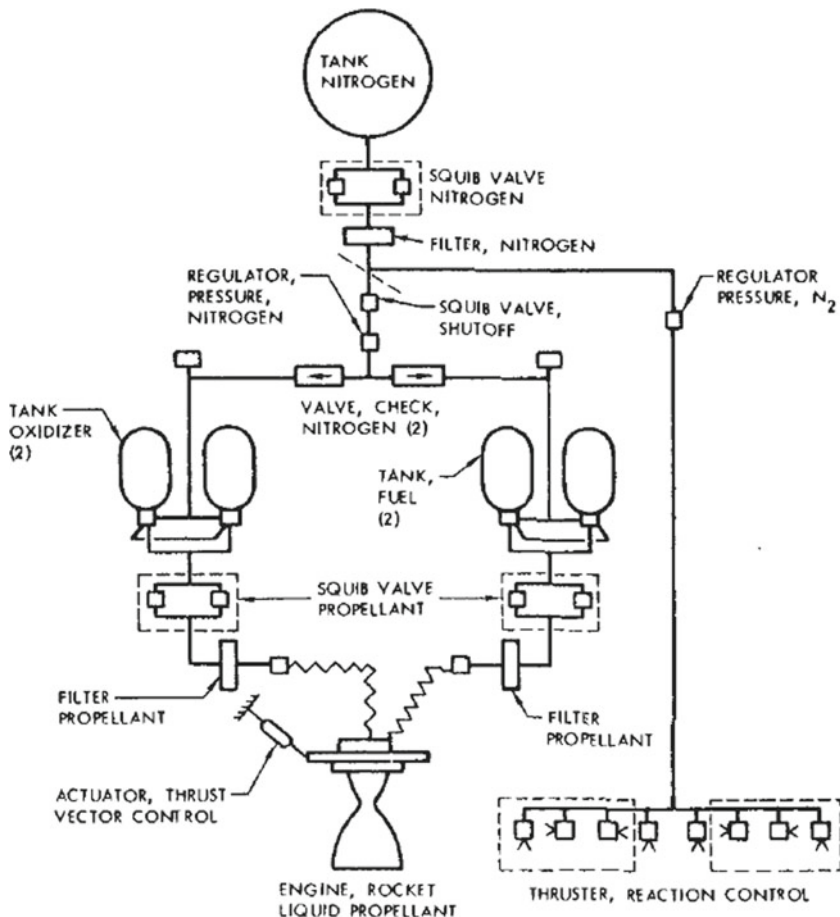
In case of a bi-propellant engine using liquid hydrogen as its fuel, gaseous hydrogen has also been used as the pressurising agent.

Helium or other pressurised gases can be stored in a vessel with or without a system for thermal conditioning. A thermal conditioning (that is, heating or cooling or both) of the gas can lead to low-mass systems. On the other hand, a thermal conditioning of the gas implies high complexity and cost. A successful system which did not condition thermally the stored gas (nitrogen) was the Lunar Orbiter velocity and reaction control system. By contrast, in the descent stage illustrated above of the Apollo lunar module, helium under pressure was stored under supercritical conditions and then heated. This led to a reduction in mass of 60% over that of an ambient-temperature high-pressure storage without thermal conditioning. These two systems of storage are briefly described below.

The velocity and reaction control system of the Lunar Orbiter IV is shown schematically in the following figure, due to the courtesy of NASA [6].

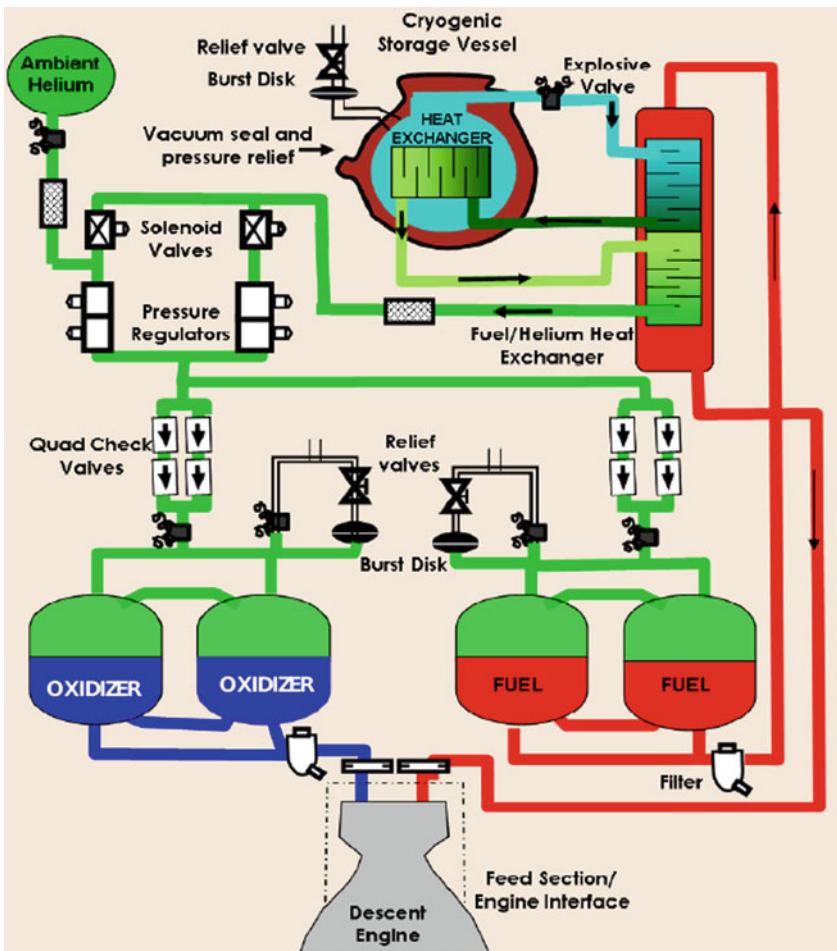
This system was designed so that its 445-N-thrust engine, using a hypergolic combination of oxidiser (N_2O_4) and fuel (Aerozine-50), could impart a velocity change of 1017 m/s to the 387 kg spacecraft for mid-course corrections, injection into an initial lunar orbit, and successive injection into a photographic orbit. The source of ullage gas was a spherical tank containing gaseous nitrogen (N_2) without provision for conditioning the temperature of this gas. The tank was made of Ti-6Al-4V alloy, with a mass of 9.9 kg and an internal volume of 0.0259 m^3 . A mass of 6.56 kg of nitrogen was stored into this sphere at a pressure of $2.4 \times 10^7 \text{ N/m}^2$ and at a temperature of 294 K. Two parallel-redundant normally-closed squib valves isolated the pressurising gas in the storage vessel from the rest of the system until the gas was required for its first use. The gas in the storage vessel was also the source for the cold-gas reaction control system, which is shown in the lower portion of the preceding figure. Only part (from 0.91 to 1.36 kg) of the nitrogen mass in the storage vessel was used to generate and maintain the pressure in the propellant tanks for the velocity control system; the remaining part was used for the reaction control system and for reserve of pressurising gas. When the squib valves were opened, the pressurising gas flowed through a normally-open shut-off squib valve to the pressure regulator of the velocity control system, which reduced the pressure of the gas to $1.3 \times 10^6 \text{ N/m}^2$. The gas was then routed through the check valves and into the oxidiser and fuel tanks. In the velocity control system, a single regulator was used to pressurise both of the propellant tanks, in order to preclude undesired in-flight shifts of propellant mixture ratio; such shifts could occur if each tank had its own pressure regulator and the regulator set-point of one changed during flight. With a single regulator, the set-point could still change, but each tank could have the same ullage pressure. Though each tank had a bladder, check valves were used to isolate the ullage gases of the fuel and oxidiser tanks. If any propellant vapour permeated one of

such bladders, the check valves prevented the vapour from entering the other system. After the velocity control system completed its function, the normally-open shut-off squib valve was set to the closed position, in order to isolate the velocity control system regulator and tankage from the gas in the storage vessel. Each ullage had a pressure relief system to protect the system from over-pressures. The pressurisation system of the Lunar Orbiter velocity and reaction control system was subject to leakages only two times during twenty-eight engine firings in five different missions [2].



The descent stage of the Apollo lunar module used just the same combination of hypergolic propellants (N_2O_4 as the oxidiser and Aerozine-50 as the fuel) as that used by the Lunar Orbiter velocity and reaction control system. In the descent stage of the Apollo lunar module, a double-walled, Mylar®-insulated, high-pressure, cryogenic vessel was used to store 22 kg of supercritical helium for the pressurisation system. The helium tank was loaded with liquid helium at 4.4 K and topped with

high-pressure gaseous helium, which increased the system temperature to approximately 6–7 K. During the 131-h (maximum) standby period, the helium pressure and temperature were increased by incoming heat leak. The maximum temperature reached by helium prior to outflow was 28 K, and the rate of pressure rise ranged from 9.6 to 19.2 N/(m²s). The feed system for the descent stage of the Apollo lunar module is illustrated schematically in the following figure, due to the courtesy of NASA [5].



With reference to the colours shown in the preceding figure, the helium fluid (cyan) passed at a maximum flow rate of 0.000668 kg/s through the first loop of the external two-pass fuel-to-helium heat exchanger, where it absorbed heat from the fuel (red). Then, the helium (dark green) was warmed and routed back through the internal helium-to-helium heat exchanger inside the cryogenic storage vessel. The warm helium transferred heat to the remaining supercritical helium in the cryogenic storage

vessel, and caused an increase in pressure, so that continuous expulsion of helium was ensured throughout the period of operation. After the helium passed through the internal helium-to-helium heat exchanger, where it was cooled, it was routed back (light green) through the second loop of the fuel-to-helium heat exchanger, and was heated to approximately 278 K before being delivered (medium green) as the pressurising agent for the fuel (red) and oxidiser (blue) tanks of the propulsion system. The use of a supercritical-helium storage tank and passive control configuration for the descent stage of the Apollo lunar module reduced the number of components required and resulted in a high degree of reliability [2].

The pressurisation systems described above are only two particular examples of component combinations. Further combinations can be found in [7].

The requirements for the gas under pressure, which have been considered in Sect. 3.2, apply only to the net or effective mass m_g of gas necessary to pressurise the tanks of propellant. However, the gross mass m_s of the stored gas depends also on the system design, on the gas expansion during operation, and on the range of the environmental temperature. The gross mass m_s of the stored gas results from a sum, whose addends are the net mass m_g of the stored gas, the mass m_{sv} of the residual gas in the storage vessel, the mass m_d of the residual gas in the lines downstream of the regulator, the mass m_{ex} of the residual mass in the heat exchanger, etc., as follows

$$m_s = m_g + m_{sv} + m_d + m_{ex} + \dots$$

A parameter which takes account of the additional terms indicated above is the use factor of the pressurising gas. This parameter, whose value is greater than unity, is defined as the ratio m_s/m_g of the gross mass to the net mass of the pressuring gas. The lowest value of pressure in a storage vessel depends on the values of the pressure drops in the various components (regulator, heat exchanger, etc.) which make up a feed system and also on a safety value. The pressurising action of a stored gas is considered to have come to an end when the pressure in its storage vessel decays to $2.758 \times 10^6 \text{ N/m}^2$ [3]. When a source of heat is present inside the storage vessel, then the expansion of the gas in the vessel is assumed to be polytropic ($pV^n = \text{constant}$), that is, such as to involve a transfer of heat and work. By contrast, when no source of heat is present in the storage vessel, then the expansion of the gas in the vessel can be assumed to be isentropic ($pV^\gamma = \text{constant}$), that is, frictionless and without heat transfer between the gas and the vessel walls. The following equation can be used to calculate the final temperature T_2 (K) of the gas in the storage vessel

$$\frac{T_2}{T_1} = \left(\frac{p_2}{p_1} \right)^{\frac{n-1}{n}}$$

where T_1 (K) is the initial temperature of the gas in the storage vessel, n is the exponent of the polytropic expansion, and p_2 (N/m^2) and p_1 (N/m^2) are respectively the final pressure and the initial pressure in the storage vessel.

The value of the exponent n is first estimated, and then verified experimentally. In case of an isentropic expansion of helium, $n = \gamma = c_p/c_v = 1.667$ [4].

In most cases, the expansion process through the regulator and the lines can be considered adiabatic, so that the total temperature remains constant. This expansion comes to an end in the propellant tanks. The temperature of the propellants in the tanks is assumed to be equal to the temperature at the outlet section of the heat exchanger. For a specified range of temperatures in a pressure-feed system, the lower value can be used to determine the mass of the pressurising gas, and the upper value can be used to determine the volume of the storage vessel, for a given storage pressure [3].

In the following example of application, an isentropic expansion process is assumed to occur in the oxidiser (N_2O_4) tank of a pressure-fed system having the following properties: temperature range 278–311 K in the storage vessel at the system start, pressure $p_s = 3.1 \times 10^7 \text{ N/m}^2$ in the storage vessel at the system start, pressure $p_u = 2.76 \times 10^6 \text{ N/m}^2$ in the storage vessel at burnout, volume $V_d = 0.0113 \text{ m}^3$ in the gas lines downstream of the regulator, volume $V_{ex} = 0.0283 \text{ m}^3$ in the heat exchanger, negligible residual volume in the gas lines, and a 2% reserve of pressurising gas. We want to compute the gross mass of the pressurising gas (helium), the volume of the gas storage vessel, and the use factor of the pressurising gas, by using the values relating to the first case (single start) of the example of Sect. 3.2. These values are also given below for convenience: absolute pressure in the oxidiser tank $p_T = 1.14 \times 10^6 \text{ N/m}^2$, vaporisation temperature of the oxidiser $T_v = 357 \text{ K}$, heat of vaporisation of the oxidiser $h_v = 414000 \text{ J/kg}$, mean value of the specific heat of the oxidiser at constant pressure in liquid state $c_{pl} = 1760 \text{ J/(kg K)}$, mean value of the specific heat of the oxidiser at constant pressure in vapour state $c_{pv} = 754 \text{ J/(kg K)}$, compressibility factor of the oxidiser $Z = 0.95$, and molar mass of the oxidiser $\mathcal{M} = 2 \times 14 + 4 \times 16 = 92 \text{ kg/kmol}$. The temperature of the gas in the ullage space at burnout is $T_u = 389 \text{ K}$. The specific heat at constant pressure of the pressurising gas (helium) at 293 K and atmospheric pressure is $c_{pg} = 5190 \text{ J/(kg K)}$ and its molar mass is $\mathcal{M} = 4 \text{ kg/kmol}$.

In Sect. 3.2, the net mass of the pressurising gas has been found to be $m_g = 4.469 \text{ kg}$. The temperature and the pressure of the residual pressurising gas in the lines downstream of the regulator after shutdown are assumed to have the same values as those of the ullage gases in the oxidiser tank at burnout, which are respectively $T_u = 389 \text{ K}$ and $p_T = 1.14 \times 10^6 \text{ N/m}^2$. Since the volume in the gas lines downstream of the regulator is $V_d = 0.0113 \text{ m}^3$ (see above), then the mass m_d of the residual pressurising gas in the lines downstream of the regulator results from the law of perfect gases, as follows

$$m_d = \frac{p_T V_d}{R_g T_u} = \frac{1.14 \times 10^6 \times 0.0113 \times 4}{8314.46 \times 389} = 0.0159 \text{ kg}$$

The temperature of the residual pressurising gas in the heat exchanger is assumed to be the same as the temperature of the pressurising gas at the inlet section of the

oxidiser tank. In Sect. 3.2, this temperature has been found to be $T_g = 554$ K. Likewise, the pressure of the residual pressurising gas in the heat exchanger is assumed to be the same as the pressure ($p_u = 2.76 \times 10^6$ N/m²) in the storage vessel at burnout. Therefore, the mass m_{ex} of the residual pressurising gas in the heat exchanger results from the law of perfect gases, as follows

$$m_{ex} = \frac{p_u V_{ex}}{R_g T_g} = \frac{2.76 \times 10^6 \times 0.0283 \times 4}{8314.46 \times 554} = 0.0678 \text{ kg}$$

By using the following equation

$$\frac{T_2}{T_1} = \left(\frac{p_2}{p_1} \right)^{\frac{n-1}{n}}$$

and solving for T_2 , where T_1 is the lower limit (311 K) of the system operating temperatures, and $p_1 = p_s = 3.1 \times 10^7$ N/m² and $p_2 = p_u = 2.76 \times 10^6$ are respectively the initial pressure and the final pressure of the helium ($n = \gamma \equiv c_p/c_v = 1.667$), the temperature of the residual helium in the storage vessel at burnout results

$$T_2 = T_1 \left(\frac{p_2}{p_1} \right)^{\frac{n-1}{n}} = 311 \times \left(\frac{2.76 \times 10^6}{3.1 \times 10^7} \right)^{\frac{1.667-1}{1.667}} = 118 \text{ K}$$

Since the pressure in the storage vessel at burnout is $p_u = 2.76 \times 10^6$ N/m² and the temperature of the residual helium in the storage vessel at burnout is $T_2 = 118$ K, then the mass m_{sv} (kg) in the storage vessel at burnout can be determined by using the equation of perfect gases, as follows

$$m_{sv} = \frac{p_u V_L}{R_g T_2} = \frac{2.76 \times 10^6 \times 4}{8314.46 \times 118} V_L$$

where V_L is the volume (m³) of the pressurising gas necessary to put the oxidiser tank under pressure.

Likewise, since the pressure in the storage vessel at start is $p_s = 3.1 \times 10^7$ N/m² and the higher temperature of the operating range is $T_s = 311$ K, then the mass m_s (kg) in the storage vessel at start can be determined by using the equation of perfect gases, as follows

$$m_s = \frac{p_s V_L}{R_g T_s} = \frac{3.1 \times 10^7 \times 4}{8314.46 \times 311} V_L$$

where, again, V_L is the volume (m³) of the pressurising gas necessary to put the oxidiser tank under pressure. Remembering the preceding equation

$$m_s = m_g + m_{sv} + m_d + m_{ex} + \dots$$

truncated after m_{ex} , and substituting the values found above, there results

$$\frac{3.1 \times 10^7 \times 4}{8314.46 \times 311} V_L = 4.469 + \frac{2.76 \times 10^6 \times 4}{8314.46 \times 118} V_L + 0.0159 + 0.0679$$

This equation, solved for V_L , yields

$$V_L = 0.124 \text{ m}^3$$

By substituting this value into

$$m_s = \frac{p_s V_L}{R_g T_s} = \frac{3.1 \times 10^7 \times 4}{8314.46 \times 311} V_L$$

the gross mass of the pressurising gas results

$$m_s = 5.949 \text{ kg}$$

By adding the 0.2% reserve of pressurising gas to the value computed above, the gross mass becomes

$$m_s = 5.949 \times 1.02 = 6.068 \text{ kg}$$

By introducing $m_s = 6.068 \text{ kg}$, $R^* = 8314.460 \text{ N m kmol}^{-1} \text{ K}^{-1}$, $\mathcal{M} = 4 \text{ kg/kmol}$, $p_s = 3.1 \times 10^7 \text{ N/m}^2$ and $T_s = 311 \text{ K}$ in the equation of perfect gases, the volume V_u of the storage vessel for the pressurising gas results

$$V_u = \frac{m_s R^* T_s}{\mathcal{M} p_s} = \frac{6.068 \times 8314.46 \times 311}{4 \times 3.1 \times 10^7} = 0.1265 \text{ m}^3$$

According to the definition given above, the use factor of the pressurising gas has the following value

$$\frac{m_s}{m_g} = \frac{6.068}{4.469} = 1.358$$

Now we want to compute the same quantities as those determined above, relating to the second case (multi-start) of the example of Sect. 3.2. There, the net mass of the pressurising gas has been found to be $m_g = 4.883 \text{ kg}$. The volume in the gas lines downstream of the regulator is $V_d = 0.0113 \text{ m}^3$ (see above). The temperature and the pressure of the pressurising gas in the lines downstream of the regulator are assumed to be the same as those in the oxidiser tank at burnout ($T_u = 367 \text{ K}$ and $p_u = 1.14 \times 10^6 \text{ N/m}^2$). Therefore, the mass m_d of the residual pressurising gas in the lines downstream of the regulator results from the law of perfect gases, as follows

$$m_d = \frac{p_u V_d}{R_g T_u} = \frac{1.14 \times 10^6 \times 0.0113 \times 4}{8314.46 \times 367} = 0.0169 \text{ kg}$$

The temperature of the residual gas under pressure in the heat exchanger is assumed to be the same as the temperature of the gas under pressure at the inlet section of the tank. In Sect. 3.2, this temperature has been found to be $T_g = 554$ K. The pressure of the same residual gas in the heat exchanger is assumed to be the same as the pressure of the gas in the storage vessel at burnout, which is (see above) $p_u = 2.76 \times 10^6 \text{ N/m}^2$. The volume in the heat exchanger is (see above) $V_{ex} = 0.0283 \text{ m}^3$. By introducing these values in the equation of perfect gases, the mass of the residual gas in the heat exchanger results

$$m_{ex} = \frac{p_u V_{ex}}{R_g T_g} = \frac{2.76 \times 10^6 \times 0.0283 \times 4}{8314.46 \times 554} = 0.0678 \text{ kg}$$

In the first case, the temperature of the residual helium in the storage vessel at burnout has been found to be $T_2 = 118$ K, and the mass of this gas in the storage vessel at burnout has been found to be

$$m_{sv} = \frac{p_u V_L}{R_g T_2} = \frac{2.76 \times 10^6 \times 4}{8314.46 \times 118} V_L$$

where $V_L (\text{m}^3)$ is the volume of the pressurising gas necessary to put the oxidiser tank under pressure.

Again, in the first case, the mass m_s (kg) of gas in the storage vessel at start has been found to be

$$m_s = \frac{p_s V_L}{R_g T_s} = \frac{3.1 \times 10^7 \times 4}{8314.46 \times 311} V_L$$

Remembering the equation

$$m_s = m_g + m_{sv} + m_d + m_{ex} + \dots$$

truncated after m_{ex} , and substituting the values found above, there results

$$\frac{3.1 \times 10^7 \times 4}{8314.46 \times 311} V_L = 4.883 + \frac{2.76 \times 10^6 \times 4}{8314.46 \times 118} V_L + 0.0169 + 0.0678$$

This equation, solved for V_L , yields

$$V_L = 0.135 \text{ m}^3$$

By substituting this value into

$$m_s = \frac{p_s V_L}{R_g T_s} = \frac{3.1 \times 10^7 \times 4}{8314.46 \times 311} V_L$$

the gross mass of the pressurising gas results

$$m_s = 6.474 \text{ kg}$$

By adding the 0.2% reserve of pressurising gas to the value computed above, the gross mass becomes

$$m_s = 6.474 \times 1.02 = 6.603 \text{ kg}$$

According to the definition given above, the use factor of the pressurising gas has the following value

$$\frac{m_s}{m_g} = \frac{6.603}{4.883} = 1.352$$

We want to compute the gross mass m_s (kg) of the gas under pressure in the oxidiser tank, the volume V_u (m^3) of the storage vessel, and the use factor of the pressurising gas for the first case (single start) of the example of Sect. 3.2, in the absence of a system for thermal conditioning. Since the pressurising gas is not heated, then its bulk temperature T_g at burnout can be assumed to be the average of the initial temperature (278 K, a datum) and the final temperature (which has been found to be $T_2 = 118$ K) in the storage vessel, as follows

$$T_g = \frac{278 + 118}{2} = 198 \text{ K}$$

Since this temperature is lower than the temperature ($T_e = 289$ K) of the propellant, then the pressurising gas does not warm the propellant. The net mass m_g of the required gas under pressure results from the law of perfect gases, as follows

$$m_g = \frac{p_T V_T}{R_g T_g} = \frac{1.14 \times 10^6 \times 3.37 \times 4}{8314.46 \times 198} = 9.335 \text{ kg}$$

The mass m_d of the residual pressurising gas in the lines downstream of the regulator results from the law of perfect gases, as follows

$$m_d = \frac{p_T V_d}{R_g T_g} = \frac{1.14 \times 10^6 \times 0.0113 \times 4}{8314.46 \times 198} = 0.0313 \text{ kg}$$

In the first case, the temperature of the residual helium in the storage vessel at burnout has been found to be $T_2 = 118$ K, and the mass of this gas in the storage vessel at burnout has been found to be

$$m_{sv} = \frac{p_u V_L}{R_g T_2} = \frac{2.76 \times 10^6 \times 4}{8314.46 \times 118} V_L$$

where V_L (m^3) is the volume of the pressurising gas necessary to put the oxidiser tank under pressure.

The gross mass m_s (kg) of gas in the storage vessel at start is

$$m_s = \frac{p_s V_L}{R_g T_s} = \frac{3.1 \times 10^7 \times 4}{8314.46 \times 278} V_L$$

Remembering the equation

$$m_s = m_g + m_{sv} + m_d + m_{ex} + \dots$$

where, in the present case, $m_{ex} = 0$, and substituting the values found above, there results

$$\frac{3.1 \times 10^7 \times 4}{8314.46 \times 278} V_L = 9.334 + \frac{2.76 \times 10^6 \times 4}{8314.46 \times 118} V_L + 0.0313$$

This equation, solved for V_L , yields

$$V_L = 0.2209 \text{ m}^3$$

Therefore, the gross mass m_s (kg) of gas in the storage vessel at start is

$$m_s = \frac{p_s V_L}{R_g T_s} = \frac{3.1 \times 10^7 \times 4 \times 0.2209}{8314.46 \times 278} = 11.85 \text{ m}^3$$

By adding the 0.2% reserve of pressurising gas to the value computed above, the gross mass becomes

$$m_s = 11.85 \times 1.02 = 12.09 \text{ kg}$$

According to the definition given above, the use factor of the pressurising gas has the following value

$$\frac{m_s}{m_g} = \frac{12.09}{9.335} = 1.295$$

Finally, it is required to compute the gross mass m_s (kg) of the gas under pressure in the oxidiser tank, the volume V_u (m^3) of the storage vessel, and the use factor of the pressurising gas for the first case (single start) of the example of Sect. 3.2, in the presence of a system for thermal conditioning, assuming a polytropic ($pV^n = \text{constant}$, with $n = 1.2$) expansion of helium in the storage vessel.

By using the following equation

$$\frac{T_2}{T_1} = \left(\frac{p_2}{p_1} \right)^{\frac{n-1}{n}}$$

and solving for T_2 , where T_1 is the initial temperature (278 K, a datum) of the helium, and $p_1 = p_s = 3.1 \times 10^7 \text{ N/m}^2$ and $p_2 = p_u = 2.76 \times 10^6$ are respectively the initial pressure and the final pressure of the same gas ($n = 1.2$), the temperature of the residual helium in the storage vessel at burnout results

$$T_2 = T_1 \left(\frac{p_2}{p_1} \right)^{\frac{n-1}{n}} = 278 \times \left(\frac{2.76 \times 10^6}{3.1 \times 10^7} \right)^{\frac{1.2-1}{1.2}} = 186 \text{ K}$$

The bulk temperature T_g of the helium at burnout can be assumed to be the average of the initial temperature $T_1 = 278 \text{ K}$ and the final temperature $T_2 = 186 \text{ K}$ in the storage vessel, as follows

$$T_g = \frac{278 + 186}{2} = 232 \text{ K}$$

The net mass m_g of the required gas under pressure results from the law of perfect gases, as follows

$$m_g = \frac{p_T V_T}{R_g T_g} = \frac{1.14 \times 10^6 \times 3.37 \times 4}{8314.46 \times 232} = 7.967 \text{ kg}$$

The mass m_d of the residual gas under pressure in the lines downstream of the regulator results from the law of perfect gases, as follows

$$m_d = \frac{p_T V_d}{R_g T_g} = \frac{1.14 \times 10^6 \times 0.0113 \times 4}{8314.46 \times 232} = 0.0267 \text{ kg}$$

The mass of this gas in the storage vessel at burnout is

$$m_{sv} = \frac{p_u V_L}{R_g T_2} = \frac{2.76 \times 10^6 \times 4}{8314.46 \times 186} V_L$$

where $V_L (\text{m}^3)$ is the volume of the pressurising gas necessary to put the oxidiser tank under pressure.

The gross mass m_s (kg) of gas in the storage vessel at start is

$$m_s = \frac{p_s V_L}{R_g T_s} = \frac{3.1 \times 10^7 \times 4}{8314.46 \times 278} V_L$$

Remembering the equation

$$m_s = m_g + m_{sv} + m_d + m_{ex} + \dots$$

where, in the present case, $m_{ex} = 0$, and substituting the values found above, there results

$$\frac{3.1 \times 10^7 \times 4}{8314.46 \times 278} V_L = 7.966 + \frac{2.76 \times 10^6 \times 4}{8314.46 \times 186} V_L + 0.0267$$

This equation, solved for V_L , yields

$$V_L = 0.1719 \text{ m}^3$$

Therefore, the gross mass m_s (kg) of gas in the storage vessel at start is

$$m_s = \frac{p_s V_L}{R_g T_s} = \frac{3.1 \times 10^7 \times 4 \times 0.1719}{8314.46 \times 278} = 9.220 \text{ kg}$$

By adding the 0.2% reserve of pressurising gas to the value computed above, the gross mass becomes

$$m_s = 9.220 \times 1.02 = 9.404 \text{ kg}$$

According to the definition given above, the use factor of the pressurising gas has the following value

$$\frac{m_s}{m_g} = \frac{9.412}{7.967} = 1.180$$

Gases under pressure are usually stored in spherical vessels, because of the structural efficiency of the spherical shape, which implies a lower mass than is possible with other shapes. Such vessels are usually of monocoque design, operate at high stress levels, are mounted within the rocket vehicle, and are insulated from deflection of the vehicle structure by appropriately designed mountings [2]. By the way, monocoque (a French word meaning single shell) is a structural technique in which a body supports loads through its external skin, with no internal frame to hold the body rigid. The alloy most often used to construct storage vessels is Ti-6Al-4V [8].

An estimate for the mass m (kg) of a spherical vessel of thickness t (m), inside diameter d (m), and made of a material having uniform density ρ (kg/m^3) can be made as follows

$$m = \rho V = \frac{4}{3}\pi\rho \left[\left(\frac{d}{2} + t\right)^3 - \left(\frac{d}{2}\right)^3 \right]$$

Another estimate, suggested by Huzel and Huang [3], for the same mass m (kg) can be made by assuming a vessel made of two hemispherical shells, such that the thickness of the weld lands is taken into account by assuming a band of width w (m) and thickness equal to one-half the wall thickness placed over the weld seam. This estimate is

$$m = \pi d^3 \rho \left(\frac{p}{4\sigma} \right) + 39.37\pi w d^2 \rho \left(\frac{p}{8\sigma} \right)$$

where p (N/m²) is the maximum pressure at which the gas is stored, and σ (N/m²) is the allowable working stress of the material of which the vessel is made.

The storage vessel must be capable of containing the gas at high pressure for long periods of time without losses due to leakage. Gases having low molar masses, such as hydrogen and helium, are less subject to leak through homogeneous metals of good quality than is the case with those having high molar masses. Leakages can occur through porous metals, for example, through castings and welded joints.

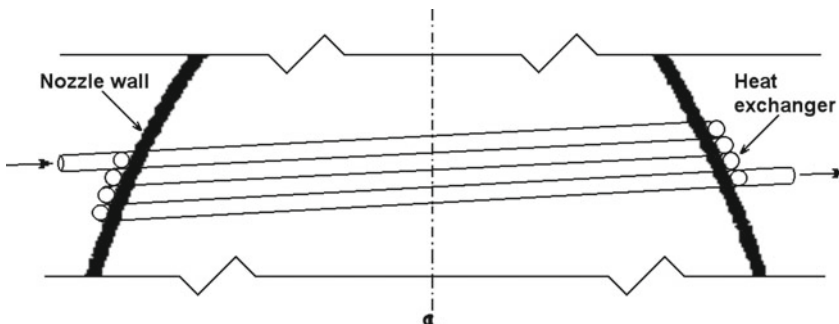
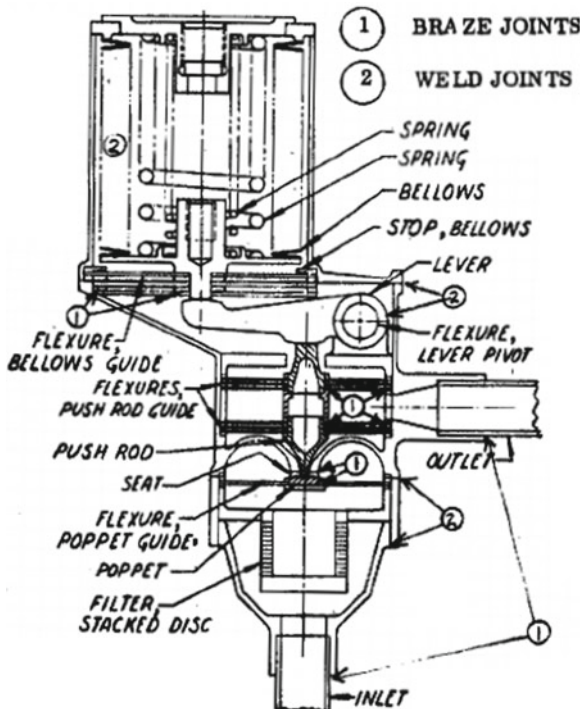
The pressure-fed systems cited above (used for the descent stage of the Apollo lunar module and for the velocity and reaction control system of the Lunar Orbiter) have, each of them, a pressure regulator for the gases (respectively, helium and nitrogen) stored under pressure. A regulator maintains the desired values of flow and pressure to the propellant tanks as the pressure of the stored gas decreases.

The example described below refers to a pressure regulator used for the Space Storable Propulsion Module, which was used for a Jupiter Orbiter mission.

With reference to the following figure, due to the courtesy of NASA [9], this pressure regulator has an unbalanced poppet, which achieves sealing to the seat by means of the upstream pressure force. In addition, the poppet is held against the seat by an axial guidance flexure.

The actuation mechanism consists of a bellows, which is exposed to space internally and to the regulator downstream pressure externally, and which is held in the null position by one or more coil springs. If the regulator downstream pressure decreases from the preset pressure, the reference spring force overcomes the bellows pressure force and the actuator exerts a net opening force on the poppet through the lever arrangement. When this net force is greater than the poppet seating force, the poppet opens and allows the gas (helium) under pressure to pressurise the downstream side of the regulator. When the downstream regulator pressure rises back up to the set pressure, the actuator returns to the null position and the poppet is caused to return to the seat by the axial guidance flexure spring force and the difference of pressure across the poppet [9].

The heat exchanger, which warms the gas under pressure, may be designed to form an integral part of the diverging portion of the nozzle, as shown in the following figure. In this case, the heat exchanger is a tube wound around the contour of the nozzle. Other types of design for heat exchangers will be shown in Sect. 3.4.



The heat transfer coefficient h_g ($\text{W m}^{-2} \text{ K}^{-1}$) on the side of the combusted gas can be determined as has been shown in Chap. 2, Sect. 2.5. The heat transferred by conduction from the nozzle wall to the heat exchanger can be assumed to be entirely

absorbed by the pressurising gas which circulates in the heat exchanger, and therefore the temperature of the pressurising gas increases. Likewise, the determination of the heat transfer coefficient h_h ($\text{W m}^{-2} \text{K}^{-1}$) on the side of the pressurising gas and the design of the heat exchanger can be done as has been shown in Chap. 2, Sect. 2.5. The number of turns in the heat exchanger around the nozzle depends on the required increase in temperature of the pressurising gas and also on the position of the heat exchanger along the nozzle. The various temperatures in the elements of the heat exchanger can be expressed by means of the following equation [3]:

$$\dot{m}_h c_p (T_o - T_i) = A \left(\frac{1}{h_g} + \frac{t}{k} + \frac{1}{h_h} \right)^{-1} \left(T_{aw} - \frac{T_i + T_o}{2} \right)$$

where \dot{m}_h (kg/s) is the mass flow rate of the pressurising gas, c_p ($\text{J kg}^{-1} \text{K}^{-1}$) is the specific heat at constant pressure of the pressurising gas, T_i (K) is the mean temperature of the pressurising gas at the inlet section of the heat exchanger, T_o (K) is the mean temperature of the pressurising gas at the outlet section of the heat exchanger, A (m^2) is the effective area of the heat exchanger, h_g ($\text{W m}^{-2} \text{K}^{-1}$) is the heat transfer coefficient on the side of the combusted gas, t (m) is the thickness of the tube of the heat exchanger, k ($\text{W m}^{-1} \text{K}^{-1}$) is the thermal conductivity of the material of which this tube is made, and T_{aw} (K) is the adiabatic wall temperature on the side of the combusted gas. The temperature of the pressurising gas which leaves the heat exchanger at any time also depends on the temperature of the same gas at the exit section of the storage vessel. The material, of which the tube of the heat exchanger is made, is to be chosen by the designer bearing in mind the necessity of attaching firmly by brazing the tube to the wall of the nozzle. The width of this tube depends on the thermal and mechanical loads to which the tube is subject.

The following example of application concerns the design of a heat exchanger of the type illustrated above, used in parallel with other heat exchangers and placed at the cross-section of area ratio $A/A_t = 10$ of a nozzle extension for a rocket engine of known characteristics.

Let $A_t = 0.02606 \text{ m}^2$ be the area at the throat, $\dot{m}_h = 0.0109 \text{ kg/s}$ be the mass flow rate of the pressurising gas (helium), and $p_{co} \equiv p_h = 3.1026 \times 10^7 \text{ N/m}^2$ its pressure in the storage vessel. The values of the specific heat ratio and of the specific heat at constant pressure of helium can be either taken from [4] ($\gamma \equiv c_p/c_v = 1.667$ and $c_p = 5190 \text{ J kg}^{-1} \text{ K}^{-1}$ at 293 K and atmospheric pressure), or determined at a given temperature and pressure, as will be shown below.

Let $T_i = 192 \text{ K}$ be the mean temperature of the helium at the inlet section of the heat exchanger, $T_o = 554 \text{ K}$ be the mean temperature of the helium at the outlet section of the heat exchanger, $T_{aw} = 2722 \text{ K}$ be the adiabatic wall temperature on the side of the combusted gas, and $h_g = 167.8 \text{ W m}^{-2} \text{ K}^{-1}$ be the heat transfer coefficient on the side of the combusted gas. We want to determine the dimensions and the number of turns for the tube of the heat exchanger, assuming this tube to be made of an alloy Ti–13V–11Cr–3Al, aged at 763 K, having the following thermal and mechanical characteristics [10]: tensile yield strength $\sigma_y = 1.3 \times 10^9 \text{ N/m}^2$,

modulus of elasticity $E = 1.1 \times 10^{11}$ N/m², thermal conductivity (at 698 K) $k = 17.1$ W m⁻¹ K⁻¹, coefficient of thermal expansion (in the range 293–923 K) $\lambda = 10.44 \times 10^{-6}$ m m⁻¹ K⁻¹, and Poisson's ratio $\nu = 0.30$. For each chosen section of the heat exchanger, the temperature of the tube at the wall depends on the bulk temperature of the pressurising gas (helium) at that section. Since the pressurising gas absorbs heat from the nozzle, the maximum temperature occurs at the outlet section of the heat exchanger. We assume the maximum allowable temperature at the outlet section of the heat exchanger on the combusted gas side to be $T_{wg} = 778$ K. Remembering the following equation of Chap. 2, Sect. 2.5

$$q = h_g(T_{aw} - T_{wg})$$

where q (W/m²) is the quantity of heat transferred per unit time per unit surface through convection at the outlet section of the heat exchanger, there results

$$q = 167.8 \times (2722 - 778) = 3.262 \times 10^5 \text{ W/m}^2$$

We take the preliminary value $t = 0.00127$ m for the thickness of the tube. This value will be checked against the results of the following calculations.

Remembering the following equation of Chap. 2, Sect. 2.5

$$T_{wc} = T_{wg} - \frac{tq}{k}$$

and substituting $T_{wg} = 778$ K, $t = 0.00127$ m, $q = 3.262 \times 10^5$ W/m², and $k = 17.1$ W m⁻¹ K⁻¹, the mean temperature of the wall on the helium side is

$$T_{wc} = 778 - \frac{0.00127 \times 3.262 \times 10^5}{17.1} = 754 \text{ K}$$

Remembering again the following equation of Chap. 2, Sect. 2.5

$$q = h_c(T_{wc} - T_{co})$$

where $T_{co} = T_o = 554$ K, and solving for h_c , the heat transfer coefficient on the helium side can be computed as follows

$$h_h \equiv h_c = \frac{q}{T_{wc} - T_{co}} = \frac{3.262 \times 10^5}{754 - 554} = 1631 \text{ W m}^{-2} \text{ K}^{-1}$$

According to Wang et al. [11, page 911, Eq. 4], the Prandtl number Pr can be computed approximately as follows

$$Pr = \frac{4\gamma}{9\gamma - 5}$$

Since in the present case $\gamma = c_p/c_v = 1.667$, then

$$Pr = \frac{4 \times 1.667}{9 \times 1.667 - 5} = 0.6667$$

The result found above for the Prandtl number takes account only of the specific heat ratio ($\gamma = 1.667$ at 293 K and atmospheric pressure, according to [4]) of helium. The pressure and the temperature of helium are not taken into account. This result can be checked by using the thermal data given by NIST [12] or by Petersen [13].

The data given by NIST at the pressure $p = 1.241 \times 10^6 \text{ N/m}^2$ (regulated pressure of helium) and at the temperature $T_{co} = 554 \text{ K}$ are: $c_p = 5192.1 \text{ J/(kg K)}$, $c_v = 3116.7 \text{ J/(kg K)}$, $\mu = 3.0488 \times 10^{-5} \text{ N s m}^{-2}$, and $k = 0.23952 \text{ W m}^{-1} \text{ K}^{-1}$. Therefore, the Prandtl number in these conditions is

$$Pr = \frac{\mu c_p}{k} = \frac{3.0488 \times 10^{-5} \times 5192.1}{0.23952} = 0.6609$$

The mass flow rate G of the coolant (helium) per unit area to be cooled can be computed as follows

$$G = \frac{\dot{m}_h}{\pi \left(\frac{d}{2}\right)^2} = \frac{0.0109 \times 4}{\pi d^2} \text{ kg s}^{-1} \text{ m}^{-2}$$

where d (m) is the inside diameter of the helium passage. In the present case, the heat is transferred through a vapour-film boundary layer, because the coolant is helium in supercritical conditions of pressure and temperature.

Therefore, the heat transfer coefficient on the helium side computed above ($h_h = 1631 \text{ W m}^{-2} \text{ K}^{-1}$) satisfies the following correlation due to McCarthy and Wolf [14, page 95, Eq. 2]:

$$h_h = 0.025 \left(\frac{c_p \mu^{0.2}}{Pr^{0.6}} \right)_{co} \frac{G^{0.8}}{d^{0.2}} \left(\frac{T_{co}}{T_{wc}} \right)^{0.55}$$

where μ (N s m^{-2}) is the coefficient of dynamic viscosity of helium, c_p ($\text{J kg}^{-1} \text{ K}^{-1}$) is the isobaric specific heat of helium, Pr is the Prandtl number of helium, T_{co} (K) is the bulk temperature of helium, T_{wc} (K) is the temperature of the wall on the helium side, and the subscript co indicates the bulk temperature ($T_{co} = 554 \text{ K}$) of the coolant (helium). By substituting the quantities computed above into the McCarthy-Wolf correlation, there results

$$1631 = 0.025 \left(\frac{5192 \times 0.00003049^{0.2}}{0.6609^{0.6}} \right) \left(\frac{0.0109 \times 4}{\pi d^2} \right)^{0.8} \frac{1}{d^{0.2}} \left(\frac{554}{754} \right)^{0.55}$$

The preceding equation, solved numerically for d , yields

$$d = 0.01205 \text{ m}$$

which is the inside diameter of the helium passage in the heat exchanger.

The maximum tensile combined pressure and thermal stress σ_t (N/m^2) at the outlet section of the heat exchanger can be determined by using the following equation of Chap. 2, Sect. 2.5

$$\sigma_t = \frac{(p_{co} - p_g)r}{t} + \frac{E\lambda qt}{2(1-\nu)k} + \frac{6M_A}{t^2}$$

where p_{co} (N/m^2) is the pressure of the coolant, p_g (N/m^2) is the pressure of the combusted gas, r (m) is the radius of the cross section of the cooling tubes, t (m) is the thickness of the cooling tubes, E (N/m^2) is the modulus of elasticity of the material of which the cooling tubes are made, λ (K^{-1}) is the coefficient of thermal expansion of the same material, q (W/m^2) is the quantity of heat per unit time per unit surface, ν is the Poisson ratio of the same material, k ($\text{W m}^{-1} \text{ K}^{-1}$) is the thermal conductivity of the same material, and M_A (Nm/m) is the bending moment per unit length acting on a cross section A-A of the circular cooling tube due to the distortion induced by discontinuities. In the present case, we assume $p_{co} - p_g \approx p_{co} = 3.103 \times 10^7 \text{ N/m}^2$ and neglect the third term (containing M_A) in comparison with the other two terms on the right-hand side of the preceding equation. Thus, the maximum stress at the outlet section of the heat exchanger is

$$\begin{aligned}\sigma_t &= \frac{3.103 \times 10^7 \times 0.01205}{2 \times 0.00127} \\ &+ \frac{1.1 \times 10^{11} \times 10.44 \times 10^{-6} \times 3.262 \times 10^5 \times 0.00127}{2 \times (1 - 0.30) \times 17.1} \\ &= 1.671 \times 10^8 \text{ N/m}^2\end{aligned}$$

This value is lower than the tensile yield strength ($\sigma_y = 1.3 \times 10^9 \text{ N/m}^2$) of the alloy Ti–13V–11Cr–3Al.

Now, in order to determine the maximum tensile combined pressure and thermal stress σ_t (N/m^2) at the inlet section of the heat exchanger, the difference between the maximum temperature of the wall on the combusted gas side (778 K) and the bulk temperature of the helium in the heat exchanger is assumed to remain approximately constant throughout the heat exchanger. The bulk temperature of the helium results from the difference $T_o - T_i = 554 - 192 = 362 \text{ K}$. Therefore, the mean temperature of the wall on the combusted gas side at the inlet section of the heat exchanger is

$$T_{wg} = 778 - 362 = 416 \text{ K}$$

Remembering again the following equation of Chap. 2, Sect. 2.5

$$q = h_g(T_{aw} - T_{wg})$$

where q (W/m^2) is the quantity of heat transferred per unit time per unit surface through convection at the inlet section of the heat exchanger, there results

$$q = 167.8 \times (2722 - 416) = 3.869 \times 10^5 \text{ W/m}^2$$

By using again the equation of Chap. 2, Sect. 2.5

$$\sigma_t = \frac{(p_{co} - p_g)r}{t} + \frac{E\lambda qt}{2(1-\nu)k} + \frac{6M_A}{t^2}$$

with $p_{co} - p_g \approx p_{co} = 3.103 \times 10^7 \text{ N/m}^2$ and neglecting the third term (containing M_A) in comparison with the other two terms on the right-hand side of the preceding equation, the maximum tensile combined pressure and thermal stress σ_t (N/m^2) at the inlet section of the heat exchanger results

$$\begin{aligned} \sigma_t &= \frac{3.103 \times 10^7 \times 0.01205}{2 \times 0.00127} \\ &+ \frac{1.1 \times 10^{11} \times 10.44 \times 10^{-6} \times 3.869 \times 10^5 \times 0.00127}{2 \times (1 - 0.30) \times 17.1} \\ &= 1.708 \times 10^8 \text{ N/m}^2 \end{aligned}$$

This value is lower than the tensile yield strength ($\sigma_y = 1.3 \times 10^9 \text{ N/m}^2$) of the alloy Ti–13V–11Cr–3Al.

Therefore, it is safe to choose a tube made of the alloy Ti–13V–11Cr–3Al, 0.00127 m in thickness and 0.01205 m in inner diameter, for the heat exchanger. The margin of safety is sufficiently large, should the temperature at the inlet section of the heat exchanger be higher than the maximum temperature considered above.

Now, in order to determine the number of turns for the tube of the heat exchanger, the effective area A (m^2) of the heat exchanger is determined by means of the following equation

$$\dot{m}_h c_p (T_o - T_i) = A \left(\frac{1}{hg} + \frac{t}{k} + \frac{1}{h_h} \right)^{-1} \left(T_{aw} - \frac{T_i + T_o}{2} \right)$$

We first substitute $\dot{m}_h = 0.0109 \text{ kg/s}$, $c_p = 5192 \text{ J/(kg K)}$, $T_o = 554 \text{ K}$, $T_i = 192 \text{ K}$, $h_g = 167.8 \text{ W m}^{-2} \text{ K}^{-1}$, $t = 0.00127 \text{ m}$, $k = 17.1 \text{ W/(m K)}$, $h_h = 1631 \text{ W m}^{-2} \text{ K}^{-1}$, and $T_{aw} = 2722 \text{ K}$, and then solve the preceding equation for A . This yields

$$\begin{aligned} A &= \frac{0.0109 \times 5192 \times (554 - 192)}{(2722 - \frac{192+554}{2})} \\ &\times \left(\frac{1}{167.8} + \frac{0.00127}{17.1} + \frac{1}{1631} \right) = 0.05797 \text{ m}^2 \end{aligned}$$

Since the area of the thrust chamber at the throat is $A_t = 0.02606 \text{ m}^2$ (see above), then the corresponding diameter at the throat is

$$D_t = \left(\frac{4A_t}{\pi} \right)^{\frac{1}{2}} = \left(\frac{4 \times 0.02606}{3.1416} \right)^{\frac{1}{2}} = 0.1822 \text{ m}$$

and the diameter of the thrust chamber at the section of area ratio $\varepsilon \equiv A/A_t = 10$ is

$$D = D_t(\varepsilon)^{\frac{1}{2}} = 0.1822 \times (10)^{\frac{1}{2}} = 0.5761 \text{ m}$$

Assuming that a portion of 40% of the internal surface of N turns of tube is the effective area $A = 0.05797 \text{ m}^2$ of the heat exchanger, A is the area of a rectangle of base πD and altitude $0.4 N \pi d$. Therefore, the number N of turns of the tube of the heat exchanger results from

$$N = \frac{A}{(\pi D)(0.4\pi d)} = \frac{0.05797}{3.1416^2 \times 0.5761 \times 0.01205 \times 0.4} = 2.115$$

where $d = 0.01205 \text{ m}$ is the inside diameter of the tube, and $D = 0.5761 \text{ m}$ is the diameter of the thrust chamber at the section of area ratio $\varepsilon = 10$. The diameter D is assumed to remain constant along the altitude of the rectangle indicated above.

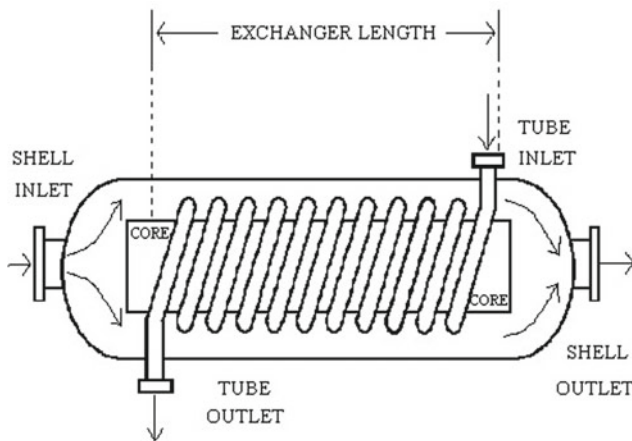
3.4 Feed Systems Using Evaporation of Two Propellants

The feed systems described here have been used prevalently, if not exclusively, in rocket engines using cryogenic or near-cryogenic propellants. A description and a list of these propellants are given in Chap. 1, Sect. 1.4.

In particular, these feed systems have been used in large rocket vehicles whose propulsion systems are fed by pumps. They have been used especially for oxidisers, because most fuels tend to boil violently when heated. However, liquid hydrogen, which is a fuel, is an exception to this rule. Since the oxidiser vapour has usually a high molar mass, feed systems using evaporation of two propellants require a mass of pressurising gas for the oxidiser tank higher than the mass required by systems using inert gases, such as those described in Sect. 3.3. This undesirable effect is counterbalanced by the elimination of storage vessels, because in feed systems using evaporation of two propellants the pressurising agent is stored as a liquid in the tank containing the main propellant.

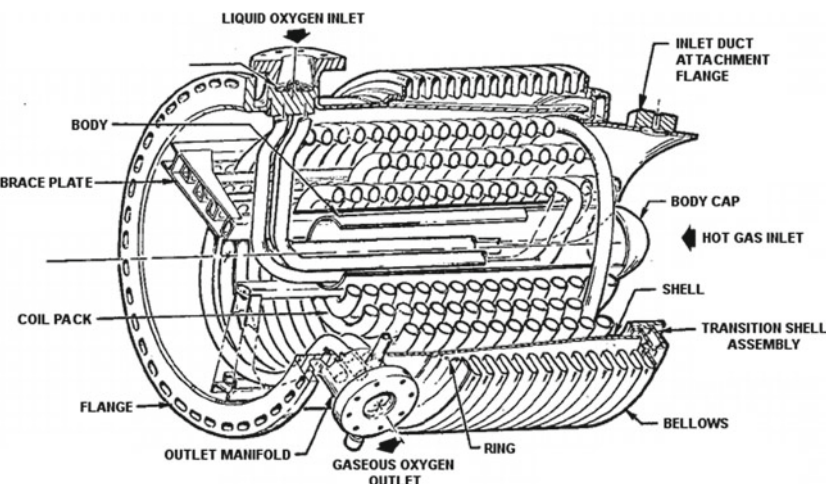
Feed systems based on evaporation of two propellants used for pump-fed rocket engines take propellants tapped off downstream of the pump and vaporised in a heat exchanger. These propellants are then used to pressurise the main propellant tank from which they have been taken. There are many types of heat exchangers. One of them is the helical-coil type, which is described below. A functional scheme of this heat exchanger is shown in the following figure, due to the courtesy of Wikimedia

[15], which illustrates a heat exchanger designed by US Army Colonel Scott S. Haraburda.



A helical-coil heat exchanger consists essentially of a shell (which is a container, usually cylindrical, designed to hold a fluid at a pressure much higher than the ambient pressure) and a tube wound around a core inside the shell. One of two fluids runs through the tube, from the inlet to the outlet section, and the other fluid flows over the tube, from the inlet to the outlet section of the shell, in order to transfer heat from one fluid to the other.

The following figure, due to the courtesy of NASA [2], illustrates another type (shell-and-tube) of heat exchanger used to vaporise liquid cryogenic propellants for evaporated-propellant pressurisation, as will be shown below.



This particular heat exchanger, which has been used for the J-2 rocket engine, is a shell assembly, consisting of a duct, bellows, flanges, and coils. It is mounted in the turbine exhaust duct between the oxidiser turbine discharge manifold and the thrust chamber. It heats and expands gaseous helium for use in the third stage of the Saturn V rocket or converts liquid oxygen to gaseous oxygen for the second stage for maintaining pressurisation in the oxidiser tank of the vehicle. During engine operation, either liquid oxygen is tapped off the oxidiser high-pressure duct or helium is provided from the vehicle stage and routed to the heat exchanger coils [16].

Heat exchangers have also been employed on the Titan rockets to vaporise liquid nitrogen tetroxide to be used as the pressurising agent [2].

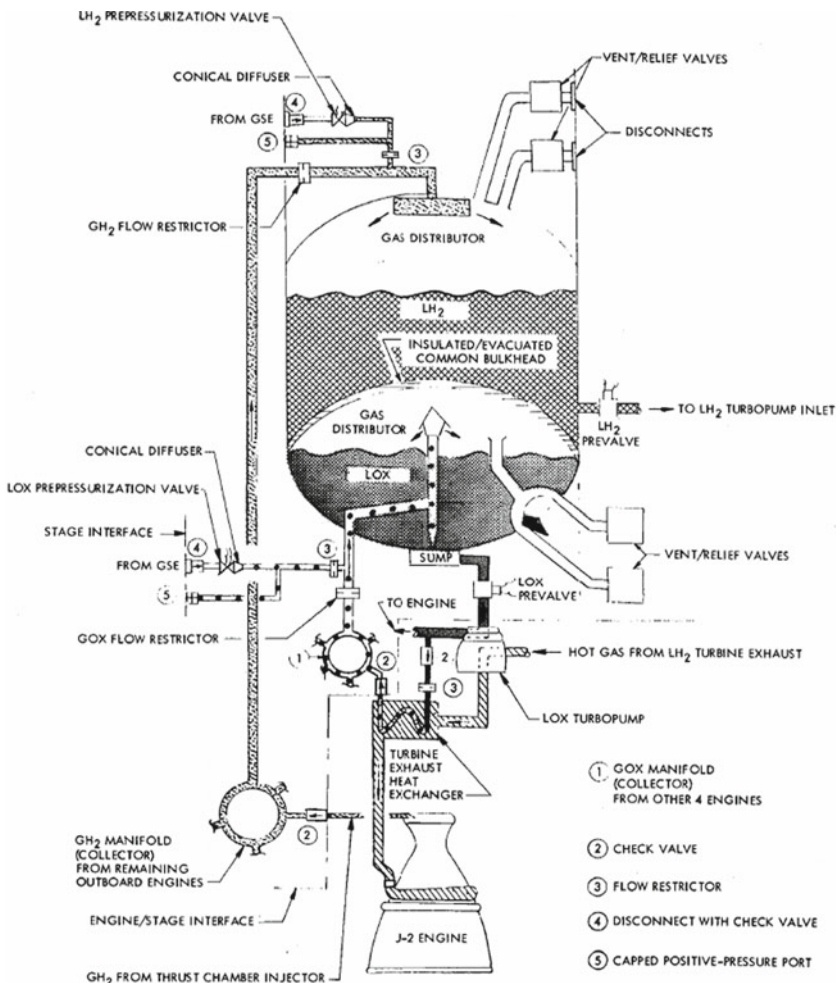
As has been shown above, evaporated-propellant pressurisation is successful with cryogenic propellants and also with the storable oxidiser nitrogen tetroxide, whose boiling point is 294.2 K. The simplest method of evaporated-propellant pressurisation is self-pressurisation (flash boiling) in a propellant tank during feed-out. By the way, flash boiling is the phenomenon which occurs in a heated liquid whose pressure is lower than the saturation vapour pressure of the liquid. When the pressure falls sufficiently below the saturation vapour pressure, then rapid boiling of the liquid can result.

The self-pressurisation method is reliable, but the mass requirements of the pressurising agent are high, because of its low temperature, and hence of its high density. In addition, pre-pressurisation from a separate system may be necessary to meet engine start requirements, as was the case with the Centaur rocket vehicle [2]. In this case, the vapour pressure of bulk propellants (hydrogen and oxygen) boiling in the tanks was used to provide the modest pressure required at the inlet of tank-mounted boost pumps. In systems requiring higher pressures, superheated vapour is obtained by passing the propellant through an engine heat exchanger or some other heat source, as will be shown below.

More favourable conditions exist in the ullage space when the pressurising agent is heated to the maximum temperature compatible with structural and propellant requirements, and when the temperature of the gas in the ullage space is stratified, that is, controlled by heating or cooling at the tank wall and upper bulkhead [2].

In the S-II (meaning by this name the second stage of the Saturn V rocket), which used evaporated-propellant pressurisation in both oxidiser and fuel systems, propellant vapour was superheated to reduce the mass of gas required to the minimum. For main stage pressurisation, the oxidiser tank of the S-II was pressurised with warm gaseous oxygen (275 ± 8 K at the maximum mixture ratio, and 250 ± 8 K at low mixture ratio). As shown in the following figure, due to the courtesy of NASA [2], the pressurising agent for the oxygen was obtained by extracting a portion of the liquid oxygen (at a temperature of approximately 94 K) leaving the discharge area of the pump and routing this fluid through the shell-and-tube heat exchanger, which has been shown in the preceding figure. The turbine outlet gas provided the heat source (at 598 ± 30 K at the maximum mixture ratio, and 548 ± 35 K at low mixture ratio) for the heat exchanger. Within the heat exchanger, the liquid oxygen was vaporised and then routed into a collector. From there, the gaseous oxygen was routed into the ullage space of the oxygen tank through a flow restrictor and gas distributor.

The fuel tank of the S-II was pressurised with gaseous hydrogen extracted from the cooling jacket of the thrust chamber, where this fluid was used as a coolant. The temperature of the pressurising hydrogen ranged from 111 ± 11 K at the maximum mixture ratio to 72 ± 17 K at low mixture ratio. The pressurising hydrogen was collected from the four outboard engines and was routed to the ullage space via the hydrogen-tank flow-control orifice and gas distributor.



The pressure in both of the propellant tanks can be adjusted by means of valves or regulators, as has been shown above. The mass flow rate of each propellant (oxidiser or fuel) required for vaporisation and pressurisation depends on the mass flow rate of that propellant at the pump inlet (or at the tank outlet) and also on the heat and mass transfer processes which occur in the propellant tanks. These processes, in

turn, depend on the temperature of the environment and on the temperature of the pressurising agent.

Let \dot{m} (kg/s) be the propellant mass flow rate at the pump inlet for each of the N engines of a rocket stage, p_T (N/m²) be pressure of one of the propellants (oxidiser or fuel) in the tank, ρ (kg/m³) be the density of the liquid propellant, R (N m kg⁻¹ K⁻¹) be the specific gas constant of the vaporised propellant, T (K) be the temperature of the gas in the ullage space of the tank, \dot{m}_e (kg/s) be the mass flow rate of evaporation of the propellant, and \dot{m}_v (kg/s) be the average flow rate of the propellant through the tank vent. When the values of these quantities are known, then the required flow rate of propellant \dot{m}_p (kg/s), for each engine, tapped off for tank pressurisation can be determined by means of the following equation [3]:

$$\dot{m}_p = \frac{\dot{m} p_T}{\rho R T} - \frac{\dot{m}_e - \dot{m}_v}{N}$$

For example, we consider a rocket stage having the following properties: oxidiser (liquid oxygen) mass flow rate at the pump inlet for each engine $\dot{m} = 131.8$ kg/s, pressure of the oxidiser in the tank $p_T = 3.103 \times 10^5$ N/m², density of the liquid oxidiser $\rho = 1141$ kg/m³, specific gas constant of the vaporised oxidiser $R = R^*/\mathcal{M} = 8314.46/32 = 259.8$ N m kg⁻¹ K⁻¹, temperature of the gas in the ullage space of the oxidiser tank $T = 122$ K, mass flow rate of evaporation of the oxidiser $\dot{m}_e = 0.7527$ kg/s, average flow rate of the oxidiser through the tank vent $\dot{m}_v = 0.7439$ kg/s, and $N = 4$ engines in the rocket stage.

By substituting these data in the preceding equation, the required mass flow rate of oxidiser \dot{m}_o , for each engine, tapped off for tank pressurisation results

$$\dot{m}_o = \frac{131.8 \times 3.103 \times 10^5}{1141 \times 259.8 \times 122} - \frac{0.7527 - 0.7439}{4} = 1.129 \text{ kg/s}$$

The same calculation can be repeated for the other propellant (liquid hydrogen) of the same rocket stage, knowing the following data: fuel mass flow rate at the pump inlet for each engine $\dot{m} = 27.12$ kg/s, pressure of the fuel in the tank $p_T = 2.62 \times 10^5$ N/m², density of the liquid fuel $\rho = 70.8$ kg/m³, specific gas constant of the vaporised fuel $R = R^*/\mathcal{M} = 8314.46/4 = 2078.6$ N m kg⁻¹ K⁻¹, temperature of the gas in the ullage space of the fuel tank $T = 67$ K, mass flow rate of evaporation of the fuel $\dot{m}_e = 1.905$ kg/s, and average flow rate of the fuel through the tank vent $\dot{m}_v = 2.994$ kg/s. The required mass flow rate of fuel \dot{m}_f , for each engine, tapped off for tank pressurisation results

$$\dot{m}_f = \frac{27.12 \times 2.62 \times 10^5}{70.8 \times 2078.6 \times 67} - \frac{1.905 - 2.994}{4} = 0.9929 \text{ kg/s}$$

3.5 Feed Systems Using Gases Stored for Mono-Propellants

These feed systems have not been employed frequently so far, because of the low specific impulses (230–240 s) which can be obtained by using traditional mono-propellants. One of these system was employed for the orbit adjust subsystem (OAS) of the Landsat satellites, which used a hydrazine (N_2H_4) propellant tank with a bladder and nitrogen (N_2) as the pressurising gas [2].

They have recently attracted considerable interest during continuous efforts aimed at replacing hydrazine with one of the so-called green propellants, which are less toxic and easier to handle and store than hydrazine.

The chemical substances considered for this purpose are ionic compounds used in concentrated aqueous solutions. Each of these compounds contains an ionic liquid (oxidiser) and a fuel (reducer). By ionic liquids we mean ionic compounds (salts) which are liquid below 373 K. More commonly, ionic liquids have melting points below room temperature [17].

According to Fahrat et al. [18], some of these oxidisers are:

- HAN (hydroxyl ammonium nitrate) $[NH_3OH]^+[NO_3]^-$
- ADN (ammonium dinitramide) $[NH_4]^+[N(NO_2)_2]^-$
- HFN (hydrazinium nitroformate) $[N_2H_5]^+[C(NO_2)_3]^-$
- AN (ammonium nitrate) $[NH_4]^+[NO_3]^-$
- HN (hydrazinium nitrate) $[N_2H_5]^+[NO_3]^-$

According to the same authors [18], ionic or molecular fuels associated with these oxidisers are:

- TEAN (trisethanol ammonium nitrate) $[NH(C_2H_4OH)_3]^+[NO_3]^-$
- AA (ammonium azide) $[NH_4]^+[N_3]^-$
- HA (hydrazinium azide) $[N_2H_5]^+[N_3]^-$
- HEHN (2-hydroxyethylhydrazinium nitrate) $[HO-C_2H_4-N_2H_4]^+[NO_3]^-$
- Methanol, ethanol, glycerol, glycine, urea

As has been shown in Chap. 1, Sect. 1.4, of all the oxidisers indicated above, those which have been attracted particular interest are hydroxyl ammonium nitrate and ammonium dinitramide.

Hydroxyl ammonium nitrate, also known as HAN, is a salt derived from hydroxyl amine (NH_2OH) and nitric acid (HNO_3). The Air Force Research Laboratory at Edwards Air Force Base in California, USA, has developed a hydroxyl ammonium nitrate-based propellant known as AF-M315E. This propellant is less toxic and easier to handle than hydrazine, and has a specific impulse $I_s = 257$ s, which is about 12% greater than the specific impulse of hydrazine, the latter being $I_s = 230$ s. It requires a catalyst bed preheating at a temperature exceeding 558 K to be ready for general operation [19].

Ammonium dinitramide, also known as ADN, whose chemical formula is $NH_4N(NO_2)_2$, is the ammonium (NH_4^+) salt of the dinitraminic acid ($HN(NO_2)_2$), and was invented in the 1970s in the former Soviet Union and independently

invented again in 1989 in the United States by SRI International. Gaseous ammonium dinitramide decomposes under heat into ammonia (NH_3), nitrous oxide (N_2O), and nitric acid (HNO_3). The Swedish company EURENCO Bofors produces a liquid mono-propellant, called LMP-103S, as a substitute for hydrazine by dissolving 65% ammonium dinitramide in 35% water solution of methanol (CH_3OH) and ammonia (NH_3). LMP-103S has 6% higher specific impulse and 30% higher impulse density (see below) than hydrazine mono-propellant [20]. LMP-103S has been tested in the PRISMA (Prototype Research Instruments and Space Mission technology Advancement, COSPAR designation 2010-028B and 2010-028F) mission in 2010.

The following table, adapted from [21], shows some performance data of the LMP-103S and AF-M315E mono-propellants in comparison with hydrazine.

	LMP-103S	AF-M315E	Hydrazine
Flame Temperature	1873 K	2173 K	873 K
I_s	252 s (theor.) 235 s (delivered)*	266 s (theor.) ~250 s (delivered)	220-224 s (1N thrusters)
Density (kg/m^3)	1240*	1465	1010
Density I_s Increase over N_2H_4	30%*	50%	-
Preheat Temperature	573 K nominal	643 K nominal	588 K Capable of cold starts (278 K)
Minimum Operational Temperature	283 - 323 K	< 273 K System dependent – Propellant becomes viscous, but no precipitation or phase change occurs.	278 - 323 K
Minimum Storage Temperature	266 K	Very low (< 295 K) Forms a glass – no crystallization occurs	274 K (Freezing Point) Reheated for re-use

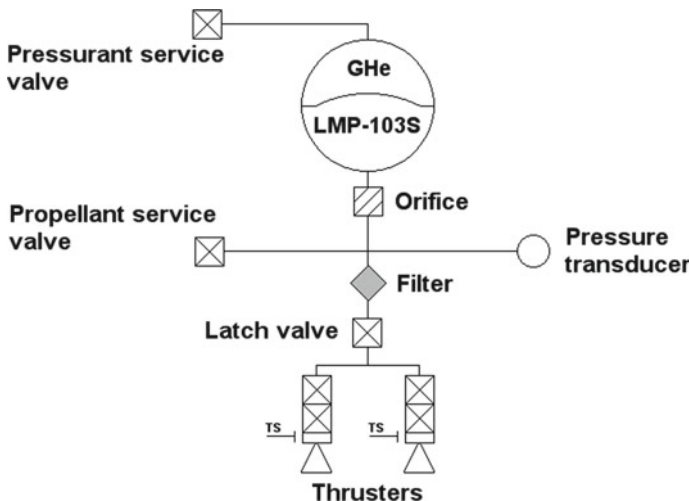
*Anfø, K. and Mollerberg, R., "Flight Demonstration of New Thruster and Green Propellant Technology on the PRISMA Satellite" ACTA Astronautica, Vol. 65, Nov.-Dec. 2009

Distribution A: Approved for public release; distribution unlimited

The following table, from [21], shows some compatibility and handling properties of the LMP-103S and AF-M315E mono-propellants in comparison with hydrazine.

Propellant	LMP-103S	AF-M315E
Thruster Materials Compatibility	High combustion temperature and oxidative environment - high temperature, corrosion resistant refractory metal (Ir and Re) chamber materials needed.	High combustion temperature and oxidative environment - high temperature, corrosion resistant refractory metal (Ir and Re) chamber materials needed.
System Materials Compatibility	Compatible with most COTS materials currently used for N ₂ H ₄ systems. Propellant is basic – compatible with many metals.	Limited material compatibility driven primarily by HAN content and acidity
Handling & Safety	Significantly reduced toxicity removes the need for SCAPE suits	Low toxicity and vapor pressure allow handling with only basic PPE Propellant will not crystallize if concentrated

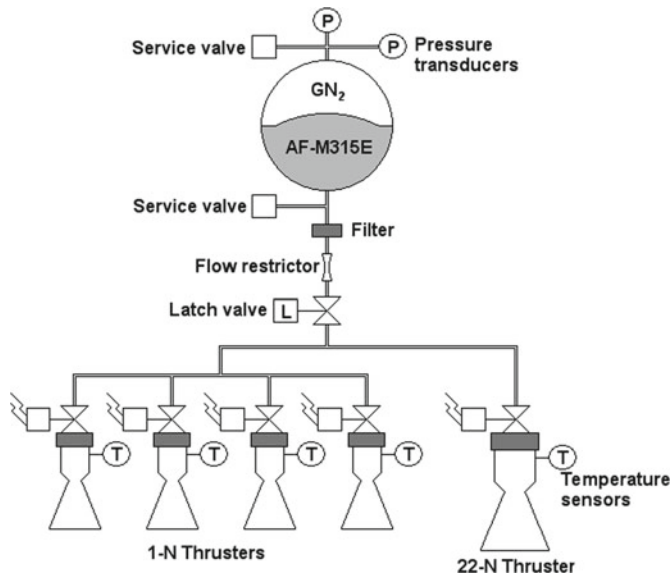
The following figure (re-drawn from [22]) illustrates the feed system used in a spacecraft during the PRISMA mission.



This system consists of one propellant tank with an internal flexible diaphragm, two service valves, one pressure transducer, one filter system, one isolation latch valve, and two 1-N mono-propellant thrusters. The tank contains 5.6 kg of LMP-103S propellant. All of these components are of the commercial off-the-shelf (COTS) type used for hydrazine thrusters. The tubes are 6 mm in diameter and are made of corrosion-resistant steel. All the components are welded to the tubes. The feed pressure decreases in proportion to the consumed propellant. The initial pressure is 2.2×10^6 N/m² at 293 K. This value decreases to 0.5×10^6 N/m² when all propellant is consumed. The thrust decreases from an initial value of 1 N to a final value of 0.25 N. The propellant and the gas (helium) under pressure are stored in the same tank and are separated by means of a flexible diaphragm. The gas acts on

this diaphragm by pushing the propellant through the system filter to the control valve, which controls the flow of propellant to the thruster. The thruster requires pre-heating before firing. When the firing command is given, the series redundant flow control valve opens and admits the propellant in the thrust chamber. There, the propellant decomposes and ignites in the pre-heated reactor bed. This generates hot gases and hence thrust. The pressure transducer and the tank temperature sensor are used to determine the correct amount of propellant. All components are powered by a remote terminal unit with 28 ± 1 V of direct current. The temperature of this unit is controlled by a thermal control remote terminal unit, and is kept in the range of 283–323 K during the entire mission [22].

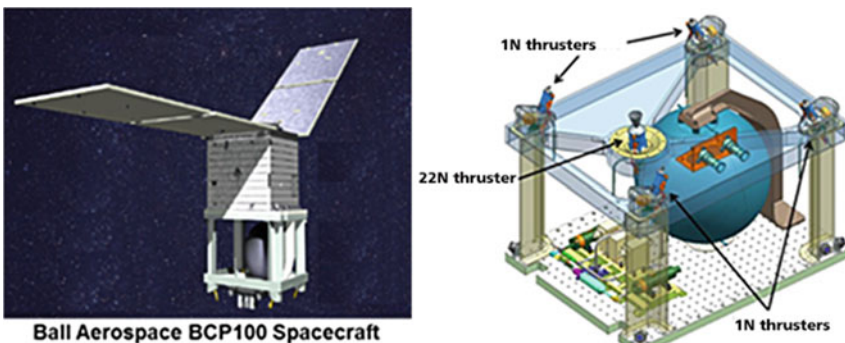
The following figure (re-drawn from [19]) illustrates the feed system to be used in the GPIM (Green Propellant Infusion Mission).



In this mission [23], scheduled for 2018, NASA wants to demonstrate the practical capabilities of the AF-M315E propellant. This feed system consists principally of one propellant tank with an internal flexible diaphragm, two service valves, two pressure transducers, one filter, one flow restrictor, one isolation latch valve, four 1-N thrusters for attitude control, and one 22-N primary divert thruster. Each of these thrusters has a single-seat valve and a temperature sensor. The feed system operates in blow-down mode, which means that the pressure decreases in proportion to the amount of consumed propellant. The gas stored under pressure over the diaphragm is nitrogen. The system components used for AF-M315E are in many cases those used for hydrazine. The 1-N thrusters and the 22-N thruster require a pre-heating of the catalyst bed before firing. The power requirements relating to this pre-heating are high, due to the elevated minimum start temperature of the thrusters. These thrusters use the LCH-240 high-temperature long-life catalyst developed by Aerojet

Rocketdyne. The use of refractory alloys, necessary to withstand the high flame temperature of the AF-M315E propellant, is confined to the thrust chamber, the nozzle, and an upper thermal isolation structure. The other parts of the thrusters can be made of conventional alloys used for hydrazine thrusters [19].

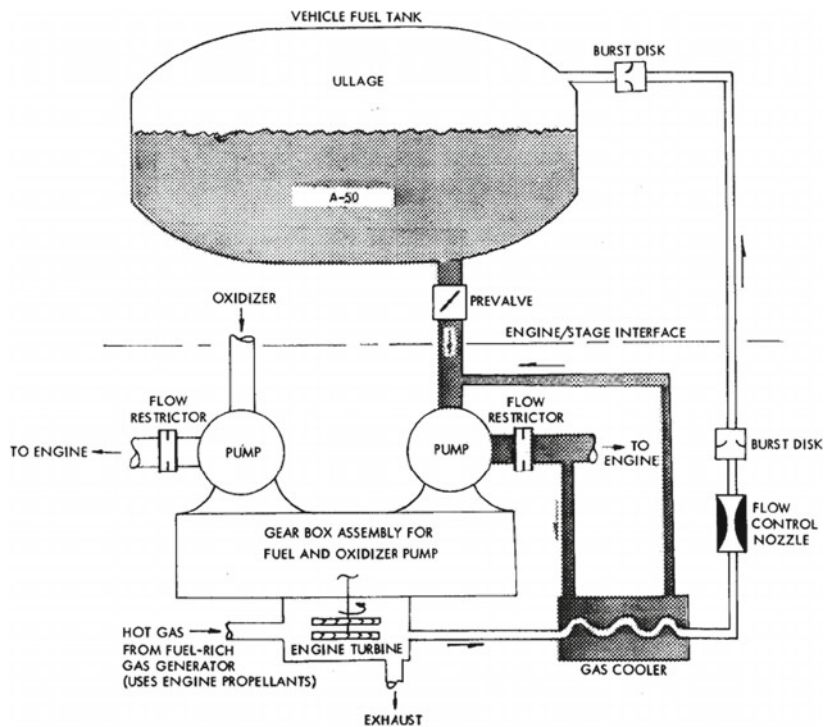
The BCP100 spacecraft, manufactured by Ball Aerospace, and its propulsion system described above are shown in the following figure, due to the courtesy of Aerojet Rocketdyne [24].



The criteria of design and the methods of calculation for the feed systems described here are similar to those described in Sect. 3.3.

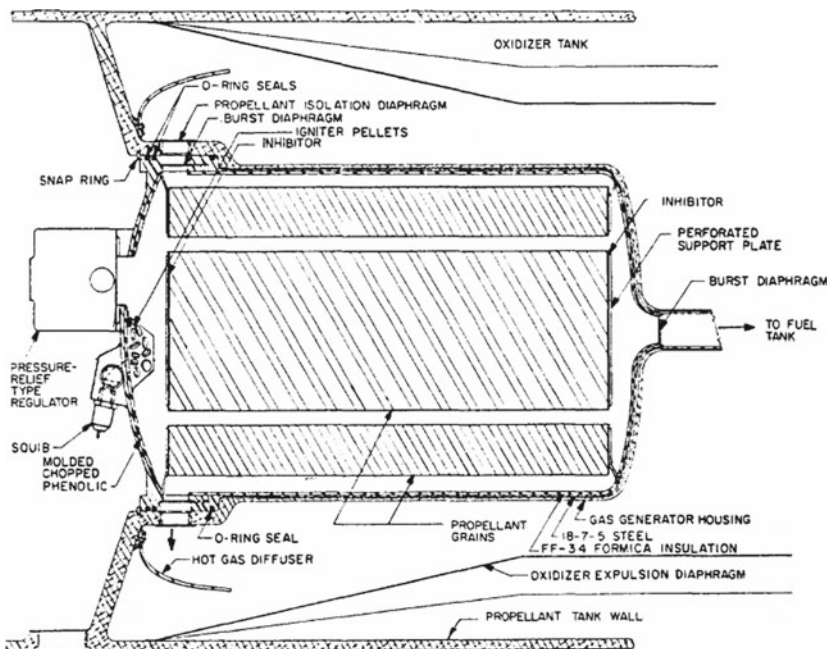
3.6 Feed Systems Using Combustion Products

In a feed system using combustion products, the pressurising gas is obtained by combustion of propellants in a turbine gas generator, or by combustion in a solid-propellant gas generator, or by injection of a hypergolic fluid into the main propellant tank. This system has been used to supply pressurising gas in several small military vehicles, and also to pressurise the fuel tanks of the Titan stages. It has rarely been used, because the pressurising gas is chemically incompatible with the propellants, or has a temperature too high, or has condensable elements. A scheme of the feed system used in the Titan stages is shown in the following figure, due to the courtesy of NASA [2].



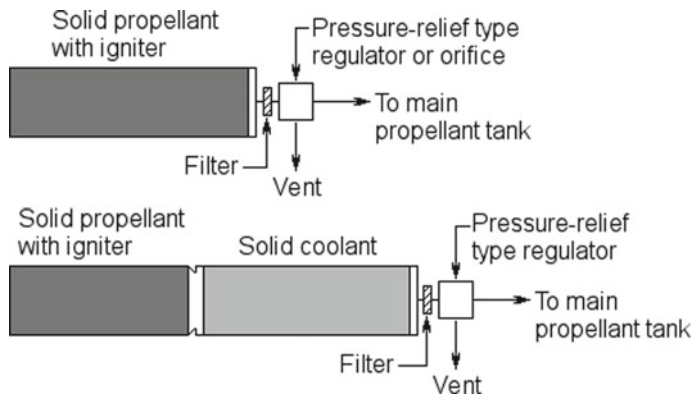
The rocket engine uses nitrogen tetroxide (N_2O_4) as the oxidiser and Aerozine 50 as the fuel. The gas generator uses the engine propellants to produce fuel-rich exhaust gases which drive the engine turbo-pumps. The combustion temperature in this gas generator is about 1256 K at a fuel-rich mixture ratio $o/f = 0.085$. The temperature at the turbine outlet is about 1183 K. The pressurising gas is tapped off at the turbine outlet, passed through a gas cooler, and then routed to the fuel tank. It is injected into the fuel tank within a temperature range of 361 K to 417 K. The flow of the pressurising gas is controlled by a flow-control nozzle located downstream of the gas cooler [2].

The following figure, due to the courtesy of NASA [3], shows a solid-propellant gas generator, which is a small device burning a solid propellant to supply hot gas under pressure to the main liquid propellants.



A gas generator like this can be employed to pressurise tanks of rocket engines using storable liquid propellants. This gas generator consists of two electrically-fired initiators (squibs), one charge of igniter pellets, some safety and arming devices, one regulator of the pressure-relief type, and two solid-propellant grains. There may also be, in some cases, a device to cool the hot gas produced. The gas generator illustrated above is contained in an insulated housing made of steel. This housing, in turn, is contained in the main propellant tank, which is made of an aluminium alloy. The gas outlets are hermetically sealed by means of burst diaphragms which assure a safe storage of the solid propellant over long periods of time. At the proper moment, the propellant grains are ignited by the igniter pellets. The gases generated by the combustion process pressurise the main propellants for the duration of the propellant grains. Such grains are designed to produce the desired pressures and flow rates within a given range of temperature. In case of the upper limit of temperature being exceeded, a regulator discharges overboard the excess gases.

Some types of solid-propellant gas generators used for feed systems are briefly described below. The following figure illustrates two solid-propellant gas generators, one of which without cooling and the other with a solid coolant.

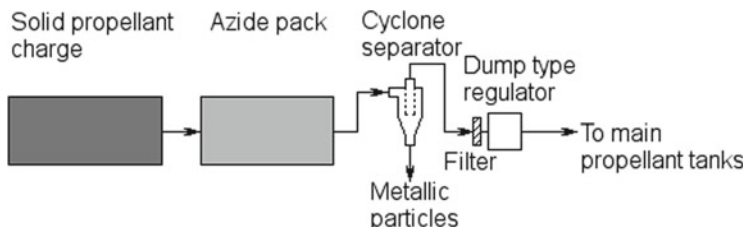


The gas generator shown in the upper part of the preceding figure consists of a solid-propellant charge with igniter, a filter, and a hot-gas regulator or an orifice. This type of gas generator can be used only for short periods of time. When the solid propellant is ignited, the hot gases are passed through the filter, regulated, and directed to the main propellant tanks. The regulator or the orifice mentioned above dumps overboard the excess gas, and therefore a vent line must be present for this purpose.

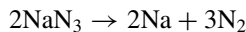
The gas generator shown in the lower part of the preceding figure consists of a solid-propellant charge with igniter, a sublimating solid coolant, a filter, and a regulator. When the solid propellant is ignited, the hot gases are cooled by passing through a solid material which decomposes or sublimates. This cooling process generates additional gases. The mixture of gases generated in this manner is passed through the filter, regulated, and directed to the main propellant tanks.

Huzel and Huang [3] describe a gas generator using ammonium nitrate (NH_4NO_3) as the solid propellant, which has a flame temperature of about 1544 K. The ammonium nitrate is used with a solid coolant made of oxalic acid (HOOCCOOH or $(\text{COOH})_2$) compressed into pellets. Oxalic acid decomposes endothermically, at a temperature above 394 K, and produces a mixture of gases consisting of carbon monoxide (CO), carbon dioxide (CO₂), and water (H₂O). The desired temperature is obtained by adjusting the ratio of the propellant to the coolant. By so doing, a temperature of 478 K has been reached [3].

The following figure illustrates a solid-propellant gas generator having an azide cooling pack.

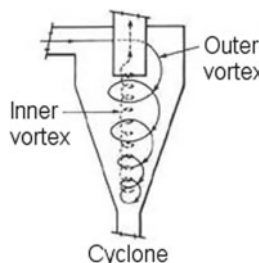


In this gas generator, the hot gas resulting from the combustion of a solid propellant is cooled by passing through an azide material. An example of this material is sodium azide (NaN_3), which decomposes after being heated at or above approximately 573 K into gaseous nitrogen (N_2) and sodium (Na) particles, as follows

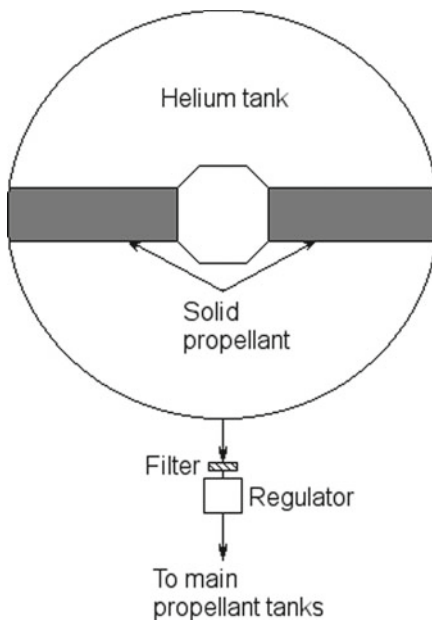


These particles are removed when the gas containing them passes through a cyclone separator. The gas coming from this separator is filtered to remove further particles, regulated, and directed to the main propellant tanks. A gas generator like this has made it possible to obtain gaseous nitrogen at a temperature of about 590 K [3].

Generally speaking, a cyclone separator is a device which removes solid particles from a gaseous or liquid stream without using filters. The solid particles are removed because they are denser than the other molecules of the stream. A fluid mixed with solid particles enters tangentially in a cyclone, which consists of a cylindrical body, a conical outlet for the particles, and a top axial pipe outlet for the clean fluid. An outer vortex is created due to the centrifugal force applied to the molecules, and the fluid circles down to the bottom end of the cone. Particles of high density are pushed against the wall and separated from the fluid. In the conical part, the fluid reverses the direction of its motion, goes up via the central part of the cyclone (inner vortex), and exits on the top by the fluid outlet pipe. The solid particles travel down the wall, and are collected into a receptacle at the bottom of the conical part. This device is shown in the following figure, due to the courtesy of the US Government [25].



Still another type of solid-propellant gas generator is the helium system with solid-propellant gas generator heating. This system consists of a spherical vessel storing helium at high pressure, a solid-propellant gas generator mounted inside this vessel, a filter, and a pressure regulator, as shown in the following figure.



This solid-propellant gas generator provides heat, which causes the helium to expand, and also additional pressurising gas. This system requires a large vessel to store the solid propellant and the helium at high pressure.

3.7 Control Systems for Liquid-Propellant Gas Generators

As has been shown in Sect. 3.6, liquid-propellant gas generators require a careful design, in order to avoid problems concerning the chemical compatibility of the pressurising gas with the propellants, or the temperature of this gas, or the presence of condensable elements into it. These problems can be solved by using control systems, which are described in the present paragraph.

As far as the chemical compatibility of the pressurising gas is concerned, hydrazine mono-propellant is considered satisfactory in view of the chemical characteristics and the molar masses of the gases (nitrogen and hydrogen) resulting from its decomposition in the presence of a catalyst. These gases contain no carbon, and therefore generate no deposits which could lower the performance of a heat exchanger. In case of gas generators using a combination of two liquid propellants, the gases generated by them can be made chemically compatible with the propellants by varying the value of the oxidiser-to-fuel mixture ratio o/f with respect to the stoichiometric value. By so doing, the same combination of propellants can be used to generate a pressurising gas compatible with both the oxidiser and the fuel. An example is given by the hypergolic combination of nitrogen tetroxide and Aerozine 50, which was used for the first and second stages of the Titan II Intercontinental Ballistic Missile and Titan space

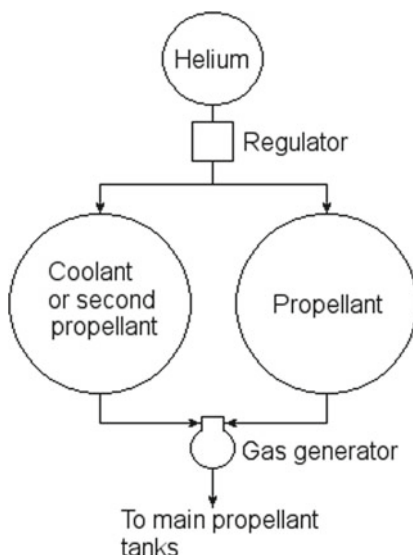
launch vehicles [26]. As has been shown in Sect. 3.6, the gas generator of the Titan engine uses the engine propellants to produce fuel-rich exhaust gases which drive the engine turbo-pumps.

As far as the temperature of the pressurising gas is concerned, more than one option can be chosen to assure compatibility. One of such options consists in varying of the value of the oxidiser-to-fuel mixture ratio to lower the combustion temperature, as has been shown above. Another option consists in injecting a non-reacting liquid into the gas generator, in order to subtract heat from the combusted gas in the evaporation of this liquid. A third option consists in cooling the gas by means of a heat exchanger, through which the gas flows with one of the liquid propellants. Of course, this option can be chosen only when the propellant can safely absorb the heat coming from the combusted gas.

The presence of condensable elements into the combusted gas can be avoided by regulating the combustion temperature, as will be shown below. In order for the molar mass of the combusted gas to be low, the combustion temperature of a fuel-rich mixture should reach a value (approximately 811 K) sufficient to break the bonds of the complex molecules of the combustion products and give rise to substances having low-mass molecules. Of course, this result can be obtained only when the fuel injected in excess into the gas generator does not reduce the combustion temperature below about 811 K. This is because, when the temperature is too low, some molecules of the combusted gas have a high molar mass, and these molecules are subject to condense.

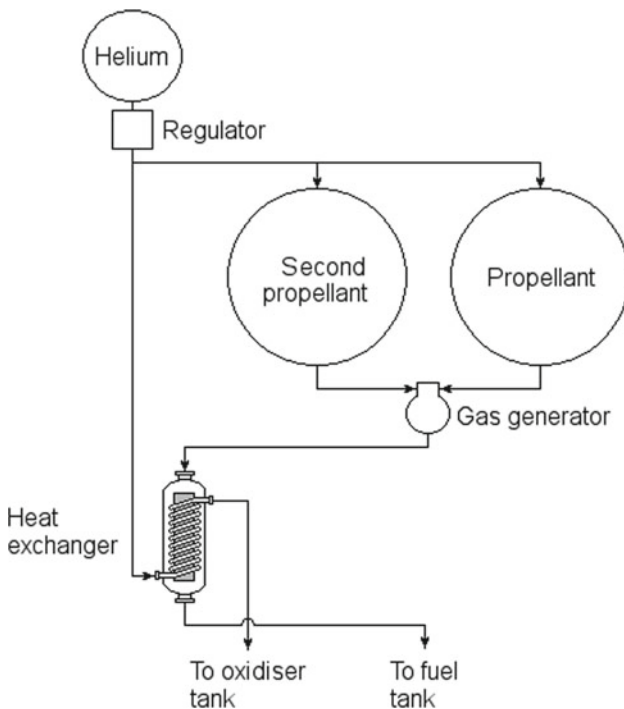
Some typical control systems used for liquid-propellant gas generators are briefly described below.

One of these control systems uses a single gas generator, which provides gas under pressure to both the fuel tank and the oxidiser tank, with injection cooling. A scheme of this system is shown in the following figure.



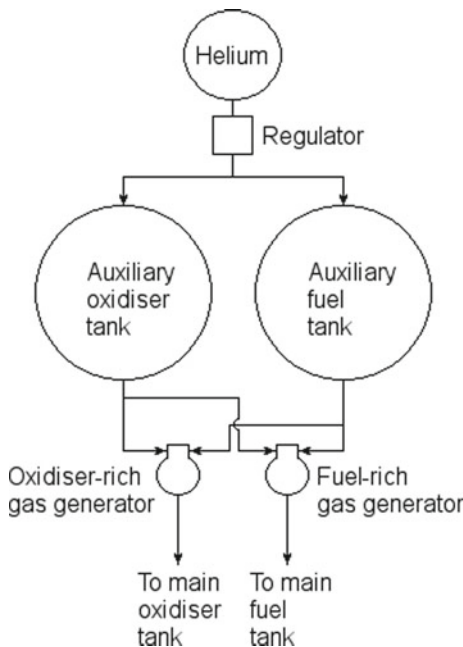
The liquid substances employed may be either a mono-propellant and an inert coolant or a combination of two propellants. In the second case, the cooling is obtained by injecting the second propellant in excess with respect to the quantity necessary for the stoichiometric mixture ratio. The mono-propellant and the coolant or the two propellants are kept under pressure by means of gaseous helium stored at a high pressure in a vessel. Downstream of this vessel, the pressure is kept to the desired value by using valves and a pressure regulator. This system makes it possible to cool the gas coming from the gas generator to a temperature compatible with the propellants. A combination of liquid substances must be studied carefully, in order to satisfy not only the temperature requirement, but also the other requirements, and in particular the one concerning the chemical compatibility of the pressurising gas with both of the propellants. To this regard, fuel-rich gases have been found apt to pressurise storable oxidisers. Examples of such oxidisers are given in [3].

Another of these control systems uses a single gas generator and a heat exchanger, as shown in the following scheme, which refers to the case of a gas generator using a combination of two propellants.



The hot gas coming from the gas generator is directed to a heat exchanger, in order to transfer heat to the cold helium. The helium expands after being heated and is used to pressurise the tank of the main oxidiser. The gas cooled through the gas generator is used to pressurise the tank of the main fuel.

Still another of these control systems uses a double gas generator, which provides gas under pressure to both the fuel tank and the oxidiser tank, with injection cooling. A scheme of this system is shown in the following figure.

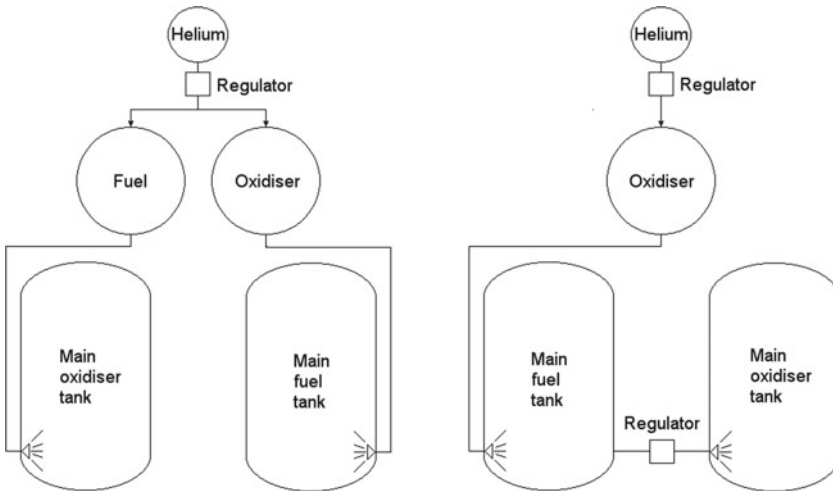


In this system, the fuel and the oxidiser are fed to two gas generators by using the pressure exerted by the helium. One of the gas generators operates with injection of excess oxidiser, and produces a cool, oxidiser-rich gas, which is used to pressurise the main oxidiser tank. The other gas generator operates with injection of excess fuel, and produces a cool, fuel-rich gas, which is used to pressurise the main fuel tank. This system requires a balance in the output of the two gas generators and also a pressure control in both of the main propellant tanks. By so doing, temperatures as low as 589 K have been reached in the gas generated [3].

3.8 Feed Systems Using Direct Injection into the Main Propellant Tanks

In these systems, a small quantity of oxidiser is injected directly into the main tank containing the fuel, and a small quantity of fuel is injected directly into the main tank containing the oxidiser. An hypergolic reaction, which takes place between the oxidiser and the fuel, produces gases used to pressurise the oxidiser and the fuel into

their respective main tanks. Two versions (parallel and serial) of the direct injection system are shown in the following figure.



The parallel version (left) of the system consists of a small vessel containing helium stored at high pressure, a helium pressure regulator, two small auxiliary propellant tanks (one for the fuel and the other for the oxidiser), and two main propellant tanks. The fuel is directly injected from its auxiliary tank into the main tank containing the oxidiser, and the oxidiser is directly injected from its auxiliary tank into the main tank containing the fuel.

The serial version (right) of the system consists of a small vessel containing helium stored at high pressure, a helium pressure regulator, only one small auxiliary propellant tank containing one of the two propellants, two main propellant tanks, and a regulator of the difference of pressure between the two main propellant tanks. The serial version takes advantage of the possibility of exerting a lower pressure in one of the two main propellant tanks than in the other. In the scheme shown on the right-hand side of the preceding figure, a small quantity of the fuel contained in its main tank passes through a regulator and is injected into the main tank containing the oxidiser.

3.9 Choice of a Feed System Using Gases Under Pressure

The choice of one of another system which uses gases stored under pressure is usually the result of a preliminary study. Huzel and Huang [3] have suggested four criteria to be considered in this study. They are:

- mission requirements for the rocket vehicle;
- chemical compatibility of the propellants with the materials;

- system reliability; and
- system performance.

The mission requirements concern the possibility of using storable propellants, the need to start the engine one or more times, and the capability of controlling the values of pressure in the ullage space.

The chemical compatibility of the propellants with the materials concern the absence of reactivity between the propellants and the materials of which their containers are made, the absence of condensable or soluble particles in the combusted gas, and the maintenance of a desired value of temperature in the gas under pressure.

The system reliability depends on the degree of complexity of the system, on the number of its failure modes, and on the number of its components. The reliability of each component, in turn, is to be evaluated considering its time of development and the funds available. To this regard, components expected to require greater efforts of development to reach desirable degrees of reliability are gas generators, heat exchangers forming an integral part of the thrust chamber, storage vessels subject to high pressures, and pipes and regulators for gases at high temperatures.

The system performance depends on the gross mass of the gas stored for pressurisation, which in turn depends on its molar mass and also on the mass of the system of pressurisation. The latter mass is part of the mass of the rocket vehicle at burnout.

References

1. Greene WD (2013) Inside the LEO doghouse, start me up! NASA, 19 Dec 2013. <https://blogs.nasa.gov/J2X/2013/12/19/inside-the-leo-doghouse-start-me-up/>
2. Lee JC, Ramirez P, Keller RB Jr (1975) Pressurization systems for liquid rockets. NASA SP-8112, 175pp. <https://ntrs.nasa.gov/archive/nasa/casi.ntrs.nasa.gov/19760015212.pdf>
3. Huzel DK, Huang DH (1967) Design of liquid propellant rocket engines, 2nd edn. NASA SP-125, NASA, Washington, D.C., 472pp. <https://ntrs.nasa.gov/archive/nasa/casi.ntrs.nasa.gov/19710019929.pdf>
4. The Engineering Toolbox, Specific heat and individual gas constant of gases. https://www.engineeringtoolbox.com/specific-heat-capacity-gases-d_159.html
5. Interbartolo M (2009) Apollo lunar module propulsion systems overview. Slide presentation, NASA, 26pp. <https://ntrs.nasa.gov/archive/nasa/casi.ntrs.nasa.gov/20090016298.pdf>
6. Boeing (1968) Lunar Orbiter IV—photographic mission summary, vol 1. NASA CR-1054, 128pp. <https://ntrs.nasa.gov/archive/nasa/casi.ntrs.nasa.gov/19680017342.pdf>
7. Childs FW, Horowitz TR, Jenisch W Jr, Sugarman B (1962) Design guide for pressurization system evaluation liquid propulsion rocket engines, vol I. Aerojet-General Corporation, 30 Sept 1962, 137pp. https://ia801401.us.archive.org/18/items/nasa_techdoc_19630008160/19630008160.pdf
8. Wagner WA, Keller RB Jr (eds) (1974, May) Liquid rocket metal tanks and tank components. NASA SP-8088, 165pp. <https://ntrs.nasa.gov/archive/nasa/casi.ntrs.nasa.gov/1975004950.pdf>
9. Wichmann H (1972, March) Design for pressure regulating components—final report. NASA-CR-139300, 271pp. <https://ntrs.nasa.gov/archive/nasa/casi.ntrs.nasa.gov/19740022135.pdf>
10. MatWeb Material property data, Titanium Ti–13V–11Cr–3Al (Ti–13–11–3) Aged 490 °C. <http://www.matweb.com/search/datasheet.aspx?MatGUID=ba6943e32b354789aa61b7517ca16b00>